ISSN: 1945-3094 (Print), 1945-3108 (Online) Volume 2, Number 3, March 2010

Journal of Water Resource and Protection

www.scirp.org/journal/jwarp

Scientific Research

Journal Editorial Board

ISSN: 1945-3094 (Print) ISSN: 1945-3108 (Online)

http://www.scirp.org/journal/jwarp

J. Water Resource and Protection, **2010, 2, 191-290**
Published Online March 2010 in SciRes (http://www.SciRP.org/journal/jwarp/).

TABLE OF CONTENTS

Volume 2 Number 3 March 2010

Journal of Water Resource and Protection (JWARP)

Journal Information

SUBSCRIPTIONS

The *Journal of Water Resource and Protection* (Online at Scientific Research Publishing, www.SciRP.org) is published monthly by Scientific Research Publishing, Inc., USA.

Subscription rates:

Print: $50 per issue.
To subscribe, please contact Journals Subscriptions Department, E-mail: sub@scirp.org

SERVICES

Advertisements
Advertisement Sales Department, E-mail: service@scirp.org

Reprints (minimum quantity 100 copies)
Reprints Co-ordinator, Scientific Research Publishing, Inc., USA.
E-mail: sub@scirp.org

COPYRIGHT

PRODUCTION INFORMATION

For manuscripts that have been accepted for publication, please contact:
E-mail: jwarp@scirp.org

J. Water Resource and Protection, **2010, 2, 191-198**
doi:10.4236/jwarp.2010.23021 Published Online March 2010 (http://www.scirp.org/journal/jwarp)

Integrated Water Resources Management and Poverty Eradication –Policy Analysis of Bangladesh and Cameroon

Emmanuel M. Nyambod, Huq Nazmul
Department of Human Ecology, Vrije Universiteit Brussel, Brussels, Belgium
E-mail: *enyambod@yahoo.co.uk, nazmulhuqrussell@gmail.com*
Received December 18, 2009; *revised December* 25, 2009; *accepted January* 27, 2010

Abstract

There is a growing recognition that the world faces water crisis that, left unchecked, will derail progress towards the Millennium Development Goals and hold back human development. Water for life in the household and water for livelihoods through production are two of the foundations for human development. This paper argues that the roots of the crisis in water can be traced to poverty, inequality and unequal power relationships, as well as flawed water management policies that exacerbate scarcity. Structured discussion on the basis of the key elements of integrated water resource management reveals that despite of more or less equivalent economic structure of both Bangladesh and Cameroon, both countries do not necessarily have the same policies in water management. This paper therefore broadly recommends inter-country experience sharing of good practices in to be able to cope with water problems in these millennia.

Keywords: Bangladesh, Cameroon, Integrated Water Management, Policies

1. Introduction

The word *crisis* is sometimes overused in development. But when it comes to water, there is a growing recognition that the world faces a crisis that, left unchecked, will derail progress towards the Millennium Development Goals[1] and hold back human development. Throughout history human progress has depended on access to clean water and on the ability of societies to harness the potential of water as a productive resource. Water for life in the household and water for livelihoods through production are two of the foundations for human development[2]. Yet for a large section of humanity these foundations are not in place. The reports argues that the roots of the crisis in water can be traced to poverty, inequality and unequal power relationships, as well as flawed water management policies[3] that exacerbate scarcity.

1.1. Human Development, Poverty and Water-Looking for the Link

Access to water for life is a basic human need and a fundamental human right[4]. Yet in our increasingly prosperous world, more than 1 billion people are denied the right to clean water and 2.6 billion people lack access to adequate sanitation[5]. These headline numbers capture only one dimension of the problem. Every year some 1.8 million children die as a result of diarrhea[6] and other diseases caused by unclean water and poor sanitation. At the start of the 21st century unclean water is the world's second biggest killer of children. Besides, every day millions of women and young girls collect water for their families—a historical ritual that reinforces gender inequalities in employment and education. Meanwhile, the ill health associated with deficits in water and sanitation undermines productivity and economic growth, reinforcing the deep inequalities that characterize current patterns of globalization and trapping vulnerable households in cycles of poverty.

[1] UN-DESA. 2008. The Millennium Development Goals Report 2008. United Nations. New York.
[2] www.hdr.undp.org/en/media/HDR06-complete.pdf accessed on 25/04/2009.
[3] Michel, D., Pandya, A. (Ed.) 2009. Troubled **Waters-Climate** Change Hydro-politics, and Transboundary Resources. The Henry L. Stimson Center. ISBN: 978-0-9821935-2-5. Washington.
[4] http://www.gwpforum.org/gwp/library/GWP_Strategy_2009-2013_final.pdf accessed on 19/03/2009.
[5] WHO/UNICEF Joint Monitoring Programme for Water Supply and Sanitation; Meeting the MDG drinking water and sanitation target: a mid-term assessment of progress, 2004.
[6] http://www.who.int/water_sanitation_health/diseases/ascariasis/en/accessed on 05/05/2009.

1.2. Integrated Water Resource Management and Poverty–Potential Remedy

At its simplest, Integrated Water Resources Management (IWRM) is a logical and appealing concept. Its basis is that the many different uses of water resources are interdependent. Interdependency among the components holds strong backward and forward linkage amongst sociophysical variable necessary for establishment of fundamental rights of ensuring water for decent living. IWRM addresses the deep-rooted problems that exacerbate poverty and simultaneously seeks cure from the water trapped poverty. The inter-related framework of IWRM includes vital components to manage the water problem which evenly valid for the water scared countries and developed countries as well though problem matters according to the context.

This report aims to establish a relation among three basic components *i.e.* IWRM, Poverty and Human Development. The issues are reinforcing each other and one's performance no matter satisfactory or unsatisfactory, influences other twos. It is now widely accepted dogma for achieving global target of ensuring decent living; poverty is the major hindrance which again is aggravated by water related poverty. On this conjecture, it seems IWRM can perform the more inclusive role than any other tools.

1.3. Scope of the Report

The paper contains huge potentiality to explore to both explicit and implicit role of IWRM for investigating of poverty eradicating role. The major highlights of this report concern two developing countries with versatile geo-sociological context, *i.e.* Bangladesh and Cameroon. Both the countries are treated as Least Developing Countries (LDCs) and in Human Development Index according to Human Development Report of United Nations, they stay at near bottom for instance 146 for Bangladesh and 153 for Cameroon in 2009[7]. The indicators pertaining to water holds back their further development in ranking and thus it can be concluded that flawed water management system and policies is the potential responsible reason behind bottom position in human development. On the midst of the Millennium Development Goals, it is not at all desirable to see still many more are crying for a single drop of water. The aspiration of this report has been evolved from this very necessary question of assessing the wrongs in the water policy or concept of IWRM and its' practice within Bangladesh and Cameroon.

[7] UNDP, (2009), Human Development Report 2009- Overcoming Barriers: Human Mobility and Development, United Nations Deve- lopment Program.

2. Methodology

The Methodology report is based on secondary data available in published and unpublished materials e.g. books, journals, magazines, periodical reports, national documents. Rigorous internet searching is one of the major sources of data and information. The consultation with the documents lays the foundation of the report. For situation analysis of the studied countries, non printed internet documents played pioneer role. Literature related to IWRM has been vigorously studied to capture the robust view of dg the role of IWRM to make the bridge between water management and poverty dimension. Alongside, intergovernmental organizational and development organizational documents, briefing papers, fact sheets provide a peer looking on the situation happening around the world. National documents and policies are the building blocks to depict the country's policies and its state relatedefinin to spirit of IWRM. The report follows the sequential path to reach conclusion as portrayed in **Figure 1**.

In description of above figure, the goals objective and primary methods of the report have been finalized through consultation between authors. Necessary documents were collected to target the goals and the objectives of the paper. Partially, analyzing policy of third world countries still appears as a cumbersome process because of low level infrastructural development and inadequate information technology systems. Despite such impasses, necessary documents were managed and somewhat translated especially from documents from Cameroon from French into English. This was specific IWRM objectives were then compared against chosen water policy guidelines for the two countries-Cameroon and Bangladesh.

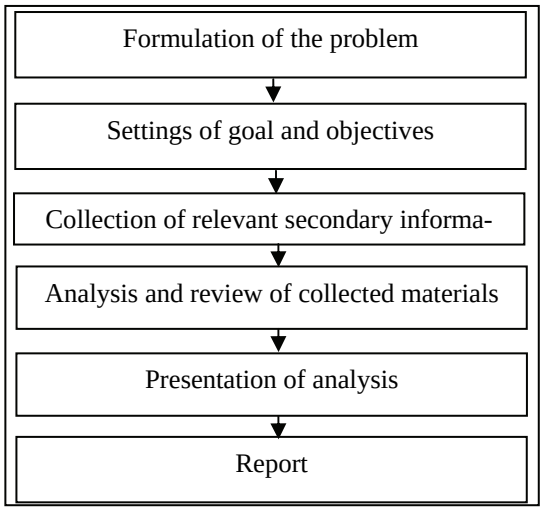

Figure 1. Steps followed to report preparation.

Source: Authors

3. Poverty and Water

3.1. Cameroon Water Poverty Situation

Cameroonians in 2001 were living with an annual income below the poverty line of CFAF 232,547 (roughly equivalent to US$1 per person, per day, or FCFA 19,000 per month), which represents the estimated annual income necessary for an individual in Yaoundé (the capital city) to buy a "minimal basket" of essential food and non-food items, including health, education, and housing expenditures. With the current price hikes in the prices of basic commodities both at the national and international scene, the poverty situation today might even be worst when compared to this 2001 [1].

Water is a basic human need and access to minimum quantities of safe water (20 liters per person per day) should be everyone's right. Lack of access to safe drinking water, sanitation, and irrigation is directly related to poverty and poor health. WHO data shows an average water consumption in 33 countries in Africa stands at 35 litres per person per day a figure seen to be far below minimum average requirement of 50 litres per person per day (WHO, 2008).

Cameroon (West-Central Africa) still live the experiences of the 16th century where safe water for this community has been a farfetched reality; where drinking from the same stream with cattle, pigs, and goats is still very rife and where the ordinary pregnant and farm battered indigenous woman has to trek for kilometres just to fetch water for household use. For the most part, most environs of this community keep on risking their lives to environmental hazards and water borne related epidemics such as diarrhea, cholera and dysentery.

Water resource management in Cameroon is a severe constraint to poverty alleviation and to sustainable development. Significant sections of the population suffer mainly due to poor water management and limited exploitation of existing water sources rather than actual water shortage/scarcity. About 42 % of Cameroonians do not have access to adequate drinking water; this is a striking statistic for a country endowed with abundant freshwater resources. In Cameroon, a cross-section of the population does not enjoy access to water either because the cost to connect the water is too high and/or the cost per meter cube is too high (the cost per meter cube has risen from 339FCFA/ m^3 in the 80's to 470FCFA/ m^3 at present–about one US dollar/ m^3). Given the general financial situation of the people, this amount is too high and this partly explains why water cuts for failure to pay or delays are significantly many.

3.2. Bangladesh Water Poverty Situation

With over 1000 people per square kilometers Bangladesh has one of the highest population densities in the world. 50 % of the population is categorized as poor and 20 % as hardcore poor. In absolute numbers, therefore, about 71 million people are under the national poverty line[8]. In spite of this serious challenge, the effort to achieve nearly universal water supply coverage has become an example of global best practice. The water supply coverage reached 97 % in 2005[9] both in urban and rural areas where it was 44 % in 1975[10].

Evidences support that Bangladesh has made commendable progress in supplying safe water to its people. For Bangladesh, the term "water poverty" is thus can be ignored as state is now guaranteeing almost 100 % safe drinking water to its people. Even, nearly same percentage of total population is enjoying safe sanitation system.

This achievement, off-course painted a bright colour on the wall of "water related poverty". No doubt, national policies and all level willingness to meet the target of meeting MDGs played the most significant role. Apart from those policies, nongovernmental organizations contribute a big deal to this achievement and keep the achievement sustained. The projected downside is not much optimistic as growing population, continuous urbanization, irrigation, salanization, climate change and trans-boundary water dispute will likely bring a huge water scarcity and quality related problem in next 25 years if the problems are left unchecked.

Safe drinking water and sanitation is the biggest problem for all developing countries which is being further accelerated due to several physical and social catalysts. Since Bangladesh overwhelmed such a big deal, its water sector problem has taken a paradigm shift from last one decade. The major problem and challenges in water sector that contributes to worsen poverty scenario to other dimension can be categorized as following:

- One of the most critical challenges Bangladesh faces is the management of water resources during their excesses and acute scarcity. It is particularly difficult when only 7 % of the catchments areas of the mighty international rivers, the Ganges, The Brahmaputra and the Meghna are in Bangladesh while 97 % is outside Bangladesh where unfortunately, Bangladesh has no control on upstream diversion and water use[11].
- There are 57 trans-border rivers including the Ganges, the Brahmaputra and the Meghna out of which 53 come from India, 1 from China and 3 from Myanmar. These rivers carry both huge quantity of floodwaters and sediments. During dry season water is scarce; the rivers

[8] http://siteresources.worldbank.org/INTBANGLADESH/Resources/AchievingtheWaterandSanitationMDGsinBangladesh_edited.doc on13/05/2006.

[9] http://hdr.undp.org/en/media/HDR_20072008_EN_Complete.pdf on 13/05/2009.

[10] http://www.bbs.gov.bd/dataindex/MDGs%20in%20Bangladesh.doc.on 13/05/2009.

[11] http://www.newagebd.com/2006/mar/04/oped.html on 13/05/2009.

suffer from extreme pollution, not enough water to keep the rivers navigable and not enough water for drinking.

- Low current from upstream rivers causes a huge problem for growing salinization, inadequate supply for irrigation and lowering water tables and lack of stakeholder participation in decision making.

4. Integrated Water Resources Management (IWRM)

At its simplest, Integrated Water Resources Management (IWRM) is a logical and appealing concept. Its basis is that the many different uses of water resources are interdependent. Integrated management means that all the different uses of water resources are considered together. Water allocations and management decisions consider the effects of each use on the others. They are able to take account of overall social and economic goals, including the achievement of sustainable development. This also means ensuring coherent policy making related to all sectors. As the basic IWRM concept has been extended to incorporate participatory decision-making. Different user groups (farmers, communities, environmentalists) can influence strategies for water resource development and management.

Management is used in its broadest sense. It emphasizes that it must not only focus on development of water resources but also must consciously manage water development in a way that ensures long term sustainable use for future generations. IWRM considers the viewpoints of human groups, factors of the human environment, and aspects of natural water systems.

Integrated water resources management is therefore a systematic process for the sustainable development, allocation and monitoring of water resource use in the context of social, economic and environmental objectives. It contrasts with the sectoral approach that applies in many countries. When responsibility for drinking water rests with one agency, for irrigation water with another and for the environment with yet another, lack of cross-sectoral linkages can lead to uncoordinated water resource development and management, results conflict, waste and unsustainable systems.

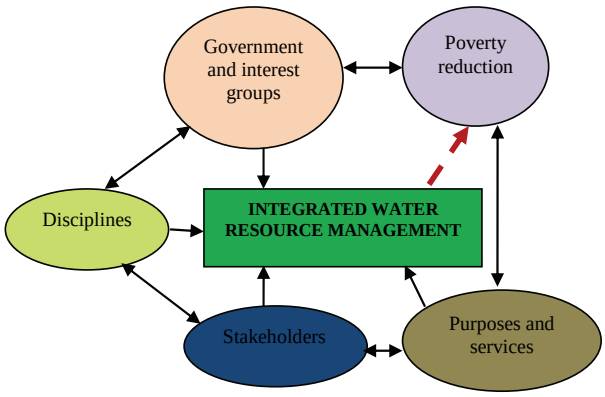

Figure 2. Relationship between IWRM and its components.

Source: Adapted from http://www.waterencyclopedia.com/Hy-La/Integrated-Water-Resources-Management.html. Accessed 13/05/2009.

According to Global Water Partnership (GWP), IWRM is based on the equitable and efficient management and sustainable use of water and recognizes that water is an integral part of the ecosystem, a natural resource, and a social and economic good, whose quantity and quality determine the nature of its utilization. The concept of IWRM, thus, introduces a kind of universal definition of IWRM.

Integrated Water Resources Management (IWRM), has been defined as a process which promotes the coordinated development and management of water, land and related resources in order to maximize the resultant economic and social welfare in an equitable manner without compromising the sustainability of vital eco-system[12].

4.1. Why IWRM?

Water is vital for human survival, health and dignity and is a fundamental resource for human development. The world's freshwater resources are under increasing pressure yet many still lack access to adequate water supply for basic needs. Growth in population, increased economic activity and improved standards of living lead to increased competition for, and conflicts over, the limited freshwater resource. Here are a few reasons why many people argue that the world faces an impending water crisis:

- Water resources are increasingly under pressure from population growth, economic activity and intensifying competition for the water among users;
- Water withdrawals have increased more than twice as fast as population growth and currently one third of the world's population live in countries that experience medium to high water stress;
- Pollution is further enhancing water scarcity by reducing water usability downstream;
- Shortcomings in the management of water, a focus on developing new sources rather than managing existing ones better, and top-down sector approaches to water management result in uncoordinated development and management of the resource;
- More and more development means greater impacts on the environment; and
- Current concerns about climate variability and climate change demand improved management of water resources to cope with more intense floods and droughts.

4.2. Emergence of IWRM as Guiding Principle

The concept of IWRM has been developed due to ill-management and non-integrated way of water resource

[12] www.unep.org/GC/GCSS-VIII/IWRMFF.OECD.doc on 11/04/2009.

management across the planet. Water is a basic human rights and very much related with the question of bread and butter for the human being from the very first moment when civilization started rolling. Over the time, new categories of water uses have appeared such as industries, irrigation schemes, rapid urbanization and corporate agriculture and etc. Special laws were enacted and special administrations were gradually placed in policy framework for better water management. However, water management was, and in most countries still is, fragmented, without any real taking into account of the global picture. This situation has resulted in many disasters: deprivation of safe drinking water supply, sanitation, intense pollution, overexploitation of aquifers, drying-up of portions of rivers, floods over densely inhabited areas, funds wasted on many inappropriate projects. This state of affairs could not continue indefinitely, and through various means and difficult experiences, a consensus progressively took form: all the users of given water resource should work together in order to try and manage "their" water in the best possible way: IWRM was born[13].

4.3. Benefits of IWRM

4.3.1. Environmental Benefits

- Ecosystems can benefit from applying an integrated approach to water management by giving environmental needs a voice in the water allocation debate. At present these needs are often not represented at the negotiating table.
- IWRM can assist the sector by raising awareness among other users of the needs of ecosystems and the benefits these generate for them. Often these are undervalued and not incorporated into planning and decision-making.
- The ecosystem approach provides a new framework for IWRM that focuses more attention on a system approach to water management: -protecting upper catchments (e.g. reforestation, good land husbandry and soil erosion control), pollution control (e.g. point source reduction, non-point source incentives, groundwater protection) and environmental flows. It provides an alternative to a sub-sector competition perspective that can join stakeholders in developing a shared view and joint action.

4.3.2. Agricultural Benefits

- As the single largest user of water and the major non-point source polluter of surface and groundwater resources, agriculture has a poor image. Taken alongside the low value added in agricultural production, this frequently means that, especially under conditions of water scarcity, water is diverted from agriculture to other water uses. However, indiscriminate reduction in water allocation for agriculture may have far-reaching economic and social consequences. With IWRM, planners are encouraged to look beyond the sector economics and take account of the implications of water management decisions on employment, the environment and social equity.
- By bringing all sectors and all stakeholders into the decision-making process, IWRM is able to reflect the combined "value" of water to society as a whole in difficult decisions on water allocations. This may mean that the contribution of food production to health, poverty reduction and gender equity, for example, could override strict economic comparisons of rates of return on each cubic meter of water. Equally, IWRM can bring into the equation the reuse potential of agricultural return flows for other sectors and the scope for agricultural reuse of municipal and industrial wastewaters.
- IWRM calls for integrated planning so that water, land and other resources are utilized in a sustainable manner. For the agricultural sector IWRM seeks to increase water productivity (*i.e.* more crops per drop) within the constraints imposed by the economic, social and ecological context of a particular region or country.

4.3.3. Water Supply and Sanitation Benefits

- Above all, properly applied IWRM would lead to the water security of the world's poor and un-served being assured. The implementation of IWRM based policies should mean increased security of domestic water supplies, as well as reduced costs of treatment as pollution is tackled more effectively.
- Recognizing the rights of people, and particularly women and the poor, to a fair share of water resources for both domestic and household-based productive uses, leads inevitably to the need to ensure proper representation of these groups on the bodies that make water resource allocation decisions.
- The focus on integrated management and efficient use should be a stimulus to the sector to push for recycling, reuse and waste reduction. High pollution charges backed by rigid enforcement have led to impressive improvements in industrial water-use efficiencies in the industrialized countries, with benefits for domestic water supplies and the environment.
- Past sanitation systems often focused on removing the waste problem from the areas of human occupation, thus keeping the human territories clean and healthy, but merely replacing the waste problem, with often detrimental environmental effects elsewhere. Introduction of IWRM will improve the opportunity for introduction of sustainable sanitation solutions that aim to minimize waste-generating inputs, and reduction of waste outputs, and to solve sanitation problems as close as possible to where they occur.
- At a practical local level, improved integration of water resource management could lead to greatly reduced costs of providing domestic water services, if for instance more irrigation schemes were designed with a domestic

[13] www.unep.org/GC/GCSS-VIII/IWRMFF.OECD.doc on 06/04/2009.

water component explicitly involved from the start.

4.4. IWRM Principles

A meeting in Dublin in 1992[14] gave rise to four principles that have been the basis for much of the subsequent water sector reform. These principles form the basis for the in-depth comparative analysis of water related policies in Cameroon and Bangladesh, described in **Table 1**.

Principle 1: Fresh water is a finite and vulnerable resource, essential to sustain life, development and the environment.

Principle 2: Water development and management should be based on a participatory approach, involving users, planners and policymakers at all levels.

Principle 3: Women play a central part in the provision, management and safeguarding of water.

Principle 4: Water has an economic value in all its competing uses and should be recognised as an economic good as well as a social good.

5. Translating IWRM from Ideology to Policy – Case of Bangladesh and Cameroon

The case for IWRM is strong – many would say incontestable. The problem for most countries is the long history of sectoral development. As the Global Water Partnership puts it:

"*IWRM is a challenge to conventional practices, attitudes and professional certainties. It confronts entrenched sectoral interests and requires that the water resource is managed holistically for the benefits of all. No one pretends that meeting the IWRM challenge will be easy but it is vital that a start is made now to avert the burgeoning crisis.*"

IWRM is, above all, a philosophy. As such it offers a guiding conceptual framework with a goal of sustainable management and development of water resources. What it does demand is that people try to change their working practices to look at the bigger picture that surrounds their actions and to realize that these do not occur independently of the actions of others. It also seeks to introduce an element of decentralized democracy into how water is managed, with its emphasis on stakeholder participation and decision making at the lowest appropriate level.

All of this implies change, which brings threats as well as opportunities. There are threats to people's power and position; and threats to their sense of themselves as professionals. IWRM requires that platforms be developed to allow very different stakeholders, often with apparently irreconcilable differences to somehow work together.

Because of the existing institutional and legislative frameworks, implementing IWRM is likely to require reform at all stages in the water planning and management cycle. An overall plan is required to envisage how the transformation can be achieved and this is likely to begin with a new water policy to reflect the principles of sustainable management of water resources. To put the policy into practice is likely to require the reform of water law and water institutions. This can be a long process and needs to involve extensive consultations with affected agencies and the public.

Based on the basic principles of the philosophy of IWRM the national water policies of case studied countries have been consulted. This rigorous consultation allows a look into the policy matters how that IWRM has been materialized. This report does not depict any field level practice of those policies but is strictly guided by the policy documents only. Mostly, the table shows synergies and gap among ideological principles, national policies and poverty connection. As the basic premise of this report to make a bridge between philosophy and policy exists compared to poverty situation, the policy related gaps surface in the table. The result of analysis is presented in a matrix form and available in Table 1 below:

6. Concluding Remarks and Recommendations

The structured discussion on the basis of the key elements of IWRM reveals that despite of more or less equivalent economic structure of both Bangladesh and Cameroon, both countries do not necessarily have the same policies in water management. A critical look shows that Bangladesh's policies are much more advanced compared to Cameroon. As said earlier, in Water and Sanitation (WATSAN) sector, Bangladesh can be one of the best practice example for the world hence Cameroon WATSAN sector can follow the guiding principles which Bangladesh is following. The implementation system must be different as societal and topographical context is much different.

However, for Bangladesh, due to Arsenic problem[15] hygienic WATSAN coverage is receding from 97 % to 80 %[16] [2]. Government should take necessary action not only for meeting arsenic problem but also for projected catastrophe related to water sector.

To manage water resources in a meaningful and effective manner, it seems crucial to incorporate IWRM policies in strata of policy level as cross cutting issue. Development is seen as an integrated and continuous process for sustainability and poverty reduction. IWRM entails the components sustainability which must be incorporated in national development agendas. At the same time, inter-country experience sharing should be encouraged so that good practice can be a universal notion for all. To conclude, the following general recommendations can applied with demystifying properly:

[14] The International Conference on Water and Environment, Dublin, Ireland, January 1992.

[15] http://www.angelfire.com/ak/medinet/file5.html accessed on 13/05 / 2009.

[16] Bangladesh PRSP, 2008.

Table 1. Policy analysis Bangladesh and Cameroon.

Components of IWRM	Cameroon[17] [3].	Bangladesh
Principle 1: Fresh water is a finite and vulnerable resource, essential to sustain life, development and the environment. The freshwater resource is a natural asset that needs to be maintained to ensure that the desired services it provides are sustained. This principle recognises that water is required for many different purposes, functions and services; management therefore, has to be holistic (integrated) and involve consideration of the demands placed on the resource and the threats to it. The integrated approach to management of water resources necessitates co-ordination of the range of human activities which create the demands for water, determine land uses and generate waterborne waste products.	According to latest water law of Cameroon recognize the principal in their article 2, 3 and 4. Those articles recognize that Water is a national property, thus the state must assure he protection and management and facilitate access to all. At the same time article 2 acknowledges the integration of surface, sub surface, spring and mineral water sources. Poverty is another philosophy that is attributed by water scarcity and deprivation. It is imperative to acknowledge the notion for effective IWRM for poverty reduction drastically.	According to National Water Policy 2001 (Section 2), • As water is essential for human survival, socio-economic development of the country and preservation of its natural environment, it is the policy of the Government of Bangladesh that all necessary means and measures will be taken to manage the water resources of the country in a comprehensive, integrated and equitable manner. • The policies enunciated in the policy are designed to ensure continued progress towards fulfilling the national goals of economic development, poverty alleviation, food security, public health and safety, decent standard of living for the people and protection of the natural environment.
Principle 2: Water development and management should be based on a participatory approach, involving users, planners and policymakers at all levels. Water is a subject in which everyone is a stakeholder. Real participation only takes place when stakeholders are part of the decision-making process. The type of participation will depend upon the spatial scale relevant to particular water management and investment decisions. A participatory approach is the best means for achieving long-lasting consensus and common agreement. Governments have to help create the opportunity and capacity to participate, particularly among women and other marginalized social groups. It has to be recognized that simply creating participatory opportunities will do nothing for currently disadvantaged groups unless their capacity to participate is enhanced. Decentralizing decision making to the lowest appropriate level is one strategy for increasing participation.	In article 24 traditional authorities are recognized as to competent to regulate litigations related to the use of the water resources on the basis of local custom and habits, without damage of the right of the parts to the litigation to seize the courts of competent jurisdiction of them. Again article 23 states that parties with a disagreement relating to management of water can regulate it of a common agreement by way of arbitration which implies a kind of notion to manage the water resources with mutual agreement with involved parties. The direct active participation of all level stakeholders is not however clearly marked which eventually treats end user as just resource user but not as right holders. As long as, users are not recognized as right holders, sustainable water management and poverty eliminating notions will remain as mirage or illusion. Community should have right to put their opinion on policy issues.	In National Water Policy 2001[18] it is clearly demarcated that (Subsection 4.2) • The Government recognizes that the process of planning and managing water resources requires a comprehensive and integrated analysis of relevant hydrological, topographical, social, political, economic, environmental and institutional factors across all related water-using sectors. • According to PRSP 2008 (p-66), the ultimate success and effectiveness of public water resources management projects depends on the people's acceptance and ownership of each project. It is important to delineate the roles and responsibilities of everyone involved in water resources management. The principle that community resources should be managed by the community concerned, along with local government institutions unless a greater national interest prevails, should guide water resource management.
Principle 3: Women play a central part in the provision, management and safeguarding of water. IWRM requires gender awareness. In developing the full and effective participation of women at all levels of decision-making, consideration has to be given to the way different societies assign particular social, economic and cultural roles to men and women. There is an important synergy between gender equity and sustainable water management. Involving men and women in influential roles at all levels of water management can speed up the achievement of sustainability; and managing water in an integrated and sustainable way contributes significantly to gender equity by improving the access of women and men to water and water-related services to meet their essential needs.	As far as water policy of Cameroon concerned, no transparent role has been earmarked to woman to leverage the policy. It is a far dream to ground water policies into practice without active role playing by woman. For Cameroon it is an urgent call to incorporate gender friendly policies to move ahead to implement IWRM for poverty reduction.	• National Water Policy 2001 recognised that women have a particular stake in water management because they are the principal providers and carriers of water, main caretaker of the family's health, and participants in many stages of pre and post harvest activities (Subsection 4.3a). • PRSP, 2008 sets five supporting strategies to implement the project fixed in the document. The first supporting strategy is to Ensuring Participation, Social Inclusion and Empowerment of woman in all decision making practice (P-160).
Principle 4: Water has an economic value in all its competing uses and should be recognised as an economic good as well as a social good. Within this principle, it is vital to recognize first the basic right of all human beings to have access to clean water and sanitation at an affordable price. Managing water as an economic good is an important way of achieving social objectives such as efficient and equitable use, and of encouraging conservation and protection of water resources. Water has a value as an economic good as well as a social good. Many past failures in water resources management are attributable to the fact that the full value of water has not been recognized.	Article 2 states that water is a national property, thus the state must assure the protection and management and facilitate access to all. Besides, in article 6, 16 and 23 contains some indication how water would be treated within the dilemma of public and private goods. Water is life and it is fundamental rights to human development. At the same time, it is becoming a scare resource all over the world and its magnitude in dry topography like Cameroon is definitely would be hard. From this point of view, government should be strict on its rational use and appropriate pricing for different sectors must be defined.	• Changes are required in the system of prices and other economic incentives affecting water demand and supply in Bangladesh. Unless the users pay a price for water, there will be a tendency to misuse and deplete it under scarcity conditions. Desirable practices such as conjunctive use, water-saving agricultural and industrial technologies, water harvesting, water transfers, and water recycling, both within and between sectors, will emerge only when users perceive the scarcity value of water (National water policy 2001, Subsection 4.14). • The policy related to pricing summarize that, Pricing structure will match the goals and needs of the water provider and the population served. Water rates will be lower for basic consumption, increasing with commercial and industrial use. The rates for surface and groundwater will reflect, to the extent possible, their actual cost of delivery (PRSP, 2008, P-70).

[17] All the articles of Cameroon water law have been extracted from LAW N° 98-005 of April 14, 1998 on water regime in Cameroon.
[18] www.mowr.gov.bd/Documents/National%20Water%20Policy%20 (English).pdf on 13/05.2009

- Address issues related to the harnessing and development of all forms of surface water and ground water and management of these resources in an efficient and equitable manner.
- Ensure the availability of water to all elements of the society including the poor and the underprivileged, and to take into account the particular needs of women and children.
- Accelerate the development of sustainable public and private water delivery systems with appropriate legal and financial measures and incentives, including delineation of water rights and water pricing.
- Bring institutional changes that will help decentralize the management of water resources and enhance the role of women in water management.
- Develop a legal and regulatory environment that will help the process of decentralization, sound environmental management, and improve the investment climate for the private sector in water development and management.
- Develop a state of knowledge and capability that will enable the country to design future water resources management plans by itself with economic efficiency, gender equity, social justice and environmental awareness.

7. References

[1] Republic of Cameroon, Poverty Reduction Strategy Paper (PRSP), 2003–2008, 2003. http://www.imf.org/external/pubs/ft/scr/2003/cr03249.pdf. Accessed on 26th February 2009.

[2] Poverty Reduction Strategy Paper (PRSP) (2008-2011), Planning Commission Bangladesh National Water Policy, 2008. Ministry of Water Resources, Bangladesh, 2001.

[3] Cameroon Water Law, N° 98-005 of April 14, 1998, "On water regime in Cameroon." http://www.gwpcm.org/eng/bibliotheque/File/code%20cameroun(2).pdf.

J. Water Resource and Protection, **2010, 2, 199-208**
doi:10.4236/jwarp.2010.23022 Published Online March 2010 (http://www.scirp.org/journal/jwarp)

Hydrochemical and Isotopic Characterisation of Groundwaters in the Eastern Region of Ghana

Samuel Y. Ganyaglo[1], Bruce Banoeng-Yakubo[2], Shiloh Osae[1], Samuel B. Dampare[1,3], Joseph R. Fianko[1], Mohammad A. H. Bhuiyan[3]
[1]*National Nuclear Research Institute, Ghana Atomic Energy Commission, Legon-Accra, Ghana*
[2]*Department of Geology, University of Ghana, Legon-Accra, Ghana*
[3]*Department of Earth Sciences, Okayama University, Okayama, Japan*
E-mail: *sganyaglo@yahoo.co.uk*
Received December 27, 2009; *revised January* 20, 2010; *accepted January* 23, 2010

Abstract

Major ions and stable isotopes of groundwater in the Cape Coast granitoid complex (G1) and Lower Birimian (LB) formations in the Eastern Region of Ghana were evaluated to establish the source of recharge to the groundwater system. Five major hydrochemical facies were identified in the various rocks in the study area. They are calcium-magnesium-bicarbonate, sodium bicarbonate, sodium chloride and calcium chloride waters and mixed or non dominant water type. Sodium chloride and calcium chloride waters dominate aquifers of the Cape Coast granitoid complex whereas calcium-magnesium-bicarbonate is the dominant hydrochemical facies in the Lower Birimian aquifers. The most probable geochemical process responsible for the evolution of these hydrochemical facies is dissolution of minerals in the various rock types. Stable isotope composition of the groundwaters established that the recharge to the groundwater system is derived from rainfall.

Keywords: Hydrochemistry, Isotopes, Groundwater, Ghana

1. Introduction

Over the years groundwater has been one of the major sources of water supply to the rural communities in the Eastern Region of Ghana. This is partially due to drying out of most streams during the dry season and to a lesser extent, pollution of the streams and rivers, which require high cost of treatment before supply. The exploitation of this vital resource dates as far back as the pre-colonial era through the construction of hand-dug wells. These wells were dug through the overburden and weathered rock material. The hand-dug wells did not yield sufficient water during the dry season and their shallow nature rendered them vulnerable to contamination from runoff and anthropogenic activities. As a result, a more effective and hygienic system of water supply in the form of boreholes as the cheapest and most reliable means of meeting the water supply needs of the people was initiated [1,2]. The region has therefore witnessed numerous borehole-drilling programmes including the 3000-borehole programme, which covered five other regions in southern Ghana.

A large amount of hydrogeological and hydrochemical data have been generated through drilling activities in this region. However, as a result of unreliability of the data generated and the lack of a database, not much has been done in understanding the hydrochemical properties of the aquifers as a means of establishing the recharge regimes for the better management of the aquifer systems. The hydrochemical nature of the groundwaters has also not been thoroughly established. It is therefore difficult to predict the chemistry of groundwater and recharge areas.

The chemical composition of groundwater is controlled by many factors including composition of precipitation, mineralogy of the watershed and aquifer materials, aquifer characteristics, climate and topography [3]. These factors combine to create diverse water types that change spatially and temporally. These spatial changes in the water types can be evaluated and used to trace the recharge source(s) to the groundwater system.

The main focus of this study is to establish the recharge regime through groundwater sampling, looking at major ions and stable isotopes of the groundwaters. Specific objectives include identification of hydrochemical

facies of the groundwaters and geochemical processes responsible for the various hydrochemical facies. It is intended to provide a database for sharing with stakeholders in the water sector, and to monitor and check land use practices in the recharge areas to ensure the safety of groundwater usage in the area.

2. Study Area

2.1. Location

The study area lies within latitudes 5° 45′ N to 6° 30′ N and longitudes 0° 00′ to 1° 00′ W. It covers an area of about 7414 km^2. It is bounded on the north by Brong Ahafo region, south by Central region, west by Ashanti region, and east by Volta region and southeast by Greater Accra region. It consists of Akwapim North and South, New Juabeng, Suhum Kraboa Coaltar, Kwabibirem and East Akim districts (**Figure 1**).

2.2. Climate

The study area lies within the wet semi-equatorial climatic zone, characterized by two rainfall maxima, followed by a prolonged dry season. The first rainy season is from May to June with the heaviest rainfall in June, and the second rainy season is from September to October. On the basis of recent meteorological data (1993 to 2003) obtained from the Ghana Meteorological Agency (GMA), annual mean rainfall varies from 1206mm at Nsawam to 1487mm at Kibi. **Figure 2** is a bar chart showing the total annual rainfall pattern in Koforidua area. The main vegetative zone is the moist semi-deciduous forest.

2.3. Geology and Hydrogeology

The study area is made up of the Cape Coast granitoid complex (G1) and the Lower Birimian (LB) rocks (**Figure 3**). The Cape Coast granitoid complex comprises a heterogeneous group of rocks occupying most of Suhum Kraboa Coal Tar, New Juabeng, the northwestern corner of the Akwapim North and part of the Akwapim South districts. The bulk of the Cape Coast granitoid complex is a granitic to quartz dioritic gneiss, which in the field is seen to change gradationally from fine to medium grained,

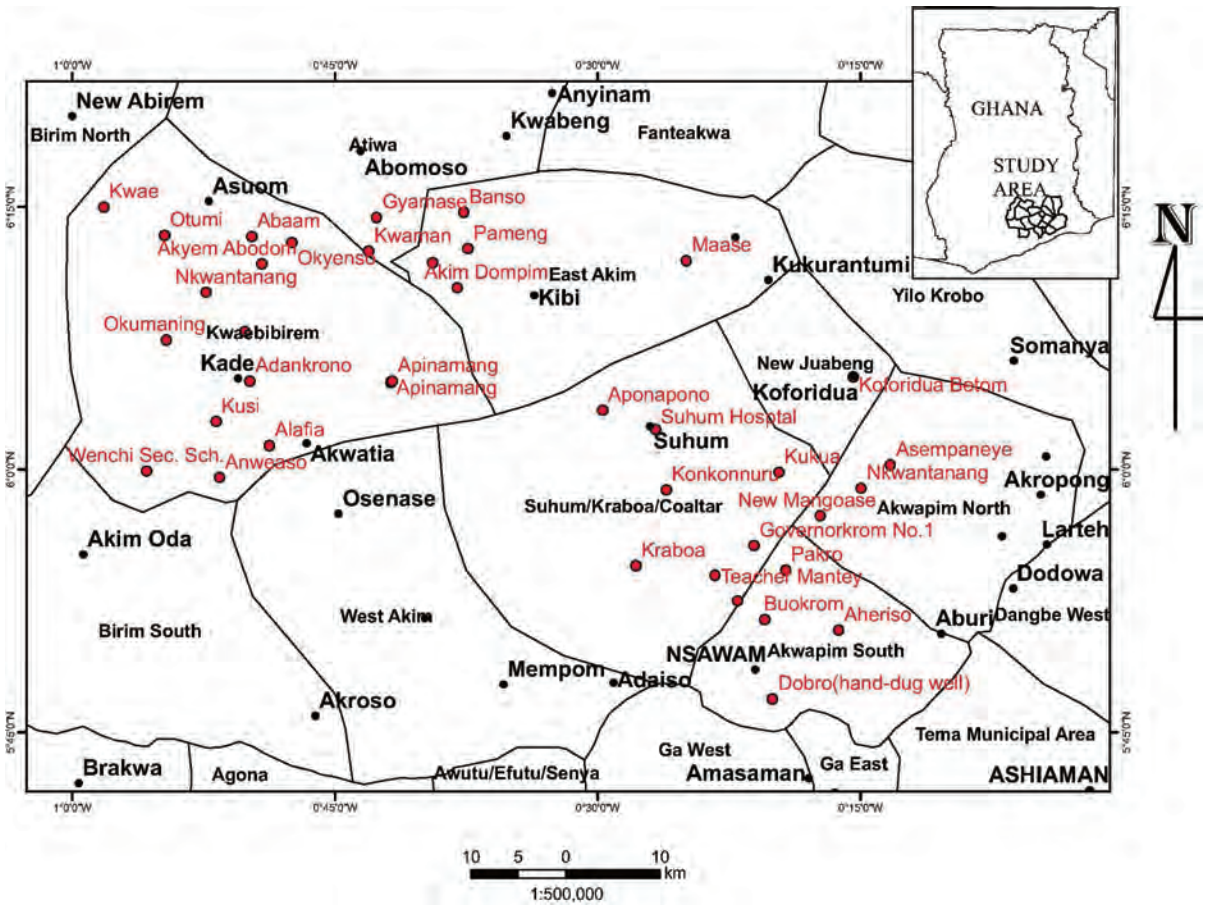

Figure 1. Location map of the study area.

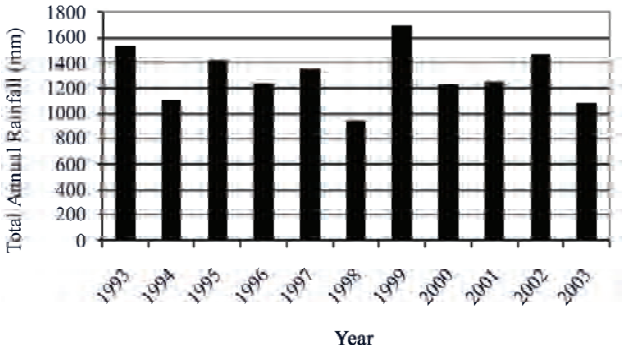

Figure 2. Total annual rainfall at Koforidua from 1993 to 2003.

foliated biotite quartz diorite gneiss to exclusively hornblende-quartz-diorite gneiss [4]. The rock types present in the Lower Birimian are greywackes with turbidite features [5], phyllites, slates, schists, weakly metamorphosed tuffs and lavas. Some of the phyllites contain pyrite and carbonaceous matter. The mode of groundwater occurrence in the study area is through the development of secondary porosities or permeabilities as a result of fracturing, jointing, shearing and deep weathering [2,6,7]. The fractures developed from tectonic movement, pressure relief due to erosion of overburden rock, shrinking during cooling of the rock mass and the compression and tensional forces caused by regional tectonic stresses [7, 8]). Most of the groundwaters in the study area occur in the weathered zone [1]. Available records indicate that borehole yield varies from 12 l/min to 150 l/min in the Cape Coast granitoid complex and 8 l/min to 360 l/min in the Lower Birimian. Average yield in the Cape Coast granitoid is 51 l/min whereas average yield in the Lower Birimian is 108 l/min. Borehole lithologic logs could not be obtained for all the boreholes sampled. Hence depth, yield and static water levels (SWL) were not recorded for some of the boreholes as shown in the data presented in Appendix 1. Estimated depth of drilling, yield, and SWL were based on boreholes for which lithologic logs were obtained. Average depth of drilling is about 33 m for aquifers in the Cape Coast granitoid and 43 m for aquifers in the Lower Birimian. The general static water level in the area ranged from 1.63 m to 10.30 m in the Lower

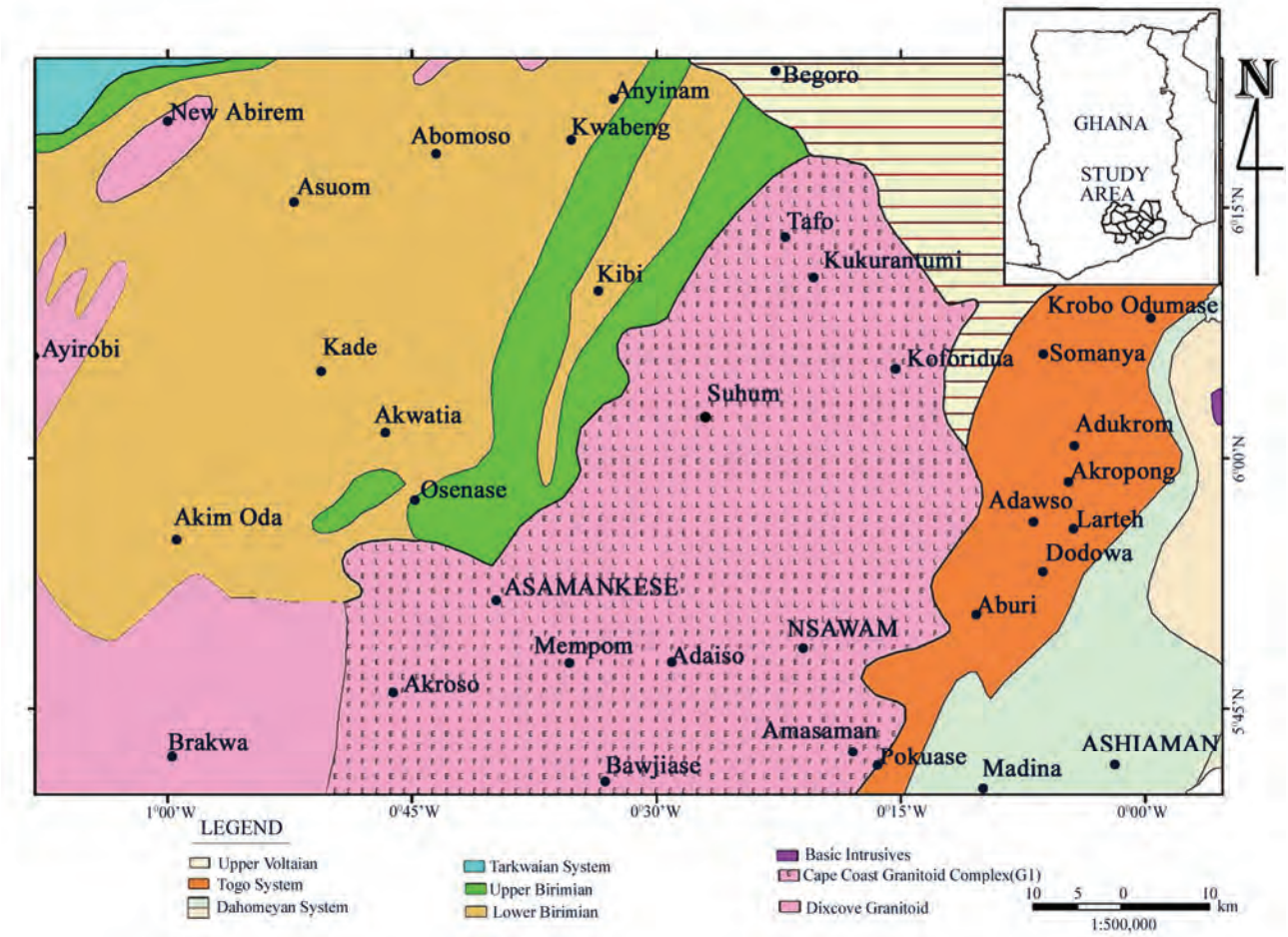

Figure 3. Geological map of the study area.

Birimian aquifers. The mean static water level is 6.15±3.0 m. The static water levels in the Cape Coast granitoid ranged from 0 to 5.14 m with the mean value of 2.35±1.54 m.

3. Methodology

A total of 38 boreholes were sampled. The sampling points are shown in **Figure 1**. Eighteen (18) samples were taken from rocks of the Cape Coast granitoid complex whereas 20 samples were from Lower Birimian rocks.

All water samples were collected in 50 ml pre-conditioned high-density polyethylene bottles. They were conditioned by washing initially with detergent, then with 10 % percent nitric acid, and finally rinsing several times with distilled water. This was carried out to ensure that the sample bottles were free from contaminants.

At the sampling point, the boreholes ware pumped for about 5 minutes to purge the aquifer of stagnant water to acquire fresh aquifer samples for analysis. 5 minutes pumping was allowed, because in most of the communities visited, pumping was already in progress. The pH and temperature were stabilised within the five minutes of pumping. Samples were initially collected in a sterilised bucket immediately after purging the aquifer and quickly transferred into sampling bottles. Samples were taken in duplicate for major ion and stable isotope analyses. Prior to this, field parameters were measured. Basic parameters measured in the field were temperature, pH, and electrical conductivity. Samples earmarked for major ion analyses were filtered on site through 0.45-micron meter cellulose filters with the aid of hand operated vacuum pump.

The samples were preserved in a refrigerator until they were transported to the laboratory for chemical analysis. The major ions were analyzed at the Ecological laboratory, University of Ghana, Legon with Dionex-120 ion chromatograph. The accuracy of the analyses was estimated from the charge balance error (CBE) [9], which is within ± 5% for all samples.

The analysis of oxygen isotope ratio of 14 samples from the study area was determined using a VG Sira 10 mass spectrometer with automatic inlet at the Geological Institute, University of Copenhagen. The measurements of deuterium in the water samples were carried out using Euro Vector elemental analyzer (EA; EuroPyrOH-3100) at the Institute of Physics and Astronomy, University of Aarhus, Denmark. The results for both isotopes were expressed in per mil (‰) deviation from the Vienna Standard Mean Ocean Water (VSMOW) using the delta (δ) – scale. Reproducibility was better than 0.1 ‰ for $\delta^{18}O$ and about 1 ‰ for $\delta^{2}H$.

The Piper 1944 Trilinear diagram was employed to define the various chemical evolution of groundwater in the area. The diagram displays the relative concentrations of the major cations and anions on two separate plots, together with a central diamond plot where the points from the two trilinear plots are projected. The central diamond-shaped field (quadrilateral field) is used to show the overall chemical character of the water. Subdivisions of the diamond field represent water type categories that form the basis for one common classification scheme for natural waters [9]. The diagram was plotted using Groundwater Chart (GW-Chart) software.

4. Results and Discussion

4.1. Hydrochemistry

A statistical summary of chemical parameters measured in the 38 groundwater samples is presented in **Tables 1** and **2**. The pH of groundwater varies from 4.2 to 7.2 in the Cape Coast granitoid complex aquifers with a mean of 6.1and standard deviation of 0.8 (**Table 1**). Majority of the samples in these aquifers falls within natural pH range of 4.5–7.0. In the Lower Birimian aquifers the pH varies from 3.0 to 6.3 with a mean of 4.1 and standard deviation of 1.0 (**Table 2**). The pH is generally low in the Lower Birimian aquifers. Field temperatures vary from 25.3 in the Lower Birimian aquifers to 31.9 ^{o}C in the Cape Coast granitoid aquifers. The lower temperatures occur at higher topographic elevations and the higher temperatures occur at lower topographic elevations. The higher topographic elevations are characterised by moist semi-deciduous forest with high amount of rainfall as mentioned in Subsection 2.2. This may have contributed to the lower temperatures at higher elevations. **Figure 4**

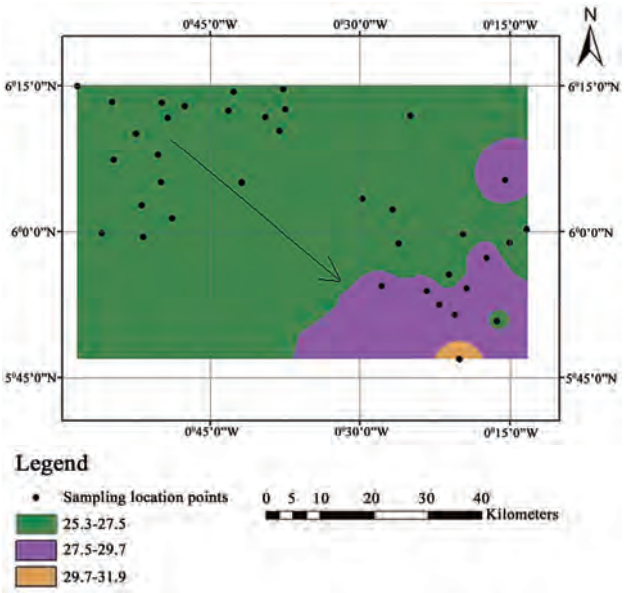

Figure 4. Spatial distribution of temperature in the study area.

shows the temperature distribution pattern in the area. The arrow points to the region of higher temperature where aquifers of the Cape Coast granitoid occur. In this region the climatic condition changes slightly to the savanna grassland with drier conditions. This may have led to the higher temperatures in the lower topographic elevation. Temperature influences dissolved mineral constituents in groundwater.

At higher temperatures groundwater dissolve more minerals resulting in elevated TDS and consequently conductivity. The higher topographic elevations which correspond to lower temperatures also correspond to lower TDS and conductivities thus describing a recharge area. The lower topographic areas of higher temperatures also correspond to higher TDS and conductivities describing a discharge area. The flow path is thus indicated in **Figure 4**. Temperature and pH influence dissolution and precipitation of minerals in groundwater. In general water with low pH (<6.5) could be acidic and corrosive. Acidic waters could leach metal ions such as: iron, manganese, copper, lead, and zinc from the aquifer. The pH of the groundwater in the lower Birimian rocks are generally lower than 6.5. It ranges from 3.0 to 6.3, showing strongly acidic to slightly acidic conditions. The acidic nature of the waters could trigger various chemical reactions in the groundwater.

Conductivity values from 55 to 1999 µS/cm were also recorded while TDS ranged from 31.9 to 968.3 mg/l. Detail hydrochemical data is presented in Appendices 1a and 1b.

The groundwater samples from the two main geological formations were plotted on the Piper 1944 Trillinear diagram to identify the chemical facies in the various aquifers in these geological terrains. The Cape Coast granitoid complex revealed five major water types (**Figure 5**). These are calcium magnesium bicarbonate ($CaMgHCO_3$), sodium bicarbonate ($NaHCO_3$), mixed water type (water type in which none of the ions is dominant), calcium chloride ($CaCl_2$) and sodium chloride (NaCl). From the plots of hydrochemistry (**Figure 5**), $CaCl_2$ and NaCl are the dominant water types in this geological terrain. The source of these water types is usually attributed to seawater intrusion for aquifers located along the coast [10]. However, the area under investigation is located in the forest zone where total annual rainfall varies from 1206 mm to 1487 mm. The granitoids weather to form thick layers composed of clay. Cation exchange reactions are therefore suspected from clay minerals and might be responsible for these NaCl and $CaCl_2$ water types. The source of Cl^- in the groundwater could also be from infiltrating rainwater and carried to the groundwater zone. It is also possible that halite from previous aerosols may have concentrated NaCl in the soil zone. This is possible in the tropical zone with rainfall events followed by prolonged dry seasons during which period; it is possible to precipitate halite in the soil.

Table 1. Statistical summary of hydrochemical data in the Cape Coast granitoid complex.

Parameter	Minimum	Maximum	Mean	Standard Deviation
pH	4.2	7.2	6.1	0.8
Temp	25.3	31.9	27.4	1.5
Conductivity	365	1999	791.1	445.9
Na+	14.2	251.6	66.3	52.8
K+	1.4	49.0	5.8	10.9
Mg2+	5.4	38.7	15.9	9.0
Ca2+	12.6	234.2	43.5	50.6
Cl-	9.3	144.6	72.9	41.1
SO42-	6.9	508.3	61.3	115.3
HCO3-	34.2	523.4	162.9	120.0
TDS	97.2	968.3	61.3	201.4

pH in pH-units, Temperature in °C, Conductivity in µS/cm, Na^+ to TDS in mg/l

Table 2. Statistical summary of hydrochemical data in the Lower Birimian aquifers.

Parameter	Minimum	Maximum	Mean	Standard Deviation
pH	3.0	6.3	4.1	1.0
Temperature	25.4	27.2	26.4	0.5
Conductivity	55.0	439.0	209.2	124.3
Na^+	3.2	19.4	10.3	5.0
K^+	0.1	4.5	1.1	0.9
Mg^{2+}	0.6	11.5	4.5	3.3
Ca^{2+}	2.1	28.8	10	7.4
Cl^-	2.2	28.5	9.5	8.6
SO_4^{2-}	0.1	20.1	3.1	6.2
HCO_3^-	32.9	184.2	76.3	44.7
TDS	31.9	180.2	81.8	42.9

pH in pH-units, Temperature in °C, Conductivity in µS/cm, Na^+ to TDS in mg/l

The other possible source of Cl^- may be from fluid inclusions in the granitic gneiss rock, which are characteristic of minerals of basement rocks [11]. **Figure 6** shows that $CaMgHCO_3$, mixed water types, NaCl and $CaCl_2$ waters occur in the granitic gneiss. The mineralogical composition of this rock type is 60 % plagioclase, 10 % microcline, 25 % quartz and 5 % biotite [4].

The higher concentration of Ca^{2+} and Na^+ in the groundwaters may therefore be due to the dissolution of plagioclase feldspars. HCO_3^- may have been generated in the soil zone en route to the groundwater zone as a result of decomposition of organic matter, which releases carbon dioxide that reacts with water in the soil zone. The reaction generates weak carbonic acid (H_2CO_3) that aids the breakdown of minerals in the rocks resulting in the release of the cations responsible for the various hydrochemical facies. Mixed water types also occur in the granodioritic gneiss and granite. Biotite granite contains NaCl water.

Two major water types are identified from the aquifers of the Lower Birimian. They include calcium–magnesium –bicarbonate and mixed water types. Phyllite, argillite, tuff and schist aquifers contain calcium–magnesium–bicarbonate water type (**Figure 7**). The occurrence of this water type in these aquifers may be due to the mineralogical composition of the rocks. The common minerals in these rocks are the calcic-plagioclase feldspars, hornblende, biotite, pyroxenes and olivine. The breakdown of the calcic-plagioclase feldspars and pyroxenes may be responsible for calcium in this water type, whereas hornblende, pyroxenes and olivine may be responsible for the magnesium in the water.

Very few samples from phyllite aquifers exhibit mixed water types.

4.2. Stable Isotopes

Analyses of stable isotopes were carried out on the sampled groundwater. The $\delta^{18}O$ values range from –2.2 ‰ to –3.4 ‰. The mean is –2.7 ‰ with a standard deviation of 0.4 ‰. The δ^2H ranges from -6 ‰ to -17 ‰. The mean is -11 ‰ with a standard deviation of 3 ‰. The negative values of Oxygen-18 and deuterium are indicative of depletion of oxygen-18 and deuterium relative to the Vienna Standard Mean Ocean Water (VSMOW). The isotopic data is presented in Appendix 2. A plot of δ^2H ‰VSMOW against $\delta^{18}O$ ‰VSMOW of the analysed samples is shown in **Figure 8**. Results of the oxygen-18 and deuterium analyses are found to cluster around the Global Meteoric Water Line (GMWL) given by the equation $\delta^2H = 8\ \delta^{18}O + 10$ [12]. The groundwater in the study area is therefore derived from rainfall. **Figures 9** and **10** show the spatial distributions of oxygen-18 and deuterium in the study area with sampling points.

5. Conclusions

The hydrochemical facies in the groundwaters in the Eastern Region of Ghana are Ca-Mg-HCO_3, $NaHCO_3$, NaCl, $CaCl_2$ and mixed water types. With respect to the underlying geological formations in the area, the major water types in the Cape Coast granitoid complex are Ca-Mg-HCO_3, $NaHCO_3$, NaCl and $CaCl_2$ and mixed water types. The most predominant water types in the

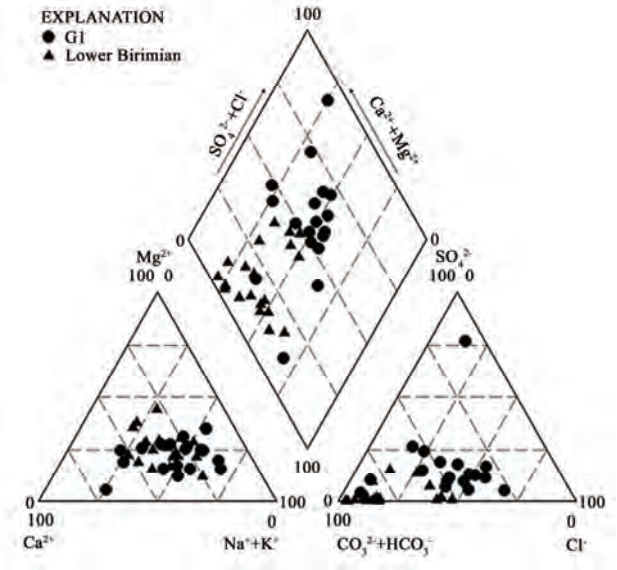

Figure 5. Trilinear piper diagram showing the chemical character of groundwater in the Cape Coast granitoid (G1) and Lower Birimian.

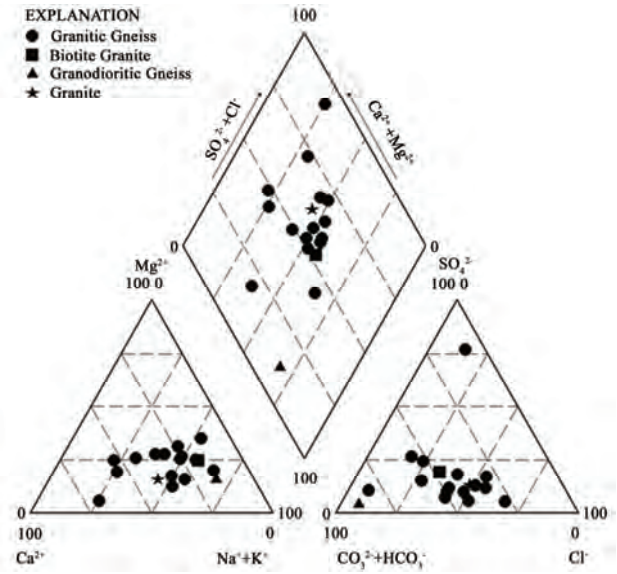

Figure 6. Trilinear piper diagram showing the hydrochemical facies in the various rock types in the Cape Coast granitoid complex.

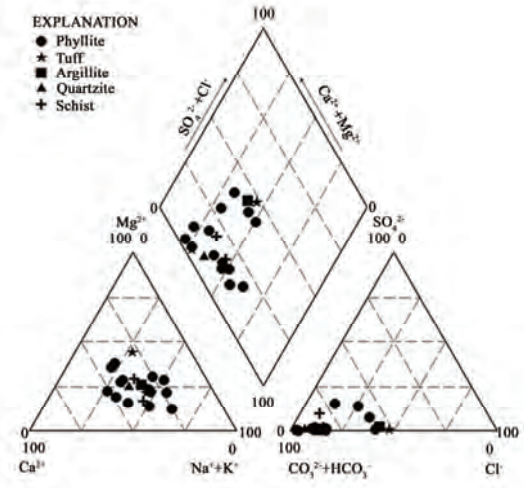

Figure 7. Trilinear piper diagram showing the hydrochemical facies in some of the rock types in the Lower Birimian.

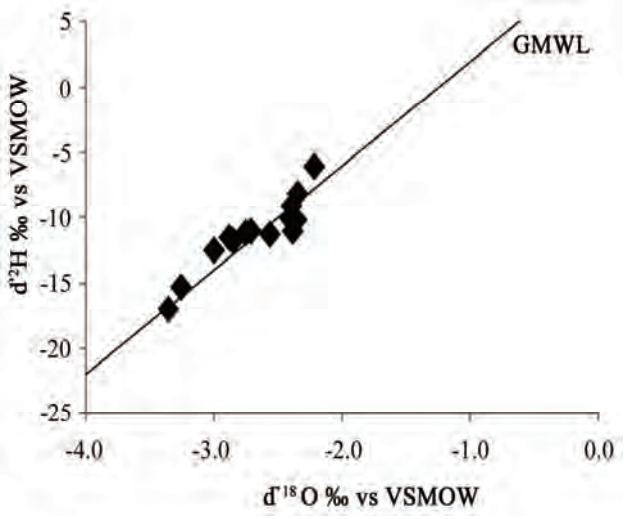

Figure 8. Stable isotopes of Eastern Region groundwaters.

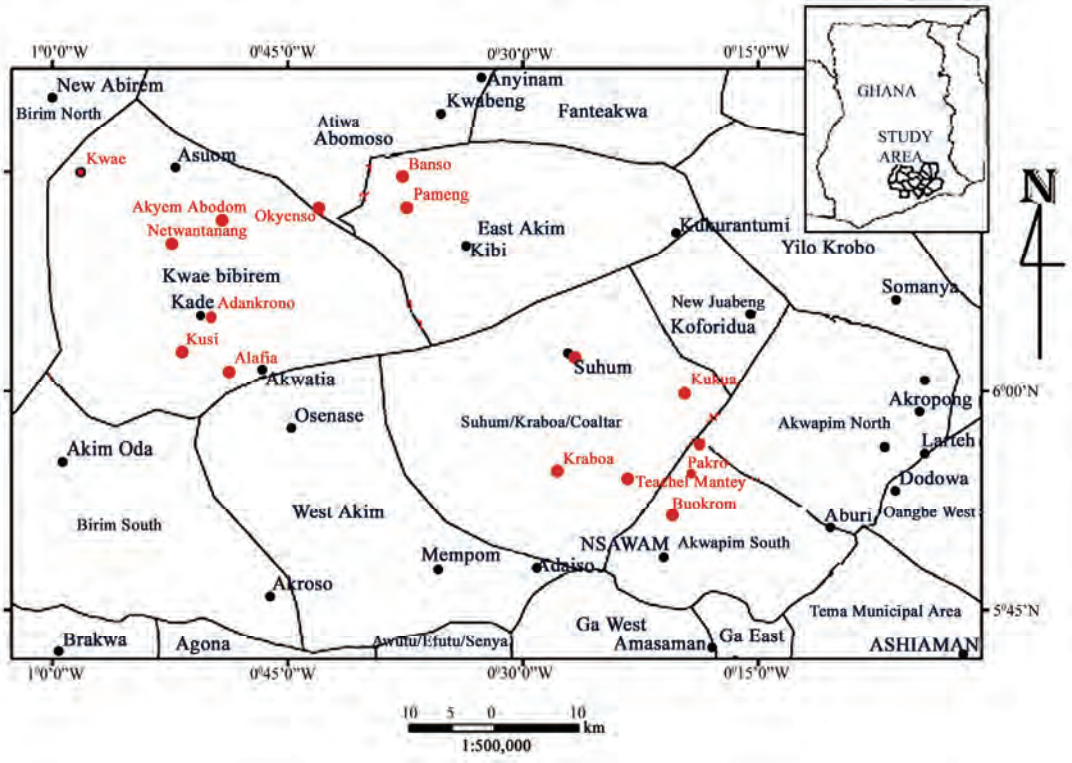

Figure 9. Sampling points for stable isotopes in the study area (highlighted in red).

Cape Coats granitoid are NaCl and $CaCl_2$ waters. The major facies in the Lower Birimian aquifers are Ca-Mg-HCO_3, and mixed water types. The geochemical processes that might be governing the presence of the various ions in solution include dissolution of minerals in the rock. A plot of δ^2H ‰VSMOW against $\delta^{18}O$ ‰VSMOW established the groundwater recharge to be from rainfall.

6. Acknowledgements

The authors gratefully acknowledge Danida-Enreca Hydrogeological Project for financial and logistical support. We thank technicians of the Ecological Laboratory of the University of Ghana, Legon, for their assistance during the chemical analysis of water samples.

7. References

[1] G. O. Kesse, "The mineral and rock resources of Ghana," Rotterdam, 1985.

[2] J. A. Akudago, K. Kankam-Yeboah, L. P. Chegbeleh, and M. Nashigaki, "Assesment of well design and sustainability in hard rock formations in northern Ghana," Hydrogeology Journal, Vol. 15, pp. 789–798, December 2006.

[3] C. Guler, G. D. Thyne, J. E. McCray, and A. K. Turner, "Evaluation of graphical and multivariate statistical methods for classification of water chemistry data," Hydrogeology Journal, Vol. 10, pp. 455–473, May 2002.

[4] S. M. Ahmed, P. K. Blay, S. B. Castor, and G. J. Coakley, "Geology of (¼)° field sheets Nos. 33 Winneba NE 59, 61, and 62 Accra SW, NW and NE," Ghana Geological Survey Bulletin, No. 32, 1997.

[5] S. S. Trashliev, "The Geology of ¼ field sheets 82 (Wiawso SE) and 46 (Asankragwa NE)," Unpublished Report of Ghana Geological Survey, 1974.

[6] B. Banoeng-Yakubo, "Occurrence of groundwater in basement complex rocks of the Upper Regions of Ghana," M.Sc. dissertation, Obefemi-Awolowo University, Geology Department, Nigeria, 1989.

[7] B. K. Banoeng-Yakubo, "The application of remote sensing and geographical information systems to hydrogeological studies in the upper west region, Ghana," Unpublished Ph.D. Thesis, University of Ghana, Legon, June 2000.

[8] S. N. Davis and L. J. Turk, "Optimum depth of wells in crystalline rocks, Groundwater," Vol. 2, No. 2, pp. 6–11, 1964.

[9] R. A. Freeze and J. A. Cherry, "Groundwater," Prentice Hall, Englewood Cliffs, NJ, USA, 1979.

[10] B. K. Kortatsi, "Hydrochemical characterization of groundwater in the Accra plains of Ghana," Environmental Geology, Vol. 50, pp. 299–311, April 2006.

[11] G. Faure, "Principles and applications of inorganic geochemistry," Prentice Hall, 1991.

[12] H. Craig, "Isotopic variations in meteoric waters," Science, Vol. 133, No. 3465, pp. 1702–1703, May 1961.

Appendix 1a. **Hydrochemical data in the Cape Coast granitoid complex aquifers.**

Community	Station	Field Borehole I.D.	Date of sampling	Depth (m)	Yield (l/min)	S.W.L (m)	pH	Temp (°C)	Cond (µs/cm)	TDS (mg/l)
Boukrom	1	BU	24-01-03	34	15	5.10	6.6	28.4	755	376.0
Aheriso	2	AH	24-01-03	40	12	1.40	6.4	27.3	765	396.4
Pakro	3	PA	24-01-03	28	50	1.87	6.6	27.9	1264	564.2
New Mangoase	4	NM	24-01-03	22	150	2.38	6.3	28.6	1084	534.9
Nkwantanang	5	NK	24-01-03				6.4	26.3	570	243.5
Kukua	6	KU	24-01-03	33	50		7.2	26.7	1582	968.3
Governorkrom No.1	7	GK	24-01-03				7.0	26.6	1999	640.6
Dobro (hand-dug well)	8	DO	21-02-03	6	6	3.30	6.4	31.9	436	235.8
Teacher Mantey	9	TM	21-02-03				6.3	27.8	955	465.6
Panpanso No.1	10	PP	21-02-03				6.5	28.0	549	297.2
Konkonnuru	11	KK	21-02-03	37	50	0	6.8	25.9	903	446
Kraboa	12	KB	21-02-03				6.6	27.8	597	335.1
Suhum Hospital	13	SU	22-02-03				5.5	27.0	406	233.6
Aponapono	14	AP	22-02-03				6	25.3	365	97.15
Koforidua Betom	15	KB	22-02-03				5.8	28.4	443	223.9
Asempaneye	16	AS	23-02-03				5.8	26.6	580	312.7
Kwae	17	KW	25-02-03	37	50	3.82	4.4	26.1	484	259.8
Maase	18	MA	26-02-03	28	40	2.20	4.2	26.7	502	267.8

Appendix 1a continued.

Community	Station	Field Borehole I.D.	Na^+ **(mg/l)**	K^+ (mg/l)	Mg^{2+} (mg/l)	Ca^{2+} (mg/l)	Cl^- (mg/l)	SO_4^{2-} (mg/l)	HCO_3^- (mg/l)	CBE
Boukrom	1	BU	83.5	2.8	29.5	16.9	110.7	55.0	142.5	3
Aheriso	2	AH	79.9	4.3	22.2	36.9	104.2	39.5	207.4	1
Pakro	3	PA	66.6	1.4	15.3	19.0	63.5	1.94	213.1	-2
New Mangoase	4	NM	103	6.5	38.7	48.9	172.5	85.9	196.8	2
Nkwantanang	5	NK	70.5	1.5	16.8	21.1	69.6	52.2	118.4	5
Kukua	6	KU	99.3	2.6	11.8	234	98.6	540.3	110.2	4
Governorkrom No.1	7	GK	252	2.0	30.3	50.1	85.97	98.2	625	4
Dobro (hand-dug well)	8	DO	35.8	7.4	15.2	31.7	13.5	22.1	203.3	5
Teacher Mantey	9	TM	57.4	3.4	16.7	25.3	120.9	29.0	97.2	-3
Panpanso No.1	10	PP	64.3	1.6	10.2	12.6	47.1	31.3	168.4	-5
Konkonnuru	11	KK	46.0	3.6	18.1	86.1	52.2	102.6	272.1	-1
Kraboa	12	KB	42.5	49	8.9	41.7	76.2	36.5	154.3	4
Suhum Hospital	13	SU	45.2	2.7	6.9	20.8	54.6	18.7	84.2	5
Aponapono	14	AP	14.2	2.4	9.0	32.3	31.9	43.0	73	1
Koforidua Betom	15	KB	31.3	2.8	11.5	21.3	57.3	4.8	123.2	-4
Asempaneye	16	AS	54.8	4.4	10.4	33.4	104.9	15.2	146.4	-6
Kwae	17	KW	28.0	2.4	5.4	22.7	56.2	18.02	75.2	-5
Maase	18	MA	19.9	4.3	9.8	27.7	67.8	11.4	50.9	-3

Appendix 1b. **Hydrochemical data in the Lower Birimian.**

Community	Station	Field Borehole I.D.	Date of Sampling	Depth (m)	Yield (m^3)	S.W.L. (l/min)	pH	Temp (°C)	Cond (µs/m)	TDS (mg/l)
Apinamang	19	AP1	24-05-03	46	50	3.45	4	26.8	167	68.36
Apinamang	20	AP2	24-05-03	45	100	5.53	3	26.6	294	146
Alafia	21	AL	24-05-03	46	36	7.25	3	26.7	439	135.8
Anweaso	22	AN	24-05-03	39	120	2.55	6	27.2	364	70.68
Wenchi Sec. Sch.	23	WE	24-05-03				4	26.7	214	117.8
Kusi	24	KU	24-05-03				4	27	127	40.53
Okumaning	25	OK	24-05-03	41	150	9.1	6	26.2	116	53.38
Subi	26	SB	24-05-03				4	25.7	55	31.94
Nkwantanang	27	NK	24-05-03	43	200	1.86	4	26.2	91	49.62
Otumi	28	OT	24-05-03	55	60	1.5	5	25.4	273	98.37
Adankrono	29	AD	25-05-03	31	60	2.49	4	27.1	170	82.67
Akyem Abodom	30	AA	25-05-03	52	120	2.76	3	26.4	120	67.29
Abaam	31	AB	25-05-03				4	25.6	239	99.99
Okyenso	32	OS	25-05-03	51	360	12.46	5	25.9	335	127.9
Kwaman	33	KW	25-05-03	43	8	10.3	3	26.6	58	35.37
Akim Akropong	34	AK	25-05-03	31	20	1.63	6	26.2	330	180.2
Gyamase	35	GY	25-05-03				3	26.8	435	34.54
Pameng	36	PA	25-05-03	48	200	8	3	26.5	63	44.68
Banso	37	BA	25-05-03	32	60	2.26	4	26.6	205	105.2
Akim Dompim	38	AM	25-05-03	43	40	7.78	3	25.8	89	44.8

Appendix 1b continued.

Community	Station	Field Borehole I.D.	Na^+ (mg/l)	K^+ (mg/l)	Mg^{2+} (mg/l)	Ca^{2+} (mg/l)	Cl^- (mg/l)	SO_4^{2-} (mg/l)	HCO_3^- (mg/l)	CBE
Apinamang	19	AP1	15.1	1.26	4.7	5.6	15.4	4.41	43.92	4
Apinamang	20	AP2	17.2	1.61	8.7	21.8	13.3	19.4	113.5	-1
Alafia	21	AL	14.6	0.85	7.4	17.2	3.2	10.2	124	-5
Anweaso	22	AN	9.18	1.63	9.1	15.7	11.8	11.2	74.5	5
Wenchi Sec. Sch.	23	WE	19	0.93	7.1	9.7	27.2	0.75	67.1	1
Kusi	24	KU	6.89	0.82	1.5	2.64	0.4	4.5	31.5	-4
Okumaning	25	OK	7.63	0.93	2	5.11	12.2	3.7	24.3	-3
Subi	26	SUB	5.58	0.95	0.6	2.13	1.3	3.3	19.9	-1
Nkwantanang	27	NK	8.22	0.76	2.3	5.06	3.6	1.4	44.5	-2
Otumi	28	OT	9.8	0.83	4.5	17.2	1	5.4	101.6	-4
Adankrono	29	AD	7.93	0.8	2.8	5.85	13.2	3.4	33.4	-5
Akyem Abodom	30	AA	8.1	0.73	3.1	8.26	0.7	5.4	59.5	-3
Abaam	31	AB	13	0.99	11	12.3	2.17	0.19	117.1	4
Okyenso	32	OS	7.94	1.29	7.6	14.9	10.8	18.8	74.9	-5
Kwaman	33	KW	4.99	0.65	0.8	3.22	1.6	2.1	24.5	-3
Akim Akropong	34	AK	19.4	4.52	6.8	28.8	28.5	20.6	113.5	-2
Gyamase	35	GY	3.15	0.76	0.7	3.49	0.5	4.7	18.2	-2
Pameng	36	PA	5.12	0.09	1	3.51	2	1.5	26.4	-4
Banso	37	BA	15.7	1.07	7	13.7	7.09	9.5	101.3	-2
Akim Dompim	38	AM	6.72	1	1.8	4.05	0.6	2.6	40.9	-5

Appendix 2. Stable isotopes data.

Community	Sample I.D.	$\delta^{18}O$	$\delta^{2}H$
Pakro	PA	-2.8	-11.0
Boukrom	BU	-2.4	-11.0
Kukua	KU	-2.6	-11.0
Alafia	AL	-2.9	-12.0
Teacher Mantey	TM	-2.4	10.0
Kraboa	KB	-2.9	-12.0
Kusi	KS	-2.4	-10.0
Kwae	KW	-2.4	-8.0
Nkwantanang	NK	-2.7	-11.0
Akyem Abodom	AA	-2.4	-9.0
Adankrono	AD	-3.3	15.0
Banso	BA	-2.2	-6.0
Okyenso	OS	-3.4	-17.0
Pameng	PA	-3.0	-13.0

J. Water Resource and Protection, **2010, 2, 209-213**
doi:10.4236/jwarp.2010.23023 Published Online February 2010 (http://www.scirp.org/journal/jwarp)

Trivalent Mn and Fe Complexes for the Degradation of Remazol Dyes

Siguara Bastos de Lemos e Silva, Anderson Arndt, Breno Pannia Espósito
Instituto de Química, Universidade de São Paulo,
Av Lineu Prestes, São Paulo, Brazil
E-mail: *breno@iq.usp.br*
Received December 31, 2009; *revised January* 20, 2010; *accepted January* 20, 2010

Abstract

Water contamination by Remazol® dyes can be remediated with the use of bleaching metal complexes. In this study, a series of Mn(III) complexes and ferric nitrilotriacetate were found to be useful in the degradation of Remazol Blue, Remazol Turquoise and Remazol Brilliant Blue. The effect of peroxide, pH, time and irradiation on the bleaching of the dyes was studied. Mn(III)-salen complexes were effective in the degradation of the diazo Remazol Blue dye in the presence of a 2-fold excess of hydrogen peroxide. This dye was also effectively bleached by a combination of hydrogen peroxide, ferric nitrilotriacetate and light irradiation. This is the first time well-defined, low molecular weight trivalent metal complexes are applied to the degradation of Remazol® dyes.

Keywords: Manganese, Iron, Remazol Dye

1. Introduction

Water contamination by remnants of organic dyes in the effluents of textile plants is of great environmental concern due to the potentially toxic effects of relatively small amounts of these compounds [1].

Vinyl sulfone (Remazol®) reactive dyes are among the pollutants whose presence in aqueous systems is undesirable. Thus, a number of physical and biological detoxification methods have been devised [2]. The use of oxidant metal species for the treatment of organic contamination is an example of chemically-assisted detoxification methods. A common strategy is to take advantage of the *in situ* generation of hydroxyl radicals through the reaction between Fe(II) species and peroxide (Fenton reaction, Equation 1) or, provided that a chromophoric metal complex is available, through a combination of UV irradiation, Fe(III) species and peroxide (Photo-Fenton reaction, Equation 2) [3].

$$Fe^{2+} + H_2O_2 \rightarrow Fe^{3+} + {}^{\bullet}OH + OH^- \quad (1)$$

$$Fe^{3+} + H_2O \rightarrow Fe(OH)^{2+} + H^+$$
$$Fe(OH)^{2+} + h\nu \rightarrow Fe^{2+} + {}^{\bullet}OH \quad (2)$$

Other high valence, oxidant metal complexes which may or may not generate reactive oxygen species in the environment may also be of use. Manganese (Mn) is a constitutive element of a number of redox-active enzymes involved in the detoxification of highly reactive oxygen species and in electron-transfer processes [4] in organisms. This catalytic role underlines the use of fungal and/or bacterial Mn-enzymes in the bioremediation of organic wastes, including dyes, such as peroxidases [5, 6] or laccases [7,8]. Also, simple Mn salts [9,10], complexes [11] or oxides [12] have been successfully applied to water remediation after dye contamination.

Mn(III) complexes have been proposed as mimetics of antioxidant enzymes such as catalase [13] and superoxide dismutase [14]. However, it is also well established that Mn(III) species are strong oxidants *per se*, leading to their use in organic catalysis [15]. Mn(III)-citrate is believed to be the main Mn species to assess the brain in humans [16], leading to a cascade of redox-active-based neurotoxic events. In combination with certain proportions of hydrogen peroxide, Mn(III) enzyme mimetics may oxidize redox-sensitive fluorescent probes [17]. Therefore, high-valence Mn complexes have also found interesting applications in advanced oxidation of dyes in wastewater [18–20].

Herein, we report for the first time the use of one Fe(III) and a number of potential Mn(III) oxidant complexes in the degradation of Remazol® dyes, which may contribute to approaches such as whole enzyme and/or

organisms in pollutant degradation. The effects of reaction time, pH, H_2O_2 and irradiation were studied photometrically in 96-well microplates.

2. Materials and Methods

The metal complexes Mn(III)-desferrioxamine B (Mn-dfb [14]), Mn(III)-pyrophosphate (Mn-pyr [21]), Mn (III)-salen chloride (EUK 8) and acetate (EUK 108) [13] were prepared and characterized by previously published methods. Iron(III) nitrilotriacetate (Fe-nta) was prepared by the direct reaction of $Fe(NH_4)(SO_4)_2.6H_2O$ with a 3-fold mol excess of sodium nitrilotriacetate under air. $MnCl_2$ was used as a divalent Mn control. The Remazol® dyes were from Dystar (Suzano, Brazil) and used as aqueous solutions in deionized water. Absorbance measurements were performed in a FluoStar Optima photometer (BMG LabTech) at 595 nm. Absorbance values were corrected for the absorption of the metal complexes and normalized in relation to the complex-untreated controls. The time of reaction between the dyes and the metal complexes was 1 h (dark; room temperature) unless otherwise noted. When required, irradiation was performed with an 8 W (12") Aqua-Glo fluorescent tube. Assays were performed in duplicate.

3. Results and Discussion

In order to determine the influence of peroxide to achieve maximum bleaching, experiments were undertaken at [dye] = 40 μM (**Figure 1**). In the absence of H_2O_2 (**Figure 1(a)**), the dyes underwent considerable bleaching induced by all the metal species (specially phthalocyanine RT and anthraquinone RBB), an effect which may be related either to the presence of O_2 in the solvents used, which can generate reactive species in the presence of metal species [22] or to the direct attack of the metal species on the dyes. This effect stabilizes at dye:complex mol ratios of *ca.* 1. The diazo dye RB is more clearly affected by higher complex concentrations (see in continuation).

Hydrogen peroxide alone did not cause any dye bleaching under the test conditions for up to a 5-fold molar excess in relation to the dye (data not shown). No improved bleaching for RT was found which could be attributed to the effect of peroxide (**Figure 1(b)**), indicating that none of the complexes studied would require peroxide to bleach this dye. However, the salen complexes EUK 8 and EUK 108 displayed considerable bleaching power towards the diazo dye RB and, to a lesser extent, to RBB in a ~ 2:1 H_2O_2:metal complex mol ratio, which is in agreement with previous studies on oxidizable fluorescent probes [17]. In both complexes, Mn(III) lies in a planar environment with a free axial coordination position available for the reaction with per-

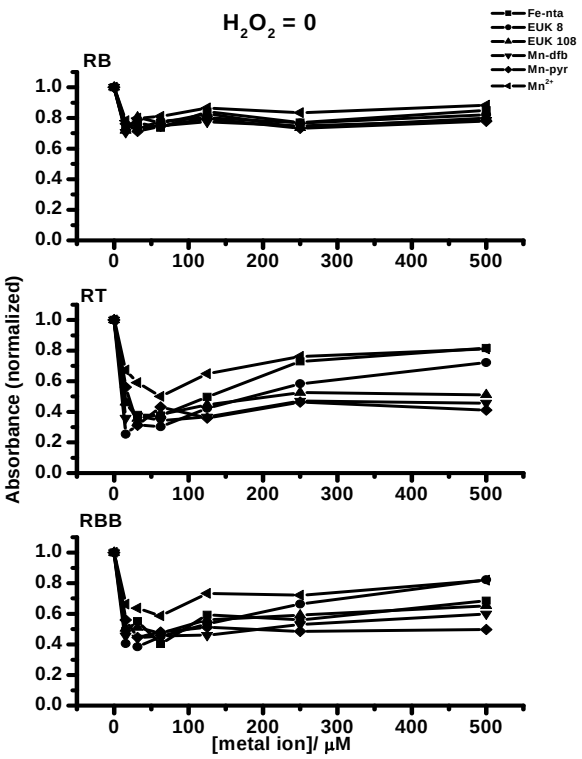

(a)

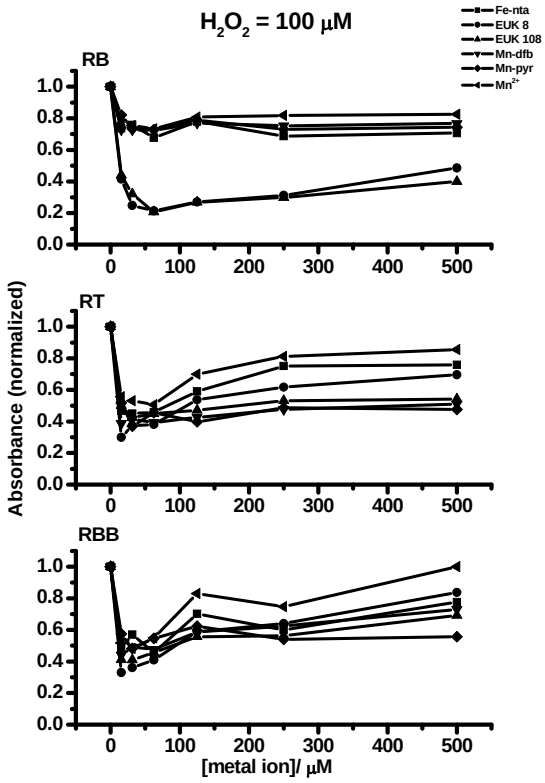

(b)

Figure 1. Effect of H_2O_2 on the bleaching induced by the metal complexes ([dye] = 40 μM).

oxide (for a detailed mechanism, see [13]). Under oxidation to Mn(V), the metal center might reasonably attack the electron-rich azo moiety, as observed in other instances of electrophilic attack [23].

In general terms, no marked trend in the effect of pH on the bleaching activity of the complexes was observed (**Figure 2**), except for RB/H_2O_2 at neutral pH values for the salen complexes EUK 8 and EUK 108, where maximum decolorization was attained. This is to be expected since the ability of salen ligands to form Mn complexes is pH-dependent, and is greatest at close to neutral pH [24]. A high proton concentration may result in reprotonation of the salen ligand, whereas alkaline conditions promote metal hydrolysis.

The effect of reaction time and dye:complex ratios were investigated for EUK 8, due to its good decolorization properties (**Figure 3**). Hydrogen peroxide was not added since it would decompose during the initial time periods investigated. Maximum bleaching was observed at *ca.* 1-2 h of incubation for RB, but was attained considerably later for the other dyes, especially at high dye concentration. Long-term expositions resulted in more efficient bleaching when dye:complex ratios are low.

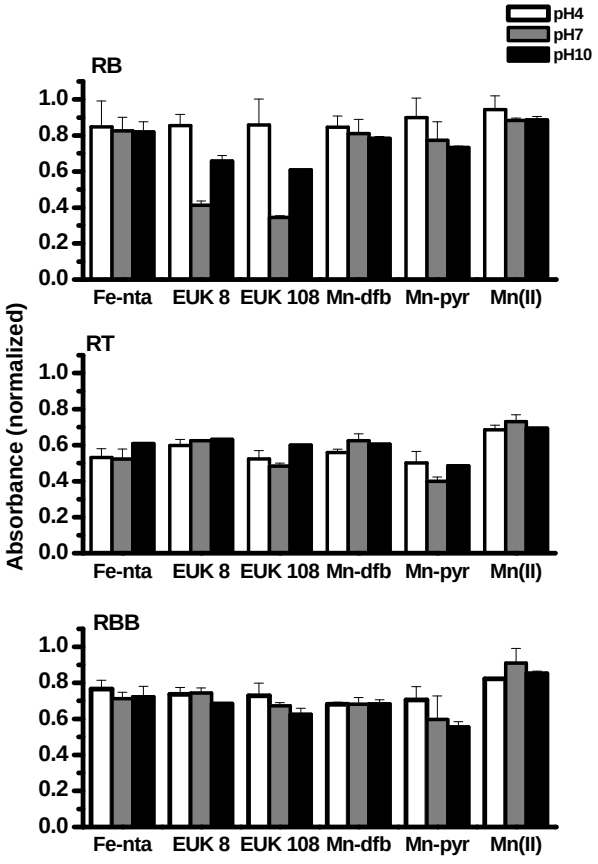

Figure 2. Effect of pH on the bleaching induced by the metal complexes ([metal complex]= 50 μM, [dye] = 40 μM; for RB: [H_2O_2]= 100 μM).

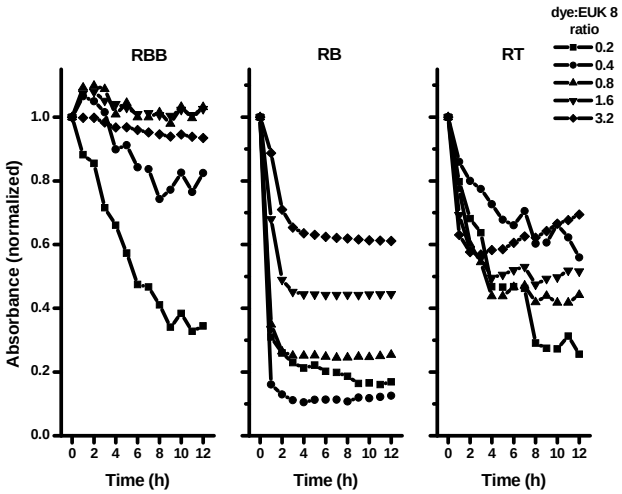

Figure 3. Effect of reaction time and dye concentration on the performance of 50 μM EUK 8.

Ferric nitrilotriacetate (Fe-nta) is an inexpensive, stable, easily obtained Fe(III) chromophoric complex that can be useful in photo-Fenton oxidative processes. There were no previous reports on the use of this complex for the remediation of dye contaminated water. Fe-nta is reduced by light to the ferrous derivative which, in aqueous aerated solution, may form reactive oxygen species [22] via a photo-Fenton process, as shown in Equation 2. In the presence of hydrogen peroxide, the divalent Fe species may undergo further generation of free radicals via the Fenton mechanism (Equation 1), indicating that a synergism exists between light and H_2O_2 in this situation. We observed this effect when comparing the effect of time and irradiation on the bleaching of RB induced by Fe-nta (**Figure 4**). In the absence of light, reactive species, if formed, do not seem to be able to degrade this dye. However, irradiation increased significantly RB bleaching in the presence of H_2O_2:Fe-nta in a *ca.* 1:1 mol ratio. To the best of our knowledge, this is the first report of the use of ferric nitrilotriacetate for degradation of a dye. We did not find evidence of irradiation-increased bleaching promoted by the Mn(III) complexes, indicating that the active Mn(III) complexes should act by either the formation of reactive oxygen species from saturation O_2 in water or, when peroxide is available, via formation of highly reactive Mn(V) species.

4. Conclusions

Trivalent metal complexes are interesting candidates for the degradation of Remazol® dyes in neutral aqueous medium. Mn(III)-salen complexes are most effective in the degradation of the diazo RB when in the presence of a *ca.* 2-fold molar excess of hydrogen peroxide. This dye is also prone to degradation via a photo-Fenton process under Fe-nta.

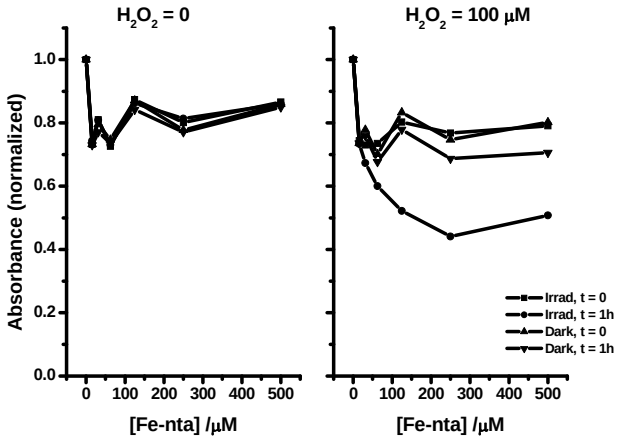

Figure 4. Effect of time and irradiation on the bleaching of 40 μM RB promoted by Fe-nta.

5. Acknowledgments

Authors are thankful for funding from the Brazilian agencies CNPq and FAPESP. Dye samples were kindly donated by Prof. Renato Freire.

6. References

[1] C. I. Pearce, J. R. Lloyd, and J. T. Guthrie, "The removal of colour from textile wastewater using whole bacterial cells: A review," Dyes and Pigments, Vol. 58, No. 3, pp. 179–196, 2003.

[2] Z. Aksu, "Application of biosorption for the removal of organic pollutants: A review," Process Biochemistry, Vol. 40, No. 3–4, pp. 997–1026, 2005.

[3] P. Bautista, A. F. Mohedano, J. A. Casas, J. A. Zazo, and J. J. Rodriguez, "An overview of the application of Fenton oxidation to industrial wastewaters treatment," Journal of Chemical Technology and Biotechnology, Vol. 83, No. 10, pp. 1323–1338, 2008.

[4] B. Halliwell and J. Gutteridge, "Free radicals in biology and medicine," Oxford University Press, 2007.

[5] M. Shakeri and M. Shoda, "Change in turnover capacity of crude recombinant dye-decolorizing peroxidase (rDyP) in batch and fed-batch decolorization of Remazol Brilliant Blue R," Applied Microbiology and Biotechnology, Vol. 76, No. 4, pp. 919–926, 2007.

[6] M. Shakeri, Y. Sugano, and M. Shoda, "Stable repeated-batch production of recombinant dye-decolorizing peroxidase (rDyP) from Aspergillus oryzae," Journal of Bioscience and Bioengineering, Vol. 105, No. 6, pp. 683–686, 2008.

[7] P. P. Champagne and J. A. Ramsay, "Contribution of manganese peroxidase and laccase to dye decoloration by Trametes versicolor," Applied Microbiology and Biotechnology, Vol. 69, No. 3, pp. 276–285, 2005.

[8] K. Svobodova, A. Majcherczyk, C. Novotny, and U. Kues, "Implication of mycelium-associated laccase from *Irpex lacteus* in the decolorization of synthetic dyes," Bioresource Technology, Vol. 99, No. 3, pp. 463–471, 2008.

[9] K. Pachhade, S. Sandhya, and K. Swaminathan, "Ozonation of reactive dye, procion red MX-5B catalyzed by metal ions," Journal of Hazardous Materials, Vol. 167, No. 1–3, pp. 313–318, 2009.

[10] E. Ember, S. Rothbart, R. Puchta R, and R. van Eldik, "Metal ion-catalyzed oxidative degradation of orange II by H_2O_2 high catalytic activity of simple manganese salts," New Journal of Chemistry, Vol. 33, No. 1, pp. 34–49, 2009.

[11] G. B. Shul'pin, Y. N. Kozlov, S. N. Kholuiskaya, and M. I. Plieva, "Oxidations by the system 'hydrogen peroxide–$[Mn_2L_2O_3]^{(2+)}$ (L=1,4,7-trimethyl-1,4,7-triazacyclononane)-oxalic acid' Part 11. Degradation of dye Rhodamine 6G and oxygenation of cyclohexene," Journal of Molecular Catalysis A-Chemical, Vol. 299, No. 1–2, pp. 77–87, 2009.

[12] A. N. Chowdhury, M. S. Azam, M. Aktaruzzaman, and A. Rahim, "Oxidative and antibacterial activity of Mn_3O_4," Journal of Hazardous Materials, Vol. 172, No. 2–3, pp. 1229–1235, 2009.

[13] S. R. Doctrow, K. Huffman, C. B. Marcus, G. Tocco, E. Malfroy, C. A. Adinolfi, H. Kruk, K. Baker, N. Lazarowych, J. Mascarenhas, and B. Malfroyt, "Salen-manganese complexes as catalytic scavengers of hydrogen peroxide and cytoprotective agents: Structure-activity relationship studies," Journal of Medicinal Chemistry, Vol. 45, No. 20, pp. 4549–4558, 2002.

[14] K. M. Faulkner, R. D. Stevens, and I. Fridovich, "Characterization of Mn(III) complexes of linear and cyclic desferrioxamines as mimics of superoxide-dismutase activity," Archives of Biochemistry and Biophysics, Vol. 310, No. 2, pp. 341–346, 1994.

[15] T. Katsuki, "Catalytic asymmetric oxidations using optically-active (salen)manganese(III) complexes as catalysts," Coordination Chemistry Reviews, Vol. 140, pp. 189–214, 1995.

[16] J. S. Crossgrove, D. D. Allen, B. L. Bukaveckas, S. S. Rhineheimer, and R. A. Yokel, "Manganese distribution across the blood-brain barrier: I. Evidence for carrier-mediated influx of manganese citrate as well as manganese and manganese transferring," Neurotoxicology, Vol. 24, No. 1, pp. 3–13, 2003.

[17] S. do Amaral and B. P. Esposito, "Fluorimetric study of the pro-oxidant activity of EUK8 in the presence of hydrogen peroxide," Biometals, Vol. 21, No. 4, pp. 425–432, 2008.

[18] J. J. Dannacher, "Catalytic bleach: Most valuable applications for smart oxidation chemistry," Journal of Molecular Catalysis A-Chemical, Vol. 251, No. 1–2, pp. 159–176, 2006.

[19] T. Wieprecht, M. Hazenkamp, H. Rohwer, G. Schlingloff, and J. T. Xia, "Design and application of transition metal catalysts for laundry bleach," Comptes Rendus Chimie, Vol. 10, No. 4–5, pp. 326–340, 2007.

[20] P. Zucca, C. Vinci, F. Sollai, A. Rescigno, and E. Sanjust, "Degradation of alizarin red S under mild experimental

conditions by immobilized 5,10,15,20-tetrakis(4-sulfonatophenyl)porphine-Mn(III) as a biomimetic peroxidase-like catalyst," Journal of Molecular Catalysis A-Chemical, Vol. 288, No. 1–2, pp. 97–102, 2008.

[21] J. K. Klewicki and J. J. Morgan, "Kinetic behavior of Mn(III) complexes of pyrophosphate, EDTA, and citrate," Environmental Science & Technology, Vol. 32, No. 19, pp. 2916–2922, 1998.

[22] K. Tsuchiya, K. Akai, A. Tokumura, S. Abe, T. Tamaki, Y. Takiguchi, and K. Fukuzawa, "Oxygen radicals photoinduced by ferric nitrilotriacetate complex," Biochimica et Biophysica Acta-General Subjects, Vol. 1725, No. 1, pp. 111–119, 2005.

[23] A. Chellamani, P. Kulanthaipandi, and S. Rajagopal, "Oxidation of aryl methyl sulfoxides by oxo (salen) manganese(V) complexes and the reactivity-selectivity principle," Journal of Organic Chemistry, Vol. 64, No. 7, pp. 2232–2239, 1999.

[24] G. Tantaru, V. Dorneanu, and M. Stan "Schiff bis bases: Analytical reagents: II. Spectrophotometric determination of manganese from pharmaceutical forms," Journal of Pharmaceutical and Biomedical Analysis, Vol. 27, No. 5, pp. 827–832, 2002.

J. Water Resource and Protection, **2010, 2, 214-221**
doi:10.4236/jwarp.2010.23024 Published Online February 2010 (http://www.scirp.org/journal/jwarp)

Removal of Hydrophobic Organic Contaminants from Aqueous Solutions by Sorption onto Biodegradable Polyesters

Yukiko Matsuzawa[1], Zen-Ichiro Kimura[1], Yoshiro Nishimura[2], Mikio Shibayama[2], Akira Hiraishi[1*]
[1]*Department of Ecological Engineering, Toyohashi University of Technology, Toyohashi, Japan*
[2]*Mikawa Textile Research Institute, Aichi Prefecture, Gamagori, Japan*
E-mail: *hiraishi@eco.tut.ac.jp*
Received November 7, 2009; *revised November* 24, 2009; *accepted January* 21, 2010

Abstract

Sorption by biodegradable polyesters of several aromatic chemicals as model compounds for hydrophobic organic contaminants (HOCs) was studied. The biodegradable polyesters used were poly(butylene succinate), poly(3-hydroxybutyrate-*co*-3-hydroxyvalerate), poly(ε-caprolactone), poly(butylene succinate/ terephthalate), and poly(L-lactic acid). Petrochemical plastics, low-density polyethylene and polyethylene terephtalate, were used for comparison. The target HOCs were biphenyl, bisphenol-A, dibenzofuran, diethylstilbestrol, nonylphenol, and chlorophenols. The treatment of the HOC solutions with each of the biodegradable polyesters resulted in the nearly complete removal of the chemicals by sorption from the aqueous phase, except for the case of poly(L-lactic acid). Low-density polyethylene adsorbed biphenyl and dibenzofuran selectively, and polyethylene terephtalate did not adsorb any of the HOCs. The adsorptive interaction between the plastics and the HOCs might be related to both the glass transition temperature of the former and the nature of the latter as defined by the Fujita's inorganicity/organicity ratio. The toxic effect of 3,5-dichlorophenol on bacterial growth in liquid culture was removed by the addition of a biodegradable polyester. These results provide a basis for the applicability of the biodegradable plastics as the adsorbents for the removal of HOCs from aquatic environments.

Keywords: Aromatic Chemicals, Hydrophobic Organic Contaminants, Sorption, Biodegradable Polyester

1. Introduction

A wide variety of aromatic chemicals released from anthropogenic sources into the environment are recognized as harmful and persistent contaminants. Such hydrophobic organic contaminants (HOCs) are concentrated in biosystems through the food chain, thereby bringing about a potential threat of biotic environments [1]. Therefore, the problem of how to detoxify and remove HOCs in the environment is central to research in environmental science and technology. One of the most widely used approaches to this subject is the removal of HOCs using appropriate sorbents such as activated carbon, siliceous materials, zeolite, and synthetic resins [2]. In recent years, biopolymers and petrochemical plastics as the sorbents of HOCs have gained more attention. It has been shown that aromatic compounds are adsorbed by soil organic matter and biopolymers such as lignin, chitin, chitosan, and cellulose [2–5]. Plastic debris dispersed as persistent pollutants in marine ecosystems [6] have been reported to act as transporters of HOCs [7,8]. Aromatic compounds in foods and liquid media are adsorbed by polyethylene [9–11]. The sorption of aromatic compounds on polyethylene as a membrane material was studied [12]. HOCs from municipal wastewater treatment plant effluents could be removed by sorption onto polypropylene [13]. Although the mechanism of adsorptive interaction between plastics and HOCs has not yet been fully elucidated, the available information suggests that sorption technology using these polymers has great promise as a tool for HOC removal from the environment.

Biodegradable polyesters, which have attracted

much attention as alternatives of conventional plastic packages have physicochemical properties resembling petrochemical plastics [14,15]. It is therefore of special interest to investigate whether biodegradable polyesters as well as petrochemical plastics adsorb HOCs. To date, there has been no fundamental information about the adsorptive interaction between biodegradable polyesters and HOCs. In this study, we report that selected biodegradable polyesters are able to adsorb aromatic chemicals more effectively than selected petrochemical plastics. We discuss the applicability of biodegradable plastics as potent adsorbents for the removal of HOCs from aquatic environments. To our knowledge, this report is the first to demonstrate that biodegradable plastics are able to adsorb HOCs.

2. Materials and Methods

2.1. Chemicals

The aromatic chemicals used as model compounds for HOCs were biphenyl (BP), bisphenol-A (BPA), dibenzofuran (DF), diethylstilbestrol (DES), and nonylphenol (NP). Also, phenol and its chlorinated derivatives, 2-monochlorophenol (2-CP) and 3,5-dichlorophenol (3,5-DCP) were used. Among these chemicals, BPA, DES, and NP are suspected of being endocrine disruptors. Some congeners of chlorophenols are known to have inhibitory effects as uncouplers on energy metabolism in organisms [16,17]. All these chemicals were purchased from Wako Pure Chemical Industries (Osaka, Japan). The physicochemical characteristics of the HOCs as defined by the Fujita's inorganicity (*i*) and organicity (*o*) characters, which are based on the concept of van der Waals interaction and electronic affinity, respectively [18, 19], were determined using an Excel Macro program available at a web site (http://www.ecosci.jp/sheet/orgs_help.html).

2.2. Biodegradable Polyesters

Commercially available biodegradable polyesters were used as the sorbents. These polymer samples were poly(ε-caprolactone) (PCL) (Daicel Chemical Industries, Tokyo, Japan), poly(butylene succinate/terephthalate) (Ecoflex, EF) (BASF Japan Ltd., Tokyo, Japan), poly(butylene-succinate) (PBS) (Showa Highpolymer Co., Hyogo, Japan), poly(3-hydroxybutyrate-*co*-8%-3-hydroxyvalerate) (PHBV) (Japan Monsanto, Tokyo, Japan), and poly(L-lactic acid) (PLA) (Mitsui Chemicals, Inc., Tokyo, Japan). For comparison, low-density polyethylene (LDPE) (Mitsui Chemicals) and polyethylene terephtalate (PET) were used as representatives of conventional petrochemicals. For testing, fibers of the plastics were prepared by the melt-spinning method. The melt spinning machine was a 35 mm single screw extruder (L/D=28) provided with a spinning nozzle having 6 holes with a diameter of 1.0 mm. The melt extrusion temperature was 200 °C for all samples. The fibers were extruded into a cooling water bath at 45 °C for PLA and 20 °C for the others; the output was about 6 g min^{-1}. The take-up speed for the fiber was 7 m min^{-1}. The diameter of the fiber was set at 1 mm in all cases. The plastic fibers thus prepared were cut into an appropriate size before use.

2.3. Characterization of Biodegradable Polyesters

Melting temperature was measured with a Rigaku TAS-100 differential scanning calorimeter heated at 10 °C min^{-1} under a nitrogen gas flow. Wide-angle X-ray diffraction measurement of polymer samples was performed using the Shimadzu XD-D1 system. Cu-Kα radiation (λ= 0.1542 nm) was used as the light source. The degree of crystallization (Xc^{Xray}) was calculated according to the following equation: Xc^{Xray} (%) = $100 \times I_{crystal} / (I_{crystal} + I_{amorphous})$, where $I_{crystal}$ is the area of the crystalline peak and $I_{crystal} + I_{amorphous}$ is the overall area. The physicochemical characteristics of the biodegradable polyesters and petrochemical plastics used are shown in **Table 1**.

2.4. Spectrophotometric Monitoring of HOC Removal

Saturated aqueous solutions of HOCs in 10 mM phosphate buffer (pH 7.0) were prepared. Before use, the saturated solutions were diluted to have an ultraviolet absorbance of 0.2 to 0.4 at 248 nm for BP, 280 nm for DF, 245 nm for DES, and 276 nm for chlorophenols. Polymer fibers measuring 10 mm in length (0.5 g each) were introduced into 10 ml screw-capped glass vials containing 5 ml of a diluted HOC solution and shaken on a reciprocal shaker (140 strokes min^{-1}) for 24 h at ambient temperature (25 °C). Then, an aliquot of the solution was sampled and analyzed spectrophotometrically with a Shimadzu BioSpec 1600 spectrophotometer.

2.5. HPLC Monitoring of HOC Removal

HOC solutions at a concentration of 0.15–0.35 mM were prepared and treated for 24 h with polymer fibers as noted above. An aliquot of the aqueous solution was sampled at an appropriate interval during the 24-h period of treatment and directly analyzed by reverse-phase HPLC or extracted with ethylacetate prior to the HPLC analysis. The solvent extraction was made twice in total of 5 ml. HPLC was performed with a Shimadzu model LC10A liquid chromatograph equipped with a Zorbax

ODS column (4.6 [i.d.] × 250 mm) and a Shimadzu SPD-2A photodiode array detector. BP and DF were eluted with 90% methanol at a flow rate of 1.0 ml min^{-1} and monitored at 248 and 280 nm, respectively. BPA, NP, and chlorophenols were eluted with 70–80% methanol at a flow rate of 0.5 ml min^{-1} and monitored at 276 nm. DES was eluted with 70 % methanol at a flow rate of 1.0 ml min^{-1} and monitored at 245 nm. The concentration of HOCs was determined by comparing HPLC peak areas of samples with those of the standards at known concentrations.

2.6. Recovery of Adsorbed HOCs

After 24 h of treatment as noted above, the polymer fibers adsorbing HOCs were collected from the aqueous phase and washed three times with pure water. The washed loss was less than the detectable limit. Then, the HOCs on the polymer were extracted twice with ethylacetate in total of 5 ml and analyzed directly by reverse-phase HPLC as noted above.

2.7. Temperature Dependency

The effect of temperature on the interaction between PLA and DF was studied. PLA fibers were cut to give a length of 5 mm and immersed in 5 ml of DF solution (2 μg ml^{-1}) in glass tubes. The test tubes were kept at ambient temperature (25 °C) and in a water bath at 50 °C and 75 °C. At appropriate intervals of incubation, DF was extracted from the solution in the test tubes and analyzed by HPLC as described above.

2.8. Bacterial Growth with 3,5-DCP and PHBV

Escherichia coli strain IAM 12119 (the type strain) and *Bacillus subtilis* IAM 12118 (the type strain), both of which were obtained from the IAM Culture Collection Center, the University of Tokyo (Tokyo, Japan) were used. The test organisms were pre-grown aerobically in PBY liquid medium [20]. A 50 μm aliquot of cultures at the late exponential phase of growth was introduced into four screw-capped test tubes (30-ml capacity) containing 6 ml of PBY medium. A small amount of a filter-sterilized 3,5-DCP solution was added to one of the test tubes at the beginning to give a concentration of 27 μg ml^{-1} and incubated aerobically at 28 °C on a reciprocal shaker (designated test 1). In tests 2 and 3, the 3,5-DCP solution was added to the culture after 3 h of incubation. In test 3, autoclaved PHBV fibers (50 mg ml^{-1}) were further added aseptically to the cultures after 6 h of incubation. The control culture was made without any additive. Growth was monitored by measuring the optical density at 660 nm (OD_{660}) using an Amar sham-Pharmacia Novaspec spectrophotometer. Cell-morphology were checked by phase-contrast microscopy and epifluorescence microscopy with SYBR Green I staining [21]. Viability of cells was estimated by the tetrazolium reduction method using 5-cyano-2,3-ditoryl tetrazolium chloride (CTC) at single cell resolution [22]. The concentration of 3,5-DCP remaining in the liquid phase was monitored by HPLC as noted above.

Table 1. Biodegradable polyesters and petrochemical polymers used.

Polyester	Crystallinity (%)	Melting temperature (°C)	Glass transition temperature (°C)
Biodegradable			
EF	21.3	115	–30
PBS	44.5	113	–32
PCL	58.8	59	–60
PHBV	52.6	158	4
PLA	20.9	163	60
Non-biodegradable			
LDPE	45.8	120	–120
PET	nd[a]	260	70

[a] nd, not determined.

3. Results and Discussion

3.1. Removal Efficiency with Different Polyesters

The aqueous solutions of different aromatic compounds as model HOCs were shaken in the presence or absence of a biodegradable polyester added as the sorbent. Then, the removal of HOCs from the aqueous phase after 24 h of treatment was checked spectrophotometrically. As examples, UV absorption spectra of BP, BPA, DF, and DES solutions with or without PCL applied are shown in **Figure 1**. These aromatic solutions showed their characteristic absorption maxima between 200 and 300 nm in the absence of PCL (**Figures 1(a)-1(d)**, traces I). On the other hand, the addition of PCL to the solutions resulted in the disappearance of absorption peaks in all cases (**Figures 1(a)-1(d)**, traces II), indicating that the HOCs were removed from the aqueous phase by sorption onto PCL. Similar effects on the aromatic solutions were observed with the addition of EF, PBS, and PHBV, whereas the addition of PLA to the solutions exerted little or no spectral change under the experimental conditions (data not shown).

HPLC experiments were performed to quantitatively estimate the efficiency of HOC removal by different biodegradable polyesters as the adsorbents compared LDPE and PET. All of the biodegradable polyesters used, except PLA, adsorbed all test HOCs effectively at a removal efficiency of more than 98 % within 24 h of treatment (**Table 2**). Much lower efficiency of HOC removal

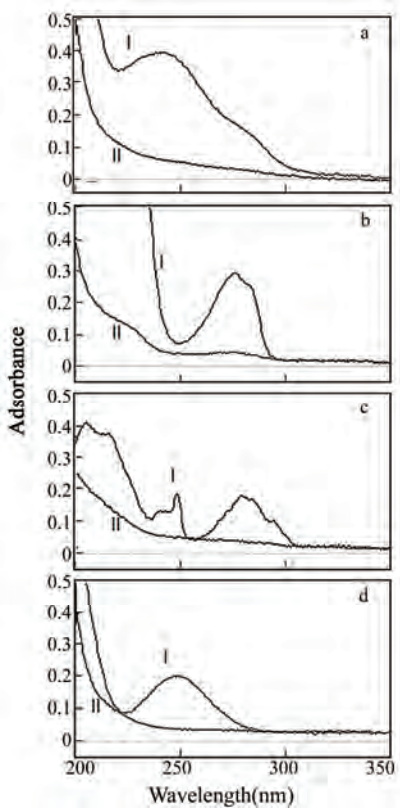

Figure 1. Absorption spectra of aqueous solutions of BP (a), BPA (b), DF (c), and DES (d) with and without PCL applied. (I) spectra without PCL applied; (II) spectra after 24 h treatment with PCL.

(≤ 22 %) was obtained with PLA and PET. The HOC removal patterns of LDPE were different in some degree from those with the biodegradable polyesters. Namely, LDPE adsorbed BP and DF effectively but removed much less amounts of BPA and DES from the solutions.

The adsorption behavior of phenol, 2-CP, and 3,5-DCP on the biodegradable polyesters was analyzed in greater detail to study whether the sorption efficiency is related to the number of chlorine substituents, *i.e.*, hydrophobicity of the chemicals. As example, the time course of the removal of phenol and the chlorophenols by PCL is shown in **Figure 2**. The removal efficiency became high with increasing numbers of chlorine substituents on phenol; the adsorbed amounts of phenol, 2-CP, and 3,5-DCP after 24 h of treatment were 20, 50, and 75 μmol g^{-1}, respectively. These results suggest that the hydrophobic interaction between the polymers and HOCs is an important factor affecting the sorption.

PBS and PHBV had similar effects on the chlorophenols but exhibited lower sorption efficiencies than PCL. The adsorbed amounts of the chlorophenols after 24 h of treatment with PBS and PHBV were 70–95 % and 50–80 % of those with PCL, respectively, whereas PLA did not adsorb the chlorophenols.

Table 2. Removal of aromatic compounds by sorption onto different biodegradable and non-biodegradable polyesters.

Polyester used	% Removal of:[a] BP	BPA	DF	DES	NP
Biodegradable					
EF	>99	>99	>99	>99	>99
PBS	>99	98±1	>99	99±1	>99
PCL	>99	>99	>99	>99	>99
PHBV	>99	98±1	>99	98±1	98±1
PLA	18±2	22±2	11±1	13±1	nt[b]
Non-biodegradable					
LDPE	97±2	9±4	>99	27±1	nt
PET	8±2	8±1	6±1	9±1	nt

[a] % Removal after 24 h of treatment; the initial concentration of aromatics ranged from 0.15 to 0.30 μmol (23–68 μg) ml^{-1}.
[b] nt, not tested.

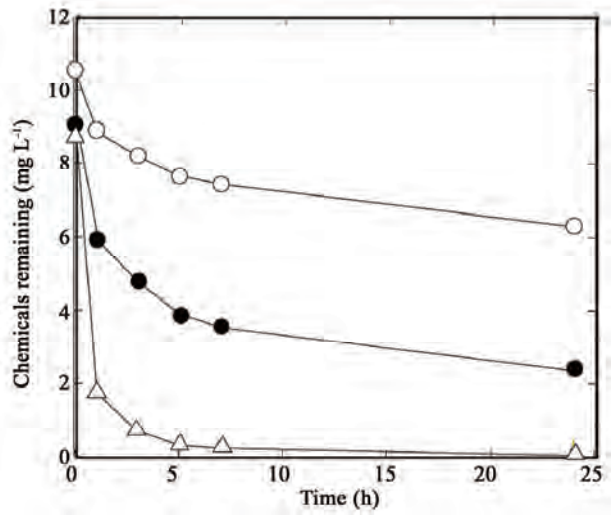

Figure 2. Removal of phenol (open circles), 2-CP (solid circles), and 3,5-DCP (triangles) from the aqueous solutions by sorption onto PCL.

3.2. HOC Removal Efficiency with Different Amounts of Adsorbents

Removal efficiency of 2-CP with different amounts of PCL added as an adsorbent was further studied under the same conditions as described for **Figure 2**. As shown in **Figure 3**, the ratio of the concentration of 2-CP in the liquid phase equilibrated after 24 h of treatment (C_e) to its initial concentration (C_0) decreased linearly with increasing amounts of PCL as the absorbent. Preliminary experiments also showed that a much faster decrease in the C_e/C_0 ratio was observed with increasing amounts of a granular type of PCL or PHBV (unpublished data). These results suggest that HOC removal efficiency depends upon the surface area of biodegradable polyesters as the absorbents.

3.2. Recovery of Adsorbed HOCs from Polymers

If the hydrophobic interaction is mainly involved in the sorption of HOCs onto the surface of polymer, the compounds absorbed should be fully recoverable by extraction with an organic solvent. To examine this, the BPA and DF solutions were treated with EF, PBS, PCL, and PHBV, and the net amounts of the chemicals extracted separately from the solution and the polymers were determined. As shown in **Table 3**, the total amount of BPA and DF recovered from each of the 4 polyesters accounted for only 19 to 56 % of the initial amount in the respective solutions. These results suggest that the mechanism of HOC sorption by the polymers is more than a simple hydrophobic interaction.

3.3. Effects of Temperature on Sorption

In view of the results noted above, the affinity between the polymers and HOCs may be related to the chemical nature of the former compounds as well as of the latter. A possible determinant of this is grass transition temperature. PCL, PBS, EF, and PHBV have a lower grass transition temperature ranging from –60 °C to 4 °C (see **Table 1**). As noted above, these polymers absorbed the HOCs effectively at room temperature, and the removal efficiency of the chlorophenols decreased in the following order: PCL (glass transition temperature, –60 °C) > PBS (–32 °C) > PHBV (4 °C). On the other hand, PLA, having a much higher glass transition temperature (60 °C), did not adsorb the chemicals effectively at room temperature. PET, whose grass transition temperature is 70 °C, showed similar behavior to PLA.

To determine the effect of temperature on the interaction of chemicals with polymers, a DF solution was treated with PLA at 25 °C, 50 °C, and 75 °C, and the chemical in the hot solution was extracted with ethylacetate. As shown in **Figure 4**, more than 90 % of DF in the hot solution at 75 °C was removed by PLA, contrasting well with the control test with the solution at 25 °C in which DF was hardly removable. The removal efficiency at 50 °C, which is lower than the glass transition temperature of PLA, was also low.

Based on the aforementioned results, it may be logical to conclude that the glass transition temperature of polymers is another important determinant of their affinity to HOCs. The mobility of the amorphous phase of plastics much increases at a higher temperature than glass transition temperature, and this physical state is possibly critical for elevating in the HOC-sorption efficiency. In this context, it is of special interest to further study the relationship between the sorption efficiency and cristallinity of the plastics. Although LDPE has a low glass transition temperature (–120 °C), it did not adsorb some of the tested HOCs (*i.e.*, BPA and DES) effectively. At this time, we are unable to find a plausible reason for this with certainty but can assume

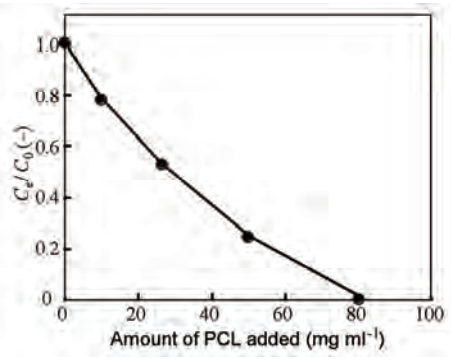

Figure 3. Removal efficiency of 2-CP as a function of the amount of PCL added as an adsorbent. C_e, equilibrated concentration of 2-CP; C_0, initial concentration of 2-CP.

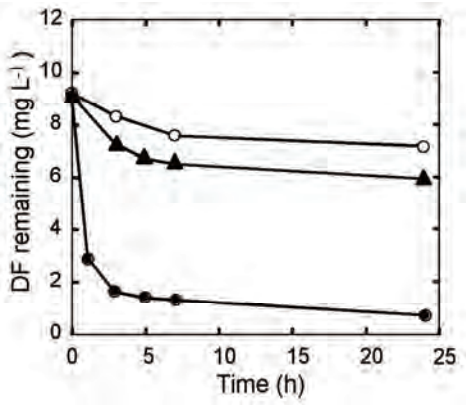

Figure 4. Removal of DF from the aqueous solution at 25 °C (open circles), 50 °C (triangles), and 75°C (closed circles) by sorption onto PLA.

Table 3. Recovery of adsorbed aromatics from biodegradable polyesters by extracting with ethylacetate.

Polyester	% Recovery of:	
	BPA	DF
EF	34±6	22±4
PBS	18±4	19±6
PCL	21±5	31±6
PHBV	55±8	56±9

that the interactions between HOCs and the plastics possibly depend upon the physicochemical nature of the former as well as of the latter.

3.4. Significance of *i/o* Characters of Chemicals in Sorption

For more comprehensive understanding of the adsorptive behavior of HOCs, we considered the Fujita's *i/o* characters, which are the parameters based on the concept of van der Waals interaction and electronic affinity, respectively. The *i/o* ratio is useful to predict the physicochemical characteristics of chemical compounds in the

liquid phase [18,19]. It can be used as a criterion of adsorbability as well as of solubility [23]. As shown in **Figure 5**, the *i* values for BP and DF are much lower than those for BPA and DES. In addition, BP and DF have a lower *i/o* ratio than BPA and DES. Thus, one can assume that chemicals having a low *i* value and a low *i/o* ratio, such as BP and DF, are adsorbed strongly by hydrophobic polymers in one fashion, while BPA and DES, having a high *i* value, interact with them in another manner. This characteristic of chemicals is an additional important factor to consider their sorption behavior onto the biodegradable polyesters as well as onto petrochemical plastics. Abe *et al*. [23] have used the *i/o* value to explain the adsorptive mechanism on activated carbon in the liquid phase.

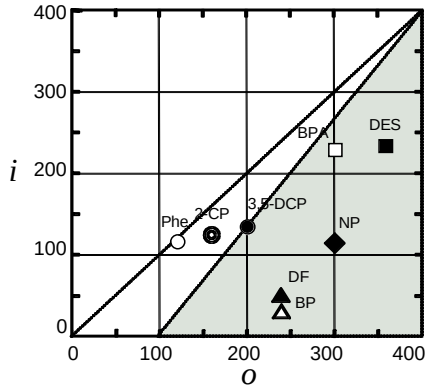

Figure 5. Fujita's *i/o* characters of HOCs used in this study. Symbols: open circle, phenol (Phe); double circle, 2-monochlorophenol (2-CP); solid circle, 3,5- dichlorophenol (3,5-DCP); open triangle, biphenyl (BP); open square, bis-phenol A (BPA); solid square, diethylstilbestrol (DES); solid triangle, dibenzofuran (DF); solid diamond, nonylphenol (NP). The compounds in the shaded area may be those adsorbed effectively by the biodegradable polyesters.

3.5. Elimination of Toxic Effects of 3,5-DCP by Sorption

A wide variety of HOCs such as 3,5-DCP have toxic effects on growth and viability of organisms. Therefore, it is important to elucidate whether these effects can be reduced by sorption using biodegradable polyesters. To know about this, two phylogenetically different bacteria were tested for growth in the presence of 3,5-DCP and PHBV. The tested organisms were *Bacillus subtilis* and *Escherichia coli*, both of which are unable to degrade PHBV and the other polyesters used in this study. The results of the experiment with *Bacillus subtilis* are shown in **Figure 6**. In tests 1 and 2, the addition of 3,5-DCP into the culture resulted in the complete inhibition of bacterial growth. In test 3, on the other hand, the addition of PHBV into the 3,5-DCP-containing cultures resulted in the restoration of its growth (**Figure 6(a)**, triangles) along with the removal of 3,5-DCP from the aqueous phase (**Figure 6(b)**). Epifluorescence microscopy showed that there were no differences in cell morphology and CTC-reducing activity at single cell resolution between the test 3 culture (**Figure 6(a)**, triangles) and the control culture (**Figure 6(a)**, solid diamonds) at the stationary phase of growth. Similar effects of PHBV were obtained with 3,5-DCP-containing cultures of *Escherichia coli* (data not shown).

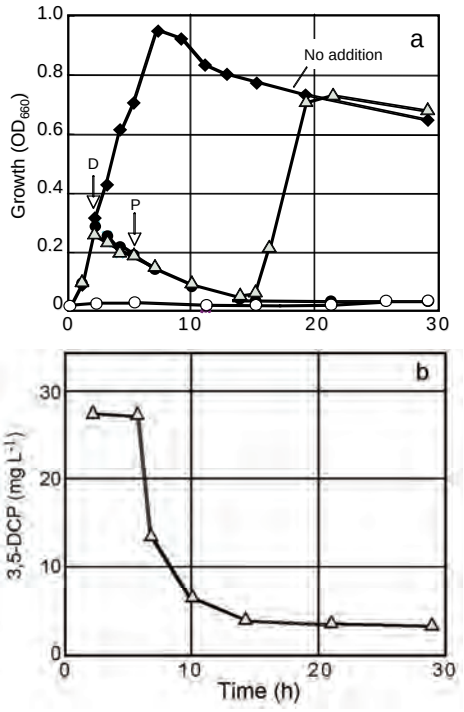

Figure 6. Effects of 3,5-DCP and PHBV on growth of *Bacillus subtilis* strain IAM 12118 (a) and change in the concentration of 3,5-DCP in the culture supernatant in test 3 (b). Symbols in Figure 4(a): diamonds, growth without 3,5-DCP (control); open circles, growth with 3,5-DCP (test 1); closed circles, growth with 3,5-DCP added after 3 h of incubation (shown by an arrow with D) (test 2); triangles, growth with 3,5-DCP and PHBV added after 3 h (shown by an arrow with D) and 5 h (shown by an arrow with P) of incubation, respectively (test 3).

As reported above, our attempt to eliminate the toxic effect of 3,5-DCP on bacteria by using PHBV as the adsorbent has given positive results. These results suggest the usefulness of sorption technology using biodegradable polyesters in protecting aquatic organisms from environmental hazards with HOCs. Our concurrent study has shown that the biodegradable polyesters are able to adsorb several other harmful aromatic compounds such as benzene, toluene, ethylbenzene, and xylene, and, in this respect, they are superior to activated carbon (unpublished observations). Further study should give more

definitive information about the applicability of the biodegradable polyesters as novel adsorbents in sorption technology for the environmental remediation of HOCs.

4. Conclusions

The present study was designed to evaluate the applicability of the biodegradable polyesters, *i.e.*, EF, PBS, PCL, PHBV, and PLA, as the sorbents for the removal of HOCs from the environment. The results of this study have demonstrated that all of the biodegradable polyesters tested, except PLA, are able to adsorb the aromatic compounds as model HOCs in aqueous solutions at room temperature. In the HOCs removal efficiency, the biodegradable polyesters are superior to conventional petrochemical plastics such as LDPE and PET. Although the sorption mechanism for this has not yet been fully understood, it is likely that both the physicochemical characteristics of the plastics (e.g., glass transition temperature) and the nature of the HOCs as defined by the Fujita's *i/o*-characters is involved. The toxic effect of 3,5-DCP on microbial growth in liquid cultures can be eliminated by sorption onto biodegradable polyesters.

5. Acknowledgments

We are grateful to Prof. H. Tsuji, Department of Ecological Engineering, Toyohashi University of Technology, for critical comments and stimulating discussions. This study was supported in part by grant K1544 from the Ministry of the Environment, Japan, and by a grant-in-aid for Scientific Research (No. 17310046) from the Ministry of Education, Culture, Sports, Science and Technology, Japan.

6. References

[1] G. Ross, "The public health implications of polychlorinated biphenyls (PCBs) in the environment," Ecotoxicology and Environmental Safety, Vol. 59, No. 3, pp. 275–291, 2004.

[2] M. Ahmaruzzaman, "Adsorption of phenolic compounds on low-cost adsorbents: A review," Advances in Colloid and Interface Science, Vol. 143, No. 1–2, pp. 48–67, 2008.

[3] A. S. Gunasekara and B. Xing, "Sorption and desorption of naphthalene by soil organic matter: Importance of aromatic and aliphatic components," Journal of Environmental Quality, Vol. 32, No. 1, pp. 240–246, 2003.

[4] X. Wang, R. Cook, S. Tao, and B. Xing, "Sorption of organic contaminants by biopolymers: Role of polarity, structure and domain spatial arrangement," Chemosphere, Vol. 66, No. 8, pp. 1476–1484, 2007.

[5] X. Wang, K. Yang, S. Tao, and B. Xing, "Sorption of aromatic organic contaminants by biopolymers: Effects of pH, copper (II) complexation, and cellulose coating," Environmental Science & Technology, Vol. 41, No. 1, pp. 185–191, 2007.

[6] J. G. Derraik, "The pollution of the marine environment by plastic debris: A review," Marine Pollution Bulletin, Vol. 44, No. 9, pp. 842–852, 2002.

[7] S. Endo, R. Takizawa, K. Okuda, H. Takada, K. Chiba, H. Kanehiro, H. Ogi, R. Yamashita, and T. Date, "Concentration of polychlorinated biphenyls (PCBs) in beached resin pellets: Variability among individual particles and regional differences," Marine Pollution Bulletin, Vol. 50, No. 10, pp. 1103–1114, 2005.

[8] Y. Mato, T. Isobe, H. Takada, H. Kanehiro, C. Ohtake, and T. Kaminuma, "Plastic resin pellets as a transport medium for toxic chemicals in the marine environment," Environmental Science & Technology, Vol. 35, No. 2, pp. 318–324, 2001.

[9] J. Chen and S. Chen, "Removal of polycyclic aromatic hydrocarbons by low density polyethylene from liquid model and roasted meat," Food Chemistry, Vol. 90, No. 3, pp. 461–469, 2004.

[10] P. Simko, "Factors affecting elimination of polycyclic aromatic hydrocarbons from smoked meat foods and liquid smoke flavorings," Molecular Nutrition & Food Research, Vol. 49, No. 7, pp. 637–647, 2005.

[11] P. Simko, P. Simon, and V. Khunova, "Removal of polycyclic aromatic hydrocarbons from water by migration into polyethylene," Food Chemistry, Vol. 64, No. 2, pp. 157–161, 1999.

[12] Y. Kiso, T. Kitao, and K. Nishimura, "Adsorption properties of aromatic compounds on polyethylene as a membrane material," Journal of Applied Polymer Science, Vol. 74, No. 5, pp. 1037–1043, 1999.

[13] V. S. Muhandiki, Y. Shimizu, Y. A. Adou, and S. Matsui, "Removal of hydrophobic micro-organic pollutants from municipal wastewater treatment plant effluents by sorption onto synthetic polymeric adsorbents: Batch sorption experiments," Environmental Technology, Vol. 28, No. 3, pp. 415–424, 2007.

[14] R. Auras, B. Harte, and S. Selke, "An overview of polylactides as packaging materials," Macromolecular Bioscience, Vol. 4, No. 9, pp. 835–864, 2004.

[15] J. M. Luengo, B. García, A. Sandoval, G. Naharro, and E. R. Olivera, "Bioplastics from microorganisms," Current Opinion in Microbiology, Vol. 6, No. 3, pp. 251–260, 2003.

[16] A. Hiraishi and T. Kawagishi, "Effects of chemical uncouplers on microbial biomass production, metabolic activity, and community structure in an activated sludge system," Microbes & Environments, Vol. 17, No. 4, pp. 197–204, 2002.

[17] F. X. Ye, D. S. Shen, and Y. Li, "Reduction in excess sludge production by addition of chemical uncouplers in activated sludge batch cultures," Journal of Applied Microbiology, Vol. 95, No. 4, pp. 781–786, 2003.

[18] H. Inoue, A. Uehara, and M. Nango, "Separation method for organic compounds (in Japanese)," Shokabo, Tokyo, 1990.

[19] S. Saito, A. Tanoue, and M. Matsuo, "The *i/o*-characters to evaluate *n*-octanol/water partition coefficient in bioconcentration of organic chemicals in fish," Chemosphere, Vol. 24, No. 1, pp. 89–95, 1992.

[20] H. Futamata, T. Uchida, N. Yoshida, Y. Yonemitsu, and A. Hiraishi, "Distribution of dibenzofuran-degrading bacterial in soils polluted with different levels of polychlorinated dioxins," Microbes & Environments, Vol. 19, No. 2, pp. 172–177, 2004.

[21] S. T. Khan, Y. Horiba, N. Takahashi, and A. Hiraishi, "Activity and community composition of denitrifying bacteria in poly(3-hydroxybutyrate-*co*-3-hydroxy-valerate)-using solid-phase denitrification processes," Microbes & Environments, Vol. 22, No. 1, pp. 20–31, 2007.

[22] Y. Fujii and A. Hiraishi, "Combined use of cyanoditolyl tetrazolium staining and flow cytometry for detection of metabolically active bacteria in a fed-batch composting process," Microbes & Environments, Vol. 24, No. 1, pp. 57–63, 2009.

[23] I. Abe, K. Hayashi, M. Kitagawa, and Y. Urahata, "Adsorptive mechanism on activated carbon in the liquid phase. III. The relationship between the physical constants of organic compounds and their adsorbabilities on activated carbon from an aqueous solution," Bulletin of the Chemical Society of Japan, Vol. 53, No. 5, pp. 1199–1205, 1980.

J. Water Resource and Protection, **2010, 2, 222-226**
doi:10.4236/jwarp.2010.23025 Published Online March 2010 (http://www.scirp.org/journal/jwarp)

Treatment of Acetonitrile by Catalytic Supercritical Water Oxidation in Compact-Sized Reactor

Benjaporn Youngprasert[1], Kunakorn Poochinda[1,2], Somkiat Ngamprasertsith[1,2]
[1]*Fuels Research Center, Department of Chemical Technology, Faculty of Science, Chulalongkorn University, Bangkok, Thailand*
[2]*Center for Petroleum, Petrochemicals and Advance Materials, Chulalongkorn University, Bangkok, Thailand*
E-mail: *somkiat.n@chula.ac.th*
Received November 20, 2009; *revised December* 18, 2009; *accepted January* 11, 2010

Abstract

The objective of this research was to study the treatment of acetonitrile by catalytic supercritical water oxidation in a compact-sized tubular reactor, with an internal volume of 4.71 mL. Manganese dioxide was used as the catalyst and H_2O_2 was used as the oxidant. The oxidation of acetonitrile in supercritical water was studied at 400-500 ^oC, 25-35 MPa, the flow rate of 2-4 mL/min, the initial concentration of acetonitrile 0.077-0.121 M and the %excess O_2 of 50-200%. As a result, the products were mainly N_2, CO_2 and CO and acetonitrile can be decomposed > 93 % within a very short contact time (1.45-6.19 s). The oxidation process was carried out with respect to the conversion of acetonitrile by 2^5 factorial design. Regression models were obtained for correlating the conversion of acetonitrile with temperature and flow rate. The complete oxidation can be achieved at a condition as moderate as 400 ^oC, 25 MPa with the flow rate of 2 mL/min.

Keywords: Acetonitrile, Supercritical Water Oxidation, Compact-Sized Reactor

1. Introduction

Laboratory wastes, which contain various types of hazardous chemicals generated from scientific research, have become a serious problem both financially and environmentally. Thus, two important and fundamental concepts of "treatment at the origin" and "self-responsibility for waste", brings about a development of a compact-sized reactor for an on-site laboratory wastewater treatment. Supercritical water oxidation (SCWO) has been proposed as a promising candidate for the treatment of various organic wastes. Organic compounds and permanent gases (such as oxygen) are completely miscible in supercritical water, so the oxidation occurs in a single-phase aqueous environment. It was reported that, above the critical point of water (374 ^oC, 22.1 MPa), most organic compounds can be converted into CO_2 and H_2O by SCWO in a very short residence time [1–3]. Recently, there has been increasing interests in the use of heterogeneous catalysts in SCWO. Many catalysts can increase the oxidation rate, reduce the residence time and temperature requirement, and possibly provide a better selectivity for competing reaction pathways, which is difficult to achieve in noncatalytic processes [4].

Acetonitrile (CH_3CN) is widely used as a solvent for the synthesis of many chemicals such as perfumes, acrylic nail removers, pharmaceuticals, rubber products, pesticides and in the manufacturing of photographic film. It is also used as a solvent in various extraction processes and HPLC analysis technique [5]. In recent years, there have been a number of studies in literature demonstrating processes for the treatment of acetonitrile wastewater [6–8]. For incineration of nitrogen-containing organic compounds, the byproducts may include NO and NO_2. At lower temperatures as required in SCWO, however, thermodynamics favor nitrogen conversion into N_2 and N_2O, rather than NO or NO_x. In addition, any NO_x formed would remain in the supercritical water, rather than being emitted to the atmosphere [9].

Thus, we have examined the oxidation of CH_3CN in supercritical water using MnO_2 as a catalyst in a compact-sized reactor [10]. The reaction is of great interest since nitrile groups are commonly found in many commercial products and they are major constituents of waste streams.

2. Methods

2.1. Apparatus and Procedure

The SCWO experiments were performed in a custom-

made tubular reactor system schematically shown in **Figure 1**. It was designed to be a compact reaction system with a similar size to a gas chromatograph, so that it can be installed in a limited space of a general laboratory. The experimental apparatus consists of a tubular reactor (0.1 m x 3/8" I.D. with an internal volume of 4.71 mL), which is heated by a 200 W vial heater. A commercial catalyst, bulk MnO_2 was packed in the reactor. The wastewater and oxidant pre-heating line (180 cm x 1/8" I.D.) is heated by a 100 W electrical heater. All wetted parts (tubing, fittings, etc.) from the feeding pumps to the gas–liquid separator, were made of SUS316 stainless steel. The oxidant feed stream was prepared by dissolving hydrogen peroxide with deionized water in a feed tank. Another feed tank was loaded with a mixture of hydrogen peroxide (oxidant) and acetonitrile solution as a simulated wastewater. The two feed streams were fed in different lines using two HPLC pumps (Jasco) and were brought together at a SUS316 stainless steel mixing tee, prior to entering the pre-heater section. Hydrogen peroxide decomposes into oxygen and water completely when it is heated in the pre-heater section (150-200 ^oC) as verified by previous experiments [11]. After preheating, the solution was fed into the reactor. The reactor inlet and outlet temperature were measured using thermocouples. The experiments were carried out at 400-500 ^oC, 25-35 MPa, the initial concentration of acetonitrile 0.077-0.121 M and the % excess O_2 of 50-200 %. Upon exiting the reactor, the effluent was cooled rapidly by passing through a heat exchanger. Then, the effluent was flowed through a 0.5 μm inline filter, before being depressurized by a back-pressure regulator (GO REGULATOR Inc.). The product stream was then separated into liquid and vapor phases. The liquid products were collected in a graduated cylinder. It was assumed that the liquid and vapor phases were in equilibrium in the phase separator, and Henry's law was used to calculate the amount of each gas dissolved in the liquid. The flow rates of both the gas and liquid phases were measured at the ambient laboratory condition.

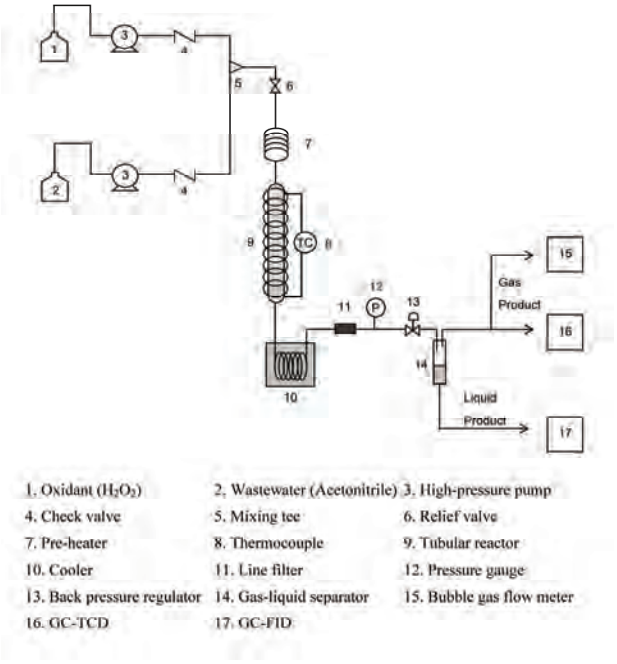

Figure 1. Schematic diagram of the compact-sized reactor.

2.2. Materials and Analytical Methods

The oxidant is oxygen which was produced by the thermal decomposition of hydrogen peroxide (Fisher, 30 %, w/v aqueous solution). Acetonitrile (Lab scan, > 99 % purity) was used as the organic compound to be oxidized in the catalytic SCWO experiments.

The effluent liquid phase was collected and then analyzed by a Shimadzu 7AG gas chromatograph with a flame ionization detector. The on-line gas samples were analyzed using a Shimadzu 2014 gas chromatograph with a thermal conductivity detector.

2.3. Experimental Design

A full 2^5 factorial design was performed to evaluate the effects of 5 factors; temperature, pressure, flow rate, initial acetonitrile concentration and % excess O_2 concentration on conversion of acetonitrile. **Table 1** summarizes these factors and their respective levels. The statistical analysis of variance, ANOVA, was carried out to determine the significance and impact of each factor as well as their interactions on the conversion. The relationships linking the main factors and interactions with the conversion were determined and presented as a quadratic equation of the general form in the following equation.

Table 1. Factors and levels used in the 2^5 factorial design.

Factor	Parameter	Level	
		(-)	(+)
A	Temperature (^oC)	400	500
B	Pressure (MPa)	25	35
C	Flow rate (mL/min)	2	4
D	Initial acetonitrile concentration (M)	0.077	0.121
E	Excess O_2 concentration (%)	50	200

$$Y = \text{mean} + \sum\text{main effects} + \sum\text{interactions} \quad (1)$$

The equation coefficients were calculated using the coded values, thus the effects of various terms can be compared directly regardless of their actual magnitude. The coding used throughout the statistical analysis denotes that −1 was taken as the lower level and +1 as the upper level. Therefore, a positive coefficient of a pa-

rameter indicates that the conversion increases with increasing level of the parameter, while a negative coefficient indicates that the conversion increases with decreasing level of the parameter.

The conversions of acetonitrile were calculated using the following equation.

$$X = (1 - C_t / C_o) \times 100 \quad (2)$$

where: X = acetonitrile conversion (%)

C_t = concentration of acetonitrile at a given time t (M)

C_o = initial concentration of acetonitrile (M)

3. Results and Discussion

The experimental data using full 2^5 factorial design were listed in **Table 2**, 32 factorial points and 4 central points included. The experiments were executed in a random order to correctly evaluate experimental errors [12]. The conversions were obtained to be between 93.63 % and 100 % at the contact times ranging from 1.45 to 6.19 s under various reaction conditions. The gas phase products were detected as CO, CO_2, CH_4, N_2O, N_2, H_2 and O_2 by GC analysis. The liquid phase products were clear and colorless. The analysis of gas and liquid products showed that acetonitrile was completely degraded and transformed into intermediate products, CO_2, H_2O and N_2. The decomposition of CH_3CN in the SCWO can be expected to follow the oxidation reaction,

$$2CH_3CN + \frac{11}{2}O_2 \longrightarrow 4CO_2 + N_2 + 3H_2O \quad (3)$$

Although catalytic SCWO was carried out at high pressures and temperatures, its advantages of short reaction time and environmental friendliness overcame its shortcomings. In comparison with other treatment techniques such as nitrile-degrading microorganisms [6,8], which needed more than 10 h of reaction time, catalytic SCWO required only in the order of seconds with the

Table 2. Results and reaction parameters for SCWO of acetonitrile.

Run order	Temperature (°C)	Pressure (MPa)	Flow Rate (mL/min)	Initial Concentration of Acetonitrile (M)	Excess Oxygen (%)	Conversion (%)
1	402	34.8	4	0.121	50	99.75
2	398	24.2	4	0.121	50	96.16
3	408	26	2	0.077	50	98.32
4	453.5	30.5	3	0.099	125	99.11
5	503.5	34.9	4	0.121	200	99.90
6	389	25.2	4	0.077	200	93.65
7	502.5	25.5	2	0.077	200	99.85
8	410	35	2	0.121	50	98.82
9	389.5	25	4	0.121	200	95.18
10	396	25	4	0.077	50	95.44
11	451.5	30.6	3	0.099	125	98.37
12	504	35.3	2	0.077	50	99.84
13	408.5	35	2	0.121	200	97.74
14	402.5	35.5	4	0.077	50	97.86
15	506	35	2	0.121	200	99.88
16	401	35.3	4	0.121	200	97.00
17	499.5	24.7	2	0.077	50	99.98
18	507	34.8	2	0.121	50	99.87
19	501.5	35	4	0.077	200	99.82
20	501	25	4	0.077	50	99.72
21	503	35.5	4	0.121	50	99.74
22	407.5	36	2	0.077	200	99.47
23	496	24	2	0.121	50	100.00
24	404	34	4	0.077	200	97.35
25	496.5	25	4	0.077	200	99.90
26	449	30.5	3	0.099	125	98.85
27	403.5	25.3	2	0.121	50	100.00
28	498.5	25	4	0.121	200	99.99
29	405	35.4	2	0.077	50	99.50
30	448.5	30	3	0.099	125	98.31
31	505.5	25.3	4	0.121	50	99.93
32	504.5	34.6	2	0.077	200	99.93
33	495.5	35	4	0.077	50	99.83
34	400	25	2	0.077	200	99.16
35	506.5	25.6	2	0.121	200	99.99
36	437.5	24.5	2	0.121	200	100.00

same conversion. In terms of environmental impact, catalytic SCWO generated less toxic components as supposed to NO or NO_x emitted from incineration [7].

The 2^5 factorial study revealed that the conversion was not significantly influenced by the initial acetonitrile concentration, pressure and % excess oxygen, while temperature, and flow rate influenced the conversions at 95 % confidence interval. A mathematical model for the conversion of acetonitrile can be written in terms of the statistically significant effects on conversion in (4) and (5) [12,13].

$$\%\text{Conversion} = 98.9+0.989T'-0.529F'+0.545T'F' \quad (4)$$

where: T' = coded value of temperature

F' = coded value of flow rate

$$\%\text{Conversion} = 106-0.013T-5.48F+0.011TF \quad (5)$$

where: T = actual value of temperature (^oC)

F = actual value of flow rate (mL/min)

A positive sign of the coefficient represents a synergistic effect, while a negative sign indicates an antagonistic effect. The temperature and flow rate have a negative relationship with the conversion, so with an increase of those factors, there will be a decrease in the conversion. However, the interaction term has a positive sign indicating that with a change in temperature and flow rate in the same direction from the central point, there will be an increase in the conversion. **Figure 2** shows a comparison between the experiment and predicted conversion for acetonitrile decomposition. The high value of the coefficient of determination, R^2 = 0.8 indicates a good correlation between the observed and the predicted values of conversion.

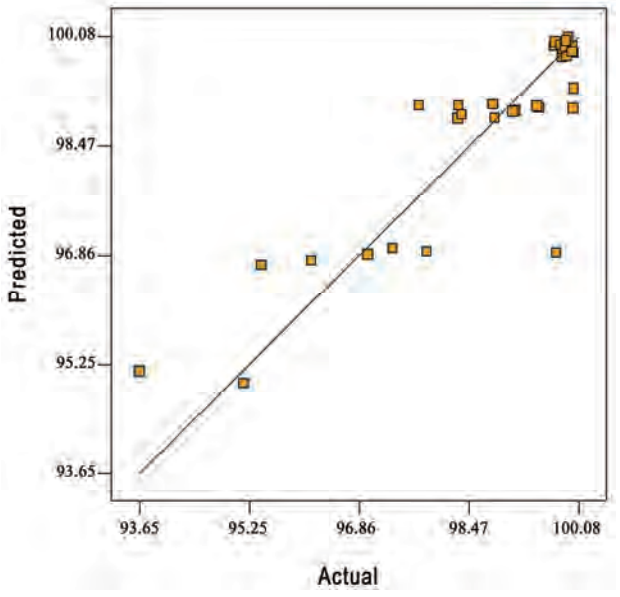

Figure 2. Comparison of the experimental and the predicted conversion.

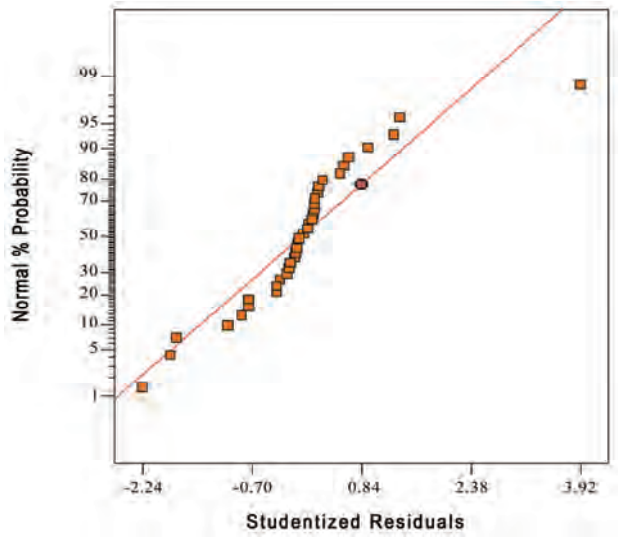

Figure 3. Normal probability plot of the difference between the observed and the predicted value.

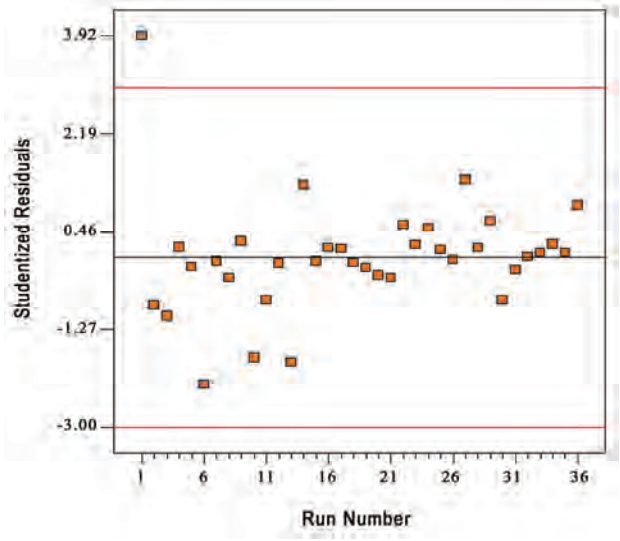

Figure 4. The residuals versus the run number when the variance is constant.

The normality of the data can be checked by plotting the normal probability plot (NPP) of the residuals. The normal probability plot is a graphical technique for assessing whether or not a data set is approximately normally distributed [14]. The residual is the difference between the observed and the predicted values (or the fitted values from the regression). **Figure 3** shows the normal probability plot of residuals. The residuals fall fairly close to the diagonal line, so the data are normally distributed. **Figure 4** illustrates the residuals for each run number. The residuals scatter randomly about zero with no specific trend, confirming that the residuals are the random error that have a normal distribution.

4. Conclusions

A compact-sized tubular reactor was designed to treat the aqueous solution of acetonitrile at the origin using catalytic supercritical water oxidation. The oxidation of acetonitrile was studied using 2^k factorial experimental design. The significant factors were found to be temperature and flow rate. The mathematical models correlating the conversion to temperature and flow rate were formulated and evaluated. The results demonstrated that the SCWO process can treat acetonitrile efficiently, with the contact times between 1.45 and 6.19 s, and the acetonitrile concentration between 0.077 and 0.121 M. It was found that acetonitrile was completely degraded and transformed into its intermediate products, CO_2, H_2O and N_2. The liquid phase products were clear and colorless. The advantage of catalytic supercritical water oxidation is the rapid oxidation of organics and the nitrogen conversion into N_2 and N_2O rather than NO or NO_x.

5. Acknowledgment

The authors would like to thank the Fuels Research Center, Department of Chemical Technology and Center for Petroleum, Petrochemicals and Advanced Materials, Chulalongkorn University, Thailand, for the financial and instrumental supports of this work. The supports are gratefully acknowledged.

6. References

[1] P. E. Savage, "Organic chemical reactions in supercritical water," Chemical Reviews, Vol. 99, pp. 603–621, February 1999.

[2] M. Watanabe, T. Sato, H. Inomata, R. L. J. Smith, K. Arai, A. Kruse, and E. Dinjus, "Chemical reactions of C_1 compounds in near-critical and supercritical water," Chemical Reviews, Vol. 104, pp. 5803–5821, December 2004.

[3] Y. Arai, T. Sato, and Y. Takebayashi, "Supercritical fluids: Molecular interaction, physical properties, and new applications," Springer-Verlag, Berlin, 2002.

[4] Z. Y. Ding, M. A. Frisch, L. Li, and E. F. Gloyna, "Catalytic oxidation in supercritical water," Industrial and Engineering Chemistry Research, Vol. 35, pp. 3257–3279, October 1996.

[5] http://www.michigan.gov/documents/MDCH_Acetonitrile_fast_sheet_approved_4–19–05_122749_7.pdf.

[6] T. Li, J. Liu, R. Bai, and F. S. Wong, "Membrane-aerated biofilm reactor for the treatment of acetonitrile wastewater," Environmental Science and Technology, Vol. 42, pp. 2099–2104, March 2008.

[7] P. Braos-García, D. Durán-Martín, A. Infantes-Molina, D. Eliche-Quesada, E. Rodríguez-Castellón, and A. Jiménez-López, "The effect of thermal treatment under different atmospheric conditions on the catalytic performance of nickel supported on porous silica in the gas-phase hydrogenation of acetonitrile," Adsorption Science and Technology, Vol. 25, pp. 185–198, April 2007.

[8] E. Kohyama, A. Yoshimura, D. Aoshima, T. Yoshida, H. Kawamoto, and T. Nagasawa, "Convenient treatment of acetonitrile-containing wastes using the tandem combination of nitrile hydratase and amidase-producing microorganisms," Applied Microbiology and Biotechnology, Vol. 72, pp. 600–606, September 2006.

[9] W. R. Killilea, K. C. Swallow, and G. T. Hong, "The fate of nitrogen in supercritical-water oxidation," The Journal of Supercritical Fluids, Vol. 5, pp. 72–78, March 1992.

[10] T. Ruamchat, R. Hayashi, S. Ngamprasertsith, and Y. Oshima, "A novel on-site system for the treatment of pharmaceutical laboratory wastewater by supercritical water oxidation," Environmental Sciences, Vol. 13, pp. 297–304, 2006.

[11] B. D. Phenix, J. L. Dinaro, J. W. Tester, J. B. Howard, and K. A. Smith, "The effects of mixing and oxidant choice on laboratory-scale measurements of supercritical water oxidation kinetics," Industrial and Engineering Chemistry Research, Vol. 41, pp. 624–631, February 2002.

[12] G. E. P. Box, J. S. Hunter, and W. G. Hunter, "Statistics for experimenters: Design, innovation and discovery," 2nd ed., Hoboken, Wiley-Interscience, NJ, 2005.

[13] R. E. Bruns, I. S. Scarminio, and B. De Barros Neto, "Statistical design: Chemometrics," Elsevier, Amsterdam, 2006.

[14] D. Montgomery, "Design and analysis of experiments," 5th ed., Wiley, New York, 2001.

J. Water Resource and Protection, **2010, 2, 227-234**
doi:10.4236/jwarp.2010.23026 Published Online March 2010 (http://www.scirp.org/journal/jwarp)

Influences of Limited Ammonium Nitrogen and Water Temperature on the Urban Stream Restoration Using Bacterial Technology – View from the Perspective of Numerical Modelling

Doddi Yudianto, Yuebo Xie
National Engineering Research Center of Water Resources Efficient Utilization and Engineering Safety, Hohai University, Nanjing, China
E-mail: *doddi_yd@yahoo.com*
Received December 2, 2009; *revised January* 5, 2010; *accepted January* 19, 2010

Abstract

To complete the previously information issued on the feasibility study and some technical challenges identified from the application of bacterial technology, this study presents another characteristics of numerical output as the bacterial growth is now also limited to ammonium nitrogen and water temperature. Based on the results obtained, it is found that the degradation of readily biodegradable COD will be much slower because of lower bacterial growth. At certain period, the COD concentration will increase and be plotted higher later on compared to the model which is limited only to substrate and oxygen. Besides the ammonium nitrogen, other parameters *i.e.* particulate products from COD decay and particulate degradable organic nitrogen will also increase soon after certain time. Considering the increase of ammonium nitrogen as it is also converted to nitrate nitrogen, it can be predicted that some algae may show up during the treatment processes. When the model is simulated under different water temperature, slower biodegradation process is presented at lower water temperature. Because the bacteria grow better at higher water temperature, more oxygen is then required. Finally, from this study, it is also identified that the artificial mixing and addition of oxygen at initial stage of treatment will considerably influence the restoration.

Keywords: Stream Restoration, Bacterial Technology, Polluted Urban Streams, Numerical Modelling, MATLAB

1. Introduction

As stream has always been the recipient of wastes discharge from human activities, be it domestic sources, industrial or agricultural effluents or mining process waters, the massive increase of industrial productions accompanied by high growth of large urban populations has led to severe water pollution problems for over the last two centuries. Such situation was found to be even worse in many lesser developed countries and some of the megalopolises with unbridled population growth and uncontrolled industrial development [1–2].

Because of its urgent necessity to find solutions for water pollution problems, there have been some methods and technologies developed and applied for the last few years. Started by the application of re-aeration using series of weir [3–5], shifting the effluent discharges location [6], pumping air into the water body using the local oxygenator [3,7] and the implementation of constructed wetland [8–13], it has been a while before the bacterial technology was then introduced to solve similar problems. In China, such technology has been implemented recently for treating the polluted lake [14] and influent of wastewater treatment plant [15]. It is also great to know that the practical application of this technology was found to be successful in speeding up the recovery processes of some streams in Shenzhen City, China. The final concentrations of BOD and COD after the treatment were informally reported to be less than 5.00 and 20.00 mg L^{-1} respectively.

Along with the practical implementation of this bacterial technology for stream restoration purpose, the feasibility and some technical challenges in relation to

Identify applicable sponsor/s here. *(sponsors)*

such technology have been previously issued by "in press" [5] and "unpublished" [16]. As it is previously stated that treating seriously polluted surface water through the self-purification process may result one or more unwanted end products [17], here other limiting parameters to the biodegradation processes *i.e.* ammonium and different water temperature are now included in this study to complete the feasibility information of bacterial technology from the perspective of numerical modelling. At the mean time, some field data from the restoration and monitoring project of Xuxi River in Wuxi City are still under collection and laboratory test. To be able to collect the data from the field site, as information, the process is not only influenced by technical factors but also administrative procedures. Under the same project, the authors have experienced more than a year to obtain the legal notice and set appropriate conditions to discharge certain amount of selected bacteria to the chosen stream reach. Because MATLAB has been proved to be highly accurate [18] and widely implemented in many fields of water quality modelling [5,19–24], therefore it is then selected to be used for all the simulations in this study.

2. Methodology

In order to understand the biodegradation processes occur as result of the implementation of bacterial technology, a combination of Streeter Phelps and some kinetic equations used in Activated Sludge Model No.1 (ASM-1) is employed here. Due to influences of hydraulics properties, the role of dispersion term in transport model becomes crucial [25–26] and therefore the flow velocity and mixing parameters are also included in the model simulations and further evaluated in relation with some selected parameters in both distance and time. Besides the readily biodegradable substrate and oxygen, ammonium nitrogen and different water temperatures are considered here to provide broader views. Furthermore, as the ASM-1 was basically developed on the basis of Chemical Oxygen Demand (COD) with homogeneous heterotrophs, all coefficients required in this study are adopted from the previous related studies. To simplify the case, it is also assumed here that all degradation processes involved occur at neutral pH.

3. Model Development

In most cases of natural stream restoration, besides the readily biodegradable COD and oxygen, the ammonium nitrogen (S_{NH_4}) also plays crucial role. As it can be initially predicted, when ammonium nitrogen is considered as another limiting parameter to the model, the results may come up with new characteristics since the bacterial growth is even lowered down to certain extent.

3.1. Brief Description of ASM-1

Generally, there are 13 substances and 8 different processes incorporated in the ASM-1. Although this model has been extended to incorporate more fractions of COD, the original model is probably still the most widely used for describing the biodegradation processes [27–28]. In the process of its development, COD was selected as the suitable parameter for defining the carbon material as it provides a link between electron equivalents in the organic substrate, bacteria, and oxygen utilized.

Representing the dynamic processes, the readily biodegradable of COD (S_S) is used for the growth of heterotrophic bacteria (X_H) and the balance is oxidized for energy giving rise to an associated oxygen demand. Here, ammonia (S_{NH_4}) is used as the nitrogen source for synthesis and incorporated into the cell mass. Both concentration of SS and oxygen may be rate limiting for the growth process as it is clearly described using the Monod kinetics. This process is generally the main contributor to the generation of bacteria and removal of COD even though modifications may be needed to satisfy the conditions of nitrification [29]. As presented in this study, some related processes to the bacterial growth are also limited by ammonia (S_{NH_4}).

In the absence of oxygen, the heterotrophs are capable of using nitrate as the terminal electron acceptor with SS as substrate. The process will lead to a production of heterotrophs and nitrogen gas (denitrification). In ASM-1, the ammonia is oxidized to nitrate via a single step process (nitrification) resulting in production of autotrophs (X_A) and giving rise to an associated oxygen demand. Because of the low yield of autotrophic nitrifiers, there is only small effect given to the formation of autotrophs. The situation for autotrophs in fact is simpler since the autotrophs do not grow in anoxic environment.

Not only growths, in this model, the decay of both heterotrophs and autotrophs are modelled according to the death regeneration hypothesis. The organisms will basically die at certain rate and a portion of the material is considered to give addition to the value of particulate products (X_P) and slowly biodegradable substrate (X_S). The organic nitrogen associated with X_S becomes available as particulate organic nitrogen. Along to those processes, the biodegradable soluble organic nitrogen (S_{ND}) is also converted to ammonia in a first order process mediated by the active heterotrophs. In addition, the X_S is slowly broken down to produce S_S under aerobic and anoxic conditions.

3.2. Kinetic Equations Applied

By adopting the basic concept of self purification and some equilibria employed in ASM-1 based on the Monod kinetics, and as the bacteria and other variables are assumed here to migrate with flow, the complete

biodegradation processes can be mathematically defined as follows.

Readily biodegradable COD (S_S):

$$\frac{dS_S}{dt} = -u_x\frac{dS_S}{dx} + E_x\frac{d^2S_S}{dx^2} - \frac{\mu_{\max H}}{Y_{XH/SS}}\frac{S_S}{K_S+S_S}\left[\frac{C}{K_{OH}+C}\frac{S_{NH_4}}{K_{NH_4}+S_{NH_4}} + \eta_g\frac{K_{OH}}{K_{OH}+C}\frac{S_{NO_3}}{K_{NO_3}+S_{NO_3}}\right]X_H + k_h\frac{X_S/X_H}{Kx+X_S/X_H}\left[\frac{C}{K_{O_2}+C} + \eta_h\frac{K_{O_2}}{K_{O_2}+C}\frac{S_{NO_3}}{K_{NO_3}+S_{NO_3}}\right]X_H \quad (1)$$

Active heterotrophic bacteria (X_H):

$$\frac{dX_H}{dt} = -u_x\frac{dX_H}{dx} + E_x\frac{d^2X_H}{dx^2} + \mu_{\max H}\frac{S_S}{K_S+S_S}\left[\frac{C}{K_{OH}+C}\frac{S_{NH_4}}{K_{NH_4}+S_{NH_4}} + \eta_g\frac{K_{OH}}{K_{OH}+C}\frac{S_{NO_3}}{K_{NO_3}+S_{NO_3}}\right]X_H - k_{dH}X_H^{nH} \quad (2)$$

Active autotrophic bacteria (X_A):

$$\frac{dX_A}{dt} = -u_x\frac{dX_A}{dx} + E_x\frac{d^2X_A}{dx^2} + \mu_{\max A}\frac{S_{NH_4}}{K_{NH_4}+S_{NH_4}}\frac{C}{K_{OA}+C}X_A - k_{dA}X_A^{nA} \quad (3)$$

Ammonium nitrogen (S_{NH_4}):

$$\frac{dS_{NH_4}}{dt} = -u_x\frac{dS_{NH_4}}{dx} + E_x\frac{d^2S_{NH_4}}{dx^2} - iX_B\mu_{\max H}\frac{S_S}{K_S+S_S}\left[\frac{C}{K_{OH}+C}\frac{S_{NH_4}}{K_{NH_4}+S_{NH_4}} + \eta_g\frac{K_{OH}}{K_{OH}+C}\frac{S_{NO_3}}{K_{NO_3}+S_{NO_3}}\right]X_H + k_{aN}S_{ND}X_H - \mu_{\max A}\left[iX_B + \frac{1}{Y_{NO_3/XA}}\right]\frac{S_{NH_4}}{K_{NH_4}+S_{NH_4}}\frac{C}{K_{OA}+C}X_A \quad (4)$$

Nitrate nitrogen (S_{NO_3}):

$$\frac{dS_{NO_3}}{dt} = -u_x\frac{dS_{NO_3}}{dx} + E_x\frac{d^2S_{NO_3}}{dx^2} - \mu_{\max H}\eta_g\frac{1-Y_{XH/SS}}{2.86Y_{XH/SS}}\frac{S_S}{K_S+S_S}\frac{K_{OH}}{K_{OH}+C}\frac{S_{NO_3}}{K_{NO_3}+S_{NO_3}}X_H + \frac{\mu_{\max A}}{Y_{NO_3/XA}}\frac{S_{NH_4}}{K_{NH_4}+S_{NH_4}}\frac{C}{K_{OA}+C}X_A \quad (5)$$

Slowly biodegradable COD (X_S):

$$\frac{dX_S}{dt} = -u_x\frac{dX_S}{dx} + E_x\frac{d^2X_S}{dx^2} + (1-f_p)k_{dH}X_H + (1-f_p)k_{dA}X_A - k_h\frac{X_S/X_H}{K_X+X_S/X_H}\left[\frac{C}{K_{OH}+C} + \eta_h\frac{K_{OH}}{K_{OH}+C}\frac{S_{NO_3}}{K_{NO_3}+S_{NO_3}}\right]X_H \quad (6)$$

Particulate products from COD decay (X_P):

$$\frac{dX_P}{dt} = -u_x\frac{dX_P}{dx} + E_x\frac{d^2X_P}{dx^2} + f_pk_{dH}X_H + f_pk_{dA}X_A \quad (7)$$

Soluble degradable organic nitrogen (S_{ND}):

$$\frac{dS_{ND}}{dt} = -u_x\frac{dS_{ND}}{dx} + E_x\frac{d^2S_{ND}}{dx^2} - k_{aN}S_{ND}X_H + k_h\frac{X_{ND}/X_H}{K_X+X_S/X_H}\left[\frac{C}{K_{OH}+C} + \eta_h\frac{K_{OH}}{K_{OH}+C}\frac{S_{NO_3}}{K_{NO_3}+S_{NO_3}}\right]X_H \quad (8)$$

Particulate degradable organic nitrogen (X_{ND}):

$$\frac{dX_{ND}}{dt} = -u_x\frac{dX_{ND}}{dx} + E_x\frac{d^2X_{ND}}{dx^2} + (iX_B - f_piX_P)(k_{dH}X_H + k_{dA}X_A) - k_h\frac{X_{ND}/X_H}{K_X+X_S/X_H}\left[\frac{C}{K_{OH}+C} + \eta_h\frac{K_{OH}}{K_{OH}+C}\frac{S_{NO_3}}{K_{NO_3}+S_{NO_3}}\right]X_H \quad (9)$$

Dissolved oxygen (C):

$$\frac{dC}{dt} = -u_x\frac{dC}{dx} + E_x\frac{d^2C}{dx^2} + k_a(C_s - C) - \mu_{\max H}\frac{1-Y_{XH/SS}}{Y_{XH/SS}}\frac{S_S}{K_S+S_S}\left(\frac{C}{K_{OH}+C}\frac{S_{NH_4}}{K_{NH_4}+S_{NH_4}}\right)X_H - \mu_{\max A}\frac{4.57-Y_{NO_3/XA}}{Y_{NO_3/XA}}\frac{S_{NH_4}}{K_{NH_4}+S_{NH_4}}\frac{C}{K_{OA}+C}X_A \quad (10)$$

where

$Y_{XH/SS}$: mg biomass COD formed per mg COD removed

F_p : mg debris COD (mg biomass COD)$^{-1}$

i_{XB} : mg N (mg COD)$^{-1}$ in active biomass

i_{XP} : mg N (mg COD)$^{-1}$ in active debris

$Y_{NO_3/XS}$: mg biomass COD formed per mg N oxidized

$\mu_{\max H}$: heterotrophic max specific growth rate

$\mu_{\max A}$: autotrophic max specific growth rate

k_{dH} : decay coefficient of heterotroph bacteria

k_{dA} : decay coefficient of autotroph bacteria

K_S : half saturation coefficient of degradable dissolves in heterotrophic growth

K_{OH} : half saturation coefficient of oxygen in heterotrophic growth

K_{NO_3} : half saturation coefficient of NO_3 in anoxic heterotrophic growth

K_X : half saturation coefficient of organic in hydrolysis

K_{NH_4} : half saturation coefficient of NH_4 in growth of heterotrophs

K_{OA} : half saturation coefficient of oxygen in nitrifying bacterial growth

k_h : maximum hydrolysis rate constant at 20 °C

k_{aN} : ammonification rate by anoxic hydrolysis of heterotrophs

k_a : reaeration coefficient

η_g : correction factor for anoxic growth of heterotrophs

η_h : correction factor for anoxic hydrolysis

3.3. Computation of Mixing Coefficient and Reaeration Coefficient

Literally, there are some available equations that can be used to technically predict the longitudinal mixing in a stream such as McQuivey and Keefer (1974), Fischer

(1975), Jain (1974), Liu (1977), Seo and Cheong (1998), and Deng *et al.* (2001) [26]. Although most of these equations have been widely applied in many research works, however, [26] showed that such equations result a wide range of values for the same hydraulic characteristics of in bank flow. Being the most accurate and mostly cited one [25], the predictive equation of Seo and Cheong is then chosen in this paper and defined as follows.

$$E_x = 5.915 \left[\frac{u_x}{u_*}\right]^{1.428} \left[\frac{W}{H}\right]^{0.62} Hu_* \quad (11)$$

$$u_x = \frac{1}{n}\left(\frac{A}{P}\right)^{2/3} S^{1/2} \quad (12)$$

where

W : width of water surface (L)
H : average water depth (L)
u_x : average water depth (LT^{-1})
u_* : shear/friction velocity (LT^{-1})
A : wet area of channel cross-section (L^2)
P : wet perimeter (L)
S : channel bed slope
n : bed roughness coefficient of Manning

Generally, there are numerous available formula for estimating the reaeration coefficient such as O'Connor and Dobbins (1958), Churchill, *et al*. (1962), Owens, *et al.* (1964), Tsivoglou and Neal (1976), USGS - Melching and Flores (1999), and Thackston and Dawson (2001) [30–31]. However, since the reaeration formula proposed by O'Connor and Dobbins (1958) is still widely used by many recent water quality models such as QUAL2Kw, WASP, et cetera, it is then selected and applied here for model simulations.

$$k_a = \frac{3.93 u_x^{0.5}}{H^{1.5}} \quad (13)$$

3.4. Numerical Computation

As the above problems are formulated in the form of partial differential equations (PDEs) and since there have been some evidences of high accuracy of numerical solution given by MATLAB using the pdepe solver function, it was therefore used in this study to conduct the whole simulations. Generally, the necessity introducing this solver method is because it offers more possibilities and flexibilities for both beginners and experts to evaluate or even invent a model since there has been a numerous number of mathematic functions developed inside MATLAB.

Besides it can be applied for broader aspect of numerical computation, in MATLAB, the PDEs with various forms of additional terms can also be easily included and solved as a system. The pdepe solver function basically converts the PDEs to ordinary differential equations (ODEs) using a second order accurate spatial discretization and is applied mostly for initial-boundary value problems consist of systems of parabolic and elliptic PDEs in one space variable and time. In this scheme, the initial conditions are allowed to be space dependent and boundary conditions to be time dependent. In solving system of PDEs, the pdepe solver function is generally written in the form of

$$c\left(x,t,u,\frac{\partial u}{\partial x}\right)\frac{\partial u}{\partial t} = x^{-m}\frac{\partial u}{\partial x}\left(x^m f\left(x,t,u,\frac{\partial u}{\partial x}\right)\right) + s\left(x,t,u,\frac{\partial u}{\partial x}\right) \quad (14)$$

Using pdepe MATLAB, various boundary conditions can also be flexibly formulated either as Dirichlet, Neumann or even Cauchy/Robin. Here, as the downstream boundary of the model is theoretically equal to zero for positive infinity, Neumann condition is considered for all model simulations.

4. Model Applications

The developed numerical model was applied to a straight and uniform rectangular channel for in bank flow case where the hydraulic dimensions used are; channel width B_1 = 5.00 m, roughness Manning coefficient n = 0.020, and bed slope of 0.00001. The flow rate applied for all model simulations was 0.50 m^3s^{-1}. Furthermore, to understand the impact of bacteria on COD removal, the concentration of heterotrophs used in the simulations is 25.00 mgL^{-1}. The autotrophs itself is set as constant of 5.00 mgL^{-1}. To simulate the biodegradation processes, this study has made use of some parameters employed by Jeppsson (1996) for modelling the activated sludge processes under different temperature. The complete parameters values and data are presented in **Tables 1-3**.

5. Results and Discussion

Based on the simulation results obtained, it can be noticed that when the bacterial growth became lower due to limited readily biodegradable COD (S_S), oxygen (O_2) and ammonium nitrogen (S_{NH_4}), the degradation of COD will be much slower (**Figure 1**). As clearly described in **Figure 2**, a contrast characteristic of COD profiles is shown in association with different limiting parameters applied to the model. When the ammonium is included as another limiting parameter, the COD concentration will increase at certain period and be plotted higher than if the model is limited only to substrate and oxygen. In addition, the bacteria will also grow slower and perform lower concentration.

Besides the ammonium nitrogen, other parameters *i.e.* particulate products from COD decay and particulate degradable organic nitrogen will also increase soon after certain time. As shown in **Figure 3**, the ammonium nitrogen starts to decrease at 0.7 day and at the same time it is converted to nitrate nitrogen. Although it is simulated under different limiting parameters but the ammonium·nitrogen will be firstly lowered the lowest point

Table 1. Typical values of ASM-1 parameters at neutral pH.

Model Parameters	20°C	10°C	Literature
$Y_{XH/SS}$	0.67	0.67	0.38 – 0.75
fp	0.08	0.08	-
iX_B	0.09	0.09	-
iX_P	0.06	0.06	-
Y_{NO_3}/XA	0.24	0.24	0.07 – 0.28
$\mu_{\max H}$ (d^{-1})	6.00	3.00	0.60 – 13.20
$\mu_{\max A}$ (d^{-1})	0.80	0.30	0.20 – 1.00
k_{dH} (d^{-1})	0.62	0.20	0.05 – 1.60
k_{dA} (d^{-1})	0.20	0.10	0.05 – 0.20
K_S (mgL^{-1} COD)	20.00	20.00	5 - 225
K_{OH} (mgL^{-1} O_2)	0.20	0.20	0.01 – 0.20
K_{NO_3} (mgL^{-1} N)	0.50	0.50	0.10 – 0.50
K_X mg COD (mg biomass COD)$^{-1}$	0.03	0.01	-
K_{NH_4} (mgL^{-1} N)	1.00	1.00	-
K_{OA} (mgL^{-1} O_2)	0.40	0.40	0.40 – 2.00
k_h (mg biomass COD d)$^{-1}$	3.00	1.00	-
k_{aN} L (mg biomass COD d)$^{-1}$	0.08	0.04	-
η_g dimensionless	0.80	0.80	0.60 – 1.00
η_h dimensionless	0.40	0.40	-

Source: Jeppsson, U (1996)

before they start to increase afterward. The ammonium nitrogen will decrease earlier when it is not included as limiting parameter of the model. Considering the increase of ammonium nitrogen, it can be predicted that some algae may show up during the treatment processes. If the domestic waste contains high concentration of such nutrient, then being accumulated with the end products of this technology, the algae will grow faster. As presented in **Figure 4**, the algae were identified to be enormous spread along the water surface of Xuxi River during biological treatment process within June to August 2009.

When the model is simulated under different water temperature, *i.e.* 10 °C and 20 °C, slower biodegradation process is presented at lower water temperature. As the bacteria work more active under higher temperature, more dissolved oxygen will be required (**Figure 5**). As shown in **Figure 6**, addition of oxygen at the initial stage of treatment process will basically enhance the rate of bacterial growth and removal of COD.

Besides the oxygen would contribute faster biodegradation, the dispersion or mixing parameter also plays crucial role to the process. As both substrate and bacteria will be moderately dispersed to the downstream as the dispersion coefficient increases, longer distance will be required for the recovery of dissolved oxygen concentration

Table 2. Characteristics of natural stream.

Characteristics of natural stream	Value
Stream flow rate, Q_r (m^3s^{-1})	0.50
Stream flow velocity, u_x (ms^{-1})	Eq. (12)
Dispersion coef, E_x (m^2s^{-1})	Eq. (11)
Reaeration rate, k_a (d^{-1})	Eq. (13)
Stream COD (mgL^{-1})	20.00
Stream soluble nitrate N (mgL^{-1})	1.00
Stream soluble ammonia N (mgL^{-1})	1.00
Stream DO, Cr (mgL^{-1})	5.00

Source: Ministry of Environmental Protection of the People's Republic of China and General Administration of Quality Supervision, Inspection and Quarantine of the People's Republic of China (2002).

Table 3. Characteristics of domestic wastewater.

Characteristics of domestic wastewater	Value
Domestic wastewater flow rate, Q_w (m^3s^{-1})	0.3 Qr
Readily biodegradable COD of wastewater, S_S (mgL^{-1})	115.00
Slowly biodegradable COD of wastewater, X_S (mgL^{-1})	150.00
Dissolved oxygen of wastewater, C (mgL^{-1})	0.00
Soluble nitrate N of wastewater, S_{NO_3} (mgL^{-1})	0.00
Soluble ammonia N of wastewater, S_{NH_4} (mgL^{-1})	25.00
Soluble biodegrad. org. N of wastewater, S_{ND} (mgL^{-1})	0.00
Particulate biodegrad. org. N of wastewater, X_{ND} (mgL^{-1})	0.00

Source: Wiesmann, *et al.* (2007).

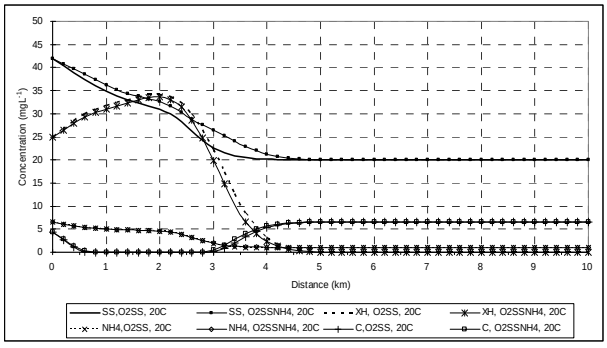

Figure 1. Concentrations of readily biodegradable COD (S_S), heterotrophs (X_H), ammonium nitrogen (S_{NH_4}), and dissolved oxygen (C) for channel with S_o = 0.00001 under different limiting parameters.

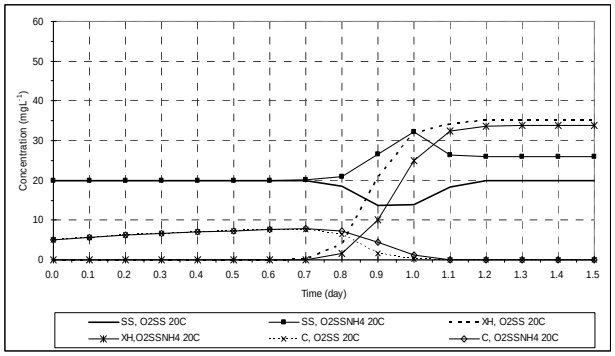

Figure 2. Transient concentrations of readily biodegradable COD (S_S), heterotrophs (X_H), and dissolved oxygen (C) for channel with S_o = 0.0001 under different limiting parameters.

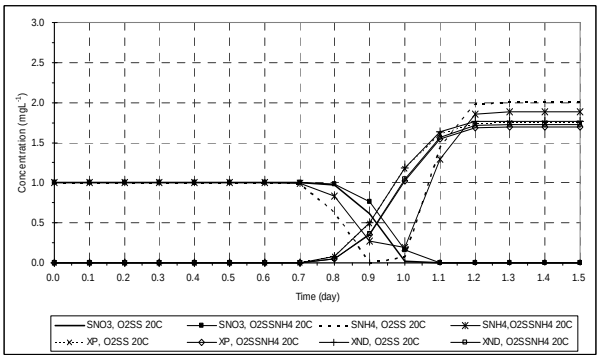

Figure 3. Transient concentrations of nitrate-N (S_{NO_3}), ammonium-N (S_{NH_4}), particulate products from COD decay (X_P), and particulate degradable organic nitrogen (X_{ND}) for channel with S_o = 0.0001 under different limiting parameters.

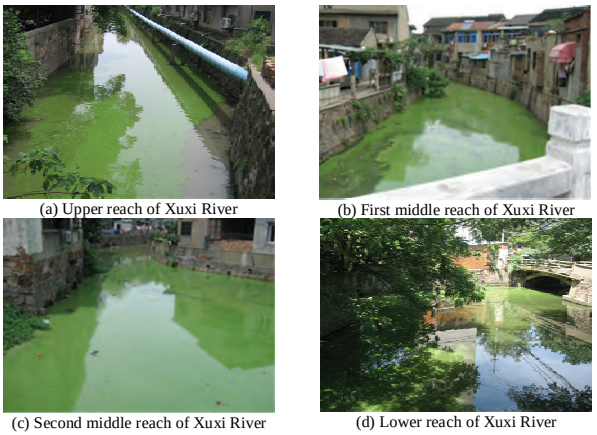

(a) Upper reach of Xuxi River (b) First middle reach of Xuxi River

(c) Second middle reach of Xuxi River (d) Lower reach of Xuxi River

Figure 4. Algae spread along the water surface of Xuxi River during biological treatment.

in the river (**Figure 7**). In practical application, the presence of different dispersion coefficient for each variable modelled will play a crucial role in association with various degree of artificial mixing employed during the process of biological river restoration. As described in **Figure 8**, when higher longitudinal dispersion coefficient applied, the bacteria will start growing at 0.5 day. Lower peak of COD concentration will also occur due to this faster biodegradation.

6. Conclusions

By adopting the concept of stream self purification and activated sludge process, the simulation results showed

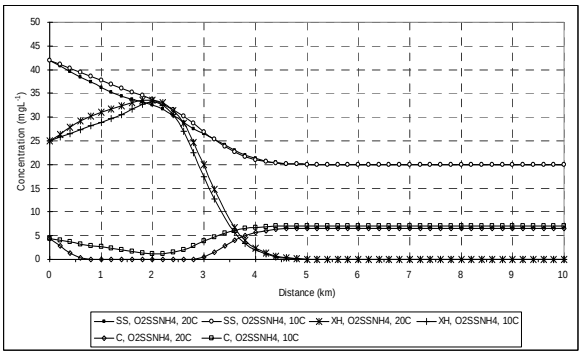

Figure 5. Concentrations of readily biodegradable COD (S_S), hete- rotrophs (X_H), and dissolved oxygen (C) for channel with S_o = 0.0001 under different water temperature.

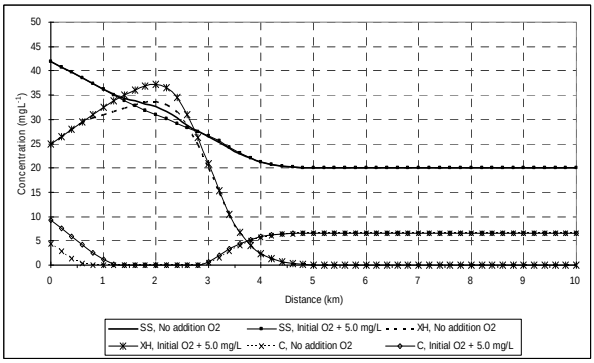

Figure 6. Concentrations of readily biodegradable COD (S_S), hete- rotrophs (X_H), and dissolved oxygen (C) for channel with S_o = 0.0001 under different initial oxygen concentration.

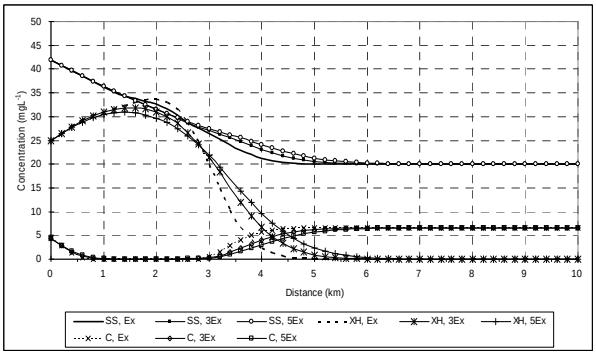

Figure 7. Influences of various values of mixing parameter to the biodegradation process applied to milder channel.

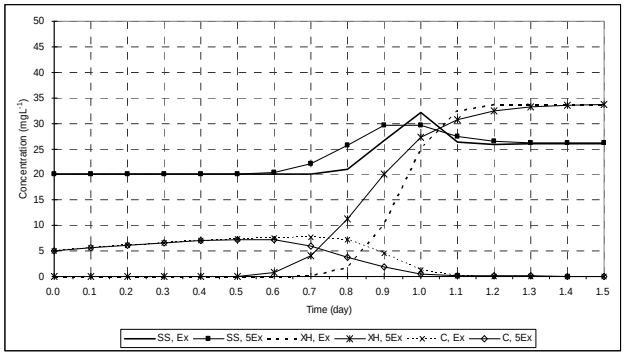

Figure 8. Transient concentrations of readily biodegradable COD (S_S), heterotrophs (X_H), slowly biodegradable COD (X_S), and dissolved oxygen (C) under various dispersion values and modified limiting parameters.

that there are some challenges to effectively apply the technology of bacteria for treating the polluted stream:

- When the ammonium nitrogen is added as limiting parameter to the bacterial growth, under neutral pH and temperature of 20 ^{o}C, the model showed that the COD concentration increases at certain period and is plotted higher at the end. Besides having additional values of some parameters such as particulate products from COD decay and particulate degradable organic nitrogen, the ammonium nitrogen will also increase after it reaches the lowest concentration.
- As consequence of having more ammonium nitrogen, there is a potency that algae may show up during the treatment process. This phenomenon is in fact strongly supported by some evidences obtained from the practical works of such technology under restoration and monitoring project of Xuxi River within June to August 2009.
- Under lower water temperature, the model simulations showed slower biodegradation process.
- Longer distance is required for the recovery of dissolved oxygen as the dispersion coefficient increases. Because of limited oxygen available in polluted stream, extra oxygen injected to the water column at the beginning of treatment may somehow help better bacterial growth and faster biodegradation processes.
- Although the alkalinity has not being modelled in this study yet, but it is realized that pH would influence the activity of bacteria and some equilibria. In addition, some toxic pollutants may also resist the growth of bacteria. Sediment, as previously reported in many works, is a crucial parameter to be included in the model especially for better understanding of nitrification process. In further research works, diversity of heterotrophs and the effects of limitations of nitrogen, phosphorus and other inorganic nutrients on the removal of organic substrate and on cell growth must also be considered.
- As soon as the field data is completely collected, calibration and validation of the model are crucial to be done.

7. References

[1] K. V. Ellis, "Surface water pollution and its control," the Macmillan Press Ltd, London, 1989.

[2] G. H. Jirka and V. Weitbrecht, "Mixing models for water quality management in rivers: Continuous and instantaneous pollutant releases," in P. M. Rowinski and W. Czernuszenko, Eds., "Water quality hazards and dispersion of pollutants," Springer, New York, pp. 1–34, 2005.

[3] M. Campolo, P. Andreussi, and A. Soldati, "Water quality control in the river Arno, technical note," Water Resources, Vol. 36, No. 10, pp. 2673–2680, 2002.

[4] P. R. Kannel, S. Lee, Y. S. Lee, S. R. Kanel, and G. J. Pelletier, "Application of automated QUAL2Kw for water quality modeling and management in the Bagmati River, Nepal," Ecological Modelling, Vol. 202, No. 3–4, pp. 503–517, 2007.

[5] D. Yudianto and Y. B. Xie, "The feasibility of bacteria application for treating the polluted urban stream from the perspective of numerical modelling," in Press for Polish Journal of Environmental Studies, 2010.

[6] I. Gupta, S. Dhage, A. A. Chandorkar, and A. Srivastav, "Numerical modeling for thane creek," Environmental Modelling and Software, Vol. 19, No. 6, pp. 571–579, 2004.

[7] A. K. Misra, P. Chandra, and J. B. Shukla, "Mathematical modeling and analysis of the depletion of dissolved oxygen in water bodies," Nonlinear Analysis: Real World Applications, Vol. 7, No. 5, pp. 980–996, 2006.

[8] M. Green, I. Safray, and M. Agami, "Constructed wetlands for river reclamation: Experimental design, start-up and preliminary results," Bioresource Technology, Vol. 55, No. 2, pp. 157–162, 1996.

[9] S. R. Jing, Y. F. Lin, D. Y. Lee, and T. W. Wang, "Nutrient removal from polluted river water by using constructed wetlands," Bioresource Technology, Vol. 76, No. 2, pp. 131–135, 2001.

[10] D. F. Juang and P. C. Chen, "Treatment of polluted river water by a new constructed wetland," International Journal of Environmental Science and Technology, Vol. 4, No. 4, pp. 481–488, 2007.

[11] J. B. Zhou, M. M. Jiang, B. Chen, and G. Q. Chen, "Emergy evaluations for constructed wetland and conventional wastewater treatments," Communications in Nonlinear Science and Numerical Simulation, Vol. 14, No. 4, pp. 1781–1789, 2007.

[12] Z. M. Chen, B. Chen, J. B. Zhou, Z. Li, Y. Zhou, X. R. Xi, C. Lin, and G. Q. Chen, "A vertical subsurface-flow constructed wetland in Beijing," Communications in Nonlinear Science and Numerical Simulation, Vol. 13, No. 9, pp. 1986–1997, 2008.

[13] H. S. Cheng, M. K. Yusoff, B. Shutes, and M. Mansor, "Nutrient removal in a pilot and full scale constructed wetland, Putrajaya city, Malaysia," Journal of Environ-

mental Management, Vol. 88, No. 2, pp. 307–317, 2008.

[14] Q. Y. Nie, Y. B. Xie, J. Zhuang, and L. L. She, "Cyanobacter ia control using microorganism," World Sci-Tech Research and Development," Vol. 30, No. 4, pp. 430–432, 2008.

[15] J. Liao, Y. B. Xie, X. C. Zong, and G. J. Cao, "Pilot study on treatment of complicated chemical industrial effluent with CABRM process," Pollution Control Technology, Vol. 21, No. 1, pp. 11–15, 2008.

[16] D. Yudianto and Y. B. Xie, "Numerical modelling perspectives on the identification of initial challenges of polluted urban stream restoration using bacterial technology," Submitted to International Journal of Environmental Research, unpublished.

[17] Q. H. Wu, R. D. Zhang, S. Huang, and H. J. Zhang, "Effects of bacteria on nitrogen and phosphorus release from river sediment," Journal of Environmental Sciences, Vol. 20, pp. 404–412, 2008.

[18] J. Kiusalaas, "Numerical method in engineering with MATLAB," Cambridge University Press, New York, 2005.

[19] S. M. Libelli, G. Pacini, C. Barresi, E. Petti, and F. Sinacori, "An interactive georeferenced water quality model," in Proceedings of the Fifth International Conference on Hydroinformatics, IWA Publishing and the Authors, Cardiff, UK, pp. 451–456. 2002.

[20] E. Holzbecher, "Environmental modelling using MATLAB," Springer, Berlin, 2007.

[21] M. Yuceer, E. Karadurmus, and R. Berber, "Simulation of river streams: Comparison of a new technique with QUAL2E," Mathematical and Computer Modelling, Vol. 46, No. 1, 2, pp. 292–305, 2007.

[22] D. Yudianto and Y. B. Xie, "Contaminant distribution under non-uniform velocity of steady flow regimes," Journal of Applied Science in Environmental Sanitation, Vol. 3, No. 1, pp. 29–40, 2008.

[23] D. Yudianto and Y. B. Xie, "The development of simple DO sag curve in lowland non-tidal river using MATLAB," Journal of Applied Science in Environmental Sanitation, Vol. 3, No. 2, pp. 80–98, 2008.

[24] D. Yudianto and Y. B. Xie, "A comparison of some numerical methods in solving 1-D steady state advection dispersion reaction equation by using MATLAB," Online Published in Civil Engineering and Environmental System, In Press for 2010.

[25] S. M. Kashefipour and R. A. Falconer, "Longitudinal dispersion coefficients in natural channels," Water Research, Vol. 36, No. 6, pp. 1596–1608, 2002.

[26] S. Wallis and R. Manson, "On the theoretical prediction of longitudinal dispersion coefficients in a compound channel," In W. Czernuszenko and P. M. Rowinski, Eds., "Water quality hazards and dispersion of pollutants," Springer, New York, pp. 69–84, 2005.

[27] U. Jeppsson, "Modelling aspects of wastewater treatment processes," Ph.D. Dissertation, Lund Institute of Technology, ISBN 91-88934-00-4, 1996.

[28] U. Wiesmann, I. S. Choi, and E. M. Dombrowski, "Fundamentals of biological wastewater treatment," Willey-VCH Verlag Gmbh & Co. KGaA, Weinheim, 2007.

[29] G. L. Jones, "A mathematical model for bacterial growth and substrate utilization in the activated sludge process," in A. James, Ed., "Mathematical models in water pollution control," John Willey and Sons, Avon, pp. 265–279, 1978.

[30] J. L. Schnoor, "Environmental modeling: Fate and transport of pollutants in water, air, and soil," John Wiley and Sons, New York, 1996.

[31] G. Pelletier and S. Chapra, "A modeling framework for simulating river and stream water quality," Environmental Assessment Program, Olympia, Washington, pp. 98504–7710, 2006.

[32] Ministry of Environmental Protection of the People's Republic of China and General Administration of Quality Supervision, Inspection and Quarantine of the People's Republic of China, Environmental Quality Standard of People's Republic of China for Surface Water (GB3838-2002), Beijing, 2002.

J. Water Resource and Protection, **2010, 2, 235-244**
doi:10.4236/jwarp.2010.23027 Published Online March 2010 (http://www.scirp.org/journal/jwarp)

Photocatalytic Degradation of Isoproturon Pesticide on C, N and S Doped TiO_2

Police Anil Kumar Reddy, Pulagurla Venkata Laxma Reddy, Vutukuri Maitrey Sharma, Basavaraju Srinivas, Valluri Durga Kumari, Machiraju Subrahmanyam*
Inorganic and Physical Chemistry Division, Indian Institute of Chemical Technology, Hyderabad, India
E-mail: *subrahmanyam@iict.res.in*
Received December 15, 2009; *revised December* 29, 2009; *accepted January* 22, 2010

Abstract

TiO_2 doped with C, N and S (TCNS photocatalyst) was prepared by hydrolysis process using titanium isopropoxide and thiourea. The prepared samples were characterized by X-ray diffraction (XRD), scanning electron microscopy (SEM), X-ray photo electron spectroscopy (XPS), BET surface area, FTIR and diffuse reflectance spectra (DRS). The results showed that the prepared catalysts are anatase type and nanosized particles. The catalysts exhibited stronger absorption in the visible light region with a red shift in the adsorption edge. The photocatalytic activity of TCNS photocatalysts was evaluated by the photocatalytic degradation of isoproturon pesticide in aqueous solution. In the present study the maximum activity was achieved for TCNS5 catalyst at neutral pH with 1 g L^{-1} catalyst amount and at 1.14 x 10^{-4} M concentration of the pesticide solution. The TCNS photocatalysts showed higher phtocatalytic activity under solar light irradiation. This is attributed to the synergetic effects of red shift in the absorption edge, higher surface area and the inhibition of charge carrier recombination process.

Keywords: Isoproturon, Pesticide Degradation, C, N and S Doped TiO_2, Visible Light Active Catalysts

1. Introduction

Organic compounds are widely used in industry and in daily life, have become common pollutants in water bodies. As they are known to be noxious and carcinogenic, an effective and economic treatment for eliminating the organic pollutants in water has been found to be an urgent demand. The treatment of water contaminated with recalcitrant compounds is an important task to attend every country in the world. To attain the standards, there is a need for new treatment. It is very much important that the treatment should be safe and economically feasible. The wastewater purification technologies are classified as physical, biological, and chemical methods. All the above processes are having some flaws during their usage. The limitations include relative slow degradation, incomplete transformations and their inability to cover many organic compounds that do not occur naturally. Several chemical processes which use oxidizing agents such as ozone, hydrogen peroxide, H_2O_2/UV, H_2O_2/ozone/UV etc. have been carried out to mineralize many synthetic organic chemicals. Sometimes intermediates formed are more hazardous than the parent compound. Therefore, alternative technologies are in demand for development to treat recalcitrant compounds in wastewater effluents. Photocatalytic process has been found to be very active in the treatment of wastewaters for the mineralization of broad range of organic pollutants. Thus, heterogeneous mediated photocatalysis treatment technique gained noteworthy importance for the treatment of wastewaters.

Semiconductor mediated photocatalytic oxidation of water pollutants offers a facile and cheap method. Among various oxide semiconductor phtocatalysts, TiO_2 has proved to be the most suitable catalyst for wide spread environmental applications because of its biological and chemical inertness, strong oxidizing power, non toxicity, long term stability against photo and chemical corrosion [1,2]. However, its applications seems to be limited by several factors, among which the most restrictive one is the need of using an UV wavelength of < 387 nm, as excitation source due to its wide band gap (3.2 eV), and this energy radiation availability is less than 5 % in solar light.

Several works reported that doping TiO_2 with anions such as carbon, nitrogen, sulphur, boron and fluorine shifts the optical absorption edge of TiO_2 towards lower energy, there by increasing the photocatalytic activity in visible light region [3–9]. The preparation of doped TiO_2 resulting in a desired band gap narrowing and an enhancement in the phtocatalytic activity under visible light.

In earlier reported studies, N doping of TiO_2 is achieved by different methods such as sputtering of TiO_2 in a gas mixture followed by annealing at higher temperatures [3], treating anatase TiO_2 powders in an NH_3/ Ar atmosphere [10], solution based methods like precipitation [11,12], sol-gel [13,14], solvothermal [15], hydrothermal processes [16] and direct oxidation of the dopent containing titanium precursors at appropriate temperatures [17]. In our earlier studies, we have concentrated on degradation of isoproturon using TiO_2 supported over various zeolites. The main idea of using Zeolite support for TiO_2 is to enhance the adsorption capacity of the pollutant over the combinate photo catalyst systems [18–20]. In the present case the main focus is on shifting the absorption edge of TiO_2 to visible light region by introducing C, N and S into the TiO_2 lattice structure. The present results obtained provides a simple route for the preparation of C, N and S doped TiO_2 with enhanced photocatalytic activity under visible light irradiation for isoproturon pesticide degradation.

2. Experimental Details

2.1. Materials and Methods

All the chemicals in the present work are of analytical grade and used as such without further purification. Isoproturon (IPU) (>99% pure, Technical grade) was obtained from Rhône-Poulenc Agrochemie, France and titanium isopropoxide was from Sigma-Aldrich chemie GmbH, Germany. HCl, NaOH and acetonitrile were obtained from Ranbaxy Limited, India. All the solutions were prepared with deionized water obtained using a Millipore device (Milli-Q).

2.2. Preparation of C, N and S Doped TiO_2 Photocatalyst

C, N and S doped TiO_2 photocatalyst was prepared by a simple hydrolysis process using titanium isopropoxide as the precursor for titanium and thiourea as the source for carbon, nitrogen and sulphur [26,34]. In a typical preparation, 10 mL of titanium isopropoxide solution was mixed with 30 mL of isopropyl alcohol solution. This solution was added drop wise to 20 mL deionized water containing in a 250 mL beaker. The solution was thoroughly mixed using a magnetic stirrer for 4 h. To this solution, required amount of thiourea, dissolved in 5 mL deionized water was added. The mixture was stirred for 6 h and dried in oven at 80 ^{0}C for 12 h. The solid product formed was further calcined at 400 ^{0}C temperature for 6 h in air to get C, N, and S doped TiO_2 photocatalyst. The weight (%) of thiourea doped TiO_2 was controlled at 0, 1, 3, 5, 10 and 15 wt% and the samples obtained were labeled as TCNS0, TCNS1, TCNS3, TCNS5, TCNS10 and TCNS15 respectively.

2.3. Characterization

The catalysts were characterized by various techniques like XRD, XPS, FTIR, SEM, BET surface area and UV-Vis DRS. The XRD of catalysts were obtained by Siemens D 5000 using Ni Filtered Cu K α radiation ($\sqrt{}$ = 1.5406 A^0) from 2θ = 1-60^0. XPS spectra were recorded on a KRATOS AXIS 165 equipped with Mg Kα radiation (1253.6 eV) at 75 W apparatus using Mg Kα anode and a hemispherical analyzer, connected to a five channel detector. The C 1s line at 284.6 eV was used as an internal standard for the correction of binding energies. The Fourier transform-infra red spectra (FTIR) were recorded on a Nicolet 740 FTIR spectrometer (USA) using KBr self-supported pellet technique. The SEM analysis samples were mounted on an aluminum support using a double adhesive tape coated with gold and observed in Hitachi S-520 SEM unit. BET data was generated on (Auto Chem) Micro Maritics 2910 instrument. UV–Vis diffused reflectance spectra (UV–Vis DRS) was from UV–Vis Cintra 10e spectrometer.

2.4. Photocatalytic Experiments

IPU solution (0.114 mM) was freshly prepared by dissolving in double distilled water. All the phtocatalytic experiments were carried out at same concentration until unless stated. The pH of the solution was adjusted with HCl and NaOH. Prior to light experiments, dark (adsorption) experiments were carried out for better adsorption of the herbicide on the catalyst. For solar experiments, isoproturon solution of 50 mL was taken in an open glass reactor with known amount of the catalyst. The solution was illuminated under bright solar light. Distilled water was added periodically to avoid concentration changes due to evaporation. The solar experiments were carried out during 10.00 A.M. to 3.00 P.M. in May and June 2009 at Hyderabad.

2.5. Analyses

The IPU degradation was monitored by Shimadzu SPD-20A HPLC using C-18 phenomenex reverse phase column with acetonitrile/water (50/50 v/v %) as mobile phase at a flow rate of 1 mL min^{-1}. The samples were collected at regular intervals, filtered through Millipore

micro syringe filters (0.2 μm).

3. Results and Discussion

3.1. Characterization

3.1.1. XRD

To investigate the phase structure of the prepared samples XRD was used and the results are shown in **Figure 1**. It can be seen that TCNS exhibits only the characteristic peaks of anatase (major peaks at 25.41^0, 38^0, 48^0, 55^0) and no rutile phase is observed. The results are in good agreement with earlier studies [21]. By applying Debye-Scherrer equation, the average particle size of the TCNS catalysts is found to be about 3.8 to 5.8 nm. It can be inferred that the ratio of thiourea to titania slightly influence the crystallization of the mesoporous titania. Also the peak intensity of anatase decreases and the catalyst becomes more amorpous. It might be due to the fact that the doped nonmetals can hinder the phase transition (anatase to rutile) and restricts the crystal growth. It is noteworthy that, even the doped samples exhibit typical structure of TiO_2 crystal without any detectable dopant related peaks. This may be caused by the lower concentration of the doped species, and moreover, the limited dopants may have moved into either the interstitial positions or the substitutional sites of the TiO_2 crystal structure [22,23].

3.1.2. XPS

To investigate the chemical sates of the possible dopants incorporated into TiO_2, Ti2p, O1s, C1s, N1s, and S2p binding energies are studied by measuring the XPS spectra. The results are shown in **Figure 2**.

The high resolution spectra of $Ti2p_{3/2}$ and $Ti2p_{1/2}$ core levels are given in the **Figure 2(a)**. The binding energy for the $Ti2p_{3/2}$ and $Ti2p_{1/2}$ core level peaks for TCNS0 appeared at 458.8 and 464.5 eV respectively which are attributed to O-Ti-O linkages in TiO_2. $Ti2p_{3/2}$ and $Ti2p_{1/2}$ core level peaks for TCNS5 are observed at 458.4 and 464.1 eV with a decrease in the binding energy value compared to TiO_2 indicating that the TiO_2 lattice is considerably modified due to C, N and S doping [24].

The chemical environment of carbon is investigated by the XPS of C1s core levels as shown in the **Figure 2(b)**. Three peaks are observed for the C1s at 284.6, 286.2 and 288.8 eV. The first peak observed at 284.6 eV is assigned to elemental carbon present on the surface, which is also in agreement with the reported studies [25]. The second and third peaks at 286.2, 288.8 eV are attributed to C-O and C=O bonds respectively [21,26].

The high resolution XPS spectra of N1s core level is shown in **Figure 2(c)**. Generally, N1s core level in N doped TiO_2 shows binding energies around 369-397.5 eV that are attributed to substitutionally doped N into the TiO_2 lattice or β nitrogen [3,27]. N1s peaks, with high intensity observed at and above 400 eV are assigned to NO, N_2O, NO_2^-, NO_3^-. Sakthivel *et al.* [28] observed an intense peak at 400.1 eV that was assigned to hyponitrile species and concluded that the higher binding energy is due to the lower valence state of N in N doped TiO_2. Many researches pointed out that intense peak at 400 eV are due to oxidized nitrogen like Ti-O-N or Ti-N-O linkages. Dong *et al.* [26] observed three peaks of N1s at 397.8, 399.9 and 401.9 eV and has attributed to N-Ti-N, O-Ti-N and Ti-N-O linkage respectively. Recently, Gopinath observed N1s binding energy at 401.3 eV and claimed the presence of Ti-N-O linkage on the surface of N doped TiO_2 nano particles [29]. **Figure 2(c)** shows the N1s spectra of TCNS5 catalyst and three peaks are observed at 397.8, 399.9 and 401.2 eV. Taking the literature support, here in the present investigation, the first peak at 397.8 eV is attributed to N-Ti-N linkages and the second and third peaks at 399.9 and 401.2 eV are ascribed to O-Ti-N, Ti-N-O linkages in the TiO_2 lattice respectively.

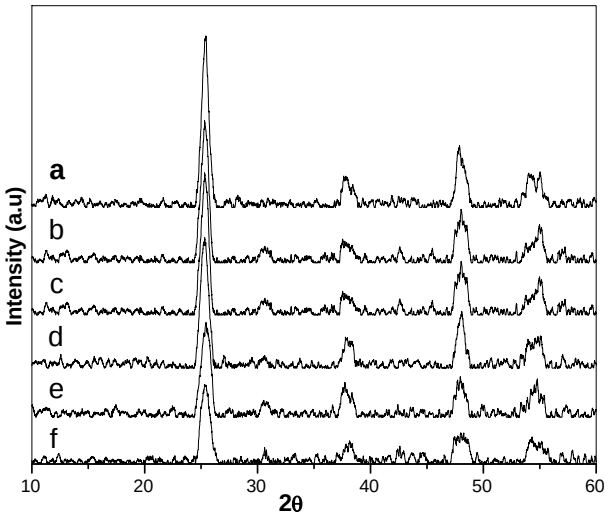

Figure 1. XRD patterns of TCNS catalysts: (a) TCNS0, (b) TCNS1, (c) TCNS3, (d) TCNS5, (e) TCNS10, (f) TCNS15.

The O1s spectra of TCNS0 and TCNS5 are shown in **Figure 2(d)**. The O1s peak for TCNS0 is observed at 529.7 and 531.6 eV. The corresponding values are 530.2 and 531.7 eV for the TCNS5 sample. The first peak is mainly attributed to the O-Ti-O linkage in the TiO_2 lattice, and the second peak is closely related to the hydroxyl groups (-OH) resulting mainly from chemisorbed water. It can be seen that the content of surface hydroxyl groups is much higher in the TCNS5 sample than in the TCNS0 sample. The increase in surface hydroxyl content is advantageous for trapping more photogenerated holes and thus preventing electron–hole recombination [26].

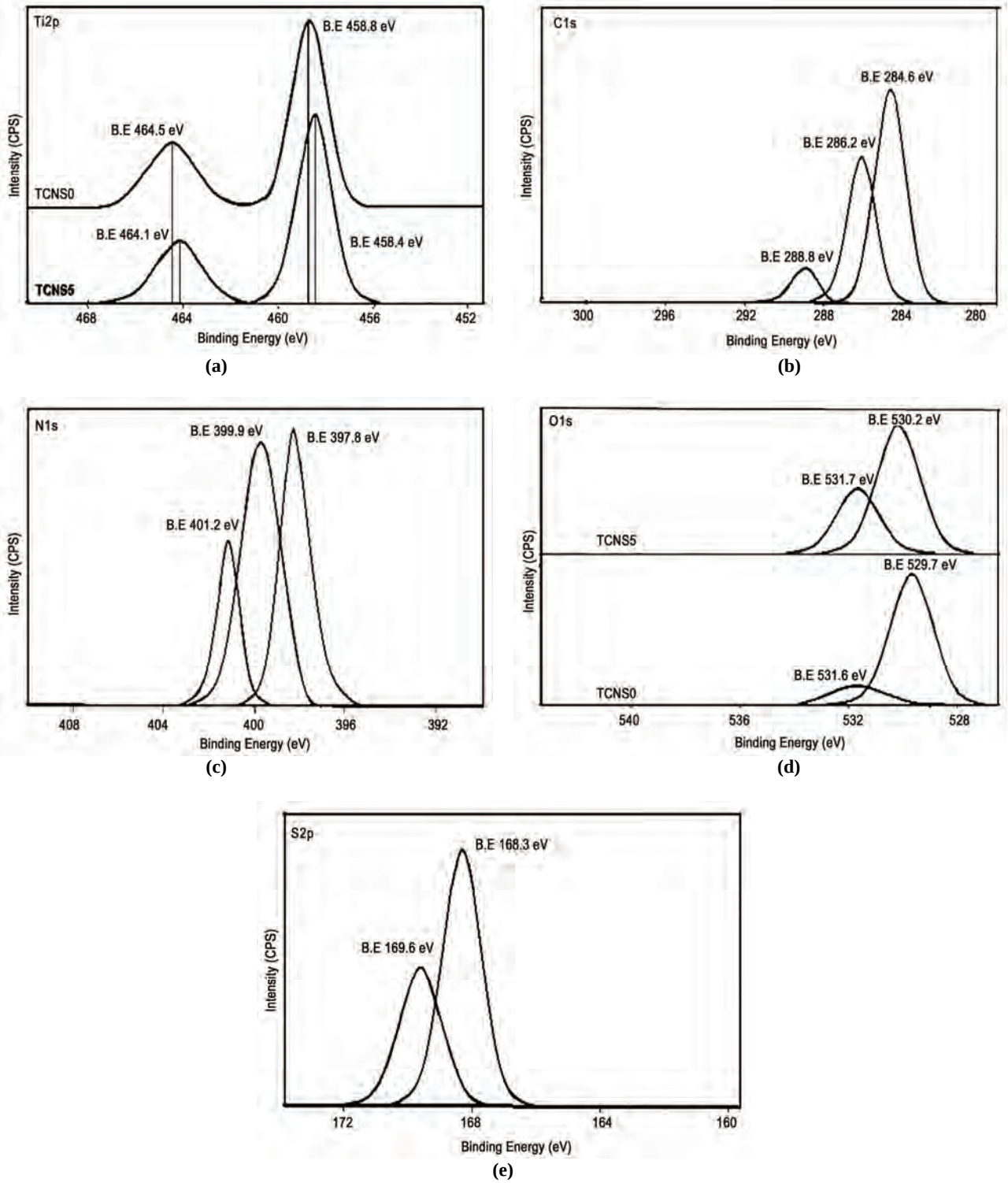

Figure 2. High resolution XPS of TCNS5 catalyst: (a)Ti2p, (b)C1s, (c)N1s, (d)O1s, (e)S2p.

S2p XPS spectra for TCNS5 are shown as **Figure 2(e)**. The oxidation state of the S-dopant is dependent on the preparation routes and sulfur precursors. Previous studies have reported that if thiourea was used, the substitution of Ti^{4+} by S^{6+} would be more favorable than replacing O^{2-} with S^{2-} [4]. S2p spectra can be resolved into four

peaks, $S2p_{1/2}^{6+}$, $S2p_{3/2}^{6+}$, $S2p_{1/2}^{4+}$ and $S2p_{3/2}^{4+}$. The **Figure 2(e)** shows two peaks at 168.3 and 169.6 eV corresponding to $S2p_{3/2}^{6+}$, $S2p_{1/2}^{6+}$ binding energies [30]. It is clear from the figure that S was doped mainly as S^{6+} and not S^{4+}or S^{2-} peaks. The sulfur doping further can be substantiated by the decrease in binding energies of the $Ti2p_{1/2}$ and $Ti2p_{3/2}$ of TCNS5 sample compared to the binding energies $Ti2p_{1/2}$ and $Ti2p_{3/2}$ of the TCNS0 sample respectively (**Figure 2(a)**). This may be caused due to the difference of ionization energy of Ti and S. Therefore, it could be concluded that the lattice titanium sites of TiO_2 were substituted by S^{6+} and formed as a new band energy structure.

3.1.3. FTIR Spectra

Figure 3 shows the FTIR spectra of TCNS0 and TCNS5 catalysts calcined at 400 ˚C. The absorption bands 2800–3500 cm^{-1}, 1600–1680 cm^{-1} are assigned to the stretching vibration and bending vibration of the hydroxyl group respectively present on the surface of TiO_2 catalyst [31,32]. The presence of surface hydroxyl groups are substantiated by XPS of O1s spectra (**Figure 2(d)**). The band around 1730 cm^{-1} is attributed to carbonyl group and bands at 1130, 1040 cm^{-1} are corresponding to nitrite and hyponitrite groups present in TCNS5 and they are absent in TCNS0 which shows successful doping of nitrogen into the lattice of TiO_2 [33,34]. No peak corresponding to NH_4^+ absence (3189 and 1400 cm^{-1}) shows that N is present only in the form of nitrite and hyponitrite species [32].

3.1.4. SEM

The surface morphology of TCNS photocatalyst is studied by scanning electron microscopy and the micrographs are presented in **Figure (4)**. The samples appeared are agglomeration of smaller particles. From this image, we can see that the surface is rough and large number of pores found to be seen. SEM images for the undoped (TCNS0) and CNS-doped (TCNS5) shows that

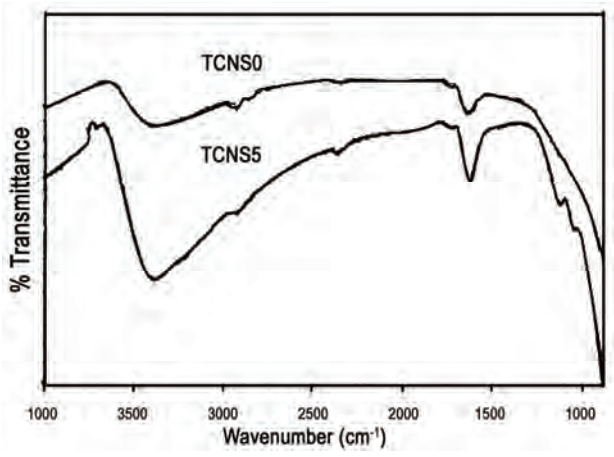

Figure 3. FTIR spectra of TCNS catalysts.

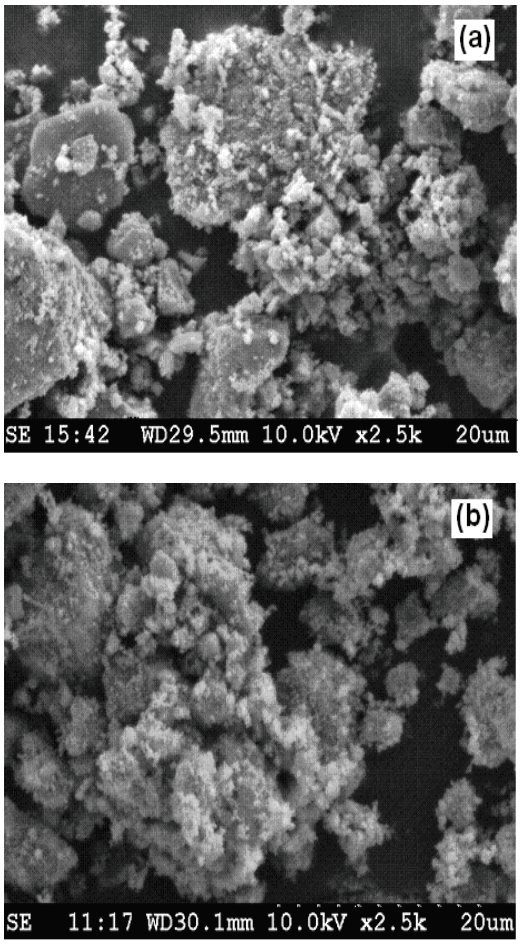

Figure 4. SEM images of (a) TCNS0 and (b) TCNS5 catalysts.

the particle morphology seems to be as spherical in both the images and there is no considerable change in morphology of both. The photograph of thiourea doped TiO_2 (TCNS5) sample is exhibiting well-dispersed crystals and the particle is homogeneous with the formation of fine and well dispersed particles.

3.1.5. UV-VIS DRS

The UV-Vis diffuse reflectance spectra (DRS) of TCNS catalysts are shown in **Figure 5**. It is seen from **Figure 5(a)** that the undoped TiO_2 nano catalyst (TCNS0) showed strong absorption band around 380 nm in the ultraviolet region. But, TCNS sample is showing absorbance at 400-470 nm with red shift (about 100 nm) towards visible region. This shift in the absorption edge decreases the direct band gap of TCNS catalyst compared to undoped TiO_2 (TCNS0) and this may be due to the insertion of C, N and S into the TiO_2 lattice [13,25,35]. Furthermore, the red shift in the DRS band increases with the increase in doped elements content into TiO_2 lattice. Band gap energy (Eg value) of all the catalysts is estimated from the plot of absorbance versus photon energy (hv). The

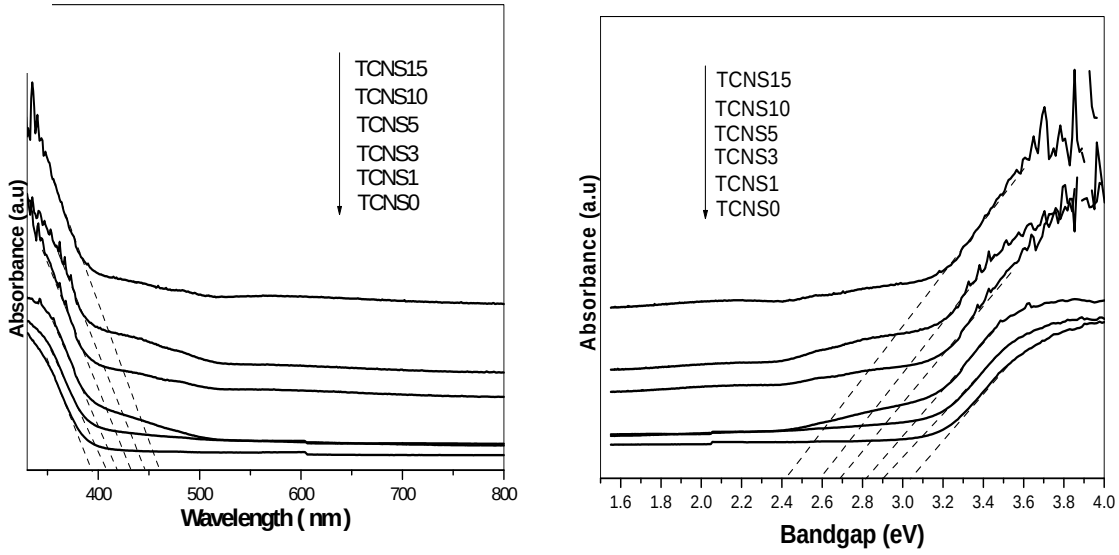

(a) (b)

Figure 5. UV-Vis diffusion reflectance spectra of TCNS catalysts. (a) Absorbance versus Wavelength; (b) Absorbance versus Bandgap.

absorbance is extrapolated to get the bandgap energy for the TCNS catalyst with good approximation as observed in **Figure 5(b)**. The estimated bandgap energies of TCNS0, TCNS1, TCNS3, TCNS5, TCNS10 and TCNS15 are 3.05, 2.91, 2.82, 2.7, 2.6 and 2.41 respectively. From the DRS results, it is clear that the C, N and S doping can shift the absorption edge of TiO_2 to the visible range and reduce the band gap, which is beneficial for improving the photo absorption and ultimately photo catalytic performance of TiO_2.

3.1.6. BET Surface Area

The surface area of TCNS catalysts calcined at 400 ^{0}C is shown in **Table 1**. The TCNS catalysts are showing high surface area. The high surface area of the prepared catalysts is due to nanosize of the particles. It is also observed that the surface area of the catalysts increases with the increase in the ratio of thiourea to TiO_2. This can be attributed to decreasing of the crystallite sizes, as discussed in XRD analysis.

3.2. Photocatalytic Activity

3.2.1. Adsorption Studies

Prior to photocatalytic experiments adsorption and photolysis studies are carried out. The isoproturon solution was kept in dark without catalyst for 10 days and no degradation is observed. Fifty milligrams of the catalyst in 50 mL of isoproturon (1.14×10^{-4} M) solution is allowed under stirring in dark. Aliquots were withdrawn at regular intervals and the change in isoproturon concentration is monitored by HPLC. Maximum adsorption is reached within 30 min for all the catalysts prepared. This illustrates the establishment of adsorption equilibrium as 30 min and is chosen as the optimum equilibrium time for all the future experiments. The photolysis (without catalyst) experiment is carried out under the solar light taking 50 mL of isoproturon solution in glass reactor and only 2–4 % of degradation is observed after 10 h of solar irradiation.

3.2.2. Determination of Thiourea Loading over TiO_2

To compare the phtotcatalytic activity of the as-prepared samples, phtocatalytic degradation of isoproturon under solar light irradiation is performed. All the studies are carried out at 1 g L^{-1} catalyst amount in 1.14×10^{-4} M isoproturon solution. The photocatalytic activity of TCNS catalysts under solar light irradiation is shown in **Figure 6**. Among all the catalysts prepared, TCNS5 is showing better phtocatalytic activity and complete degradation. The visible light activity of the samples has increased gradually with the increasing amount of dopent and it reaches optimum at 5 wt % loading (TCNS5) and further increase results an activity decrease gradually.

Table 1. BET surface area and particle size of the TCNS catalysts.

Catalyst	Particle size by XRD (nm)	BET surface area (m^2/g)
TCNS0	5.8	80.53
TCNS1	5.2	82.47
TCNS3	5.1	83.97
TCNS5	4.6	89.14
TCNS10	4.2	92.98
TCNS15	3.8	124.28

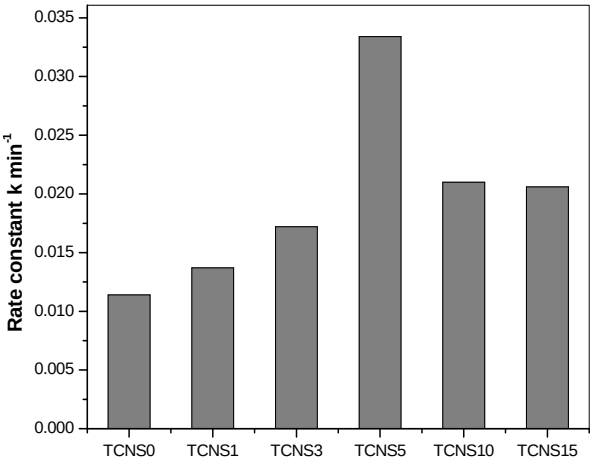

Figure 6. Photocatalytic activity of C, N and S doped TiO_2 for the degradation of isoproturon aqueous solution (1.14×10^{-4} M) under solar-light irradiation.

The different samples photo catalytic activity can be attributed to the following factors. It is known that the doping of C, N and S elements in titania brings visible light absorption photocatalytic activity of titania. It can be seen from the DRS spectra that C, N, and S doping resulted in an intense increase in absorption in the visible light region and a red shift in the absorption edge of the titania (**Figure 5(a)**). The band-gap narrowing of titania by C, N, S doping lead to enhanced photocatalytic activity of the titania under visible light. Because the prepared doped samples can be activated by visible light, thus more electrons and holes can be generated and participate in the photocatalytic redox reactions [21]. All together, the C, N, and S doped samples show much higher photocatalytic activity than undoped tiantia. But we can also see that at higher loadings photocatalytic activity of TCNS samples has decreased though they show more red shift in the absorption edge. It might be due to the fact that, the excess dopent acts as recombination centers which facilitates electron-hole recombination thus lowering the activity. So, the photocatalytic activity is depressed to a certain extent. To conclude, the higher activity of the TCNS5 sample can be ascribed to the high surface area, strong adsorption in visible region and lower recombination of electron-hole pair due to high concentration of surface hydroxyl groups (**Figure 2(d)**) which can trap the photo generated holes and thus decreasing the electron hole recombination process [26].

3.2.3. Effect of Substrate Concentration

The effect of substrate concentration is an important parameter for photocatalytic degradation activity over known catalyst amount. The 7.28×10^{-5}, 1.14×10^{-4} and 2.42×10^{-4} M concentrations of isoproturon are studied over TCNS5 catalyst with 1.0 g L^{-1} catalyst amount. It is seen from **Figure 7** a slight difference in degradation rate over titania supported catalyst for 7.28×10^{-5}, 1.14×10^{-4} M concentrations are observed compared to 2.42×10^{-4} M. This indicates, at higher concentrations OH radicals produced by the catalyst are not sufficient to degrade the pollutant molecules which are adsorbed or near to the catalyst surface. Hence, 1.14×10^{-4} M solutions is chosen for the degradation as there is an equilibrium between adsorption of reactant molecules and the generation of OH radicals from the active sites.

3.2.4. Effect of Catalyst Amount

The catalyst amounts 0.5, 1.0 and 2.0 g L^{-1} of TCNS5 are investigated for effective isoproturon degradation (**Figure 8**). It is observed that, increasing amounts 0.5–1.0 g L^{-1}, the photocatalytic activity has increased and at the higher amounts the activity trend is not encouraging. This is due to the higher amounts of the catalyst makes the solution turbid which obstructs the light path into the solution and inturn reducing the formation of OH radicals. In the present study, 1.0 g L^{-1} is found to be the optimum catalyst amount for efficient degradation of isoproturon.

3.2.5. Effect of pH

The effect of pH is an important parameter because it commands the surface charge properties of the catalyst and therefore the adsorption of the pollutant. The pH studies at 3–10 are carried over TCNS5 catalyst using 1.0 g L^{-1} of 1.14×10^{-4}M isoproturon solution. The adsorption capacity of the catalyst in different pH ranges is not much affected due to the non-ionic nature of isoproturon. The results depicted in **Figure 9** are showing that at neutral pH, the rate of degradation is faster compared to acidic or basic medium [36]. This may be due to the non-ionic nature of isoproturon. In basic medium, there is a slight increase in degradation rate and is observed when compared to the acidic medium. This may be because, the OH radicals are mainly attacking methyl groups

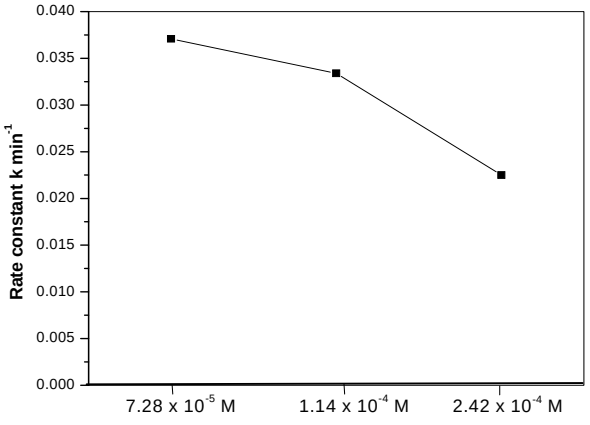

Figure 7. Effect of initial concentration on the rate of solar photocatalytic degradation of isoproturon over TCNS5.

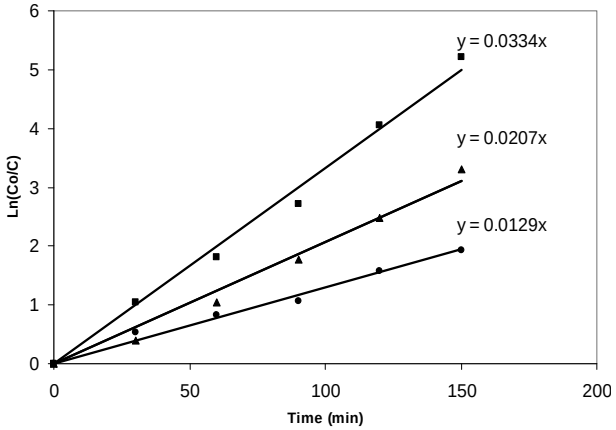

Figure 8. Effect of catalyst amount on photocatalytic degradation of isoproturon over TCNS5 catalyst under solar light irradiation: 0.5 g L^{-1} (●), 1g L^{-1}(■) and 2 g L^{-1} (▲).

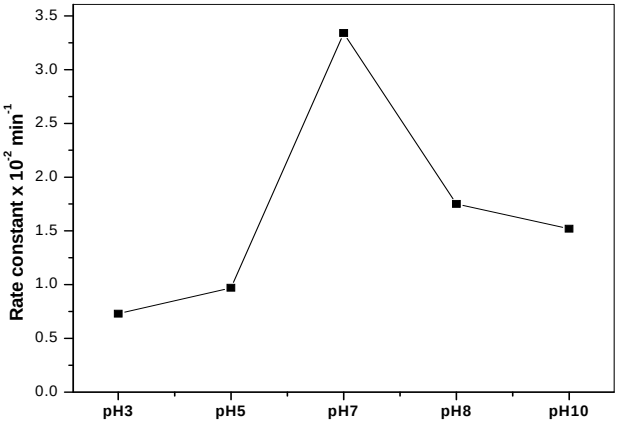

Figure 9. Effect of pH on solar photocatalytic isoproturon degradation over TCNS5. (Experimental conditions: C_0 =1.14×10^{-4} M; catalyst amount = 1.0 g L^{-1}.)

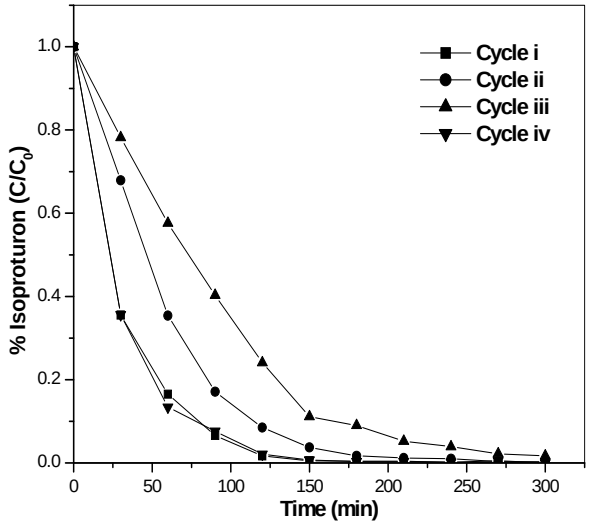

(a)

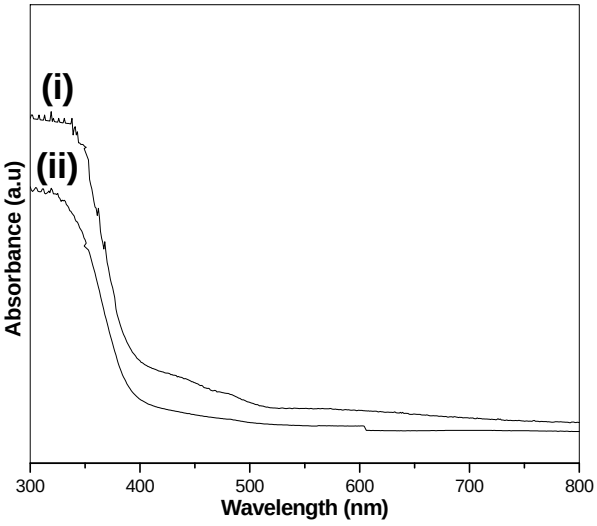

(b)

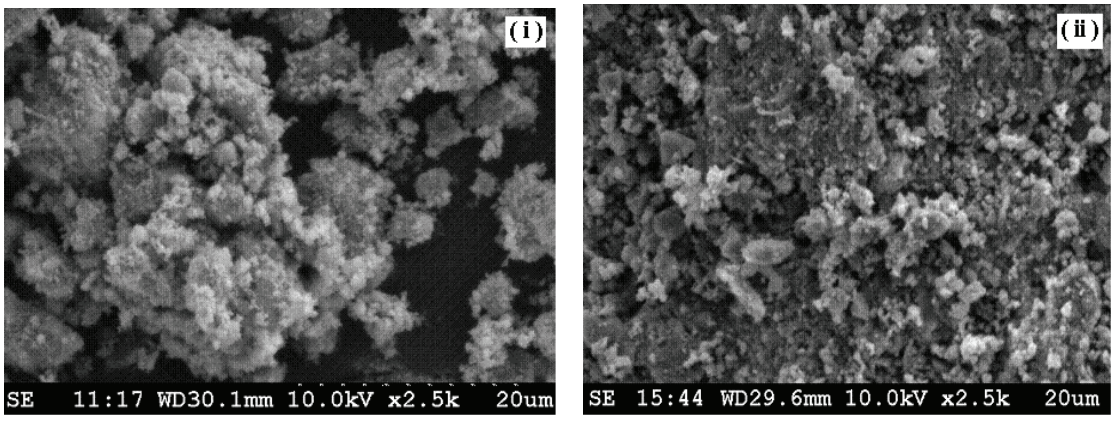

(c)

Figure 10. Isoproturon degradation over TCNS5 catalyst. (a) Recycling activity studies. (Experimental conditions: C_0 =1.14×10^{-4} M; pH 7; catalyst amount = 1.0 g L^{-1}.) Characterization of 1) Fresh and 2) Used (after 4th cycle) catalysts (b) UV–Vis DRS spectra and (c) SEM photographs.

and the hydroxylation of aromatic ring is clearly unfavored with decrease in pH, whereas in basic medium the hydroxylation of aromatic ring is favored but not the methyl groups. In neutral medium, the OH radicals attack both on the aromatic ring and on the methyl groups. This cumulative effect results a maximum degradation rate of the pollutant [20].

3.2.6. Catalyst Recycling Studies

To evaluate stability/activity of the catalyst for photocatalytic degradation, the recycling studies are conducted over TCNS5 using 1.0 g L^{-1} catalyst and the results are provided in **Figure 10(a)**. After completion of the 1st cycle, the catalyst is recovered, dried and is reused as such (without any calcination) for the 2nd cycle, a slight decrease in the rate of degradation is observed compared to the first cycle. When same catalyst is reused without calcination for the third cycle, there is a slight decrease in degradation rate observed compared to first and second cycle. The differences in rates are due to the accumulated organic intermediates on the surface of the catalyst, affecting the adsorption in turn reducing the activity. This is confirmed by calcining the 3rd cycle used sample at 400 ^{0}C for 3 h and reused for the 4th cycle activity. The original activity of the catalyst for degradation is restored. This indicates that calcination of the used catalyst is necessary in order to regain the activity. Furthermore, this is substantiated by comparison of the surface characterization studies like SEM and UV–Vis DRS techniques on the fresh and 4th cycle used samples **Figures 10(b)-10(c)**. The band gap as well as wavelength excitations are not having any changes in the UV–Vis DRS spectra of the fresh and used catalysts. From SEM photographs, it is clear that the surface morphology is not changed much and it indicates that catalyst is intact even after the 4th cycle. Thus, the above studies prove that the catalyst is reusable for number of cycles without any loss in activity and stable for longer life.

4. Conclusions

The present study demonstrates preparation of a C, N, and S doped TiO_2 photocatalyst and its role in photocatalytic pesticide degradation. The results conclude that 5 wt% thiourea doped TiO_2 (TCNS5) is an efficient catalyst for the photocatalytic degradation of isoproturon. The higher activity of TCNS5 catalyst may be due to the high surface area, lower electron-hole recombination and the stronger adsorption in visible light region. The substrate concentration of 1.14×10^{-4} M, catalyst amounts 1 g L^{-1} and neutral pH are found to be favorable for higher degradation rates of isoproturon. The catalyst activity is found to be sustainable even after the 4th cycle (as evidenced by SEM and UV–Vis DRS techniques).

5. Acknowledgements

The authors PAKR, MS thank CSIR, New Delhi for funding this work under Emeritus Scientist Scheme.

6. References

[1] A. Fujishima, K. Hashimoto, and T. Watanabe, "TiO_2 photocatalysis: Fundamentals and applications," BKC, Tokyo, 1999.

[2] L. Q. Wu, N. Xu, and J. Shi, "Leak growth mechanism in composite Pd membranes," Industrial & Engineering Chemistry Research, Vol. 39, pp. 342–348, 2000.

[3] R. Asahi, T. Morikawa, T. Ohwaki, K. Aoki, and Y. Taga, "Visible-light photocatalysis in Nitrogen-Doped titanium oxides," Science, Vol. 293, pp. 269–71, July 2001.

[4] T. Ohnoa, M. Akiyoshi, T. Umebayashi, K. Asai, T. Mitsui, and M. Matsumura, "Preparation of S-doped TiO_2 photocatalysts and their photocatalytic activities under visible light," Applied Catalysis A: General, Vol. 265, pp. 115–121, February 2004.

[5] X. Chen and S. S. Mao, "Titanium dioxide nano-materials: Synthesis, properties, modifications, and applications," Chemical Review, Vol. 107, pp. 2891–2959, 2007.

[6] H. Irie, Y. Watanabe, and K. Hashimoto, "Carbon-doped anatase TiO_2 powders as a visible-light sensitive photocatalyst," Chemistry Letters, Vol. 32, pp. 772–773, May 2003.

[7] W. Ho, J. C. Yu, and S. Lee, "Synthesis of hierarchical nanoporous F-doped TiO2 spheres with visible light photocatalytic activity," Chemical Communications, pp. 1115–1117, January 2006.

[8] L. Lin, W. Lin, Y. Zhu, B. Zhao, and Y. Xie, "Phosphor-doped titania —A novel photocatalyst active in visible light," Chemistry Letters, Vol. 34, pp. 284–285, November 2004.

[9] T. Ohno, T. Mitsui, and M. Matsumura, "Photocatalytic activity of S-doped TiO_2 photocatalyst under visible light," Chemistry Letters, Vol. 32, pp. 364–365, January 2003.

[10] H. Irie, Y. Watanabe, and K. Hashimoto, "Nitrogen-concentration dependence on photocatalytic activity of $TiO_{2-x}N_x$ powders," Journal of Physical Chemistry B, Vol. 107, pp. 5483–5486, January 2003.

[11] J. G. Yu, M. H. Zou, B. Cheng, and X. J. Zhao, "Preparation, characterization and photocatalytic activity of in situ N, S-codoped TiO_2 powders," Journal of Molecular Catalysis A: Chemical, Vol. 246, pp. 176–184, December 2005.

[12] Y. Q. Wang, X. J. Yu, and D. Z. Sun, "Synthesis, characteri- zation, and photocatalytic activity of $TiO_{2-x}N_x$ nanocatalysts," Journal of Hazardous Materials, Vol. 144, pp. 328–333, October 2006.

[13] J. L. Gole and J. D. Stout, C. Burda, Y. Lou, and X. Chen, "Highly efficient formation of visible light tunable

$TiO_{2-x}N_x$ photocatalysts and their transformation at the nanoscale," Journal of Physical Chemistry B, Vol. 108, pp. 1230–1240, September 2003.

[14] C. Burda, Y. Lou, X. Chen, A. C. S. Samia, J. Stout, and J. L. Gole, "Enhanced nitrogen doping in TiO_2 nanoparticles," Nano Letters, Vol. 3, pp. 1049–1051, June 2003.

[15] B. Chi, L. Zhao, and T. Jin, "One-step template-free route for synthesis of mesoporous N-doped titania spheres," Journal of Physical Chemistry C, Vol. 111, pp. 6189–6193, February 2007.

[16] X. W. Bao, S. S. Yan, F. Chen, and J. L. Zhang , "Preparation of TiO2 photocatalyst by hydrothermal method from aqueous peroxotitanium acid gel," Material Letters, Vol. 59, pp. 412–415, October 2004.

[17] T. Morikawa, R. Asahi, T. Ohwaki, K. Aoki, and Y. Taga, "Band-gap narrowing of titanium dioxide by nitrogen doping," Japan Journal of Applied Physics, Vol. 40, pp. 561–563, April 2001.

[18] M. V. Phanikrishna Sharma, V. Durgakumari, and M. Subrahmanyam, "Solar photocatalytic degradation of isoproturon over TiO_2/H-MOR composite systems," Journal of Hazardous Materials, Vol. 160, pp. 568–575, March 2008.

[19] M. V. Phanikrishna Sharma, V. Durga Kumari, and M. Subrahmanyam, "Photocatalytic degradation of isoproturon herbicide over TiO_2/Al-MCM-41 composite systems using solar light," Chemosphere, Vol. 72, pp. 644–651, April 2008.

[20] M. V. Phanikrishna Sharma, G. Sadanandam, A. Ratnamala, V. Durga Kumari, and M. Subrahmanyam, "An efficient and novel porous nanosilica supported TiO_2 photocatalyst for pesticide degradation using solar light," Journal of Hazardous Materials, Vol. 171, pp. 626–633, June 2009.

[21] Y. Ao, J. Xu, D. Fu, and C. Yuan, "Synthesis of C,N,S-tridoped mesoporous titania with enhanced visible light-induced photocatalytic activity," Microporous and Mesoporous Materials, Vol. 122, pp. 1–6, November 2008.

[22] S. I. Shah, W. Li, C. P. Huang, O. Jung, and C. Ni, "Study of Nd^{3+}, Pd^{2+}, Pt^{4+}, and Fe^{3+} dopant effect on photo reactivity of TiO_2 nanoparticles," Proceedings of the National Academy of Sciences, Vol. 99, pp. 6482–6486, January 2002.

[23] J. Sun, L. Qiao, S. Sun, and G. Wang, "Photocatalytic degradation of orange G on nitrogen-doped TiO_2 catalysts under visible light and sunlight irradiation," Journal of Hazardous Materials, Vol. 155, pp. 312–319, November 2007.

[24] F. Peng, L. Cai, H. Yu, H. Wang, and J. Yang, "Synthesis and characterization of substitutional and interstitial nitrogen-doped titanium dioxides with visible light photocatalytic activity," Journal of Solid State Chemistry, Vol. 181, pp. 130–136, November 2007.

[25] Y. Park, W. Kim, H. Park, T. Tachikawa, T. Majima, and W. Choi, "Carbon-doped TiO_2 photocatalyst synthesized without using an external carbon precursor and the visible light activity," Applied Catalysis B, Vol. 91, pp. 355–361, June 2009.

[26] F. Dong, W. Zhao, and Z. Wu, "Characterization and photocatalytic activities of C, N and S co-doped TiO_2 with ^1D nanostructure prepared by the nano-confinement effect," Nanotechnology, Vol. 19, pp. 365–607, July 2008.

[27] I. C. Kang, Q. Zhang, S. Yin, T. Sato, and F. Saito, "Novel method for preparation of high visible active N-doped TiO_2 photocatalyst with its grinding in solvent," Applied Catalysis B, Vol. 84, pp. 570–576, May 2008.

[28] S. Sakthivel and H. Kisch, "Daylight photocatalysis by carbon-modified titanium dioxide," Angewandte Chemie International Edition, Vol. 42, pp. 4908–4911, 2003.

[29] C. Gopinath, "Comment on photoelectron spectroscopic investigation of nitrogen-doped titania nanoparticles," Journal of Physical Chemistry B, Vol. 110, pp. 7079–7080, January 2006.

[30] S. Liu and X. Chen, "A visible light response TiO_2 photocatalyst realized by cationic S-doping and its application for phenol degradation," Journal of Hazardous Materials, Vol. 152, pp. 48–55, June 2007.

[31] J. Geng, D. Yang, J. Zhu, D. Chen, and Z. Jiang, "Nitrogen-doped TiO_2 nanotubes with enhanced photo- catalytic activity synthesized by a facile wet chemistry method," Material Research Bulletin, Vol. 44, pp. 146–150, March 2008.

[32] Y. Li, C. Xie, S. Peng, G. Lub, and S. Li, "Eosin Y-sensitized nitrogen-doped TiO_2 for efficient visible light photocatalytic hydrogen evolution," Journal of Molecular Catalysis A: Chemical, Vol. 282, pp. 117–123, December 2007.

[33] S. Sakthivel, M. Janczarek, and H. Kisch, "Visible light activity and photoelectrochemical properties of nitrogen-doped TiO_2," Journal of Physical Chemistry B, Vol. 108, pp. 19384–19387, September 2004.

[34] Y. Yokosuka, K. Oki, H. Nishikiori, Y. Tatsumi, N. Tanaka, and T. Fujii, "Photocatalytic degradation of trichloroethylene using N-doped TiO_2 prepared by a simple sol–gel process," Research on Chemical Intermediates, Vol. 35, pp. 43–53, January 2009.

[35] J. A. Rengifo-Herrera, K. Pierzchała, A. Sienkiewicz, L. Forro, J. Kiwi, and C. Pulgarin, "Abatement of organics and escherichia coli by N, S co-doped TiO_2 under UV and visible light. Implications of the formation of singlet oxygen ($^1O_2$) under visible light," Applied Catalysis B, Vol. 88, pp. 398–406, November 2008.

[36] H. S. Lee, T. Hura, S. Kimb, J. H. Kima, and H. I. Lee, "Effects of pH and surface modification of TiO_2 with SiO_x on the photocatalytic degradation of a pyrimidine derivative," Catalysis Today, Vol. 84, pp. 173–180, July 2003.

J. Water Resource and Protection, **2010, 2, 245-250**
doi:10.4236/jwarp.2010.23028 Published Online March 2010 (http://www.scirp.org/journal/jwarp)

Evaluation and Improvement of Bed Load Formula Using Tapi River Data, India

S. M. Yadav, B. K. Samtani
Civil Engineering Department, S.V. National Institute of Technology, Surat, India
E-mail: *smy@ced.svnit.ac.in, samtanibk@yahoo.com*
Received December 16, 2009; *revised December* 28, 2009; *accepted January* 20, 2010

Abstract

The effect of non uniformity of bed material on the sediment transport has been studied by various investigators in the past. In the present paper the bed load transport rate has been estimated for non uniform bed material considering the various variables like discharge, hydraulic mean depth, flow velocity, bed slope, average diameter of particle etc. by collecting field data of Tapi River. The majority of the bed load formulae represent a functional relationship between bed load discharge and shear stress. This study focuses on evaluating the bed load using Einstein's formulae. The bed load of pre monsoon season is estimated using various field parameters. The mathematical model has been developed using effective shear stress and bed load discharge. The statistical analysis, multiple regression and curve fitting (by nonlinear square fitter) is carried out using allometric function of Micro cal Origin 7.5. The proposed model has been tested using five years field data of Tapi River other than that used for the development of model. The value of rmse is close to zero indicates a perfect fit between measured and predicted values. The inequality coefficient is close to 0.50 suggest moderate relationship between estimated and computed bed load.

Keywords: Sediment Transportation, Bed Load Equation, Einstein, Ripple Factor, Mathematical Model

1. Introduction

The subject of sediment transport and flow in alluvial streams are gaining importance with the increasing utilization of water resources. Einstein [1] has developed bed load equation as a function of sediment transport in the open channel flow, Bathurst *et al*. [2] proposed bed load discharge equations for steep mountain gravel bed rivers, Beschta [3] proposed conceptual models of sediment transport in streams, Emmett [4] studied bed load transport in two large, gravel-bed rivers, Idaho and Washington, Elliot *et al.* [5] studied the sediment transportation in Yampa river, North western Colorado, Gomez *et al.* [6] assessed bed load transport formula for gravel bed rivers, Bravo–Espinosa [7] tested the bed load equations for 22 alluvial streams, Helmut *et al.* [8] evaluated and improved bed load discharge formulae for gravel bed rivers, Nian-Sheng Cheng [9] developed an exponential formula that does not involve the concept of the critical shear stress and Samtani [10] studied sediment transport characteristics of major rivers of South Gujarat, India. The majority of the bed load formulae represent a functional relation between bed load discharge and shear stress (Garde and Ranga Raju [11]). The formulae are characterized by three aspects:

1) The basic function $q_b = A\, f\,(t_0\text{-}t_c)$.
2) The characteristic grain-size to be used.
3) The bed load correction factor.

The bed load transport formulae are site specific in nature and therefore can not be compared easily. In the present analysis the Einstein's approach is used to find out the bed load transport for Tapi River, India. Using field data of Savkheda gauging station of Tapi River, Einstein's bed load equation is evaluated and a new bed load equation is proposed which is tested using Tapi river data other than that used for the development of model. The main objectives of this paper are:

1) Using various measured parameters determine q_b, t_0 and t_c.
2) To evaluate and propose modified bed load equation.

2. Study Area and Data Collection

Tapi is the second largest westward flowing river of peninsular India. The total length of the river is 724 km

from origin to Arabian Sea. The Tapi basin is situated between latitudes 20' N to 22' N, 80% of the basin lies in Maharashtra and the balance in the state of Madhya Pradesh and Gujarat as shown in **Figure 1**. The Savkheda is one of the gauging station on the river Tapi. (**Figure 2**). Central Water Commission, Tapi Division, Surat is regularly collecting daily data of discharge and sediment at gauging site Savkheda on river Tapi. Savkheda is situated at a distance of about 488 kms from origin. The daily data during pre monsoon were collected for 15 years period from 1981 to 1995 [12]. Bed load data (seasonal) from 1981–95 [13] were collected for study. The validation of model is carried out using data of 2000-2005.

3. Discharge and Sediment Observations

Discharges were observed once in a day at 08:00 hours at all the sites and calculated by area-velocity methods. Cross-section is divided into 15 to 25 segments as per IS1192:1981. Depths were measured by sounding rods as per IS 3912: 1966. Necessary air and wet line corrections were done as per IS 1192: 1981. Velocity was measured by cup-type current meter as per IS 3910:1966. Suspended sediment samples were collected in Punjab Bottle Samplers at a depth of 0.6 D from the water surface.

4. Method of Analysis

The factor which is mainly responsible for the movement of the bed grains is the fluid drag. This drag force per unit of wetted area is called unit tractive force, and is given by

$$\tau_0 = \gamma RS \tag{1}$$

where, τ_0 is shear stress in kg/m^2, R is hydraulic radius in meters and S is bed slope. A certain minimum value of shear stress is required to move the grain, depending upon the internal friction of soil. The Einstein Brown equation follows semi theoretical approach based on fall velocity criteria. Einstein – Brown's bed load transport equation is given by,

$$\frac{q_b}{w.d} = 40\left(\frac{\tau_0}{\gamma_d (Ss - 1)}\right)^3 \tag{2}$$

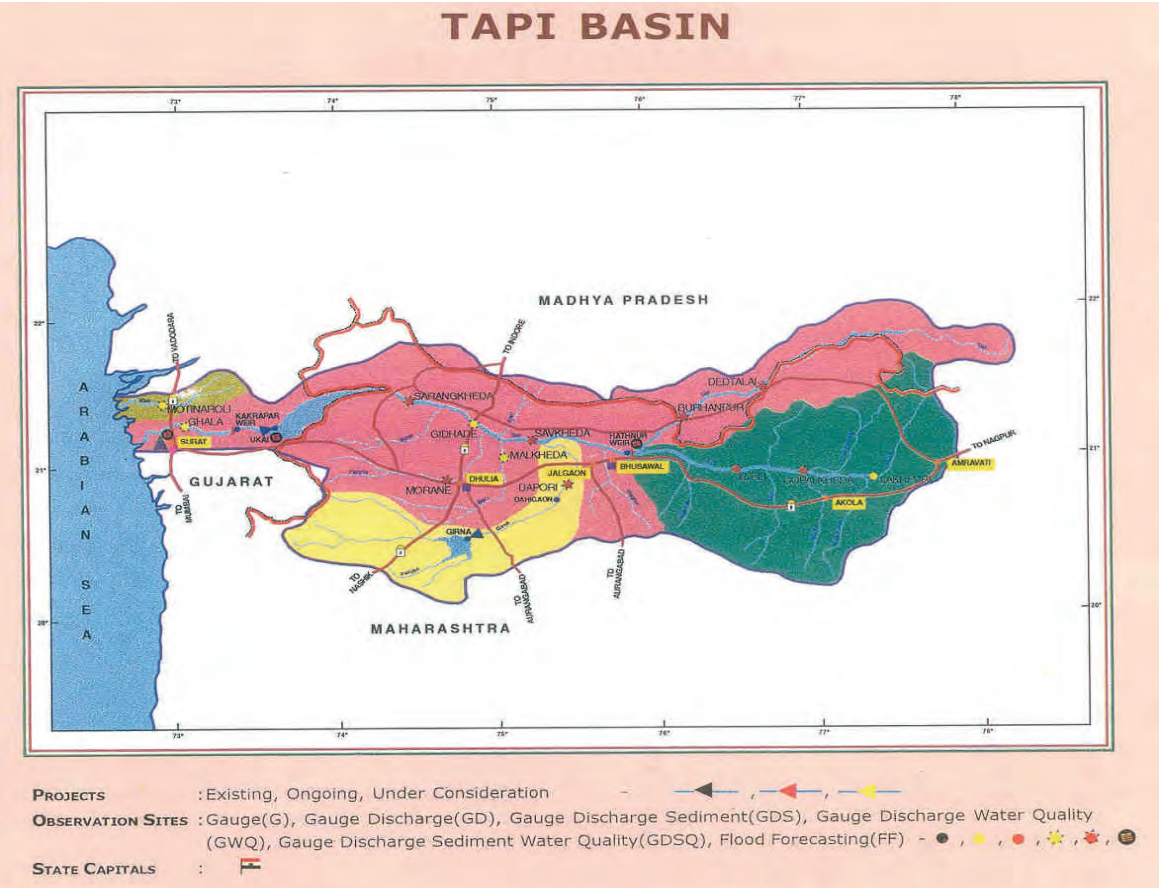

Figure 1. Map of study area.

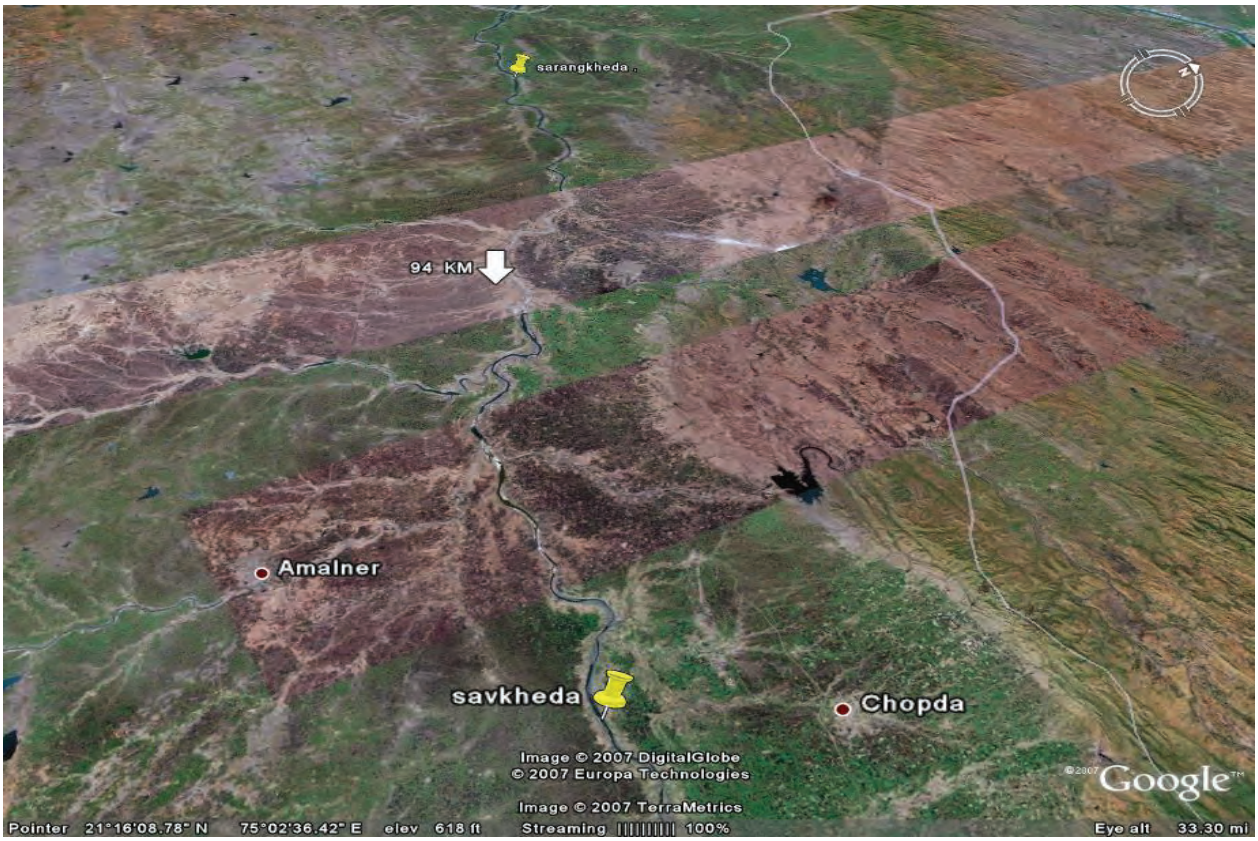

Figure 2. Digital image of study area showing Sarangkheda and Savkheda gauging station.

where, q_b = bed load transport rate weight per kg per meter width

t_0 = average shear stress on channel boundary

γ_d = unit weight of sediments

Ss = specific gravity of the stone or grain

S = bed slope.

γ = unit weight of fluid

d = Mean diameter of stone or grain.

The functional relationship $q_b = A\, f\,(t_0\text{-}t_c)$ can be approximated by an power function $Y = a\, X^{\,b}$.

5. Computation of Bed Load and Related Parameters

From the observed and calculated daily data like discharge, area, velocity, wetted perimeter, hydraulic mean depth, Manning's and Chezy's constants, average diameter of sediment, mean diameter of sediment etc. are grouped under mainly five heads *i.e.*, daily, monthly, pre monsoon, post-monsoon and yearly to facilitate the use of these data in analysis. In this paper analysis is carried out for pre monsoon season for Einstein's approach. The equations stated above were used to find out bed load, shear stress and critical shear stress. The functional relationship is appropriated as following model:

$$Y = a\, X^{\,b} \tag{3}$$

Following steps has been followed to develop the model.

Step 1. The field daily data of 15 years has been converted in to monthly and seasonal data.

Step 2. Using the field data such as bed width, slope, hydraulic mean depth, discharge, velocity, temperature, mean diameter of particle the average and critical shear stress are computed.

Step 3. The Einstein's equation is used to compute bed load transport in weight per unit width.

Step 4. The model $Y = a\, X^{\,b}$ is developed using 15 years of field data of Tapi river using Origin software 7.5.

Step 5. The model is tested using five years of data other than that used for model development.

Step 6. The testing of model is carried out by determining the statistical measures like root mean square error, inequality coefficient and discrepancy ratio.

The statistical analysis, multiple regression and curve fitting (by nonlinear square fitter) is using allometric function of Micro cal Origin 7.5.

6. Proposed Bed Load Formula

During pre monsoon, the estimated values of bed load

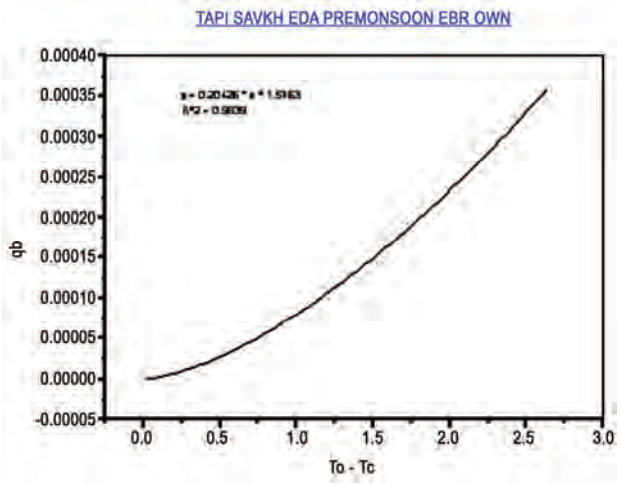

Figure 3. Relationship between effective shear stress and bed load transport rate.

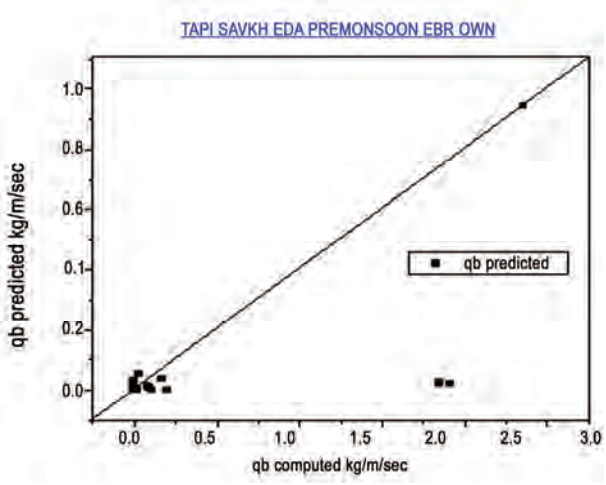

Figure 4. Computed versus predicted bed load transport rates.

Table 1. Model validation.

Sr.No	Equation	River	Site	RMSE	Discrepancy Ratio	Inequality coefficient U
1	Einstein's	Einstein's	Savkheda	0.027	>2	0.54

discharge, shear stress and critical shear stress obtained using Einstein's approach are plotted as shown in **Figure 3**. The stastical analysis is carried out using Micro cal Origin 7.5. The modified bed load equation is proposed as under:

$$Y = 0.20426 * X^{0.98326}$$

The value of coefficient comes out to be 0.20426 while value of index is 1.57634 with value of R^2 =0.98. The above equation may be used to calculate the correct bed load transported by Tapi River.

7. Model Validation

The above mathematical model is tested using five years of Tapi River data. The root mean square error (rmse) is one of the most convenient approaches for assessing simulation models. It measures the deviation between the trend of the predicted values and measured ones.

$$rmse = \left[\sum_{i=1}^{n} \frac{(q_{bo} - q_{bp})^2 i}{n} \right]^{1/2} \quad (4)$$

The value of rmse is zero indicates a perfect fit between measured and predicted values.

The discrepancy ratio is the measure of an equation to replicate data accurately. It is the ratio of a predicted to the measured bed load discharge. If this ratio is one, the equation exactly predicts the measured rate. If the ratio is less than one or greater than one the equation under or over predicts measured data respectively.

The inequality coefficient is a simulation statistics related to the rmse, defined as under,

$$U = \frac{rmse}{\left[\frac{1}{n} \sum_{i=1}^{n} (q_{bo})_i^2 \right]^{1/2} + \left[\frac{1}{n} \sum_{i=1}^{n} (q_{bp})_i^2 \right]^{1/2}} \quad (5)$$

The numerator is the root mean square error. If U=0 then $q_{bp} = q_{bo}$ and there is a perfect fit. If U=1, then $q_{bp} \neq q_{bo}$ and the lacks predicative value. The value of root mean square error, Discrepancy coefficient and inequality coefficient for above model are presented in **Table 1**.

The value of rmse 0.027 is close to zero, discrepancy ratio is more than one and inequality ratio is close to zero which confirms the models moderate agreement. To examine more closely the accuracy of model, the computed bed load transport rates per unit channel width, $q_{computed}$ using field data are plotted in **Figure 4** against the corresponding predicted values, $q_{predicted}$. In this figure the solid line represents the condition of perfect agreement.

8. Result Analysis

A new bed load transport relation for alluvial river has been proposed. The relation is an empirical fit to the data of Tapi river are considered to represent the two limits of the spectrum of bed load transport rate observed in the field and computed. The modified bed load equation based on Einstein's bed load computation for Tapi River, pre monsoon season, Savkheda gauging station is as under.

$$Y = 0.20426\ X^{1.57634} \quad (6)$$

The value of coefficient obtained by above analysis is 0.20426 and the value of index is 1.57634. The above model is tested using five years field data of Tapi River. Bravo-Espinosa, M. [7] tested the bed load equations using 22 streams data. He used rmse, inequality ratio and discrepancy ratio to evaluate bed load equations. The rmse, inequality ratio and discrepancy ratio suggest good agreement between computed and predicted bed load. The increase in the channel discharge increase the rate of bed load transport but decreases the bed shear stress and increases critical shear stress responsible for the movement of bed particles. Helmut and Jonathan [8] derived form their study that Einstein formula is particularly appropriate for flood analysis. They concluded from their study that shear stress based formulae using single values for the threshold of motion do not perform well but shear stress formula modified on the basis of some measured data is improved considerably. In the present analysis the proposed bed load formula perform well for the Tapi river data.

9. Conclusions

Following findings can be summarized as conclusions:

- For Tapi River data the proposed bed load equation shows good agreement between estimated and computed bed load.
- Application of local hydraulics and sediment logic parameters improved formula prediction.
- The value of discrepancy ratio, which is a measure of an equation to replicate data accurately, is more than 2 which suggest moderate agreement between estimated and computed values of bed load.
- The value of rmse is close to zero indicates a perfect fit between estimated and computed values.
- In case of any other river across the globe, the proposed bed load equation gives considerable variation therefore the values of coefficient (a) and index (b) required to be modified to bring predicted and measured bed load in the close prediction band (Helmut and Jonathan).

10. Acknowledgement

It is to be acknowledging that without the permission given by Chief Engineer, Central Water Commission C.W.C., Narmada and Tapi River Basin Organization Baroda; this paper would not have seen the light of the day. The enormous assistance provided by the office of the Executive Engineer Central Water Commission (Tapi Division, C.W.C., Surat) during the preparation of this paper is duly acknowledged.

11. References

[1] H. A. Einstein, "Formular for the transportation of bed load," Transportation ASCE, Vol. 107, pp. 561–573, 1942.

[2] J. C. Bathurst, W. H. Graf, and H. H. Cao "Bed load discharge equations for steep mountain rivers, Sediment transport in gravel Bed Rivers," Wiley, U. K. Chichester, pp. 453–477, 1987.

[3] R. L. Beschta "Conceptual models of sediment transport in streams, sediment transport in gravel-bed rivers," C. R. Thorne, J. C. Bathurst, and R. D. Hey, eds., Wiley, U. K. Chichester, pp. 387–419, 1987.

[4] W. W. Emmett "Bed load transport in two large, gravel-bed rivers," Idaho and Washington Proceedings of 3rd Federal Inter-Agency Sedimentation Conference, Denver, Vol. 4, pp. 101–114, 1976.

[5] J. G. Elliott, J. E. Kircher, and P. Von Guerard "Sediment transport in the lower Yampa River, northwestern Colorado," US Geology Survey Water Resource Investigations Report, No. 84–4141, pp. 44, 1984.

[6] B. Gomez and M. Church, "An assessment of bed loads sediment transport formulae for gravel Bed Rivers," Water Resources Research, Vol. 25, No. 6, pp. 1161–1186, 1989.

[7] M. Bravo-Espinosa, "Prediction of bed load discharges for alluvial channels," PhD dissertation, University of Arizona, Tucson, Arizona, pp. 276, 1999.

[8] M. H. Helmut and B. L. Jonathan, "Evaluation and improvement of bed load discharge formulas based on Helly –Smith sampling in an Alpine gravel bed rivers," Journal of Hydraulic Engineering, Vol. 128, No. 5, pp 484–499, 2002.

[9] N. S. Cheng, "Exponential formula for bed load transport, JHE, ASCE, Vol. 128, No. 10, October 2002.

[10] B. K. Samtani, "Study of sediment transport characteristics with reference to major Rivers of South Gujarat," Ph.D. Thesis, Faculty of Technology and Engineering, M. S. University of Baroda, India, 2002.

[11] R. J. Garde and K. G. Ranga Raju, "Mechanics of sediment transportation and alluvial stream problems, Third ed., New Age Publication, New Delhi, 2006.

[12] Central Water Commission (1980–1995), Water Resources Organization (NR), Integrated Water Year Book, Tapi Basin, Western River Circle, Nagpur, Tapi Division.

[13] Central Water Commission (1980–1995), Bed Material Analysis Data, Western River Circle, Nagpur, Tapi Division.

Notations

d = sieve diameter of particle
R = hydraulic radius
S = bed slope
q_{bp} = predicted bed load transport in weight per unit width
q_{bo} = measured/computed bed load transport in weight per unit width
U = inequality coefficient
q_b = rate of bed load transport in weight per unit width
t_0 = average shear stress on channel boundary
t_c = critical tractive stress
a,b = regression parameters
ω = fall velocity
μ = ripple factor

J. Water Resource and Protection, **2010, 2, 251-258**
doi:10.4236/jwarp.2010.23029 Published Online March 2010 (http://www.scirp.org/journal/jwarp)

Measuring Salinity within Shallow Piezometers: Comparison of Two Field Methods

Enrico Balugani, Marco Antonellini
I.G.R.G, University of Bologna, Via San Alberto, Ravenna, Italy
E-mail: *balugani.enrico@libero.it, m.antonellini@unibo.it*
Received December 21, 2009; *revised January* 14, 2010; *accepted January* 26, 2010

Abstract

The objective of this study is to understand the validity of salinity vertical profiles collected from shallow piezometers that are not previously flushed. This study shows that salinity data collected from boreholes are only an average value along the entire screened section of the piezometer. In order to collect data that is representative for the salinity of the adjacent aquifer, a new monitoring strategy has been developed. This strategy includes measurement of the salinity at the top of the watertable in an auger hole which is a shallow boreholes made with an handheld drill. This should be combined with measurements in piezometers that are first flushed to take out stagnant water. From the piezometers on can measure the average salinity of the screened part and the salinity at the bottom of the aquifer. By using this monitoring strategy it is also possible to define where the piezometers screens are located if this is not known beforehand.

Keywords: Coastal Aquifer, Salt-Water Intrusion, Piezometers, Monitoring

1. Introduction

1.1. Overview

A large part of the world population lives along the coasts exerting a strong pressure on freshwater resources [1]. Overexploitation of coastal groundwater often results in subsidence and saltwater intrusion. The area considered in this study is part of the Po Plain coast, particularly affected by salt-water intrusion problems, because of the low topography with respect to sea level and the anthropogenic pressure connected to tourism, agriculture, and the gas industry [2]. Italy is one of the countries most affected by saltwater intrusion, due to the relatively high population density (196,6 inhabitants/km^2) and the length of its coastline (more than 8000 km). To the best of our knowledge, a standard monitoring methodology and protocols to characterize this phenomenon has not yet been developed, so that approaches in different areas of the world may be quite different according to local knowledge of the saltwater intrusion problem. There are different approaches to study saltwater intrusion in coastal aquifers, for example geophysical methods [3], borehole investigations, and numerical models [4]. Borehole data are widely used in these kinds of studies, especially for calibrating numerical models, but in recent years the validity of data collected directly from wells and piezometers is under discussion [5–9]. Characterizing piezometric heads and salinity within a large coastal phreatic aquifer is a complex endeavour. The point water head measured in a salty aquifer needs to be corrected and transformed to equivalent freshwater head or environmental head [10] in order to have a correct representation of the hydraulic gradients. As pointed out by the numerical experiments described in [9], the salinity measured in a borehole or a piezometer, that happens to be in the mixing zone of a coastal aquifer, may not be representative for the fluids within the porous medium. In long-screened boreholes, preferential flow within the borehole (**Figure 1**), driven by gradients in concentration, results in biased data for groundwater samples or measurements collected from the well-water profile [9]. These data have poor relationships with the effective environmental concentrations of chemicals [6]. Flow in the borehole (**Figure 1**) does not only affect the chemical concentrations in the well, but also affects the near-borehole aquifer acting as a preferred flow channel for solutes [11–13]. Shallow conventional wells and piezometers are, especially, prone to this problem [14]. The reliability of data collected from boreholes is strongly connected to the length of the screened section; the longer the screen the greater the bias [14]. From Britt's experiments [8] it is clear that the assumption of

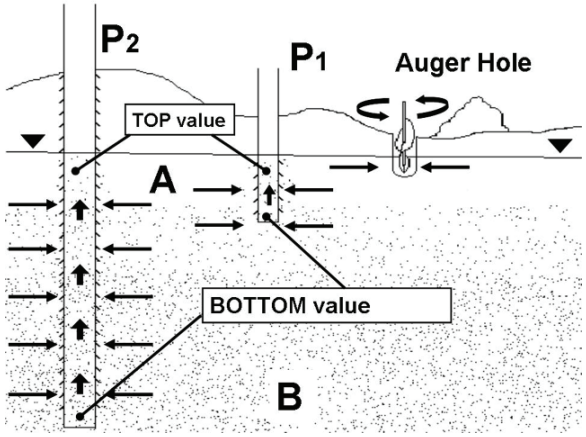

Figure 1. Hypothesis on salt distribution inside and near the piezometer, based on Britt (2005) and Elci *et al.* (2001). P1 = type 1 piezometer; P2 = type 2 piezometer; A = fresh water; B = salt water; points represent salt, arrows represent the directions of salt movement.

linear flow in a piezometer under normal conditions is questionable.

1.2. Objective of the Study

This paper presents field measurements of watertable elevation and salinity made with two different methods in shallow wells within a coastal phreatic aquifer. Our study site, the San Vitale pine forest, is strongly affected by saltwater intrusion [2,15], and the monitoring system in place since the last fifteen years consists of more than 20 conventional piezometers 6,4 cm in diameter, with a screen along their whole length (**Figure 1**); the monitoring system used so far (method A) is based on salinity measurements from conventional shallow piezometers without flushing the stagnant water. A four year long collection of monthly data already exists for this area (starting from 2004). Given the importance of past data in the study of the evolution of saltwater intrusion along the coast, we decided to find a way to test their validity in view of their integration with measurements from current and future surveys. The specific objectives of this study were to understand how the borehole-flow related bias affects salinity measurements collected during sampling in a piezometer network within a phreatic aquifer, what exactly the data represent, infer the validity of the data collected during the past years and to develop an appropriate method of sampling. This has been done by means of field experiments on the existing piezometers, by comparison with previously collected data (method A - CTD probe and no flushing), and by drilling auger holes to the top of the watertable combined with salinity measurements in flushed piezometer (method B). Another objective of the study was to assess the position of the screens along existing boreholes in the phreatic aquifer that for some piezometers was not reported before.

1.3. Setting

Our study area is located in the San Vitale pine forest, north of Ravenna, on the north Adriatic coast of Italy. The area borders on the south with the city of Ravenna, on the north with the Destra Reno canal (not shown), on the west with two freshwater wetlands (Boundary Water Bodies, in **Figure 2**), on the south with the Romea highway (S.S. 309), and on the east with farmland and the Piallassa Baiona lagoon (B.W.B. on the right in **Figure 2**). This latter lagoon is divided by dikes in several water bodies and is partly connected to the sea: the westernmost water bodies have been closed and remain filled with freshwater, whereas those in the east have salinity similar to that of the sea and experience tide-induced water level fluctuations. The area is covered by a pine forest planted by the Romans on paleodunes with belts that run in a north–south direction. The surface hydrographic system consists of east-west oriented river and channels, open surface water bodies, and drainage ditches with pumping machines that discharge water towards the sea. The area is undergoing subsidence due to natural and anthropogenic causes; the subsidence has dropped most of the forest below mean sea level [15,16]. Soils are mostly sandy and their specific characteristics depend on morphology and watertable depth. The area stratigraphy is consists of multiple series of transgressive-regressive deposits [17–20]. These sediments forming the aquifers are composed of clay layers

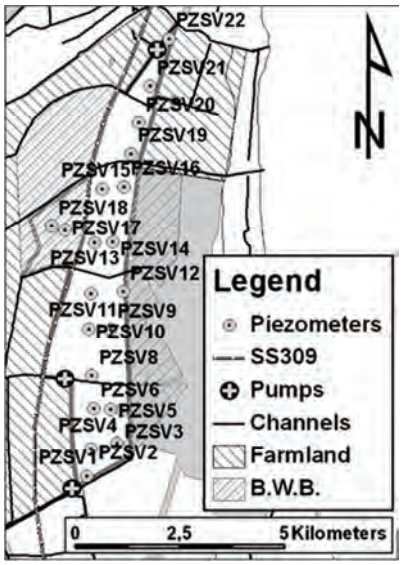

Figure 2. Detail of the study area with boundaries and piezometers location (called PZ), rivers and canals, water bodies and wetlands in proximity to the San Vitale pine forest. B.W.B. stands for Boundary Surface Water Bodies.

(aquiclude) stratified with sand layers (**Figure 3**). The phreatic aquifer corresponds to the upper sand layer; it is confined at the bottom by a clay-silt and sand-silt unit that acts as aquiclude (from -10 m to -21 m) [21]. The aquifer hydraulic conductivity (K) is known by slug tests [2,22], the range in K vary between 14 and 30 m/day [22]. Depth of watertable from the surface ranges from 0 to -4 m. The piezometer network covers the whole pine forest area with an irregular grid: the maximum distance between two piezometers is 1 km, and the minimum is 200 m. All piezometers are in the forested area except PZ17 and PZ18, that are located in the Punte Alberete wetland (**Figure 2**).There are two types of piezometers (**Figure 1**): the first one consists of short piezometers (type 1; PZ4, 5 and 6) that are 3 m long and have 3,8 inch diameter whereas the second one (type 2) consists of piezometers that are 6 m long and have a 6,4 inches diameter. The total length of the screen in these piezometers is unknown. The common procedure in the area was to screen the last meter of the short piezometers (type 1) and to screen completely the long piezometers (type 2).

2. Methods

Until now, the monitoring procedure (method A) used in our study area consisted of watertable head, electric conductivity, and temperature measurements directly in the piezometers by means of a CTD probe (AQUATroll-®200) that records a profile of these parameters in each piezometer. The piezometers were not flushed by pumping before the measurements were made. Electrical conductivity data are then converted into salinity values using the equations by Lewis & Perkins [23]. Watertable level data were measured with a standard water-level meter (resolution: 1 cm). The new method (method B) uses a different approach; in order to reduce the bias due to stagnant water above the screens, we decided to flush away from the piezometer a water quantity equivalent to 3 wet borehole volumes [24] and to measure the electric conductivity and temperature at the top and bottom of the piezometer. Pumping has been conducted from the top of the watertable (see **Figure 1**) at an approximate rate of 4 liters per minute.

In this way, we collected two different types of information:

1) from the difference between top and bottom salinity (see **Figure 1**) we infer the length of the screened section

2) from the electrical conductivity data recorded post-flushing we obtain a more representative average salinity value for the part of the aquifer in contact with the bottom of the piezometer.

A large difference between top salinity before and after flushing occurs in piezometers that are screened only in the last bottom meter because stagnant water is removed and replaced with ground water coming from the screened section.

However, a small difference occurs in piezometers that are fully screened, because there is less stagnant water.

After this, we compared the salinity measured within the borehole with that in the adjacent aquifer. The salinity at the top of the watertable was obtained by digging a shallow auger hole (5 cm deeper than the watertable, just to submerge the probe; **Figure 1**) near the piezometer (distance between 5 to 20 m) to reach the watertable top and take measurements of electric conductivity and temperature.

The experiment has been conducted in three days distributed within two weeks from 6 to 15 august 2008 without any rainfall event. The water extracted was red to brown colored (iron oxides in the water from the steel casing) at the beginning of the pumping, and then turned clear once the stagnant water was flushed away.

In order to better evaluate the results of the experiment, the problem has been simplified by dividing the area into subareas bordered by natural hydrologic boundaries, such as rivers or canals.

3. Result and Discussion

The results of our monitoring campaign show that the watertable levels are below or equal to the mean sea level in the whole area (**Table 1**). Groundwater levels are close to 0 m msl in the southeastern part of the aquifer and in its northwestern part. The regions where the interpolated water table is close to 0 m msl correspond to the boundaries of surface water bodies. The lowest watertable level is -2,22 m msl and it has been observed in the northern part of the forest at piezometer SVPZ21. The highest watertable level is 0.02 m and it has been observed in the central part of the forest at PZSV17.

The measurements done in piezometers 1, 4, 5, 6, 8, 10, 11, 13, 18, 20, 22. before flushing show a salinity at the top of the watertable below 1,5 g/l which is the limit salinity for fresh water; [25] The salinity measured at the bottom of the piezometers before flushing ranges from 6 to 27 g/l in the southern area (piezometers from

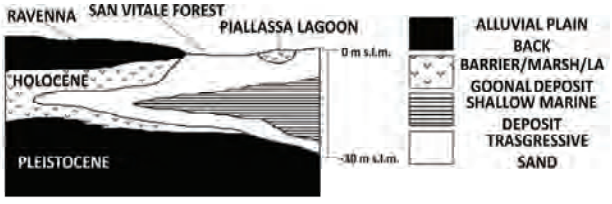

Figure 3. Schematic stratigraphic reconstruction of the coastal aquifer below the study area (modified after Amorosi *et al.*, 1999 and Marchesini *et al.*, 2000).

Identify applicable sponsor/s here. *(sponsors).*

Table 1. Salinity and groundwater level data measured in piezometers before and post-flushing the stagnant water during this study.

Piezometer name	Groundwater level from well head (m)	Water Table Level (m m.s.l.)	Before Purging		After Purging		Auger hole	Piezometer length (m)	Piezometer diameter (cm)	Inferred screen length
			top	Bottom	top	Bottom				
			Sal g/l	Sal g/l	Sal g/l	Sal g/l	Sal g/l			
SVPZ1	1,62	-0,46	0,64	14,4	1,63	14,65	0,7	6	6,4	A
SVPZ2	1,81	-0,46	3,14	18,33	2,54	18,9	0,32	6	6,4	A
SVPZ3	1,55	-0,54	5,85	6,83	18,58	24,82	3,58	6	6,4	A
SVPZ4	2,02	-0,67	0,61	27,31	25,45	28,29	7,32	3	3,8	B
SVPZ5	1,47	-0,57	0,59	8,43	8	11,31	5,27	3	3,8	B
SVPZ6	2,12	-0,93	0,42	8,98	6,19	8,19	0,46	3	3,8	B
SVPZ8	1,99	-0,67	0,57	17,92	0,71	18,16	0,87	6	6,4	A
SVPZ9	2,54	-0,71	3,3	15,59	3,99	16,02	1,1	6	6,4	C
SVPZ10	2,58	-0,96	0,6	0,8	0,65	0,78	-------	6	6,4	C
SVPZ11	2,52	-0,74	0,26	1,14	0,27	1,11	0,36	6	6,4	C
SVPZ12	1,54	-0,07	30,38	30,86	9,35	24,63	10,04	6	6,4	C
SVPZ13	2,32	-0,43	0,59	0,97	0,59	0,99	-------	6	6,4	C
SVPZ14	2,1	-0,6	9,19	22,34	9,61	22,09	5,83	6	6,4	C
SVPZ15	2,6	-0,33	1,68	6,89	1,67	7,09	-------	6	6,4	C
SVPZ16	2,9	-1,57	3,64	18,97	3,19	20,27	-------	6	6,4	C
SVPZ17	1,98	-0,1	4,38	12,08	2,51	12	0,47	6	6,4	C
SVPZ18	1,69	-0,49	1	9,5	1,61	9,51	2,01	6	6,4	C
SVPZ19	2,5	-0,67	3,23	13,42	4,28	14,19	3,75	6	6,4	C
SVPZ20	3,25	-1,6	0,36	9,51	0,42	7,41		6	6,4	C
SVPZ21	3,75	-2,22	0,48	2,27	Purging not Possible					
SVPZ22	2,95	-1,07	4,52	5,52	1,85	5,59		6	6,4	C

1 to 6), from 2 to 13 g/l in the northern area (piezometers from 19 to 22), and is rather variable in the central area (salinity values range from 0.8 to 31 g/l). After flushing away the stagnant water, the salinity values at the top of the watertable in the piezometers remain below 1,5 g/l in boreholes 8, 10, 11, 13, 20. The salinity measured at the bottom of the piezometers post-flushing the stagnant water, ranges from 8 to 28 g/l in the southern area, from 5 to 14 g/l in the northern area, it is about 10 g/l in Punte Alberete, and it varies between 0,8 to 25 g/l in the central area.

The salinity measured in the Auger holes is below 1,5 g/l next to piezometers 1, 2, 6, 8, 9, 11, 13, 17 and it is above 5 g/l next to piezometers 4, 5, 12, 14 (again, **Table 1**).

3.1. Data Analysis

The watertable levels have not changed after pumping for flushing the stagnant water. This is due to the high hydraulic conductivity of the aquifer (K = 14 - 30 m/d, [2]). The highest watertable levels (0.02 m in PZSV17) have always been observed in proximity to open surface water bodies, such as the Piallassa lagoon in the south (**Figure 3**). The different gradients cause two main groundwater fluxes: one from west to east in the northern part of the study area, and one from west and south to the northwest in the southern part.

3.1.1. Measurements at Top of the Watertable

We compared the salinity at the top of the watertable measured in the piezometers with that measured in the auger holes. The salinity measurements at the top of the watertable within the piezometers, collected during our study campaign before flushing the stagnant water (**Table 1**), are similar to the previous measurements collected in the same season during 2007 (**Table 2**). It appears that the salinity remained more or less the same in the central and northern parts, with the exception of piezometer 12 where the salinity is higher than it was before (16,39 g/l during 2007, 30,38 g/l during 2008, see **Tables 1** and **2**) and decreased (from 22 g/l to 0.5 g/l in PZSV4) in the southern part of the forest. Post-flushing (**Figure 4**), the situation changes. The largest variations with respect to pre-flushing salinity occur in piezometer 12 (decrease in salinity of 21,03 g/l) and in the southern part of the area where the salinity decreases (for all piezometers, differences in salinity are more than 100 %, see **Table 1**). In some cases the saltwater-freshwater interface is apparently so close to the bottom of the piezometer that flushing the stagnant water causes up-coning of seawater. This is shown in piezometer 4, where before pumping there was a fresh-water lens (salinity 0.61 g/l), and after pumping the salinity increased to 35 g/l. The observed variation in salinity values induced by pumping are related to two different factors: the first one is the different response of wells to pumping due to differences

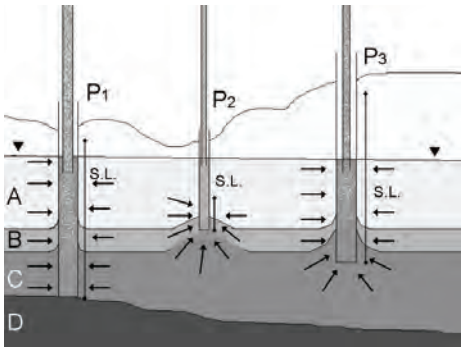

Figure 4. Different borehole behaviour in response to pumping. In a fully penetrating borehole the laminar flux from the aquifer remains mainly horizontal, whereas in incomplete penetrating well a vertical flow component is present. P1 = type 1 piezometer; P2 = type 2 piezometer, fully penetrating; P3 = type 2 piezometer, partially penetrating; D = aquifer bottom; S.L. = screen length. Arrows represent water flow directions.

in length of the piezometers and position of the screens, on which depends the amount of stagnant water before pumping and the level from which groundwater flows into the piezometer during pumping, the second one is natural mixing with saltwater due to up-coning where the freshwater-saltwater interface is in close proximity to the bottom of the piezometer. The salinity measured in the auger holes (or auger drills, **Figure 1**) is generally lower than that measured in the piezometers (mean difference is 1,58 g/l). The salinity measurements made in the auger holes remain high near the Piallassa lagoon, but they are 10 or more g/l lower than what was measured in the piezometers (**Table 1**).

3.1.2 Measurements at bottom of piezometers

The salinity measurements at the bottom of the piezometers (6 m c.a.), that we made in this study before flushing the stagnant water, fit well to the data collected in previous years [22] and the local public records (**Table 2**); the only relevant variation from previous years is in the southern part, between the two pumps shown in **Figure 2**. In this latter area, the salinity in piezometers PZSV3, PZSV4 and PZSV8 is less than what was measured previously (5 % of mean difference – see **Tables 1** and **2**). After pumping, the salinity varies with respect to the pre-pumping data; in the northern and central part of the forest the differences are minimal, in the northeastern part (piezometers 16, 19, 20), the salinity decreases after pumping.

3.2. Interpretation of Salinity Changes

The salinity measured after pumping was interpreted using the work described in [24] on wellbore responses to pump-induced flow and mixing in controlled laboratory conditions. Our idea was to interpret field salinity profile variations in wells due to pumping in controlled conditions for different well screen lengths in a way to relate these variations to different well geometries. Differences between the situation before and after pumping vary widely from piezometer to piezometer. Bottom salinity measured after pumping is always higher than bottom salinity measured before pumping, whereas the top watertable salinity measurements are sometimes higher and sometimes lower with respect to pre-pumping value. The distribution in variations among salinity measurements pre- and after pumping show that the San Vitale pine forest can be divided into two areas: the northcentral one and the southern one (**Figure 3**). In the southern area piezometers of type 1 (3 piezometers) and 2 (4 piezometers) are present and the cause of the differences in salinity is likely the different lengths of the screens in the two types of piezometers. In the northern area, the salinity at both top and bottom is the same regardless of the monitoring method, therefore also previous measurements made without flushing could be considered to be representative for the aquifer. In the central-northern area, all piezometers have the same geometry; differences between top-piezometer and auger hole salinity data increase slowly at increasing salt concentration (Difference for PZSV14 was 36 %; for PZSV22 was 10,6 %). There are also small differences (mean 1 g/l) in salinity measured in piezometers from the northern area before and after-flushing and in auger holes (**Table 1**). This suggests that the screen length coincides with the total length of the piezometer .The salinity data measured in the piezometers at the top of the watertable in the northern area are similar to those measured in the auger-holes, because the aquifer is in connection with the screened profile. The mean difference between the salinity measurements collected at the top of the watertable post-flushing and in auger holes for the southern area is over 1000 % (7,46 g/l) for the type 1 piezometers. Differences between the salinity at the top of the piezometers before and post-flushing for piezometers 12 and 22 are difficult to understand: a possible explanation for piezometer 12 could be the relatively high watertable (1,54 m from well head, whereas all others have a watertable deeper than 2 meters from the well head) and proximity to water body that is influenced bu the tides, resulting in strong well mixing caused by water level fluctuations in the piezometer [9]. Differences between auger holes measurements and piezometers measurements show no apparent relationships with other variables such as borehole geometry, morphology, vegetation, proximity to water bodies, and lithology. We conclude that type 2 piezometers are screened from 2 to 6 meters from the borehole head, so that they can be interpreted to be fully penetrating (P2 in **Figure 4**) the phreatic aquifer in the northern area of the pine forest where the depth of the bottom acquiclude is at a depth between -6 and -7 m [2].

Table 2. Salinity and watertable level measurements in piezometers for the months of August 2007 and 2008.

Piezometer name	August 2007			August 2008		
	Watertable Level (m m.s.l.)	Top	Bottom	Watertable Level (m m.s.l.)	Top	Bottom
		Sal g/l	Sal g/l		Sal g/l	Sal g/l
SVPZ1	-0,49	1,54	9,9	-0,36	1,54	15,32
SVPZ2	-0,45	4,73	14,97	-0,5	4,56	18,78
SVPZ3	-0,35	10,28	10,4	-0,46	17,2	25,22
SVPZ4	-0,65	14,94	20,2	-0,57	23,01	28,67
SVPZ5	-0,6	9,71	8,54	-0,55	11,85	11,52
SVPZ6	-0,91	3,03	6,05	-0,87	5,58	7,83
SVPZ8	-0,73	1,44	14,66	-0,68	0,62	19,12
SVPZ9	-0,67	2,27	12,13	-0,61	4,46	19,38
SVPZ10	-0,88	0,37	0,69	-1,23	0,76	0,72
SVPZ11	-1,02	0,2	0,5	-0,99	0,45	0,77
SVPZ12	-0,23	10,24	22,37	-0,08	16,39	32,41
SVPZ13	-0,61	0,48	0,65	-0,67	0,9	0,85
SVPZ14	-0,6	4,07	14,2	-0,7	9,28	21,46
SVPZ15	-0,43	0,82	2,86	-0,48	1,11	5,41
SVPZ16	-0,67	1,7	14,46	-0,56	2,82	0
SVPZ17	-0,07	3,21	7,78	0,02	3,19	12,49
SVPZ18	-0,32	1,19	9,3	-0,34	0,21	9,6
SVPZ19	-0,57	3,5	7,96	-0,81	5,27	13,41
SVPZ20	-1,65	0,41	5,86	-1,57	0,31	8,83
SVPZ21	-1,87	1,94	4,65	-2,2	0,61	1,47
SVPZ22	-0,92	3,69	2,79	-0,97	4,45	5,36

In the southern area, differences between bottom salinity data before and after pumping show a dual behaviour (**Table 1**): salinity measurements in piezometers 1, 2 and 6 remain unchanged, whereas in the other piezometers they change significantly (mean difference of 100 % salinity for PZSV3, 4 and 5, respectively). This suggests that the differences are not related to borehole geometry. In the southern area, the electric conductivity profiles made before pumping, suggest that the driving factor controlling bottom salinity data variations should be proximity to the saltwater of the Piallassa lagoon (**Figure 2**): the borehole bottom remains just above a sharp interface between freshwater and saltwater and during pumping, saltwater up-coning takes place causing strong mixing in the piezometer (**Figure 4**). The differences in top watertable salinity measured before and after pumping have a similar pattern to the bottom salinity differences previously described: piezometers 1 and 2 show small differences (0,98 and 0,6 g/l, respectively) whereas, for the other piezometers in the southern area, top salinity values change considerably (7 % for PZSV3, 4, 5 and 6, respectively). This shows that borehole screen length is different in the two types of piezometers belonging to the two network sets. The type 1 piezometer is screened only in the last meter: this explain both similarity between bottom salinity values before and after pumping and the marked difference between top salinity values before and after pumping.

Few of the salinity values at the top of the piezometers measured after pumping are close to those measured in the auger holes (**Table 1**): this shows that effective groundwater density stratification is lost in boreholes, because of internal fluxes and mixing.

The large difference in salinity (see **Tables 1** and **2**) between the two measurement methods (A and B) in both northern and southern areas could be the depth of the clay aquiclude. In the northern and central area the piezometers are almost completely penetrating, because

the depth of the aquiclude and the length of the piezometer coincide (6 m). In the southern area, however, the clay layer at the bottom of the aquifer is at a depth that is twice the piezometer's length (13 m). For this reason, at the bottom of the piezometer, fluxes occur in both an horizontal and vertical direction and there is vertical seepage of saltwater into the piezometer (**Figure 4** [26]).

3.3. Determination of the Position and Length of the Screen

A study of the piezometers/well response to pumping, like the one we performed in this study, could be used to determine the position and length of the screens if such position and length are not known. This requires also knowledge of the aquifer's thickness in order to avoid the use of partially penetrating piezometers. If the groundwater at the top of the aquifer is sampled using the auger holes method, and a salinity profile is measured along the piezometers before and after pumping, the comparison between the field data and the numerical models for different screen/length configurations [13] allows to infer the position and length of the screened section (our results have been confirmed by using a straddle-packer multilevel system on the same piezometers).

This study shows that the use of partially penetrating piezometers should be avoided in monitoring acquifer salinization. Auger holes, on the contrary, seem a reliable way to obtain representative data about the salinity at the top of the groundwater. Fully penetrating and screened piezometers could be used to obtain the average water salinity data through the whole aquifer column after proper flushing of the stagnant water. More representative values for groundwater salinity at different depths could only be obtained by using cluster piezometers or multilevel samplers.

4. Conclusions

The salinity measurement method used in this study has certain advantages in characterizing the salinity at the top of the watertable and it has allowed us to critically evaluate salinity values measured before in previous studies that did not include flushing the wells.

If the piezometer is not fully penetrating, measurement obtained is an average comprehensive of deeper parts of the aquifer. Surface groundwater salinity obtained by auger holes measurements is considerably lower than what expected from the piezometers data.

Our study has shown that it is important, in the design of networks to monitor salinity, that piezometers are fully penetrating and screened through the aquifer of interest.

We have also developed a methodology to indirectly assess the length and position of the screened section of the piezometers for which no record is available. With this method it is, therefore, possible to obtain information about the screened section of old piezometers already present in an area and use them in a hydrogeology study.

5. Acknowledgment

We thank the Municipality of Ravenna and a strategic funding project of the University of Bologna for financial support. We thank also V. Marconi for the field help and the inspired suggestions. The revision of P. Mollema helped to improve this manuscript.

6. References

[1] T. Beatley, D. J. Brower, and A. K. Schwab, "An introduction to coastal zone management," Published by Island Press, 2002.

[2] M. Antonellini, P. Mollema, B. Giambastiani, K. Bishop, L. Caruso, A. Minchio, L. Pellegrini, M. Sabia, E. Ulazzi, and G. Gabbianelli, "Salt water intrusion in the coastal aquifer of the southern Po Plain, Italy," Hydrogeology Journal, Vol. 16, No. 8, December 2008.

[3] S. S. A. Nassir, M. H. Loke, C. Y. Lee, M. N. M. Nawawi, "Salt-water intrusion mapping by geoelectrical maging surveys," Geophysical Prospecting, Vol. 48, pp. 647–661, 2000.

[4] O. E. GHP, "Salt water intrusion in a three-dimensional groundwater system in the Netherlands: a numerical study," Transp Porous Media, Vol. 43, No. 1, pp. 137–158, 2001.

[5] R. M. Powell and R. W. Puls, "Passive sampling of groundwater monitoring wells without purging: Multilevel well chemistry and tracer disappearance," Journal of Contaminant Hydrology, Vol. 12, No. 1–2, pp. 57–77, 1993.

[6] P. E. Church and G. E. Granato, "Bias in groundwater data caused by well-bore flow in long-screen wells," Ground Water, Vol. 34, No. 2, pp. 262–273, 1996.

[7] J. M. Martin-Hayden and G. A. Robbins, "Plume distortion and apparent attenuation due to concentration averaging in monitoring wells," Ground Water, Vol. 35, No. 2, pp. 339–346, 1997.

[8] L. S. Britt, "Testing the in-well horizontal laminar flow assumption with a sand-tank well model," Ground Water Monitoring & Remediation, Vol. 25, No. 3, pp. 73–81, 2005.

[9] E. Shalev, A. Lazar, S. Wollman, S. Kington, Y. Yechieli, and H. Gvirtzman, "Biased monitoring of fresh water-salt water mixing zone in coastal aquifers, Ground Water, Vol. 47, No. 1, pp. 49–56, 2009.

[10] C. W. Fetter, Applied Hydrogeology, 4th ed., Upper Saddle River, Prentice-Hall, New Jersey, 2001.

[11] T. E. Reilly and D. R. LeBlanc, "Experimental evaluation

of factors affecting temporal variability of water samples obtained from long-screened wells," Ground Water, Vol. 36, No. 4, pp. 566–576, 1998.

[12] J. M. Martin-Hayden, "Sample concentration response to laminar wellbore flow: Implication to groundwater data variability," Ground Water, Vol. 38, No. 1, pp. 12–19. 2000.

[13] A. Elci, F. J. Molz III, and W. R. Waldrop, "Implication of observed and simulated ambient flow in monitoring wells," Ground Water, Vol. 39, No. 6, pp. 853–862, 2001.

[14] S. R. Hutchins and S. D. Acree, "Ground water sampling bias observed in shallow, convenional wells," Ground Water Monitoring and Remediation, Vol. 20, No. 1, pp. 86–93, 2000.

[15] B. M. S. Giambastiani, M. Antonellini, G. H. P. Oude Essink, R. J. Stuurman, "Saltwater intrusion in he unconfined coastal aquifer of Ravenna (Italy): A numerical model," Journal of Hydrology, Vol. 340, pp. 91–104, 2007.

[16] P. Teatini, M. Ferronato, G. Gambolati, and M. Gonella, "Groundwater pumping and land subsidence in the Emilia-Romagna coastland, Italy: Modeling the past occurrence and the future trend," Water Resources Research, Vol. 42, 2006.

[17] M. Bondesan, G. Calderoni, and R. Dal Cin, "Il litorale delle province di Ferrara e di Ravenna (alto Adriatico), evoluzione morfologica e distribuzione dei sedimenti," Boll Soc Geol, pp. 247–287, 1978.

[18] A. Amorosi, M. L. Colalongo, G. Pasini, D. Preti, "Sedimentary response to Late Quaternary sea-level changes in the Romagna coastal plain (Northern Italy)," Sedimentology, Vol. 46, pp. 99–121. 1999.

[19] M. Bondesan, V. Favero, and M. J. Viñals, "New evidence on the evolution of the Po delta coastal plain during the Holocene," Quaternary International, Vol. 29/30, pp. 105–110, 1995.

[20] L. Marchesini, A. Amorosi, U. Cibin, A. Zuffa, E. Spadafora, and D. Preti, "Sand composition and sedimentary evolution of a late quaternary depositional sequence, Northwestern Adriatic Coast, Italy," Journal of Sedimentary Research, Vol. 70, No. 4, pp. 829–838, 2000.

[21] A. Veggiani, "Le ultime vicende geologiche del Ravennate," In: Influenza di insediamenti industriali sul circostante ambiente naturale, Studio sulla pineta di S. Vitale di Ravenna. Ed. Compositori, Bologna, pp. 48–58, 1974.

[22] B. M. S. Giambastiani, "Evoluzione idrologica ed idrogeologica della pineta di San Vitale (Ravenna)," Ph.D. Thesis, Bologna University, 2007.

[23] UNESCO, "Algorithms for computation of fundamental properties of seawater. Unesco technical papers in marine science 44," Unesco/SCOR/ICES/IAPSO Joint Panel on Oceanographic Tables and Standards and SCOR Working Group 51, 1983.

[24] J. M. Martin-Hayden, "Controlled laboratory investi- gations of wellbore concentration response to pumping," Ground Water, Vol. 38, No. 1, pp. 121–128, 2000.

[25] P. E. Wendell, "Introduction to environmental engineering and science," Prentice Hall, 3rd ed. ISBN, No. 0–13–148193–2, 2007.

[26] M. S. Hantush, "Hydraulics of wells," in Advances in Hydroscience," Vol. 1, Ed.: V. T. Chow, Academic Press, New York, pp. 281–432, 1964.

J. Water Resource and Protection, **2010, 2, 259-266**
doi:10.4236/jwarp.2010.23030 Published Online March 2010 (http://www.scirp.org/journal/jwarp)

Production of Natural Coagulant from Moringa Oleifera Seed for Application in Treatment of Low Turbidity Water

Eman N. Ali*, Suleyman A. Muyibi, Hamzah M. Salleh, Md Zahangir Alam, Mohd Ramlan M. Salleh
Biotechnology Engineering Department, Faculty of Engineering, International Islamic University Malaysia, Kuala Lumpur, Malaysia
E-mail: *iman*129@yahoo.com
Received September 29, 2009; *revised October* 7, 2009; *accepted October* 19, 2009

Abstract

This study focused on developing an efficient and cost effective processing technique for *Moringa oleifera* seeds to produce natural coagulant for use in drinking water treatment. The produced natural coagulant can be used as an alternative to aluminum sulphate and other coagulants and used worldwide for water treatment. This study investigates processing *Moringa oleifera* seeds to concentrate the bio-active constituents which have coagulation activity. *Moringa oleifera* seeds were processed for oil extraction using electro thermal soxhlet. Isolation and purification of bio-active constituents using chromatography technique were used to determine the molecular weight of the bio-active constituents. The molecular weight of bio-active constituents found to be in a low molecular weight range of between 1000 – 6500 Dalton. The proposed method to isolate and purify the bio-active constituents was the cross flow filtration method, which produced the natural coagulant with very simple technique (oil extraction; salt extraction; and microfiltration through 0.45 µm). The turbidity removal was up to 96.23 % using 0.4 mg/L of processed *Moringa oleifera* seeds to treat low initial turbidity river water between 34-36 Nephelometric Turbidity Units (NTU) without any additives. The microfiltration method is considered to be a practical method which needs no chemicals to be added compared to other researchers proposed methods. The natural coagulant produced was used with low dosages to get high turbidity removal which considered to be a breakthrough in this study and recommended to be scaled up for industry level. The product is commercially valuable at the same time it is minimizing the cost of water treatment.

Keywords: Moringa Oleifera, Drinking Water Treatment, Bioactive Constituents, Coagulation, Flocculation, Turbidity

1. Introduction

Developing countries are facing potable water supply problems because of inadequate financial resources. The cost of water treatment is increasing and the quality of river water is not stable due to a suspended and colloidal particle load caused by land development and high storm runoff during rainy season, such is experienced in a country like Malaysia.

About 1.2 billion people still lack safe drinking water and more than 6 million children die from diarrhea in developing countries every year. In many parts of the world, river water that can be highly turbid is used for drinking purposes. World Health Organization (WHO) has set the guideline value for the residual turbidity in drinking water at 5 Nephelometric Turbidity Units (NTU) [1]. As identified by the United States Environmental Protection Agency (USEPA), turbidity is a measure of the cloudiness of water; it is used to indicate water quality and filtration effectiveness. Higher turbidity levels are often associated with higher levels of disease-causing micro organisms such as viruses, parasites and some bacteria. These organisms can cause symptoms such as nausea, cramps, diarrhea, and associated headaches [2].

Water-borne infectious disease caused by viruses, bacteria, protozoa and other micro organisms is associated

with outbreaks of and background rates of disease in developed and developing countries worldwide [3].

Naturally occurring coagulants are usually presumed safe for human health. Earlier studies have found the *Moringa oleifera* seeds are non-toxic, and recommended its use as coagulant in water treatment in developing countries.

Moringa oleifera is the best natural coagulant discovered so far that can replace aluminum sulphate (alum), which is used widely for water treatment around the world.

The consumption of alum is very high in water treatment in Malaysia. The main concern in this study is low turbidity water which was difficult to be treated according to other researcher's presentations. The ideal plant for low turbidity water treatment in Malaysia is Wangsa Maju Water Treatment Plant (Puncak Niaga (M) Sdn Bhd) which was used for comparison in this study, the process flow sheet (Appendix A). The plant is working to treat the low turbid water with initial turbidity of 30 NTU or less. The process depends on using several additives to get residual turbidity of less that 5 NTU. The dose of alum usually used is between 13-18 mg/L, chlorine is added with an amount of 3.55 Kg/hour, and for post chlorination 5.5 Kg/hour, besides adding fluoride 0.5-0.6 mg/L, lime ($CaCO_3$) for pH adjustment, and Chamfloc 151 sludge dewatering with an amount of 3% w/w. Some chemicals are local and some are imported (Personal communications). Therefore, this study focused on the treatment of low turbidity water.

2. Materials and Methods

The proposed method to isolate and purify the bio-active constituents is the cross flow filtration method, which produced the natural coagulant with very simple technique (oil extraction; salt extraction; and microfiltration through 0.45 µm). Process flow chart is shown in **Figure 1**.

2.1 Preparation of *Moringa oleifera* seeds

Good quality dry seeds of *Moringa oleifera* were selected from the pods that were collected from Serdang, Selangor Darul Ehsan, Malaysia. The pods collected were allowed to completely dry on the tree (the brown colour pods) because the green pods do not possess any coagulation activity [4].

The pods length ranged between (40-60) cm, and each pod contained around (20-30) seeds. The seeds coat and wings were removed manually, followed by the grinding of the seeds into a fine powder using a domestic blender (National, MX-896TM), then sieving the ground powder through 250 µm sieve (**Figure 2**).

2.2. Oil Extraction

Prior to extraction of bioactive constituents through ion exchange resin, the ground and sieved *Moringa oleifera* seed powder with size of < 250 µm was defatted with hexane by using electro thermal soxhlet apparatus (ROSS, UK). This was done by weighing of 10 gm of *Moringa oleifera* seed powder and setting it in the thimbles of the electro thermal soxhlet extraction chamber, adding 170 ml of hexane in the heating chamber, then evaporating of hexane through three cycles each for 30 min to ensure the extraction of oil from the seeds, until the hexane became colorless, drying of *Moringa oleifera* cake residue from the soxhlet thimbles and weighing the dry sample [5].

The *Moringa oleifera* cake residue stock after oil extraction was used in this study; the oil percentage was 35 % w/w. The sample of 1 Kg was defatted and kept to be used throughout the study period at room temperature a round 23±2 ºC.

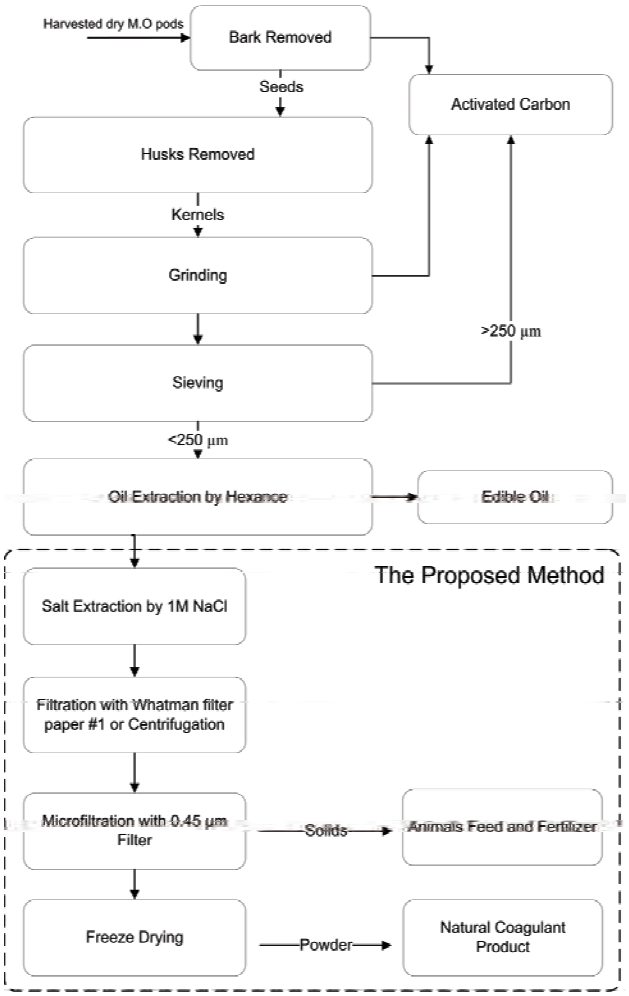

Figure 1. Proposed production process flow chart.

Figure 2. *Moringa oleifera* pods and seeds.

2.3. Salt Extraction

The extraction was done by adding a sloution of 1 Molar NaCl to the sample and mixed for 30 minutes using the magnetic stirrer (ERLA, ERLA Technologies (M) Sdn. Bhd. Malaysia). The extracted solution was centrifuged at 6000 rpm for a period of 10 minutes using the centrifuge (Eppendorf, 5804R, Germany). The supernatant was injected to ion exchange column.

2.4. Ion Exchange Process

The ion exchange technique was followed to isolate and purify the bioactive constituents for molecular weight measurements. The steps of the process were as follows:

2.4.1. Buffers Preparation

Two buffers were prepared for this stage of research as follows:

- **Phosphate buffer stock (1 M):** Phosphate buffer stock (1 M) with pH 7.5 was made by adding 174.16 gm of di-potassium hydrated phosphate (K_2HPO_4, GmBH Chemicals, Germany) into 900 ml of distilled water. The pH of the solution was 9.41 which were adjusted to 7.5 by adding 5 M HCl. The preparation of the buffer stock solution was finalized by adjusting the volume to 1000 ml by adding distilled water.
- **Buffer A** (0.1 M phosphate buffer): Preparation of 0.1 M phosphate buffer was by adding 100 ml of 1 M phosphate buffer stock into 900 ml of distilled water, 0.02 % NaN_3 was added to the solution as anti-bacterial agent.
- **Buffer B** (1.0 M NaCl in 0.1M phosphate buffer): This buffer was prepared by adding 58.44 gm of NaCl (GmBH Chemicals, Germany) to 900 ml of buffer A, and adjusting the volume to 1000 ml.

2.4.2. Preparation of the Column

The Glass Column (300×25 mm, with Bio-Rex Resin 70, Bio-Rad, USA) was used for ion exchange. The resin (Bio-Rex 70) was prepared by adding the resin powder to buffer A, and mixing the contents until the slurry was homogenous. Afterwards, the slurry was loaded to the glass column. The resin was then washed with 2 M NaCl to remove any impurities that may be present in the resin. It was then washed with buffer A to equilibrate the column to be ready for the loading of the sample.

2.4.3. Loading of the Sample to Ion Exchange Column

Equilibrate the column with 300 ml of 0.1 M phosphate buffer**.** Loading 30 ml of the extracted proteins sample as prepared in 2.3 above. Applying buffer A with an amount equal to twice of the column volume (300 ml) to wash all the unwanted negative charged proteins. Applying buffer B with 1 M NaCl, and buffer (A and B) and mixing them before sending to ion exchange. The flow rate was adjusted at 2 ml/min, and the fractions collected were 120 fractions with 5 ml volume each. Measuring absorbance of fractions using spectrophotometer (SEC-OMAM, Anthelie Advanced, France) at wave length 280 nm. The absorbance for the eluted fractions is plotted and 11 points were chosen for molecular weight measurements as shown in **Figure 3**.

2.5. Determination of Molecular Weight

High performance liquid chromatography (HPLC) equipment was used. The bio-active constituents purified by chromatography technique were injected to HPLC to determine the molecular weight. Eleven points were

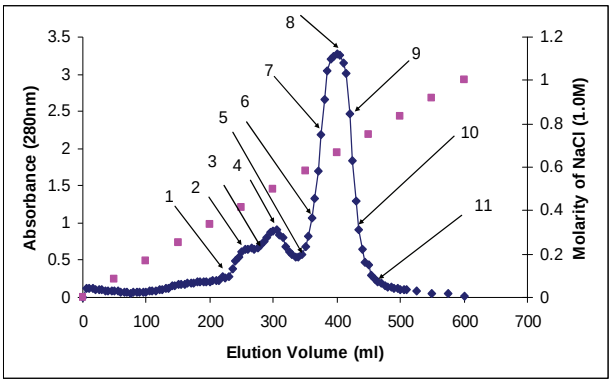

Figure 3. Eluted fraction from Ion exchange column.

selected from **Figure 3** to measure the molecular weight of different eluted fractions. HPLC (Waters 1525 with Binary HPLC Pump, Waters 2487 Dual λ Absorbance Detector, and Breeze GPC software, from Waters, 34 Maple Street Milford, MA 01757, USA) was used to measure the molecular weight of the bioactive constituents with Gel Filtration Column 300×7.8 mm (Bio-Sil SEC-125) for molecular weight measurement besides guard column 80×7.8 mm (Bio-Sil 125)was connected before the column to the HPLC to protect the column. The standard used was Bio-Rad Gel Filtration Standard with Thyroglobulin, IgG, Ovalbumin, Myoglobin, and Vitamin B12. The molecular weight is 670, 158, 44, 17, and 1.35 kDa, respectively. The buffer used was sodium phosphate (GmBH Chemicals, Germany). Filter paper (Waters GHP 0.45 µm) was used to filter the sample before injecting into HPLC.

The buffer used for HPLC was prepared as follows: 0.5 M NaH_2PO_4; 0.5 M Na_2HPO_4: 1.5 M NaCl; and 0.10 M NaN_3. The buffer used as a mobile phase for the HPLC is mixture from the above solutions as follows: 100 ml of 0.5 M NaH_2PO_4, 100 ml of 0.5 M Na_2HPO_4, 100 ml of 1.5 M NaCl, 100 ml of 0.10 M NaN_3. Subsequently by adding the above solution to one litre flask and completing the volume to 1000 ml by adding distilled water. The buffer prepared is contained the following concentration: 0.05 M NaH_2PO_4, 0.05 M Na_2HPO_4, 0.15 M NaCl, 0.01 M NaN_3 with pH = 6.8, and this Eluant is used as mobile phase in HPLC.

2.6. Cross Flow Filtration

The proposed method of microfiltration and ultrafiltration were performed for bioactive constituent's separation. The microfiltration followed by ultrafiltration was carried out as follows:

2.6.1. Microfiltration

The use of microfiltration was to reduce the organic load in the processed *Moringa oleifera* seeds. Cross flow filtration (QuixStand Benchtop System, Sweden), with peristaltic pump (Watson-Marlow Bredel Pumps, Falmonth Cornwall TR 11 4RU, England) was used. The microfiltration cartridge (CFP-4-E-3MA) were used for sample filtration with pore size of 0.45 µm with a fiber ID 1mm, membrane area 110 cm^2, and nominal flow path length 30 cm. The structure is a polysulfone membrane which operates in a vertical orientation complete process fluid drainage. It is typical for concentration and purification of proteins, and suitable for scaling-up studies (GE Healthcare Bio-Science Corp. USA). The supernatant was then injected to ultrafiltration cartridge.

The new cartridge needs to be washed although it is shipped dry. It was washed with warm distilled water (55 °C) and rinsed for 5 minutes at a pressure of 0.3 bar (5 psig).

2.6.2. Ultrafiltration Process

The Xampler ultrafiltration cartridge (UFP-1-C-3M) was used for bioactive constituents separation with cutoff of 1000 Dalton, with fibre ID 0.5 mm, membrane area 140 cm^2, and nominal flow path length 30 cm, the type of membrane is polysulfone hollow fibre type (GE Healthcare Bio-Science Corp. USA).

2.7. Coagulation Activity Tests

The jar test was performed to monitor the coagulation activity of the processed *Moringa oleifera* seed in water treatment.

2.7.1. Synthetic Water (Kaoline Suspension) Preparation

A weight of 5 gm of Kaoline, laboratory grade (K7375, particle size 0.1-4 µm, Sigma-Aldrich), was dissolved with 500 ml of distilled water. Sodium bicarbonate solution with concentration of 100 mg/l was prepared by adding 100 mg of sodium bicarbonate (GmBH Chemicals, Germany) to 1000 ml of distilled water; Adding 500 ml of the sodium bicarbonate solution to the kaoline; Stirring the mixture at 200 rpm for 60 minutes to uniform the dispersion of clay particles. The suspension then was allowed to stand for 24 hours for complete hydration of the kaoline [4,6,7]. This is the stock kaoline solution for the coagulation activity evaluation throughout the study period and this stock was diluted a few times to get the turbidity needed for each particular test.

2.7.2. Jar Test

The jar test was performed for each stage of purification process to monitor the coagulation activity. The method applied was according to [5] with rapid mixing of 125 rpm for 4 minutes, followed by slow mixing of 40 rpm for 25 minutes and settling time of 1 hour. The jar test was carried out using (Stuart Flocculator SW6, Barloworld, UK) equipped with six paddles rotating in a set of six beakers. A turbidimeter 2100P (HACH company, USA) was used for all turbidity measurements.

3. Results and Discussion

The molecular weight of the chosen eleven points for this study showed different low range molecualr weight (**Table 1**). All the points have low molecular weight which is ranged from 6500 to less than 1350 Dalton. The eluted fractions from the ion exchange column were used to monitor the coagulation activity and measuring the turbidity removal using the conventional jar test method. The results of turbidity removal percentage are tabulated in **Table 2**.

Table 1. Molecular weight for 11 points selected in Figure 3.

Point #	Retention time (min)	Molecular weight Range (Dalton)
1	11.40	~4000
2	11.20, 11.50, 12.20	~5000, ~3500, < 1350
3	11.20, 11.40	~5000,~ 4000
4	11.10, 11.40	~6000, ~4000
5	11.50, 13.20	~3500, < 1350
6	11.387, 12.167, 13.070	~4000, < 1350
7	11.10, 11.50, 12.20, 13.00	~6000, ~3500, < 1350
8	11.00, 11.40, 12.00	~6500, ~4000, 1500
9	11.50, 12.30, 13.05	~3500, < 1350
10	11.374, 12.162, 13.016	~4000, < 1350
11	11.383, 12.107, 13.110	~4000, < 1350

Table 2. Turbidity removal percentage for 11 selected points.

Sample #	Optimum residual turbidity (NTU)	Turbidity removal %
1	10.62	64.60
2	2.23	92.13
3	2.95	90.16
4	1.78	94.08
5	2.03	93.24
6	1.38	95.39
7	5.21	82.63
8	4.71	84.29
9	1.65	94.49
10	0.64	97.12
11	1.56	94.80

The main concern in using *Moringa oleifera* for water treatment is the significant increase in organic load, as organic matters originating from the seeds can be released into the water during treatment [8,9]. The presence of organic matter in treated water can cause problems of colour, taste, and odour, and also facilitates the development of microorganisms upon storage [10]. Jahn [11] reported that water treated with crude *Moringa oleifera* extract should not be stored for more than 24 hours. The crude extract is therefore not generally suitable for large water supply systems where the hydraulic residence time is very high. Oil extraction is of a great advantage here, to reduce the organic load from the seeds, and to produce edible oil as a by-product. It is clearly possible to extract oil first and then use the aqueous extract as a coagulant. This dual exploitation is even advantageous for isolation and purifying the active agents in the coagulation with *Moringa oleifera* seed and also for the reduction of organic matter concentration in the treated water [4].

Two steps were followed to produce the natural coagulant by cross flow filtration. The first step was microfiltration, which is important for reducing the organic matters concentration. The main concern here is to filter all the oil from the seeds to reduce the organic content, because it can act as a precursor of trihalomethane formation during the disinfection process by chlorine which may be carcinogenic [8]. It is also may be postulated that the oil content in the seed will form an emulsion or film coating which may inhibit the contact with the surface of reaction and thus reduce floc formation. Extraction of the oil may therefore enhance the turbidity removal, resulting in better coagulation and flocculation [12].

The second step was ultrafiltration with 1000 Dalton cutoff membrane. In this study a simple scalable purification method was found. This is a straightforward production method of processed *Moringa oleifera* for water treatment.

The sample of *Moringa oleifera* seeds was processed as mentioned in Subsections 2.1, 2.2, and 2.3. The extract from the salt extraction process was filtered with Whatman filter paper #1 to remove all the solids from the extract. It was then applied for microfiltration with 0.45 μm microfiltration cartridge. Ndabigengesere & Narasiah [8] used 0.45 μm for microfiltration but the extraction method was with water, followed by many complicated steps to produce the coagulant, and the chemical oxygen demand increased by increasing the dose. No other research has been done on the microfiltration process. Permeate collected from microfiltration process was applied in the QuixStand Benchtop System apparatus to separate the retentate and permeate according to the molecular weight cutoff of 1000 Dalton.

The jar test was performed by using synthetic water and applying the three samples produced from: 1) microfiltration (0.45 μm), 2) the retentate of ultrafiltration (1000 Dalton), and 3) permeate of ultrafiltration (1000 Dalton), and the results of residual turbidity are shown in

Figures 4, **5**, and **6**, respectively.

From the results obtained, 0.45µm microfiltration, showed a low residual turbidity of 1.32 NTU by adding 0.4 mg/L of processed *Moringa oleifera* to the synthetic water samples (**Figure 4**) with turbidity removal of 96.23 %. Also, there is no significant improvement by using ultrafiltration with 1000 Dalton after using microfiltration (**Figure 5**) because the retentate was 95 % of the total volume of the sample which is not economically feasible. By using a dose of 0.4 mg/L of the retentate, the residual turbidity was 2.29 NTU which is not much different from the result obtained from microfiltered sample through a 0.45 µm membrane. On the other hand, the use of permeate, gives residual turbidity of 2.38 NTU by using a double dose which is 0.8 mg/L (**Figure 6**) compared to the retentate dosage. This means that the bioactive compounds were passing to the permeate. Furthermore, for the ultrafiltration, it was observed that the bioactive constituents were covering all the molecular weights presented in the sample, because 5% of permeate of ultrafiltration gave good coagulation activity only by using the double dose (0.8 mg/L gave 93.20 removal efficiency and 0.4 mg/L of retentate gave 93.46 % removal efficiency). The result indicated that there was no improvement in the product quality using 1000 Dalton ultrafiltration membrane.

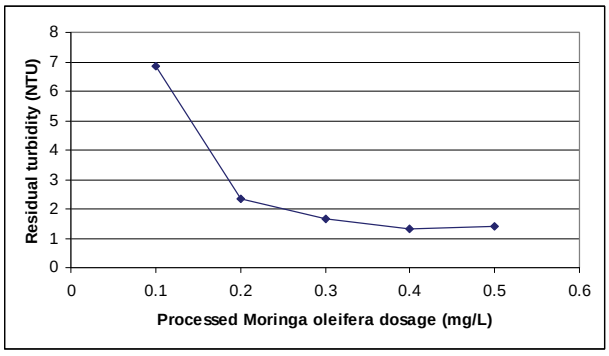

Figure 4. Residual Turbidity for microfiltration with 0.45 µm.

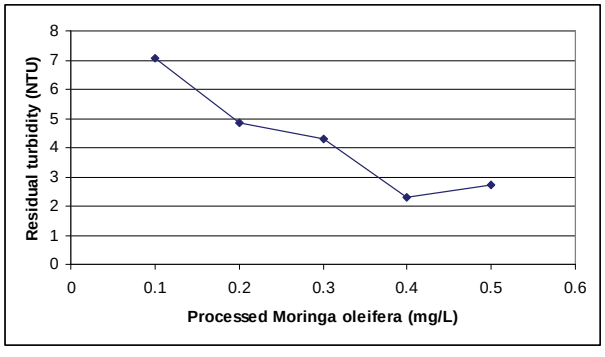

Figure 5. Residual Turbidity for microfiltration with 0.45 µm followed by 1000 Dalton (Retentate).

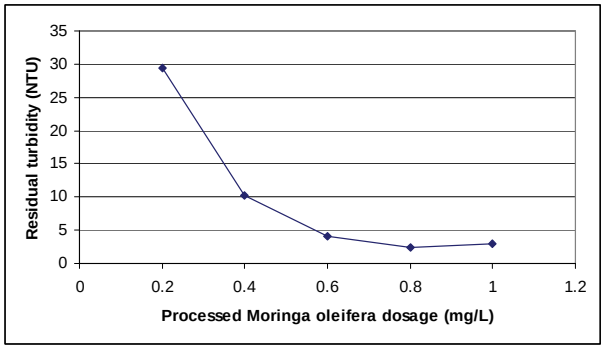

Figure 6. Residual Turbidity for microfiltration with 0.45 µm followed by 1000 Dalton (Permeate).

The ultrafiltration method involved the use of 1000 Dalton due to low molecular weight of less than 6500 Dalton (salt extraction method), in contrast with Ndabigengesere *et al*. [4] where the molecular weight was 13000 Dalton (water extraction method). The latter discovered out that the active components were retained on the 10000 Dalton membrane, while passed through the 30000 Dalton membrane.

4. Conclusions

The results showed that the cross flow filtration with microfiltration was sufficient to produce the natural coagulant with a more efficient and cost effective technique. It was observed that microfiltration with filter size of 0.45 µm is enough to produce a natural coagulant with good coagulation activity. It was clear in this study that to include ultrafiltration step in the production process was considered as a loss, besides the waste of time and labour. The ultrafiltration was not beneficial because permeate was very low, and separation was inadequate to improve the coagulation activity.

5. Acknowledgements

The authors are grateful to the Ministry of Science Technology and Innovation of Malaysia for funding the Project (IRPA 09-02-08-10002 EAR).

6. References

[1] G. L. McConnachie, G. K. Folkard, M. A. Mtawali, and J. P. Sutherland, "Field trials of appropriate hydraulic flocculation processes," Water Research, Vol. 33, No. 6, pp. 1425–1434, 1999.

[2] http://www.who.int/water_sanitation_health/dwq/infectdis/en/index.html.Retrieved October 24, 2008.

[3] http://www.epa.gov/safewater/contaminants/index.html.Retrieved October 24, 2008.

[4] A. Ndabigengesere, K. S. Narasiah, and B. G. Talbot, "Active agents and mechanism of coagulant of turbid waters using *Moringa oleifera*," Water Research, Vol. 29, No. 2, pp. 703–710, 1995.

[5] S. A. Muyibi, S. A. Abbas, M. J. M. M. Noor, F. R. Ahmadon, "Enhanced coagulation efficiency of *Moringa oleifera* seeds through selective oil extraction," IIUM Engineering Journal, Vol. 4, No. 1, pp. 1–11, 2003.

[6] S. A. Muyibi and L. M. Evison, "Optimizing physical parameters affecting coagulation of turbid water with *Moringa oleifera* seeds," Water Research, Vol. 29, No. 12, pp. 2689–2695, 1995.

[7] T. Okuda, A. U. Baes, W. Nishijima, and M. Okada, "Improvement of extraction method of coagulation active components from *Moringa oleifera* seed," Water Research, Vol. 33, pp. 3373–3378, 1999.

[8] A. Ndabigengesere and K. S. Narasiah, "Quality of water treated by coagulation using *Moringa oleifera* seeds," Water Research, Vol. 32, No. 3, pp. 781–791, 1998.

[9] T. Okuda, A. U. Baes, W. Nishijima, and M. Okada, "Coagulation mechanism of salt solution extracted active component in *Moringa oleifera* seeds," Water Research, Vol. 35, No. 3, pp. 830–834, 2001.

[10] M. Broin, C. Santaella, S. Cuine, K. Kokou, G. Peltier, and T. Joët, "Flocculant activity of a recombinant protein from *Moringa oleifera* Lam Seeds," Applied Microbiol Biotechnol, Vol. 60, pp. 114–119, 2002.

[11] S. A. A. Jahn, "Using *Moringa oleifera* seeds as coagulant in developing countries," J. Am. Wat. Wks Ass., Vol. 6, pp. 43–50, 1988.

[12] S. A. Muyibi, M. J. M. M. Noor, T. K. Leong, and L. H. Loon, "Effect of oil extraction from *Moringa oleifera* seeds on coagulation of turbid water," Environment Studies, Vol. 59, No. 2, pp. 243–254, 2002.

Appendix A

WANGSA MAJU WATER TREATMENT PLANT

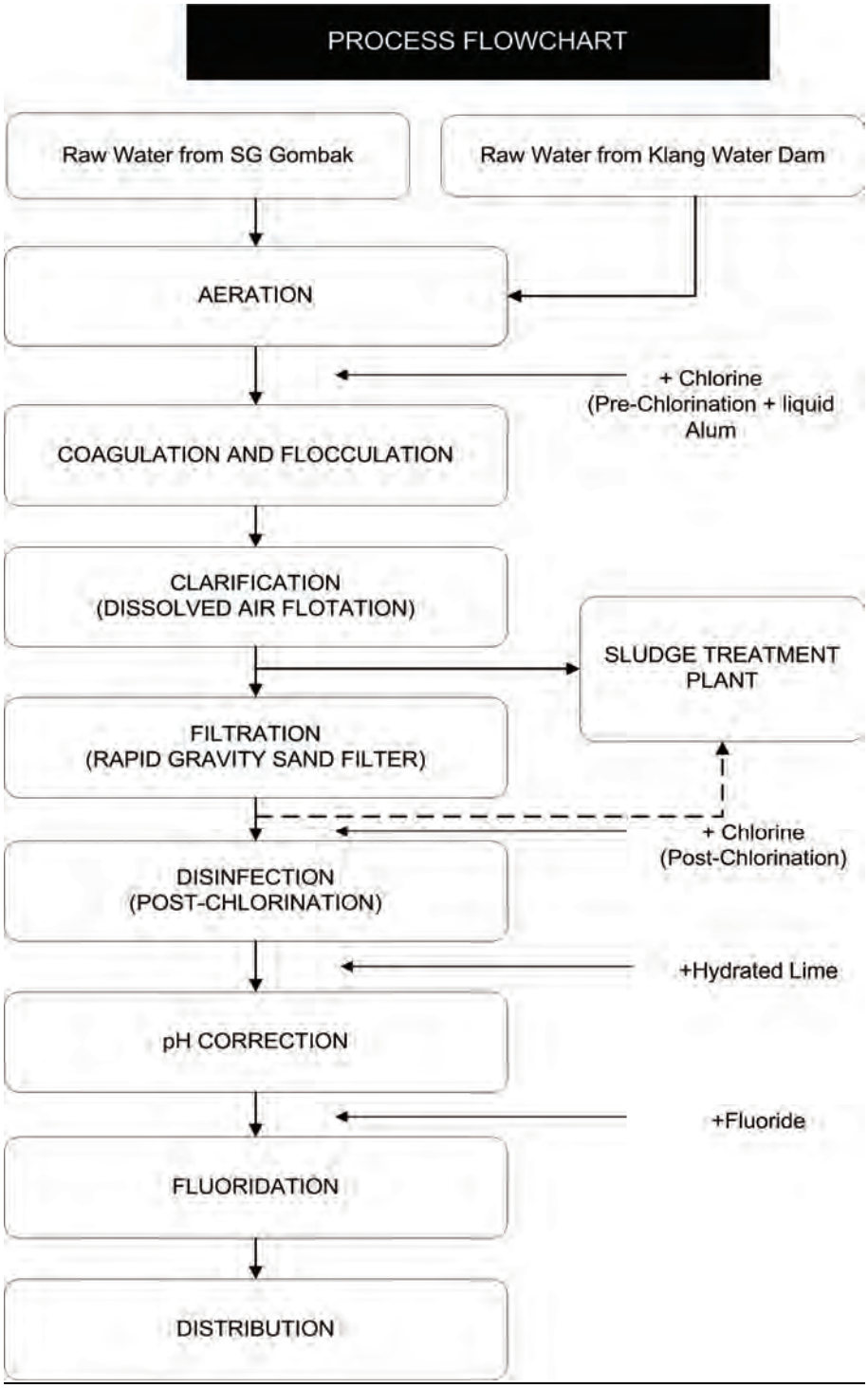

J. Water Resource and Protection, **2010, 2, 267-281**
doi:10.4236/jwarp.2010.23031 Published Online March 2010 (http://www.scirp.org/journal/jwarp)

Simulation of Runoff and Sediment Yield for a Himalayan Watershed Using SWAT Model

Sanjay K. Jain[1], Jaivir Tyagi[1], Vishal Singh[2]
[1]*National Institute of Hydrology, Roorkee, India*
[2]*Alternate Hydro-Energy Centre, I IT, Roorkee, India*
E-mail: *sjain@nih.ernet.in*
Received October 12, 2009; *revised December* 7, 2009; *accepted January* 25, 2010

Abstract

Watershed is considered to be the ideal unit for management of the natural resources. Extraction of watershed parameters using Remote Sensing and Geographical Information System (GIS) and use of mathematical models is the current trend for hydrologic evaluation of watersheds. The Soil and Water Assessment Tool (SWAT) having an interface with ArcView GIS software (AVSWAT2000/X) was selected for the estimation of runoff and sediment yield from an area of Suni to Kasol, an intermediate watershed of Satluj river, located in Western Himalayan region. The model was calibrated for the years 1993 & 1994 and validated with the observed runoff and sediment yield for the years 1995, 1996 and 1997. The performance of the model was evaluated using statistical and graphical methods to assess the capability of the model in simulating the runoff and sediment yield from the study area. The coefficient of determination (R^2) for the daily and monthly runoff was obtained as 0.53 and 0.90 respectively for the calibration period and 0.33 and 0.62 respectively for the validation period. The R^2 value in estimating the daily and monthly sediment yield during calibration was computed as 0.33 and 0.38 respectively. The R^2 for daily and monthly sediment yield values for 1995 to 1997 was observed to be 0.26 and 0.47.

Keywords: AVSWATX, Calibration, Validation, Image Processing, Remote Sensing, GIS, Runoff, Sediment Yield

1. Introduction

A Watershed is a hydrologic unit which produces water as an end product by interaction of precipitation and the land surface. The quantity and quality of water produced by the watershed are an index of amount and intensity of precipitation and the nature of watershed management. In some watersheds the aim may be to harvest maximum total quantity of water throughout the year for irrigation and drinking purpose. In another watershed the objectives may be to reduce the peak rate of runoff for minimizing soil erosion and sediment yield or to increase ground water recharge. Hence, the modeling of runoff, soil erosion and sediment yield are essential for sustainable development. Further, the reliable estimates of the various hydrological parameters including runoff and sediment yield for remote and inaccessible areas are tedious and time consuming by conventional methods. So it is desirable that some suitable methods and techniques are used/ evolved for quantifying the hydrological parameters from all parts of the watersheds. Use of mathematical models for hydrologic evaluation of watersheds is the current trend and extraction of watershed parameters using remote sensing and geographical information system (GIS) in high speed computers are the aiding tools and techniques for it.

The Satluj river basin as a whole receives a good amount of rainfall throughout the year, which flows through the Western Himalayan region. Apart from the hill topography, faulty cultivation practices and deforestation within the basin result in huge loss of productive soil and water as runoff. There is an urgent need for developing integrated watershed management plan based on hydrological simulation studies using suitable modeling approach. Considering hydrological behaviour of the basin and applicability of the existing models for the solutions of aforesaid problems, the current study was undertaken with the application of SWAT 2000 in integration with remote sensing and GIS to estimate the surface runoff and sediment yield of an intermediate watershed of Satluj river (Suni to Kasol). The AVSWAT is a preprocessor and as well as a user interface to SWAT

model. The application of AVSWAT2000/X in the present study provided the capabilities to stream line GIS processes tailored towards hydrologic modeling and to automate data entry communication and editing environment between GIS and the hydrologic model. The time series data on rainfall, runoff and sediment yield were available at the gauging station of the catchment and these were used to calibrate and validate the SWAT model and to assess its applicability in simulating runoff and sediment yield from the intermediate watershed in the Himalayan region.

2. The Study Area

The data of an intermediate watershed of Satluj river was used for assessment of runoff and sediment yield in the present study. The study watershed (**Figure 1**) lying between Suni to Kasol in the state of Himachal Pradesh, India is located between latitudes 31˚ 5` to 31˚ 30` N and longitudes 76˚ 50` to 77˚15` E. The watershed covers an area of about 681.5 sq km with an elevation between 600 to 3200 m above mean sea level (msl). The Satluj River flows through the Western Himalayan region. The Western Himalayas cover the hilly areas of Jammu- Kashmir, Himachal Pradesh and Uttarakhand states in India. Two important river systems originating from the Western Himalayan region are 1) Indus system consisting of Indus, Jhelum, Chenab, Ravi, Beas and Satluj rivers, and 2) Ganga system consisting of Yamuna, Ramganga, Sarda, and Karnali rivers. These rivers are fed by snowmelt and rainfall during the summer and by groundwater flow during the winter.

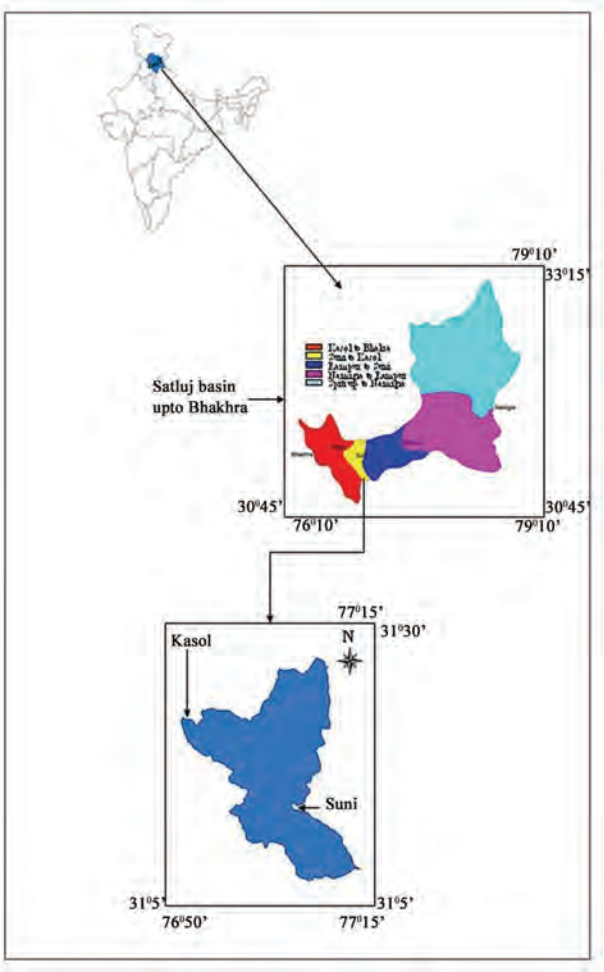

Figure 1. Study area between Suni to Kasol.

3. Swat Model

The SWAT (Soil and Water Assessment Tool) is one of the most recent models developed jointly by the United States Department of Agriculture - Agricultural Research Services (USDA-ARS) and Agricultural Experiment Station in Temple, Texas [1]. It is a physically based, continuous time, long-term simulation, lumped parameter, deterministic, and originated from agricultural models. The computational components of SWAT can be placed into eight major divisions: hydrology, weather, sedimentation, soil temperature, crop growth, nutrients, pesticides, and agricultural management. The SWAT model uses physically based inputs such as weather variables, soil properties, topography, and vegetation and land management practices occurring in the catchment. The physical processes associated with water flow, sediment transport, crop growth, nutrient cycling, etc. are directly modeled by SWAT [2,3]. Some of the advantages of the model include: modeling of ungauged catchments, prediction of relative impacts of scenarios (alternative input data) such as changes in management practices, climate and vegetation on water quality, quantity or other variables. SWAT has a weather simulation model also that generates daily data for rainfall, solar radiation, relative humidity, wind speed and temperature from the average monthly variables of these data. This provides a useful tool to fill in missing daily data in the observed records. The hydrologic cycle as simulated by SWAT is based on the water balance equation:

$$SW_t = SW_o + \sum_{i=1}^{n}(R_{day} - Q_{surf} - E_a - w_{seep} - Q_{gw})$$

where, SW_t is the final soil water content (mm H_2O), SW_o is the initial soil water content (mm H_2O), t is time in days, R_{day} is amount of precipitation on day i (mm H_2O), Q_{surf} is the amount of surface runoff on day i (mm H_2O), E_a is the amount of evapotranspiration on day i (mm H_2O), w_{seep} is the amount of percolation and bypass exiting the soil profile bottom on day i (mm H_2O), Q_{gw} is

the amount of return flow on day *i* (mm H_2O).

In SWAT, a basin is delineated into sub-basins, which are then further subdivided into hydrologic response units (HRUs). HRUs consist of homogeneous land use and soil type (also, management characteristics) and based on two options in SWAT, they may either represent different parts of the sub-basin or sub-basin area with a dominant land use or soil type (also, management characteristics). With this semi-distributed (sub-basins) set-up, SWAT is attractive for its computational efficiency as it offers some compromise between the constraints imposed by the other model types such as lumped, conceptual or fully distributed, physically based models. A full model description and operation is presented in Neitsch *et al.* [4,5]. SWAT uses hourly and daily time steps to calculate surface runoff. The Green and Ampt equation is used for hourly and an empirical SCS curve number (CN) method is used for the daily computation.

Spruill *et al.* [6] evaluated the SWAT model and parameter sensitivities were determined while modeling daily streamflow in a small central Kentucky watershed comprising an area of 5.5 km^2 over a two year period. Streamflow data from 1996 were used to calibrate the model and streamflow data from 1995 were used for evaluation. The model accurately predicted the trends in daily streamflow during this period. The Nash-Sutcliffe [7] R^2 for monthly total flow was 0.58 for 1995 and 0.89 for 1996 whereas for daily flows it was observed to be 0.04 and 0.19. The monthly total tends to smooth the data which in turn increases the R^2 value. Overall the results indicated that SWAT model can be an effective tool for describing monthly runoff from small watersheds.

Fohrer *et al.* [8] applied three GIS based models from the field of agricultural economy (ProLand), ecology (YELL) and hydrology (SWAT-G) in a mountainous meso-scale watershed of Aar, Germany covering an area of 59.8 km^2 with the objective of developing a multidisciplinary approach for integrated river basin management. For the SWAT–G model daily stream flow were predicted. The model was calibrated and validated followed by model efficiency using Nash and Sutcliffe test. In general the predicted streamflow showed a satisfying correlation for the actual landuse with the observed data.

Francos *et al.* [9] applied the SWAT model to the Kerava watershed (South of Finland), covering an area of 400 km^2. The temporal series comprised temperature and precipitation records for a number of meteorological stations, water flows and nitrogen and phosphorus loads at the river outlets. The model was adapted to the specific conditions of the catchment by adding a weather generator and a snowmelt submodel calibrated for Finland. Calibration was made against water flows, nitrate and total phosphorus concentrations at the basin outlet. Simulations were carried out and simulated results were compared with daily measured series and monthly averages. In order to measure the accuracy obtained, Nash and Suttcliffe efficiency coefficient was employed which indicated a good agreement between measured and predicted values.

Eckhartd and Arnold [10] outlined the strategy of imposing the constraints on the parameters to limit the number of interdependently calibrated values of SWAT. Subsequently an automatic calibration of the version SWAT-G of the SWAT model with a stochastic global optimization algorithm and Shuffled Complex Evolution algorithm is presented for a mesoscale catchment.

Tripathi *et al.* [11] applied the SWAT model for Nagwan watershed (92.46km^2) with the objective of identifying and prioritizing of critical sub-watersheds to develop an effective management plan. Daily rainfall, runoff and sediment yield data of 7 years (1992-1998) were used for the study. Apart from hydro-meteorological data, topographical map, soil map, land resource map and satellite imageries for the study area were also used. The model was verified for the monsoon season on daily basis for the year 1997 and monthly basis for the years 1992-1998 for both surface runoff and sediment yield.

Singh *et al.* [12] made a comparative study for the Iroquois river watershed covering an area of 2137 sq. miles with the objectives to assess the suitability of two watershed scale hydrologic and water quality simulation models namely HSPF and AVSWAT 2000. Based on the completeness of meteorological data, calibration and validation of the hydrological components were carried out for both the models. Time series plots as well as statistical measures such as Nash-Sutcliffe efficiency, coefficient of correlation and percent volume errors between observed and simulated streamflow values on both monthly and annual basis were used to verify the simulation abilities of the models.

The review indicated that SWAT is capable of simulating hydrological processes with reasonable accuracy and can be applied to large ungauged basin. Therefore, to test the capability of model in determining the effect of spatial variability of the watershed on runoff, AVSWAT 2000 with arcview interface was selected for the present study.

3. Methodology

3.1. Creation of Data Base

Digital elevation model (DEM) is one of the main inputs of SWAT Model. For preparation of DEM, the vector map with contour lines (from topographic maps) was converted to raster format (Grid) before the surface was interpolated. Grids are especially suited to representing geographic phenomena that vary continuously over space,

and for performing spatial modeling and analysis of flows, trends, and surfaces such as hydrology. Raster data records spatial information in a regular grid or matrix organized as a set of rows and columns. The DEM of the study watershed is shown in **Figure 2**. The drainage map (**Figure 3**) was digitized using Survey of India toposheets at a scale of 1:50,000. The drainage map can be entered into AVSWAT as shape file and grid format.

Landuse map is a critical input for SWAT model. Land use/land cover map was prepared using remote sensing data of Landsat ETM+. The classification of satellite data mainly follows two approaches *i.e.* supervised and unsupervised classification. The intent of the classification process is to categorize all pixels in a digital image into one of several land cover classes, or "*themes*". This categorized data may then be used to produce thematic maps of the land cover present in an image. In the present study, the unsupervised classification method was used for preparation of the land use map (**Figure 4**). The various land use categories and their coverage in the study watershed are presented in **Table 1**.

Soil map of the study area was digitized using soil map of the National Bureau of Soil Survey and Land Use Planning (NBSS&LUP) at a scale of 1:50,000. Soil plays an important role in modeling various hydrological processes. In the AVSWATX model, various soil properties like soil texture, hydraulic conductivity, organic carbon content, bulk density, available water content are required to be analyzed to make an input in the model for simulation purpose. While carrying out the soil sampling, the soil map prepared by NBSS&LUP was used as a base map. The collected 26 soil samples were then analyzed in a standard soil laboratory. Based on the analysis it was observed that the soils in the study area were mostly clayey soils (**Figure 5**) and falls in the hydrologic soil group C & D.

A hydro-meteorological observation network was set up in the Satluj River basin by Bhakra Beas Management Board (BBMB), Nangal. The rainfall is observed at 10 stations namely Bhakra, Berthin, Kahu, Suni, Kasol, Rampur, Kalpa, Rackchham, Namgia and Kaza. In the present study, the rainfall data of Suni and Kasol stations were used. The flows were monitored at Suni and Kasol gauging sites on the main Satluj river. The gauge-discharge sites were monitored for 24 hours during the monsoon period to observe the high floods. The daily runoff and sediment load data of two stations namely Suni and Kasol were collected for the years 1993 through 1997. The processing of meteorological data was done statistically. The simulated daily weather data on maximum and minimum temperature, rainfall, wind speed and relative humidity at all the grid locations for 5 years representing the series approximating 1993 to 1997 time period were processed.

Table 1. Coverage of various land use categories in the study.

Land use category	Code	Area (ha)	% age of Watershed Area
Urban Low Density	URLD	79.00	0.12
Urban High Density	URHD	400.00	0.58
River Water	WATR	886.05	1.30
Scrub	BROM	2584.53	3.74
Agriculture	AGRC	12244.80	17.97
Barren/ Fallow	PAST	7461.00	10.95
Forest Deciduous/ Mixed	FRSD	44514.90	65.34

3.2. Model Set up

AVSWATX automatically delineates a watershed into sub-watersheds based on DEM and drainage network. After the DEM was imported in the model a masking polygon of the study area was created in Arc Info grid format and was loaded in the model in order to extract out only the area of interest. The critical source area or the minimum drainage area required to form the origin of a stream was taken as 2500 ha which formed 13 sub watersheds (**Figure 6**). The area delineated by the AVSWATX interface was found to be 68,134.23 ha against the manually delineated area of 68,170.28 ha. The error of calculation was found to be 0.02%.

The land use and soil map in Arcshape format were imported in the AVSWATX model. Both the maps were made to overlay to subdivide the study watershed into hydrologic response units (HRU) based on the land use and soil types. Subdividing the areas into hydrologic response units enables the model to reflect the evapotranspiration and other hydrologic conditions for different land cover/crops and soils. One of the main sets of input for simulating the hydrological processes in SWAT is climate data. Climate data input consists of precipitation, maximum and minimum temperature, wind speed, relative humidity and the weather generator (.dbf) file. The climate data for study periods were prepared in .dbf format and then imported in the SWAT model. After importing the climatic data, the next step was to set up a few additional inputs for running the SWAT model. These inputs were management data, soil-chemical data, manning's roughness coefficient for overland flow and in-stream water quality parameters. These input files were set up and edited as per the requirement and objective of the study. In the management data file, runoff curve numbers for Indian conditions as well as those prescribed in SWAT user manual were adopted for different land use classes based on the land use type and hydrologic soil group (HSG). Finally the SWAT model was run to simulate the various hydrological components.

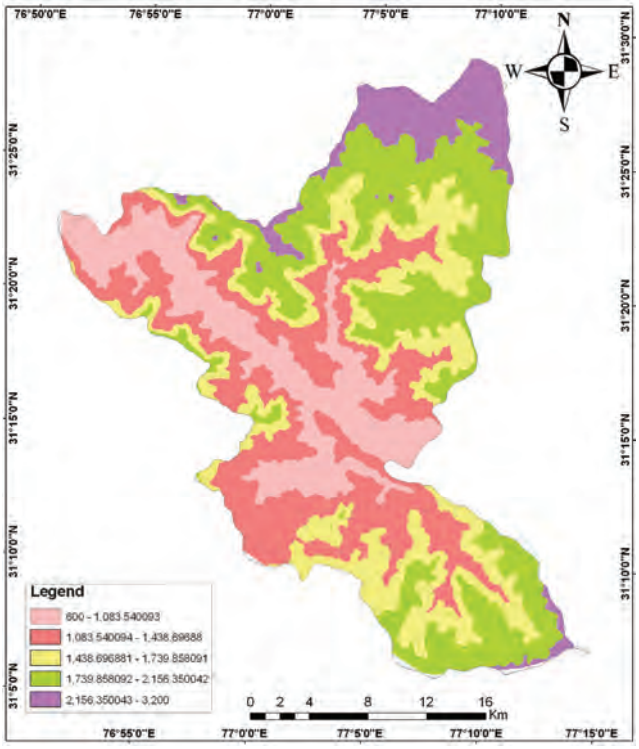

Figure 2. Digital elevation model of the study watershed.

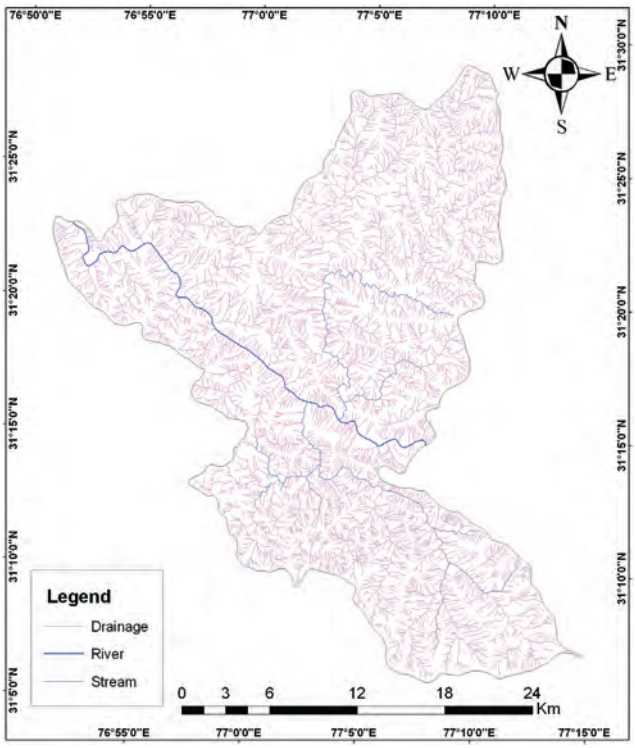

Figure 3. Drainage network in the study area.

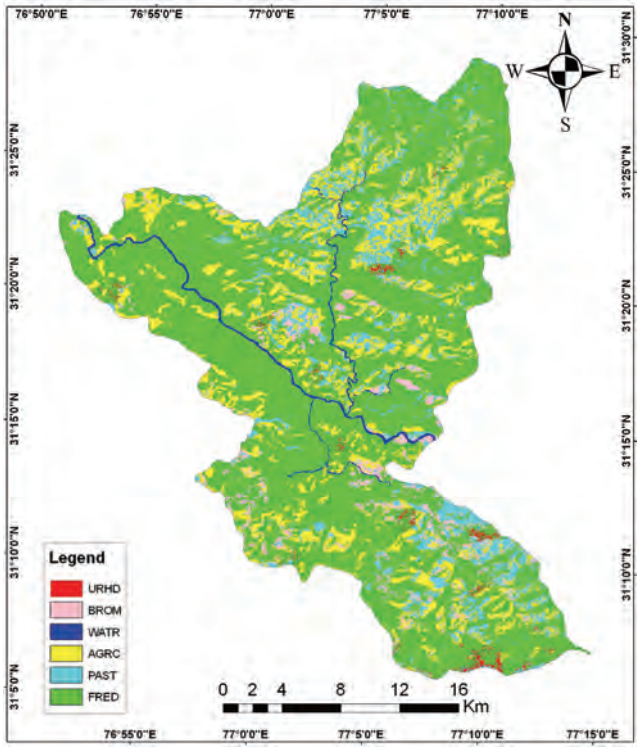

Figure 4. Landuse / landcover of the study area.

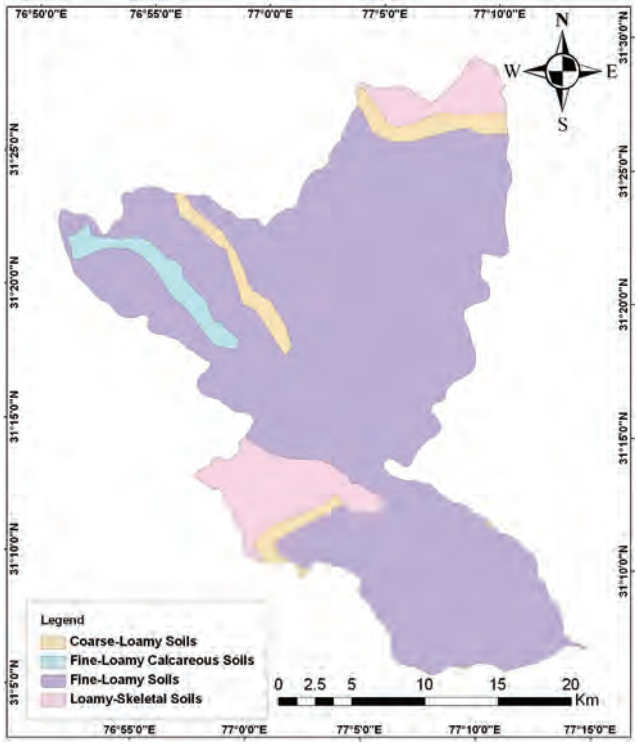

Figure 5. Soil texture map of the study area.

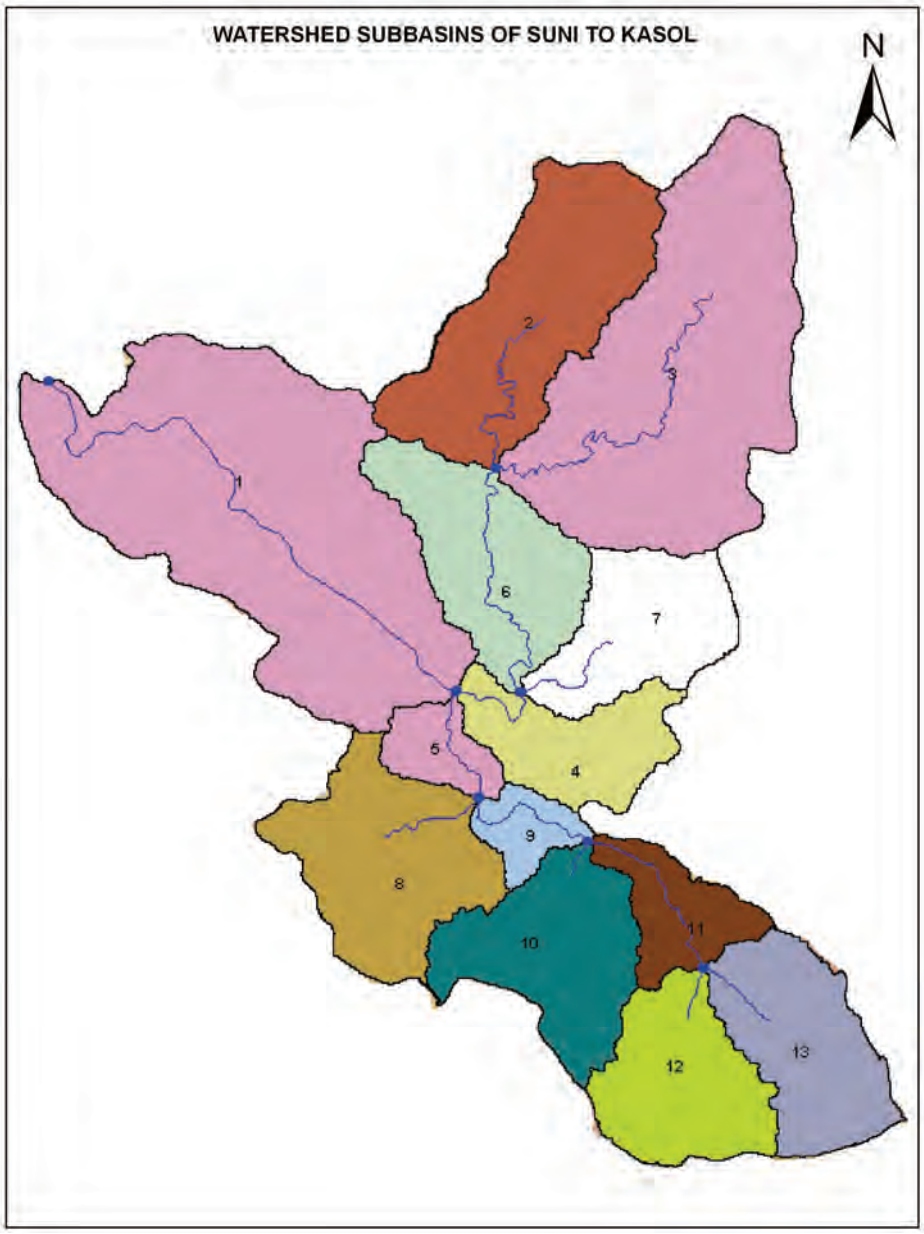

Figure 6. Delineation of sub-watersheds of the study area.

3.3. Performance Evaluation of the Model

Performance of the model was evaluated in order to assess how the model simulated values fitted with the observed values. Several statistical measures are available for evaluating the performance of a hydrologic model. These include coefficient of determination, relative error, standard error, volume error, coefficient of efficiency [13], among others. The coefficient of determination (R^2) is one of the frequently used criteria and was employed in this study. R^2 describes the proportion of the total variance in the measured data that can be explained by the model. It ranges from 0.0 to 1.0, with higher values indicating better agreement, and is given by,

$$R^2 = \left[\frac{\sum_{i=1}^{N} [O(i) - O_{avg}][S(i) - S_{avg}]}{\left[\sum_{i=1}^{N} (O(i) - O_{avg})^2\right]^{0.5} \left[\sum_{I=1}^{N} (S(i) - S_{avg})^2\right]^{0.5}} \right]^2$$

where, $O(i)$ is the i^{th} observed parameter, O_{avg} is the mean of the observed parameters, $S(i)$ is the i^{th} simulated parameter, S_{avg} is the mean of model simulated parameters and N is the total number of events.

4. Results and Discussion

4.1. Model Calibration

The AVSWATX model was calibrated using the daily data of runoff and sediment yield recorded at the outlet of the study watershed for the years 1993 & 1994. The model was calibrated using the values of parameters for available water content (AWC) and soil evaporation compensation factor (SECO) within the prescribed range of the model. Several simulation runs were applied to achieve the model calibration. The time series of the observed and simulated daily and monthly runoff (**Figure 7(a)**, (**b)**) and daily and monthly sediment yield (**Figure 8(a)**, **(b)**) for the calibration period were plotted for visual comparison. From these figures, it can be observed in general that the model

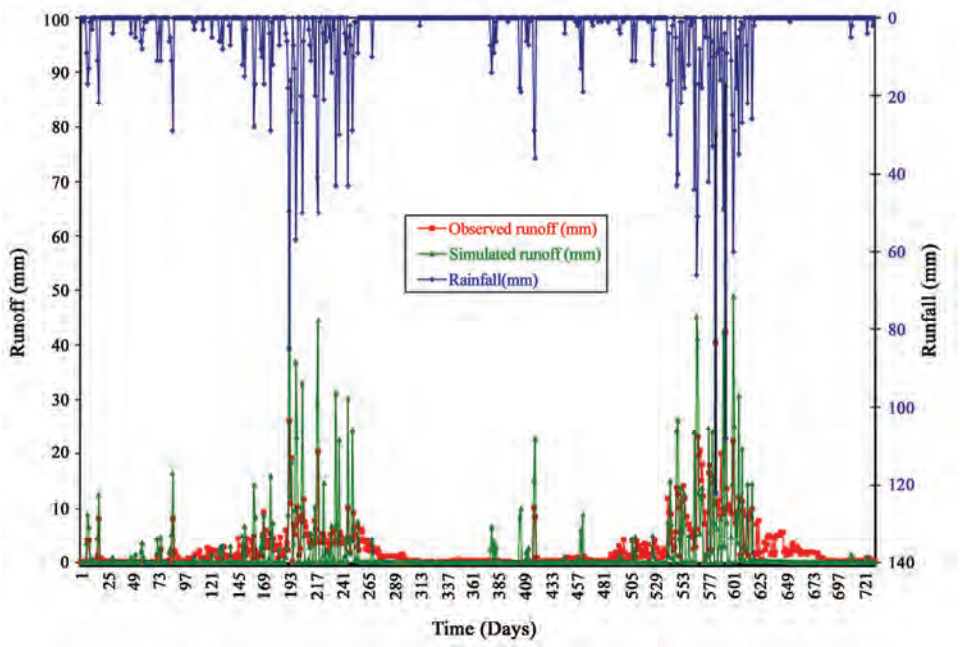

(a)

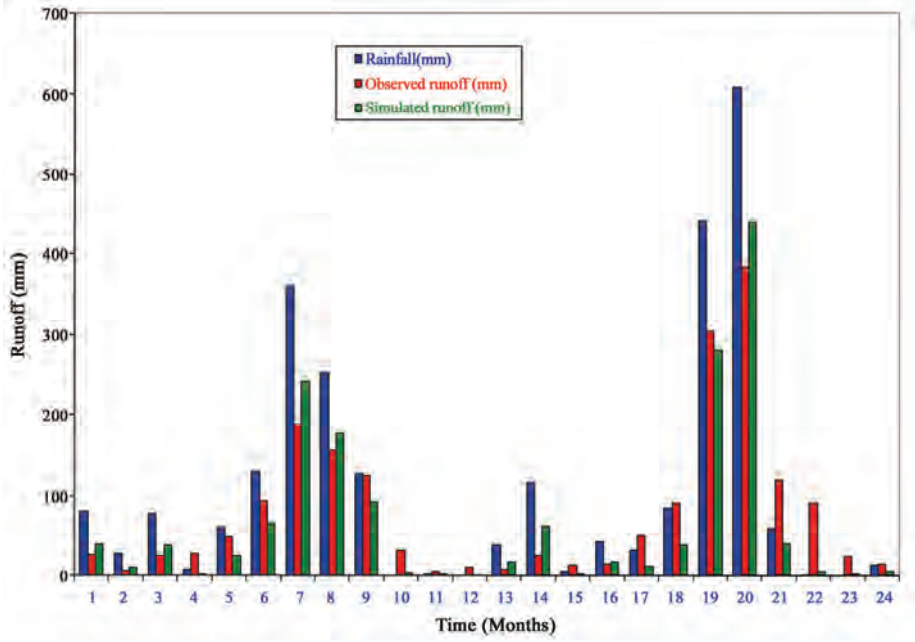

(b)

Figure 7. Comparison of observed and simulated. (a) daily runoff; (b) monthly runoff for the calibration period 1993-94.

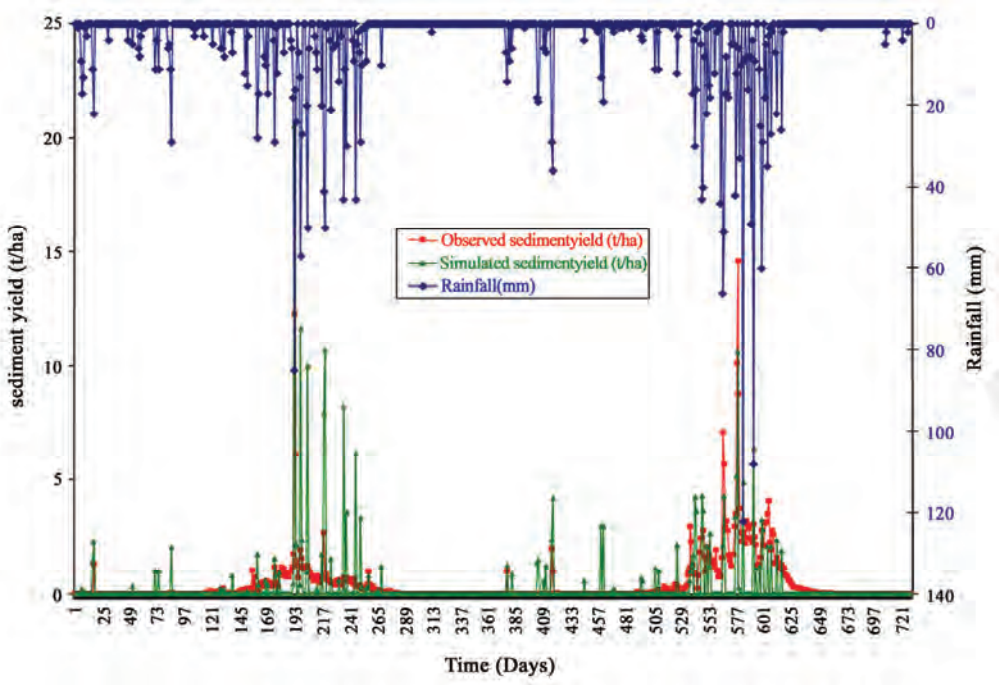

(a)

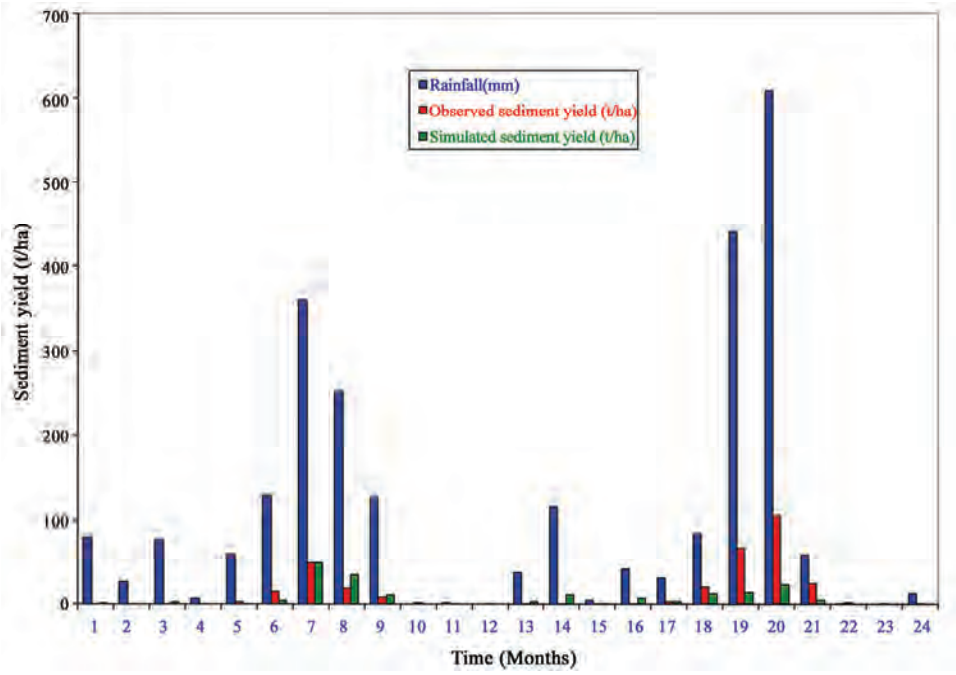

(b)

Figure 8. Comparison of observed and simulated. (a) daily sediment yield; (b) monthly sediment yield for the calibration period 1993-1994.

overestimated the peaks of both runoff and sediment yield in both the years of calibration. The total runoff computed by the model was, however, found to be 691.67 mm and 911.85 mm against the observed runoff of 729.82 mm and 1127.66 mm during 1993 and 1994 respectively. The sediment yield computed by the model during respective years was obtained as 114.72 t/ha and 106.27 t/ha against the observed sediment yield of 99.10 t/ha and 223.83 t/ha respectively. The observed and simulated values were plotted against each other in order to determine the goodness-of fit criterion of coefficient of determination (R^2) both for runoff and sediment

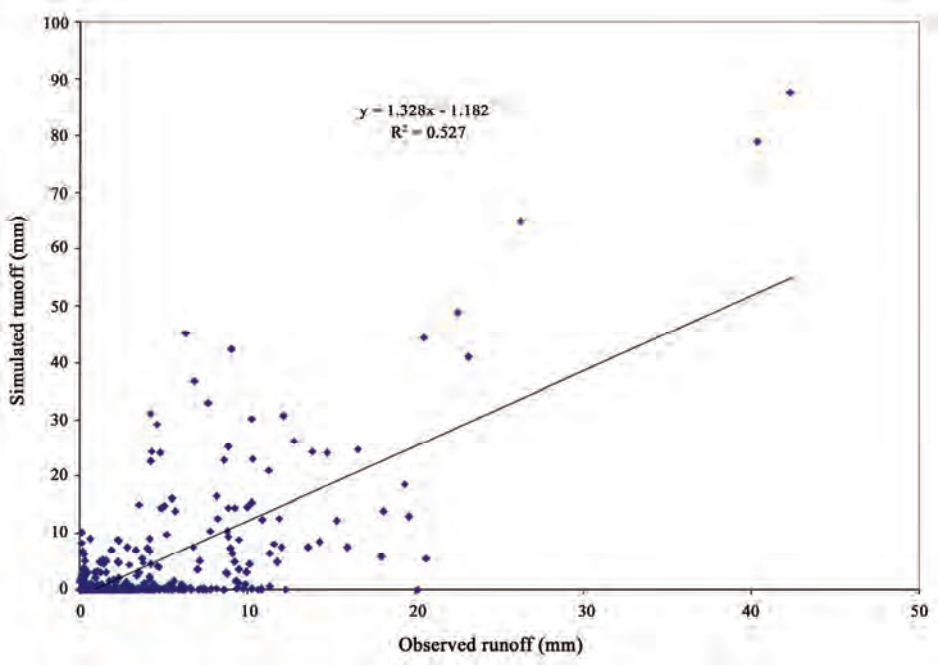

(a)

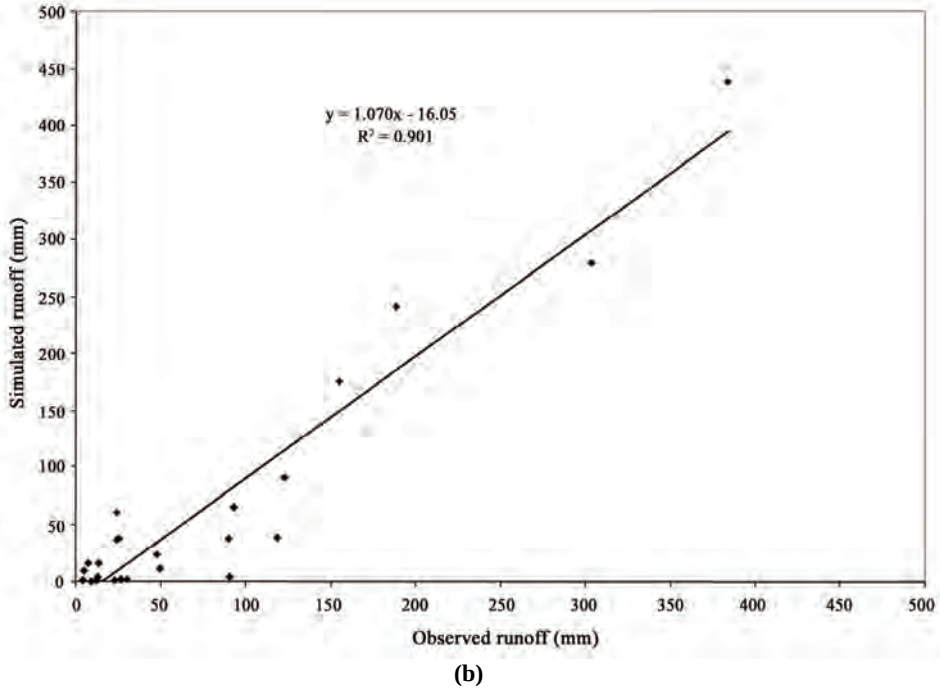

(b)

Figure 9. Goodness-of-fit for observed and simulated. (a) daily runoff; and (b) monthly runoff for the calibration period 1993-94.

yield. The R^2 value for daily and monthly values was obtained as 0.53 and 0.90 respectively for runoff (**Figure 9(a)**, **(b)**) and 0.33 and 0.38 respectively for sediment yield (**Figure 10(a)**, **(b)**). The analysis reveals that the monthly comparison showed a better correlation than the daily values. The poor correlation among daily values in the present study can be supported by the inferences of Peterson and Hamlett [14], Benaman *et al*. [15], Varanou *et al*. [16], Spruill *et al*. [6], and King *et al*. [17]. It was reported that SWAT's daily flow predictions, in general, were not as good as monthly flow predictions. Simulated and observed daily flow comparisons yielded much

lower Nash-Sutcliffe Coefficient (NSC) than monthly comparisons. The monthly totals tend to smooth the data, which in turn increases the NSC [6,18]. While simulating sediment loadings in the Cannonsville Reservoir watershed (1,178 km^2) in New York, Benaman *et al.* [15] noted that the model generally simulated watershed response on sediment, but it grossly under predicted sediment yields during high flow months. In the present study, the error in simulation may also be attributed to some extent perhaps to the unreliable observed data. Another reason could be the number of delineated sub-watersheds. It is reported that watershed subdivision has an effect on the sediment load [19].

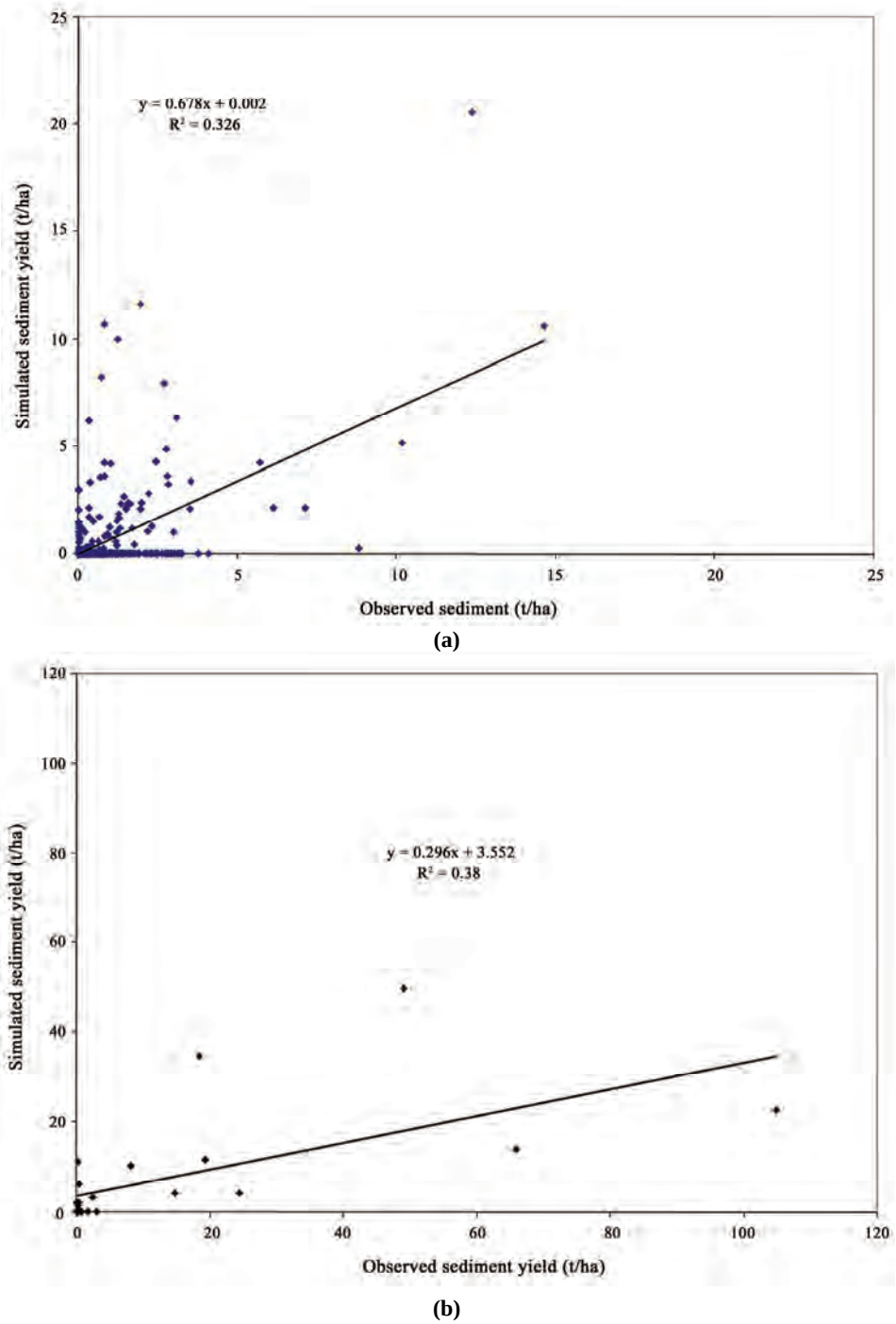

Figure 10. Goodness-of-fit for observed and simulated. (a) daily sediment yield; (b) monthly sediment yield for the calibration period 1993-94.

4.2. Model Validation

The model validation was carried out for daily and monthly surface runoff and sediment yield for the years 1995 to 1997. A graphical comparison of the observed and simulated daily and monthly flows (**Figure 11(a)**, **(b)**) show that the peaks of the surface runoff were over-estimated in most of the events. During the years 1995,

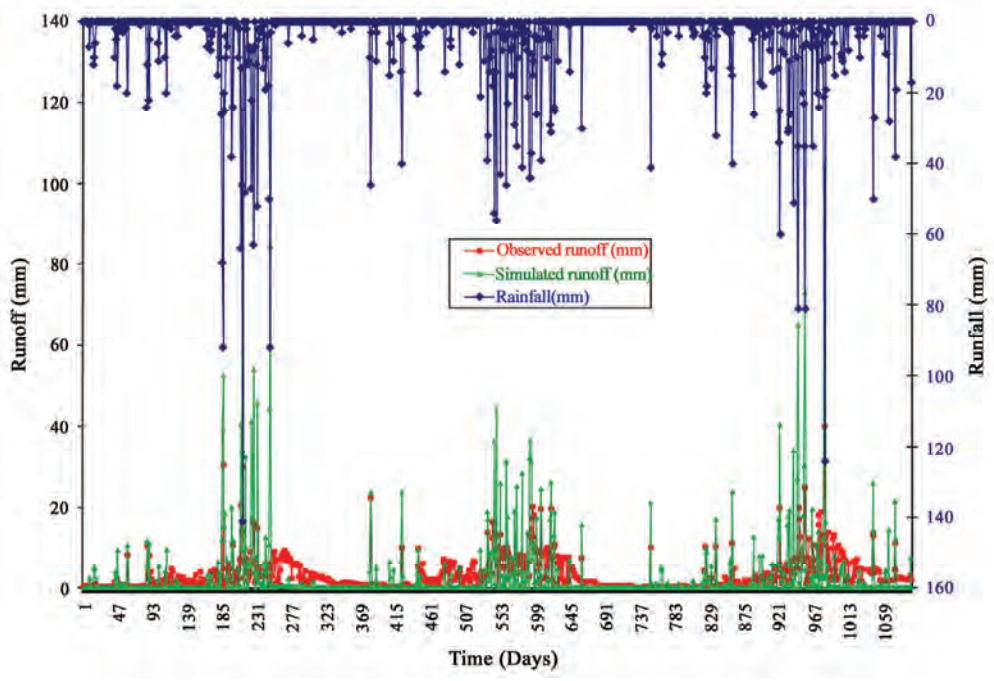

(a)

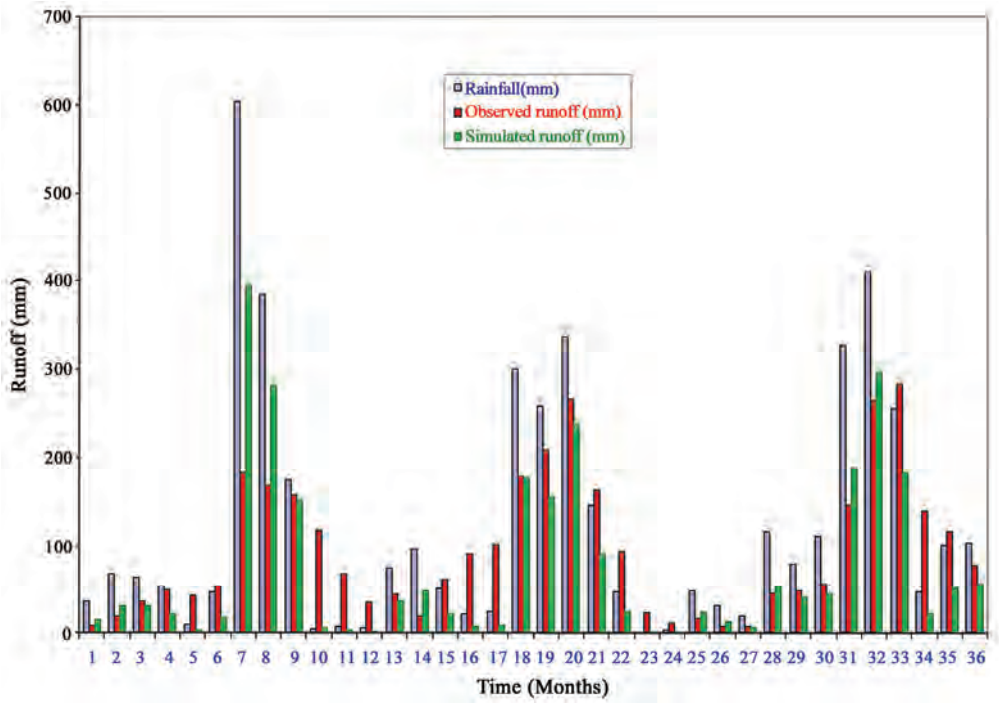

(b)

Figure 11. Comparison of observed and simulated (a) daily runoff, and (b) monthly runoff for the validation period 1995-97.

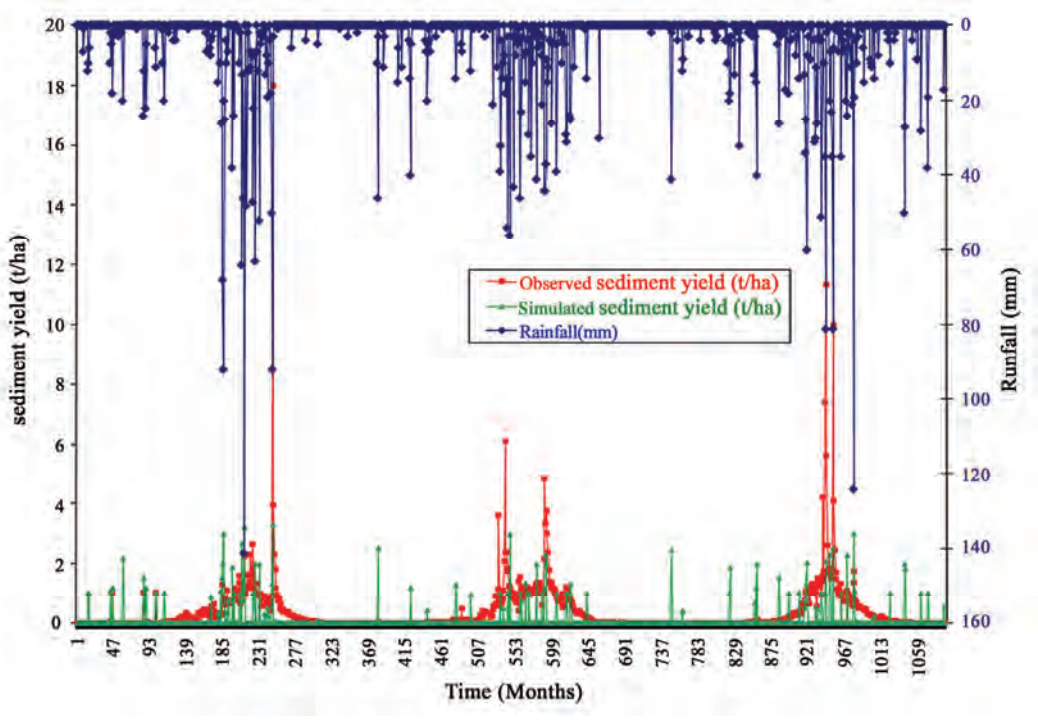

(a)

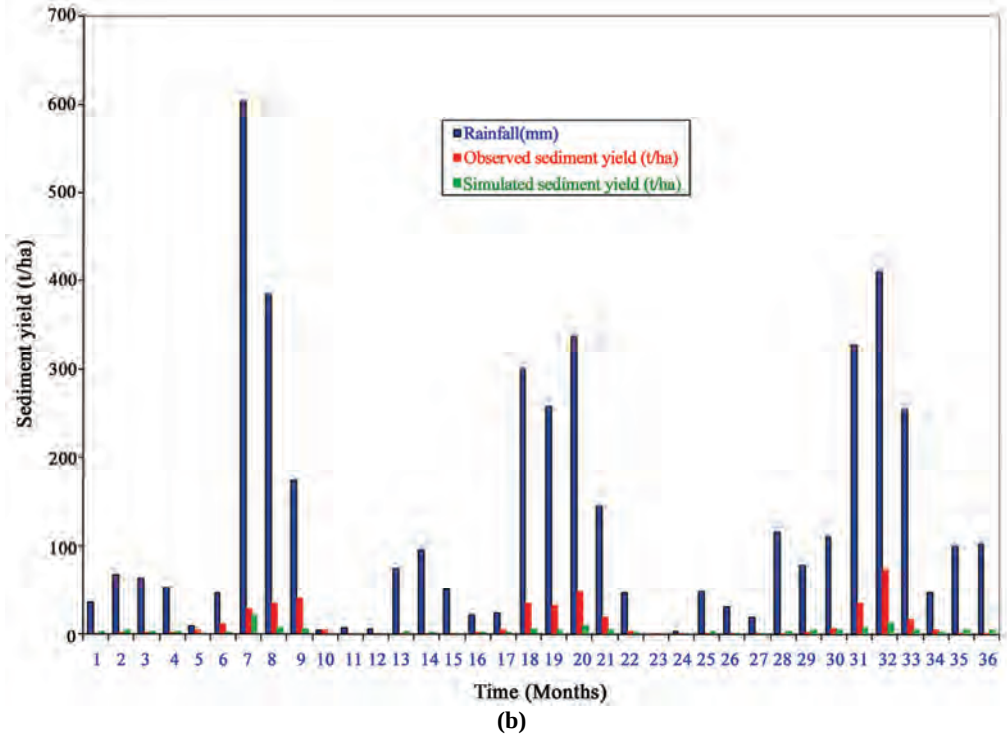

(b)

Figure 12. Comparison of observed and simulated. (a) daily sediment yield; (b) monthly sediment yield for the validation period 1995-97.

1996 and 1997, the simulated runoff was 957.13, 804.92 & 974.80 mm respectively as against the observed runoff of 931.47, 1252.68 and 1197.77 mm from a corresponding total rainfall of 1453, 1350 & 1641 mm. The plots of daily and monthly sediment yield (**Figure 12(a)**, **(b)**) show that the sediment yield was underestimated by the model. The total sediment yield simulated by the model was computed to be 46.33, 31.13 & 44.36 t/ha as against

the observed sediment yield of 125.21, 143.75 and 137.35 t/ha respectively for the years of 1995, 1996 and 1997. The R^2 values for the daily and monthly runoff (**Figure 13(a)**, **(b)**) were obtained as 0.33 and 0.62 respectively, while these values for sediment yield (**Figure 14(a)**, **(b)**) were computed as 0.26 and 0.47 respectively for the validation period of 1995 to 1997.

The results of the study can further be assessed keeping in view the unreliability of the input data. The parameter values derived from various sources need to be

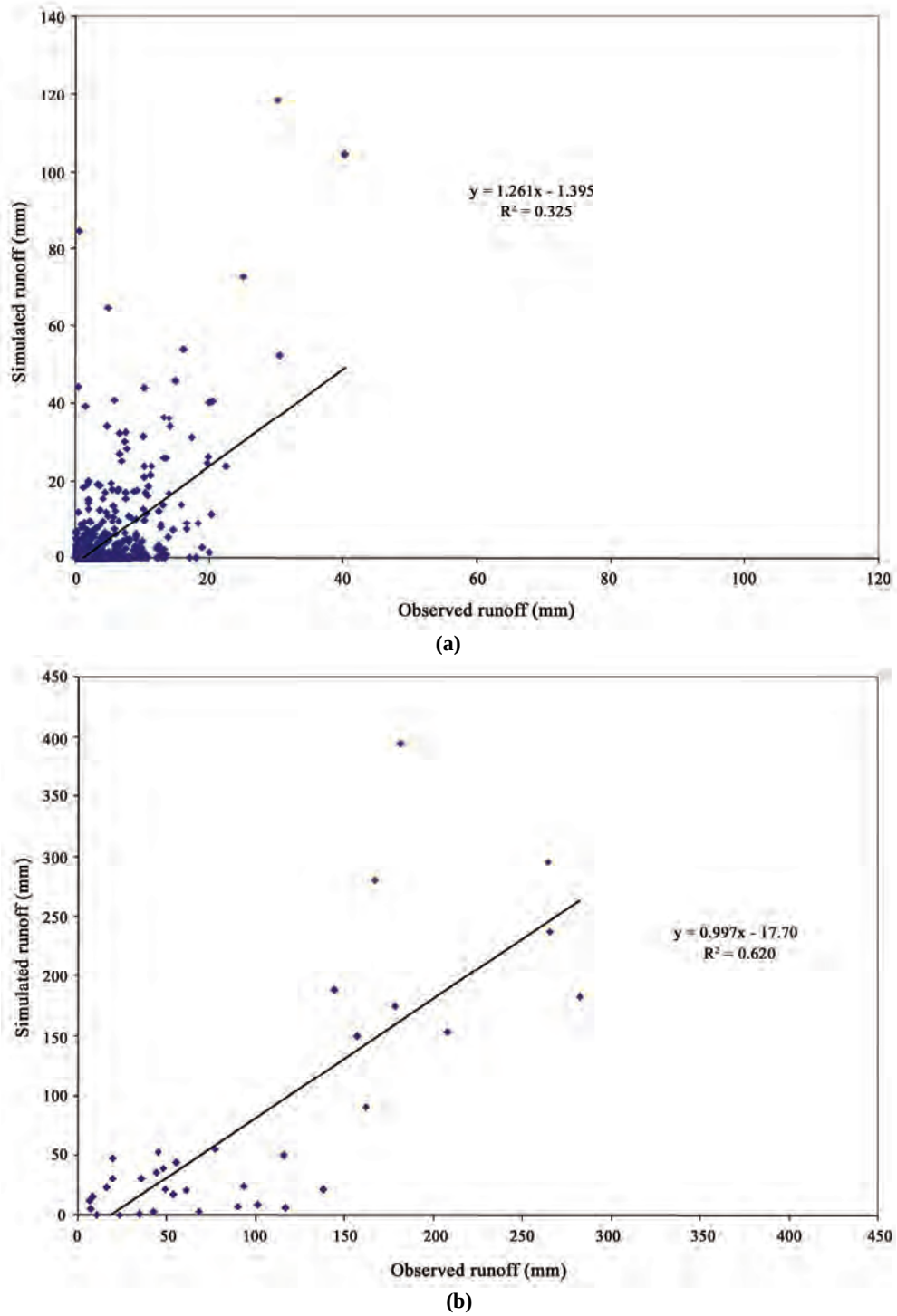

Figure 13. Goodness-of-fit for observed and simulated. (a) daily runoff; (b) monthly runoff for the validation period 1995-97.

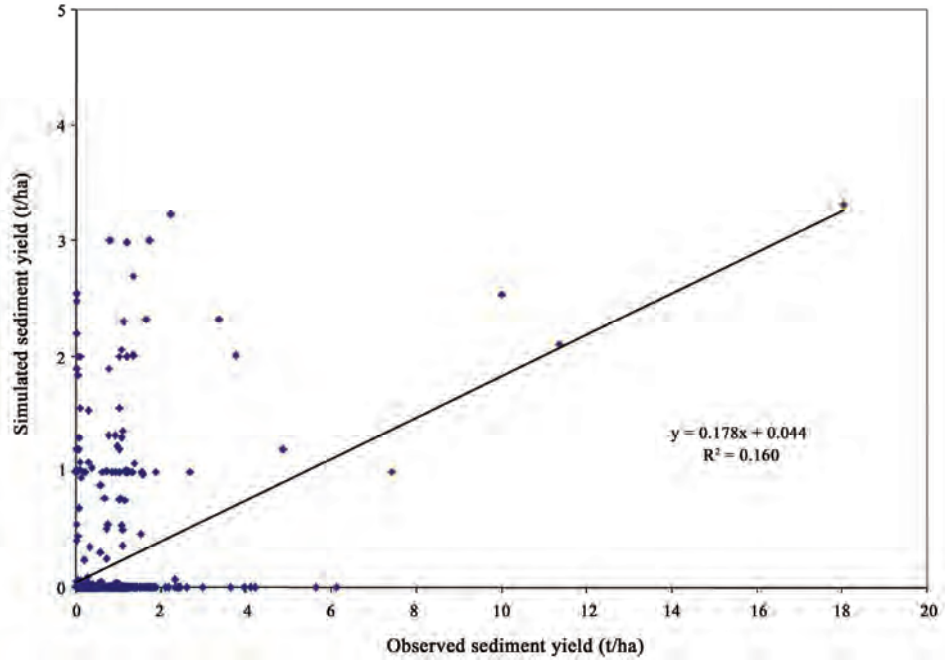

(a)

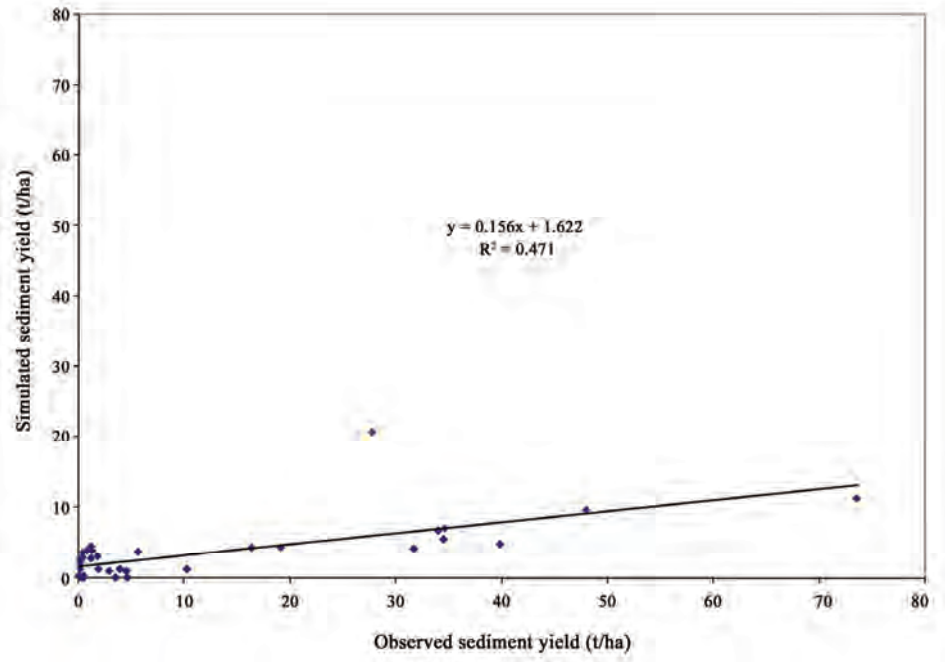

(b)

Figure 14. Goodness-of-fit for observed and simulated. (a) daily sediment yield; (b) monthly sediment yield for the validation period 1995-97.

verified in the field which is a difficult task in view of its approachability and mostly covered by thick forest. Similarly, the land use derived from remote sensing data was based on unsupervised classification. Further, the rainfall, runoff and sediment yield data used in the study may involve a number of possible human and instrumental errors. Keeping in view the above, it can be concluded from the simulation results of the study that the SWAT model has simulated the runoff and sediment yield reasonably well from an intermediate watershed in Himalayan region. The enhanced performance of the model could be achieved with some refinement in the input data.

5. Conclusions

In the present study, SWAT 2000, a physical based semi distributed hydrological model having an interface with ArcView GIS software was applied to a Himalayan watershed for modeling runoff and sediment yield. After preparing all the thematic maps and database as per the format of AVSWAT model, the model was calibrated for the daily and monthly surface runoff and sediment yield using the observed data of 1993 and 1994. The model validation was carried out for a data set of three years of 1995 through 1997. The simulation performance of the model for calibration and validation was evaluated using graphical and statistical methods.

The coefficient of determination (R^2) for the daily and monthly runoff was obtained as 0.53 and 0.90 respectively for the calibration period and 0.33 and 0.62 respectively for the validation period. The R^2 value in estimating the daily and monthly sediment yield during calibration was computed as 0.33 and 0.38 respectively. The R^2 for daily and monthly sediment yield values for 1995 to 1997 was observed to be 0.26 and 0.47. The values of R^2 can be considered reasonably satisfactory for estimating runoff and sediment yield from a remote watershed with scarce data.

6. References

[1] J. G. Arnold, P. M. Allen, and D. Morgan, "Hydrologic model for design of constructed wetlands," Wetlands, Vol. 21, No. 2, pp. 167–178, 2001.

[2] J. G. Arnold, and N. Fohrer, "SWAT2000: Current capabilities and research opportunities in applied watershed modeling," Hydrology Process, Vol. 19, pp. 563–572, 2005.

[3] J. G. Arnold, R. S. Srinivasan, and J. R. Williams, "Large area hydrologic modeling and assessment: Part 1. Model development," Journal of the American Water Resources Association, Vol. 34, No. 7389, 1998.

[4] J. Benaman, C. A. Shoemaker, and D. A. Haith, "Modeling non-point source pollution using a distributed watershed model for the Cannonsville Reservoir Basin," Delaware County, New York. Proceedings of the World Water & Environmental Resources Congress, May 20-24, 2001.

[5] D. K. Borah and M. Bera, "SWAT model background and application reviews," Paper Number: 032054, Presented at the ASAE Annual International Meeting, July 27-July 30, 2003, Las Vegas, Nevada, USA.

[6] K. Eckhartd and J. G. Arnold, "Automatic calibration of a distributed catchment model," Journal of Hydrology, Vol. 251, pp. 103–109, 2001.

[7] N. Fohrer, D. Moller, and N. Steiner, "An interdisciplinary modeling approach to evaluate the effects of land use change," Physics and Chemistry of the Earth, Vol. 27, pp. 655–662, 2002.

[8] A. Francos, G. Bidoglio, L. Galbiati, F. Bouraoui, F. J. Elorza, S. Rekolainen, K. Manni, and K. Granlund, "Hydrological and water quality modelling in medium sized coastal basin," Physics Chemistry Earth (B), Vol. 26, No. 1, pp. 47–52, 2001.

[9] N. S. Hsu, J. -T. Kuo, and W. S. Chu, "Proposed daily streamflow-forecasting model for reservoir operation," Journal of Water Resource Planning and Management, ASCE, Vol. 121, No. 2, 1995.

[10] M. Jha, W. Philip Gassman, S. Secchi, R. Gu, and J. Arnold, "Effect of watershed subdivision on SWAT flow, sediment and nutrient predictions," Journal of American Water Resources Association, Vol. 40, No. 3, pp. 811–825, 2004.

[11] K. W. King, J. G. Arnold, and R. L. Bingner, "Comparison of Green-Ampt and curve number methods on Goodwin Creek watershed using SWAT," Transactions of the ASAE, Vol. 42, No. 4, pp. 919–925, 1999.

[12] J. E. Nash and J. V. Sutcliffe, "River flow forecasting through conceptual models Part I-a discussion of principles," Journal of Hydrology, Vol. 10, pp. 282–290, 1970.

[13] S. L. Neitsch, J. G. Arnold, J. R. Kiniry, J. R. Williams, and K. W. King, "Soil and water assessment tool thereotical documentation - version 2000," Soil and Water Research Laboratory, Agricultural Research Service, Grassland, 808 East Blackland Road, Temple, Texas.

[14] S. L. Neitsch, J. G. Arnold, J. R. Kiniry, R. Srinivasan, and J. R. Williams, "Soil and water assessment tool user's manual - version 2000," Soil and Water Research Laboratory, Agricultural Research Service, Grassland, 808 East Blackland Road, Temple, Texas.

[15] J. R. Peterson and J. M. Hamlett, "Hydrologic calibration of the SWAT model in a watershed containing fragipan soils," Journal of the American Water Resources Association, Vol. 37, No. 2, pp. 295–303, 1998.

[16] J. Singh, K. H. Verman, and M. Demissie, "Hydrologic modelling of the iroquois river watershed using HSPF and SWAT," Illinous State Water Survey Contract Report, 2004–2008, 2008.

[17] C. A. Spruill, S. R. Workman, and J. L. Taraba, "Simulation of daily and monthly stream discharge from small watersheds using the SWAT model," Transactions of ASAE, Vol. 43, No. 6, pp. 1431–1439, 2000.

[18] M. P. Tripathi, R. K. Panda, and N. S. Raghuwanshi, "Identification and prioritisation of critical sub-watersheds for soil conservation management using SWAT model," Biosystems Engineering, Vol. 85, No. 3, pp. 365 –379, 2003.

[19] E. Varanou, E. Gkouvatsou, E. Baltas, and M. Mimikou, "Quantity and quality integrated catchment modeling under climate change with use of soil and water assessment tool model" Journal of Hydrologic Engineering, Vol. 7, No. 3, pp. 228–244, 2002.

J. Water Resource and Protection, **2010, 2, 282-290**
doi:10.4236/jwarp.2010.23032 Published Online March 2010 (http://www.scirp.org/journal/jwarp)

Comparison of Alkaline Treatment of Lead Contaminated Wastewater Using Lime and Sodium Hydroxide

Sudhakar M. Rao[1*], G. C. Raju[2]
[1]*Department of Civil Engineering & Chairman, Center for Sustainable Technologies, Indian Institute of Science, Bangalore, India*
[2]*Department of Civil Engineering, BMS College of Engineering, Bangalore, India*
E-mail: *msrao@civil.iisc.ernet.in*
Received July 13, 2009; *revised August* 20, 2010; *accepted August* 26, 2010

Abstract

A lead-acid storage battery manufacturing industry in India produces several thousand liters of lead contaminated acidic wastewater on a daily basis and uses hydrated lime to render the lead-contaminated acidic wastewater alkaline (pH = 8.0). Alkaline treatment of the acidic wastewater with lime though a cost-effective method, generates copious amount of lead-contaminated gypsum sludge. Other alkali agents such as sodium hydroxide, sodium carbonate and dolomite are also used for alkali treatment of the acid wastewaters. The present paper compares the relative efficiency of hydrated lime and 0.05 M to 1 M NaOH solutions with respect to 1) amounts of sludge produced, 2) immobilization of the soluble lead in the acidic wastewater (AWW) and 3) increase in TDS (total dissolved solids) levels upon treatment of AWW with NaOH solutions and lime. The study also performs equilibrium speciation upon alkaline treatment of AWW with lime and NaOH (sodium hydroxide) solutions using the Visual MINTEQ program to understand the chemical reactions occurring during treatment process.

Keywords: Acid, Alkali Agents, Alkaline Treatment, Battery, Lead, Speciation, TDS

1. Introduction

A lead-acid storage battery manufacturing industry in India produces several thousand liters of lead contaminated acidic wastewater on a daily basis. The acidic wastewater (AWW) contains lead concentration of 4.24 mg/L and has pH of 0.96. Macchi *et al*. [1] report similar ranges of pH (1.6 and 2.9) but higher lead concentrations (5–15 mg/L) in acidic wastewaters of lead-acid storage battery units in Italy. Neutralization of the lead-contaminated acidic wastewaters are achieved by adjusting their pH values to a desirable range of 5.5 to 9.5 using alkaline agents such as, sodium hydroxide, sodium carbonate, lime and dolomite [2]. The lead-acid storage battery manufacturing industry in India uses hydrated lime to treat the lead-contaminated acidic wastewater to pH 8.0. Alkaline treatment of acidic wastewater by lime addition occurs according to the reaction:

$$Ca(OH)_2 + H_2SO_4 \rightarrow CaSO_4 \cdot 2H_2O \qquad (1)$$

Alkaline treatment with lime also precipitates the soluble lead in the acidic wastewater as hydroxides, carbonates and sulfates that is incorporated in the gypsum sludge. Guided by the minimum solubility of lead compounds in the alkaline pH (8-10) range [3] the lead-acid battery manufacturing industry in India chose to treat their acidic wastewater to this pH (8.0).

Alkaline treatment of the acidic wastewater with lime though a cost-effective method, generates copious amount of sludge material. For example, calculations show that treatment of 1000 liters of acidic wastewater produces 100 kg of moist sludge. As mentioned earlier, pH of acidic wastewaters are also rendered alkaline by addition of sodium hydroxide, sodium carbonate, and dolomite [2]. Sodium hydroxide solution neutralizes the acidic wastewater according to the reaction:

$$2NaOH + H_2SO_4 \rightarrow Na_2SO_4 + 2H_2O \qquad (2)$$

The advantage of employing sodium hydroxide solution is that the neutralization reaction (reaction 2) leads to minimum sludge formation as the reaction product Na_2SO_4 (sodium sulfate) is water-soluble. Macchi *et al.* [1] observe that neutralization of acidic battery wastewater using sodium hydroxide solution has an added advantage as the resident ferric ions in the battery

wastewater precipitate (as hydroxides) and scavenge the lead ions from the wastewater. A possible disadvantage of neutralizing the acid wastewater with sodium hydroxide solution is an increase in total dissolved solids (TDS) concentration of the treated water owing to the formation of soluble sodium sulfate. Increase in TDS levels of the treated water is a concern as MOEF (Ministry of Environment and Forests) regulations [4] state that TDS levels of treated leachate for disposal on land or inland surface water bodies should not exceed 2100 mg/L.

Earlier studies have not considered the relative impacts of lime and sodium hydroxide neutralization of lead-contaminated acidic wastewater on the amounts of sludge produced, lead removal efficiency and TDS levels of the treated wastewater. This paper hence compares the relative efficiency of lime and sodium hydroxide solutions with respect to 1) amounts of sludge produced upon alkaline treatment (pH=8) of AWW, 2) immobilization of available lead in AWW upon alkaline treatment and 3) increase in TDS levels of AWW upon alkaline treatment. Ion speciation studies are performed using the Visual MINTEQ program to obtain insight into changes in hydrogen ion concentration and equilibrium concentrations of aqueous and solid phases formed during the alkaline treatment process.

2. Materials and Methods

2.1. Wastewater Sample and Chemicals

Lead contaminated acidic wastewater (AWW) was supplied by the lead-acid battery industry in India. Laboratory reagent grade hydrated lime and sodium hydroxide were used in the AWW neutralization studies.

2.2. Alkaline Treatment Assays

The pH of the acidic wastewater was increased by adding incremental amounts of laboratory reagent grade hydrated lime to separate one-liter batches (of acid wastewater) with manual stirring until the pH of the wastewater stabilized for the given lime addition. Experimental results estimated that addition of 15.5 g of lime per liter of acidic wastewater altered its pH to 8.0. The acidic wastewater was elevated to this pH to simulate the alkaline treatment process of the lead acid battery industry. To estimate the sludge generated by this lime addition process, a separate experiment was performed; 15.5 g of hydrated lime was added to one liter of acidic wastewater (pH = 0.96). The lime-treated solution was filtered and analyzed for lead concentration using atomic absorption spectrophotometer. The resultant sludge was weighed in the moist condition.

The pH of the acidic wastewater was also increased by adding incremental amounts of 1 molar (M), 0.1 M and 0.05 M NaOH solutions to separate, one-liter batches of AWW. The incremental volumetric additions were continued until the acidic wastewater was rendered sufficiently alkaline (pH 10.1 to 10.7). In separate experiments 0.405 L (liter), 3.78 L and 8.2 L of 1 M, 0.1 M and 0.05 M NaOH solutions were added to separate 1 L batches of acidic wastewater; the treated solutions were filtered and the resulting sludge were weighed in the moist condition. Lead concentrations in the filtrates were analyzed using atomic absorption spectrophotometer.

2.3. Equilibrium Ion Speciation Estimation

The study performed equilibrium speciation of AWW upon neutralization by lime and NaOH solutions using the Visual MINTEQ program [http://www.lwr.kth.se/English/OurSoftware/vminteq/#download]. Visual MINTEQ is a geochemical program to model aqueous solutions and the interactions of aqueous solutions with hypothesized assemblages of solid phases. It applies the fundamental principles of thermodynamics to solve geochemical equilibria from a set of mass balance equations. The input parameters to the Visual MINTEQ program were the chemical composition of AWW (**Table 1**), the pH of AWW on addition of lime or 1 M NaOH solution (**Figure 1**), mass of lime added (incorporated as solid finite phase) and increase in sodium ion concentration from addition of 1 M NaOH solution. Speciation of the lead by Visual MINTEQ program at various lime and 1 M NaOH solution additions provided information on the relative amounts of lead occurring in the soluble and precipitated states during the treatment process.

2.4. Analytical Methods

Lead contaminated acidic wastewater (AWW) supplied by the lead-acid battery industry in India was filtered through 0.45 micron filter. The filtrate was analyzed for lead, iron, calcium, magnesium, sodium and potassium concentrations using atomic absorption spectrophotometer (model-Perkin Elmer Analyst 200). The concentration of, sulfate ions was determined by the turbidity method, while the chloride concentration was determined by ion

Table 1. Acidic wastewater composition.

Parameter	Value
Lead (mg/L)	4.24
Iron (mg/L)	80
Calcium (mg/L)	336
Magnesium (mg/L)	10.0
Sodium (mg/L)	195
Potassium (mg/L)	7
Sulfate (mg/L)	9100
Chloride (mg/L)	383
pH	0.96

meter method using an ionmeter (Orion, 720A) with a chloride ion-selective electrode. The pH and electric conductivity of the acidic wastewater were also determined.

3. Results and Discussion

3.1. Characteristic of Acidic Wastewater

Table 1 presents the chemical composition of the acidic wastewater. The AWW has an acidic pH of 0.96 and soluble lead concentration of 4.24 mg/l. The lead concentration of 4.24 mg/l in the acidic wastewater greatly exceeds the permissible limit (0.1 mg/l) for disposal of treated lead-acid battery effluent into the environment [5]. Besides, containing excess lead concentration, the acidic pH of the acidic wastewater (0.96) classifies the wastewater as a corrosive liquid [6]. High sulfate ion concentrations occur in the acidic wastewater of lead-acid storage battery units (**Table 1**), as sulfuric acid mainly constitutes the acidic wastewater. Soluble iron (80 ppm) occurs in the acidic wastewater (**Table 1**) due to corrosion reactions [1]. Speciation by the Visual MINTEQ program indicated hydrogen ion concentration of 0.1096 M for the AWW which is expected for its pH value of 0.96. Further, the speciation results show that bulk of the sulfate concentration in the AWW (0.1 M) occurs as HSO_4^- (0.08 M) species.

3.2. Lime Treatment of AWW

Figure 1 presents the experimentally obtained plot of OH addition (in meq/L) versus pH of AWW (**Figure 1**). The OH values in meq/L are obtained by converting mass of lime addition /L of AWW to equivalent OH concentration. The figure shows that hydroxyl ion additions up to 405 meq/liter marginally change the pH of the acidic wastewater. Increasing the hydroxyl ion concentration from 405 to 432 meq/L sharply increased the pH of AWW to 11.5. Addition of 422 meq of OH ions per liter of acidic wastewater is necessary to increase its pH to 8 (**Figure 1**). Alkaline treatment (pH=8) of 1 liter of AWW with hydrated lime generated 0.102 kg of moist sludge. The prominent peaks at 7.63Å, 4.28Å and 3.07Å in the X-ray diffraction of the air-dried (at 45 ^{0}C) sludge (**Figure 2**)

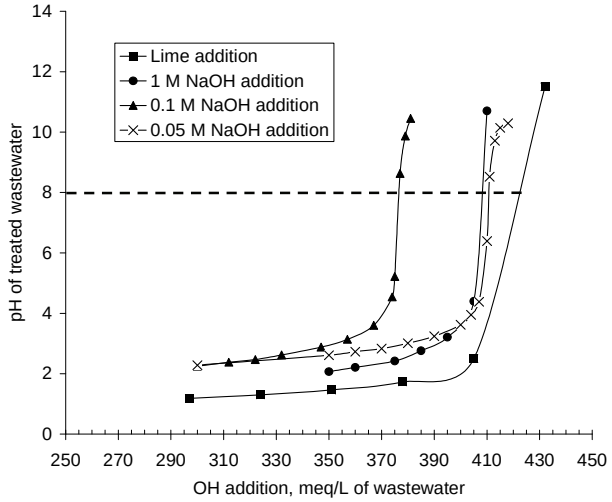

Figure 1. pH of acidic wastewater upon lime and NaOH solution addition.

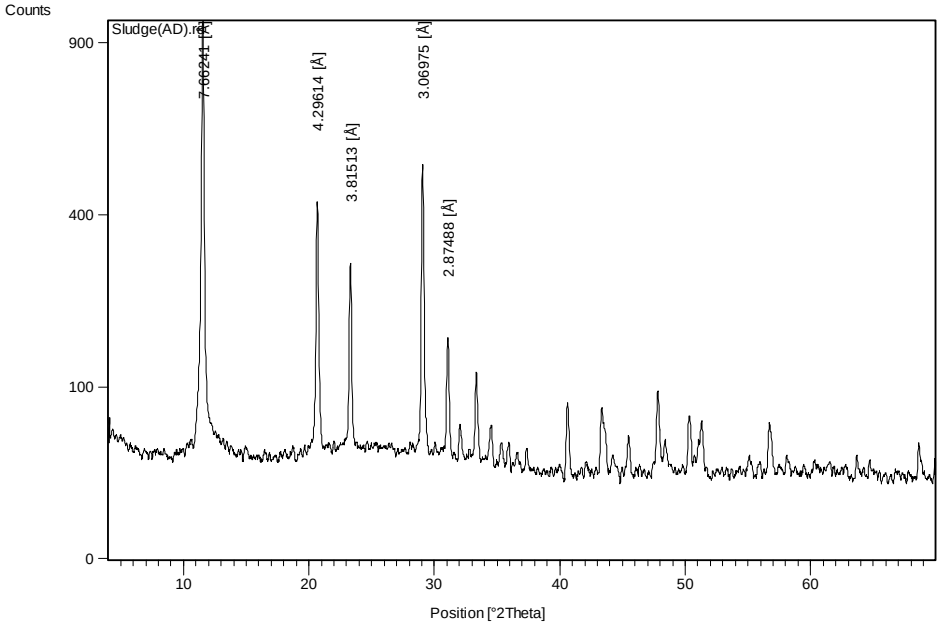

Figure 2. X-ray diffraction pattern of air-dried sludge.

reveal the presence of gypsum mineral (calcium sulfate dihydrate, $CaSO_4.2H_2O$).

The speciation results show that alkaline treatment of AWW with lime reduces its initial hydrogen ion concentration from 0.1096 M to 4.35×10^{-12} M. Correspondingly the HSO_4^- concentration reduced from 0.08 M to 2.25×10^{-13} M and the calcium ion concentration increased from 0.074 M to 0.16 M (**Figure 3**). The increase in calcium ion concentration and reduction in hydrogen ion concentration upon lime treatment of AWW is explained

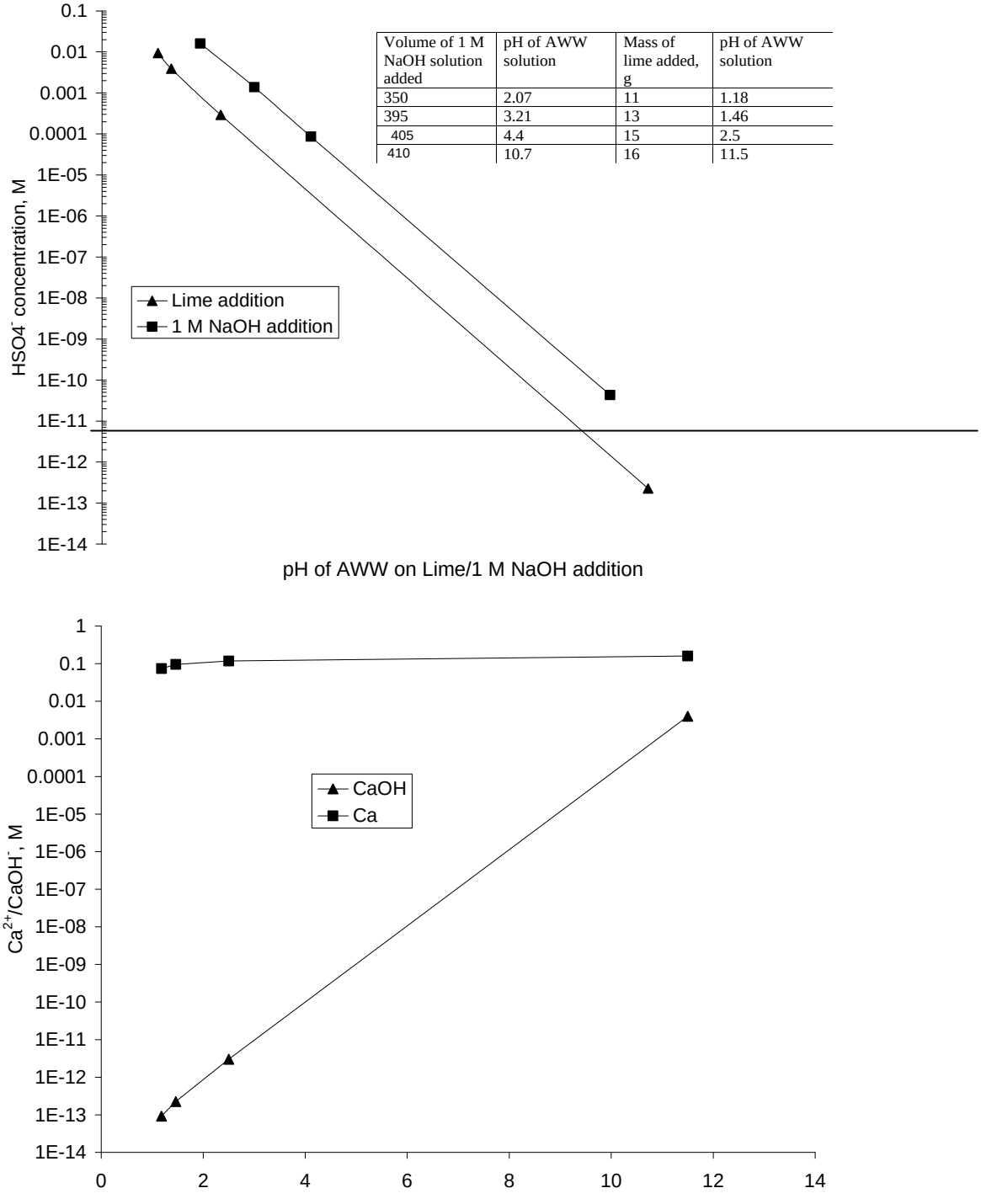

Volume of 1 M NaOH solution added	pH of AWW solution	Mass of lime added, g	pH of AWW solution
350	2.07	11	1.18
395	3.21	13	1.46
405	4.4	15	2.5
410	10.7	16	11.5

Figure 3. Variations in ion concentrations upon AWW neutralization with lime and 1 M NaOH solution-visual MINTEQ results.

from the following reactions. Lime dissociates into calcium and hydroxyl ions (reaction 4); the dissociated hydroxyl ions reduce the hydrogen ions with the formation of H_2O (reaction 5). Increasing addition of lime to AWW shifts the equilibrium to the right enhancing the hydroxyl ion concentration.

$$Ca(OH)_2 \leftrightarrow Ca^{2+} + 2H_2O^- \quad (4)$$

$$2OH^- + 2H^+ \rightarrow 2H_2O \quad (5)$$

The sharp increase in CaOH- concentration (**Figure 3**) from 9.2×10^{-14} M at pH 1.18 (lime addition = 11 g/liter) to 3.99×10^{-3} M at pH 11.5 (lime addition 16 g/Liter) is attributed to the enhanced formation $CaOH^-$ in the strongly alkaline pH medium according to reaction:

$$Ca^{2+} + OH^- \rightarrow CaOH^- \quad (6)$$

The speciation results show that the HSO_4^- concentration decreases from 0.009 M to 2.25×10^{-13} on increasing the pH of the AWW from 1.18 to 11.5 (**Figure 3**). Decrease in HSO_4^- concentration is attributed to the reduction of bisulfate to sulfate (reaction 7) and combination of calcium and sulfate ions to form $CaSO_4$ (aq):

$$HSO_4^- + OH^- \rightarrow H_2O + SO_4^{2-} \quad (7)$$

$$Ca^{2+} + SO_4^{2-} \rightarrow CaSO_4(aq) \quad (8)$$

Speciation results showed that alkaline treatment (pH=8) of AWW with lime leads to the formation of 0.0052 M to 0.0054 M $CaSO_4$ (aq) species.

The lead ion concentration in lime-treated AWW (pH=8) correspond to 0.11 mg/L which marginally exceeds the permissible limit (0.1 mg/L) for disposal of treated effluent into environment [5]. The initial lead concentration in AWW corresponds to 4.24 mg/L or 2.046×10^{-5} M. Speciation of the lead by Visual MINTEQ program at various lime additions provided information on the relative amounts of lead occurring in the soluble and precipitated forms during the lime treatment process. **Figure 4** plots the soluble lead content as function of pH on lime addition. Lime addition up to 15 g/L causes the entire lead to remain in soluble form (pH of treated effluent = 2.5). Addition of 15.7 g/L increases the AWW pH to 8 and causes near complete (99.48 %) precipitation of lead.

Figure 5 shows that 0.215 kg of moist sludge is generated upon alkaline treatment (pH=8) of AWW (volume = 1L) by lime addition. **Figure 6** shows that the TDS level of lime-treated AWW (pH 8) corresponds to 2100 mg/L which meets the TDS limit (2100 mg/L) recommended for disposal of treated leachate to land, inland surface water or public sewers [4].

3.3. Sodium Hydroxide Treatment of Acidic Wastewater

Figure 1 includes the experimentally obtained plots of OH addition (in meq/L) versus pH of AWW (**Figure 1**) for volumetric additions of 1M, 0.1 M and 0.05 M

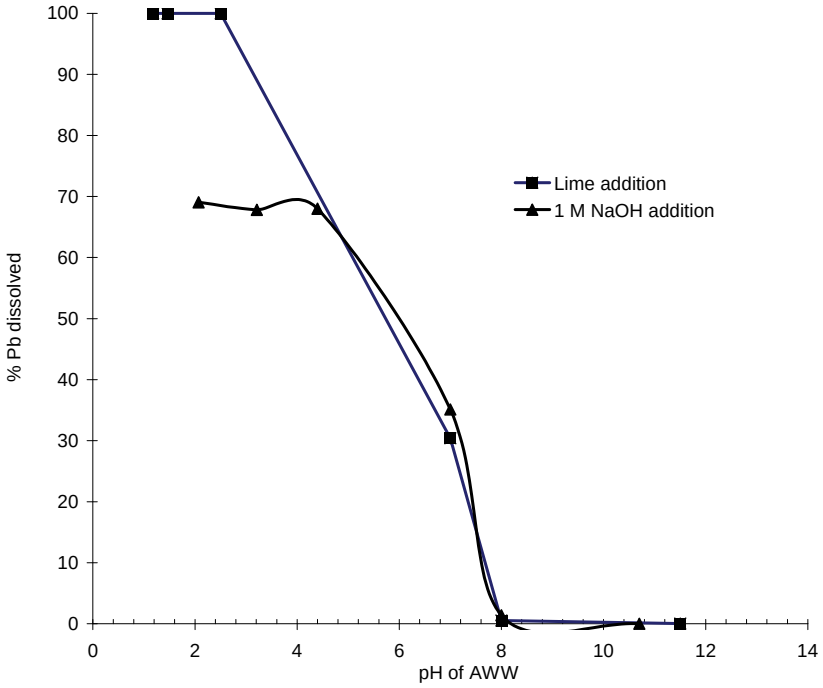

Figure 4. Variations of soluble lead concentrations as a function of pH upon AWW neutralization with lime and 1 M NaOH solution.

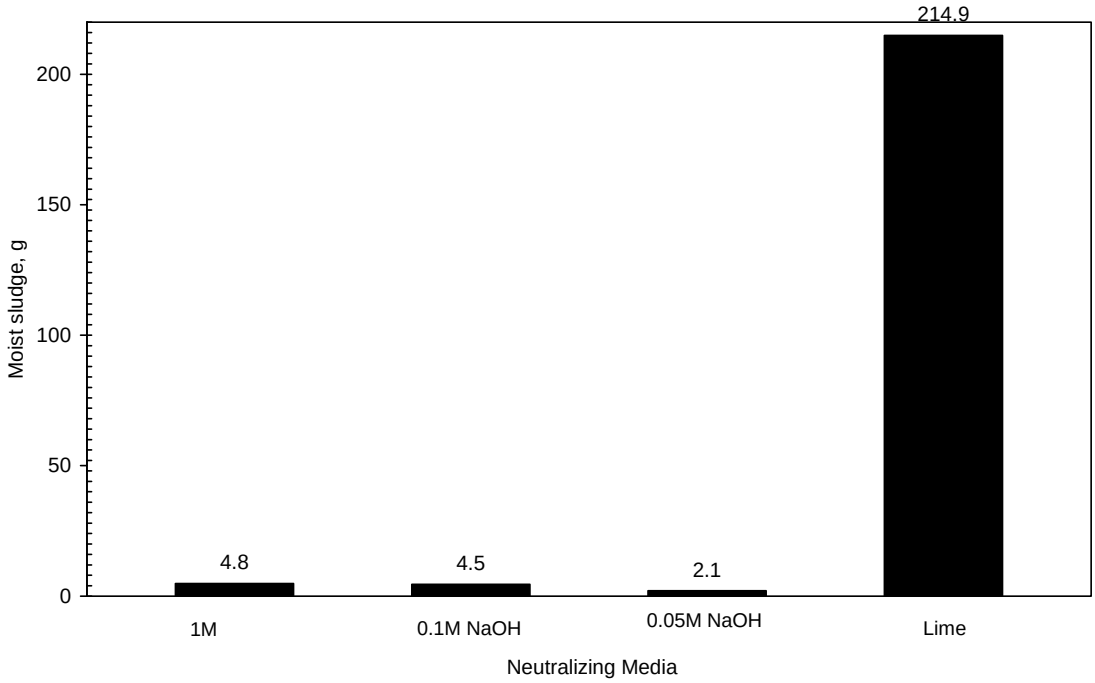

Figure 5. Comparison of moist sludge produced by different alkali agents.

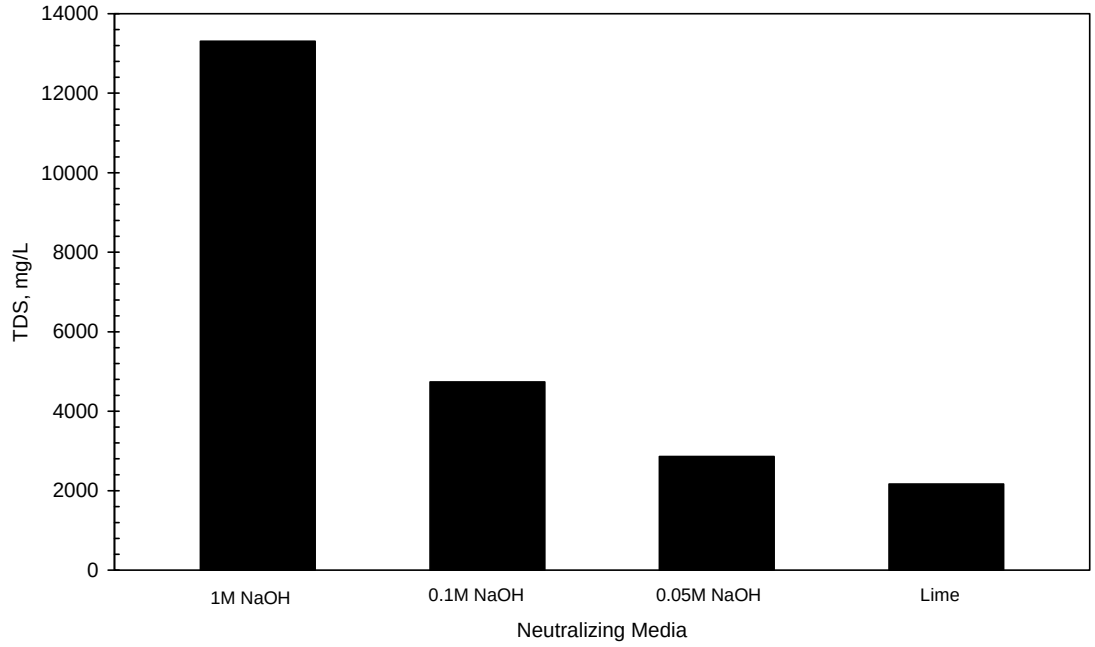

Figure 6. TDS levels in AWW neutralized with different alkali agents.

NaOH solutions. The figures show that the pH of the acidic wastewater responds to NaOH addition in two phases; the rate of increase in pH is gradual up to pH values of 3.6 to 4.4; thereafter rate of increase in pH with addition of NaOH solutions is a rapid process. These plots estimate that 407 meq/L, 377 meq/L and 410 meq/L of hydroxyl ions are required to modify the pH of the acidic wastewater from an initial value of 0.96 to desired value of 8.0 on addition of 1 M, 0.1 M and 0.05 M NaOH solutions.

Visual MITEQ speciation results show that alkaline treatment (pH=8) of AWW with 1 M NaOH solution reduces the initial hydrogen ion concentration from 0.1096 M to 2.72×10^{-11} M and the HSO_4^- concentration from 0.08 M to 4.32×10^{-11} M (**Figure 3**); concomitantly, sodium ion concentration increases from 0.33 M to 0.38

M (**Figure 7**). The increase in sodium ion concentration and reduction in hydrogen ion concentration upon NaOH addition is attributed to the reactions:

$$NaOH \rightarrow Na^{+} + OH^{-} \quad (9)$$

$$OH^{-} + H^{+} \rightarrow H_2O \quad (10)$$

Speciation results show that the HSO_4^- concentration decreases from 0.016 M to 4.31×10^{-11} M on increasing the pH of the AWW from 2.07 to 10.7 (**Figure 3**). The reduction in HSO_4^- concentration is attributed to the reaction:

$$HSO_4^- + Na^+ + OH^- \rightarrow NaSO_4^- + H_2O \quad (11)$$

The concentration of $NaSO_4^-$ species varies from 0.026 M at pH 2.07 (350 ml addition) to 0.034 M at pH 10.7 (410 ml addition, **Figure 7**). Experimental measurements showed that the lead concentration in AWW treated with1 M NaOH solution (0.24 mg/L) does not meet the permissible limit (0.1 mg/l) for disposal of treated effluent into inland surface water [5], while, AWW treated with 0.1 M (lead concentration = 0.07 mg/L) and 0.05 M NaOH (lead concentration = 0.06 mg/L) solutions meet this requirement. The inverse relation between concentration of sodium hydroxide solution and lead ion concentration in treated effluent is apparently related to volumes of the alkali solution used in the treatment process. **Figure 1** had earlier estimated that 0.405 L, 3.78 L and 8.2 L of 1 M, 0.1 M and 0.05 M NaOH solutions are required to modify the pH of the acidic wastewater from an initial value of 0.96 to desired value of 8.0. Smaller lead concentrations apparently occurs in the effluents treated with 0.1 M and 0.05 M NaOH solutions owing to 9 to 20 times greater dilution of the acidic wastewater in comparison to treatment with 1 M NaOH solution. Visual MINTEQ results however did not show differences in the soluble/precipitated lead concentrations of AWW treated to pH 8 with 1M, 0.1 M and 0.05 M NaOH solutions. The speciation results showed that identical levels (98.7 %) of lead precipitate (as $Pb(OH)_2$, 2.02×10^{-5} M) on treating the AWW to pH 8 with the three NaOH solutions.

Figure 4 includes the Visual MINTEQ results for the soluble lead content (as a percentage) as function of pH on addition of 1 M NaOH solution. Treatment of AWW with NaOH solution renders significant fraction of lead insoluble (30 to 32 %) in the acidic pH range of 2.07 to 4.4 (**Figure 4**). Increasing the AWW pH to 8.0 (408 ml addition) rendered almost the entire lead fraction (98.7 %) insoluble. **Figure 8** reveals that treating AWW with NaOH solution results in precipitation of $PbSO_4$ species (anglesite) in the acidic pH range of 2.07 to 4.4. The much larger equilibrium constant (log K_{eq}) for anglesite formation (log K_{eq} = 7.79) in comparison to $Pb(OH)_2$ formation (log K_{eq} = -8) is apparently responsible for precipitation of lead in the acidic pH range.

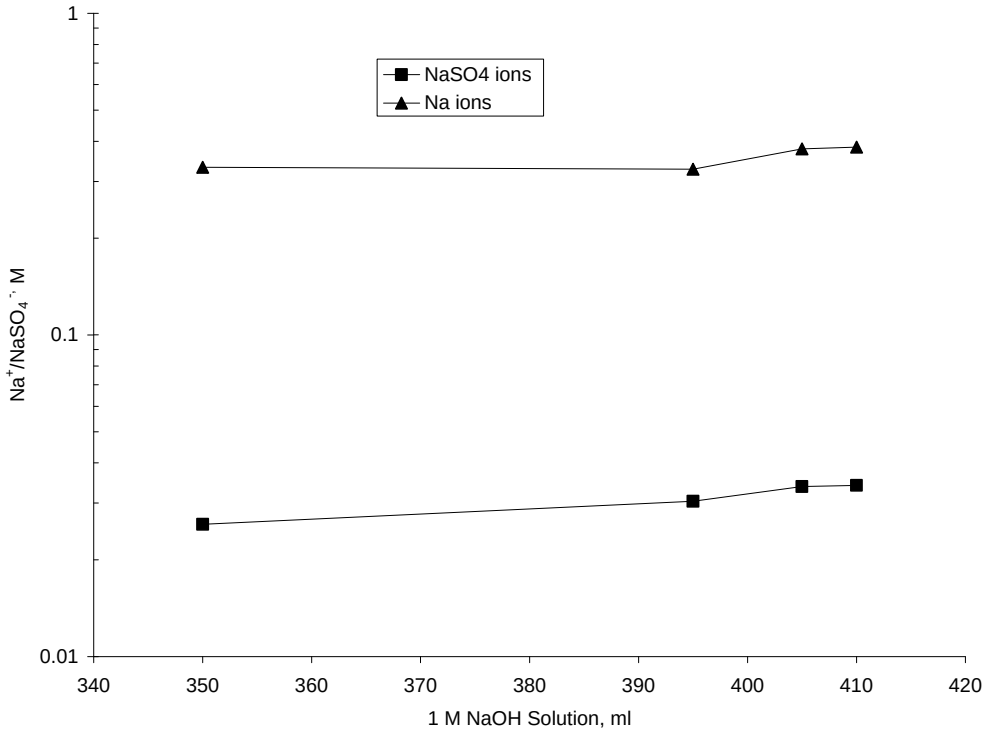

Figure 7. Variations in Na^+ and $NaSO_4^-$ ion concentrations upon AWW neutralization with 1 M NaOH solution-visual MINTEQ results.

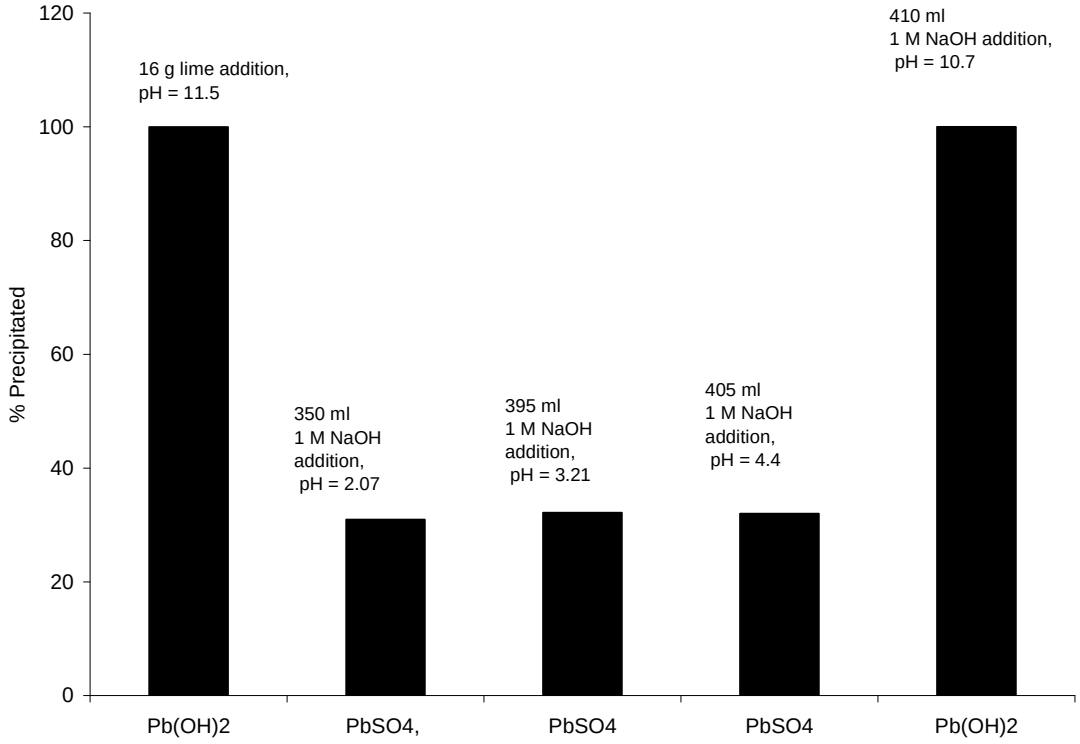

Figure 8. Relative distribution of precipitated lead as a function of pH upon AWW neutralization with lime and 1 M NaOH solution.

Figure 5 reveals that alkaline treatment of AWW (pH 8) with 0.05 M, 0.1 M and 1 M NaOH solutions produce 0.0021 kg, 0.0045 kg and 0.0048 kg of moist sludge respectively. **Figure 6** compares the total dissolved solid concentration (TDS) of AWW treated to pH 8 with 1 M, 0.1 M, 0.05 M NaOH solutions respectively. Expectedly, the acidic wastewater treated with 1 M NaOH solution exhibits maximum TDS level of 13,310 mg/L; the acidic wastewater treated with 0.05 M NaOH solution exhibits the minimum TDS level (2800 mg/L) which is higher than TDS limit recommended [4] for disposal of treated leachate to land, inland surface water or public sewers (2100 mg/L).

3.4. Comparison of Lime and Sodium Hydroxide Treatments

Figure 1 reveals that NaOH solutions are more effective than lime for alkaline treatment of AWW as the pH of the acidic wastewater is modified to 8.0 at lower OH concentrations (377 to 410 meq/L) on addition of NaOH solutions than on lime addition (OH concentration = 422 meq/L at pH=8). Experimental results in **Figure 5** show that treatment with NaOH solutions produce much lesser (45 to 103 folds) masses of moist sludge than lime. Alkaline treatment (pH 8) with 0.1 M and 0.05 M NaOH solutions generate acceptable levels of residual lead concentrations (< 0.1 mg/L) in the treated AWW, while lime treatment results in residual lead concentration (0.11 mg/L) which is slightly in excess of the permissible limit. The disadvantage of using NaOH solutions is that the treated wastewater is characterized by higher total dissolved salt concentrations (2860 to 13310 mg/L, **Figure 6**). For example, acidic wastewater treated with 0.05 M NaOH solution has 33 % higher TDS (TDS=2860 mg/L) than the sample treated with lime (TDS = 2100 mg/L).

4. Conclusions

Speciation results showed that AWW is characterized by the presence of 0.196 molar H^+ and 0.08 molar HSO_4^- ion concentrations. Upon lime/NaOH treatment, hydroxyl ions released by alkali dissociation, reduce hydrogen ions to form H_2O molecules. Decrease in HSO_4^- concentration is attributed to the reduction of bisulfate to sulfate ions; the sulfate ions combine with calcium/sodium ions to form $CaSO_4(aq)/NaSO_4^-$ species. AWW is characterized by lead concentration of 4.24 mg/L. Speciation results showed that almost the entire lead fraction is precipitated (98.7 to 99.48 %) upon increasing the pH of AWW to 8.0 with lime or 1 M NaOH solution. Treating AWW with 0.1 M and 0.05 M NaOH solutions generated acceptable residual lead concentra-

tions (lower than the permissible limit of 0.1 mg/L) in the treated wastewater owing to greater dilution of AWW by the weaker alkali solutions.

Comparison of NaOH and lime treatments reveal that lower OH concentrations (in meq/L) are required to modify the pH of AWW from 0.96 to 8.0. Further, smaller mass of moist sludge and environmentally acceptable levels of residual lead concentrations (for additions of 0.1 M and 0.05 M solutions) are generated upon NaOH treatment in comparison to lime treatment of AWW. Based on the minimal mass of moist sludge produced, acceptable residual lead concentration and lowest (among NaOH solutions) TDS of treated AWW, 0.05 M NaOH solution is suggested as an alternative agent to remediate the acidic wastewater from lead-acid battery manufacturing industry. The treated AWW will however have to be subjected to some form of desalination before it is discharged on land or to inland water bodies to meet environmental norms for discharge of treated effluent into the environment.

5. References

[1] G. Macchi, M. Pagang, M. Santori, and G. Tiravanti, "Battery industrial wastewater: Pb removal and produced sludge," Water Research, Vol. 27, pp. 1511–1518, 1993.

[2] J. W. Patterson, "Lead in wastewater treatment technology," Ann Arbor Science, Ann Arbor, Michigan, pp. 129–138, 1975.

[3] R. M. Harrisom and D. P. H. Laxen, "Lead pollution causes and control," Chapman and Hall, London, 1981.

[4] Ministry of Environment and Forests. Municipal Solid Wastes (Management and Handling) Rules 2000. MOEF, New Delhi, 2000.

[5] "Liquid effluent discharge standards for lead acid battery manufacturing," Central Pollution Control Board. http://cpcb.nic.in.

[6] CPCB. "Guidelines for proper functioning and upkeep of disposal sites," Hazardous Waste Management Series: HAZWAMS/32/2005–2006, Central Pollution Control Board (CPCB), New Delhi, 2005.

Call For Papers

Journal of Water Resource and Protection (JWARP)

http://www.scirp.org/journal/jwarp
ISSN:1945-3094 (Print), 1945-3108 (Online)

JWARP is an international refereed journal dedicated to the latest advancement of water resource and protection. The goal of this journal is to keep a record of the state-of-the-art research and promote the research work in these fast moving areas.

Editor-in-Chief

Prof. Jian SHEN — College of William and Mary, USA

Editorial Board

Subject Coverage

This journal invites original research and review papers that address the following issues in water resource and protection. Topics of interest include, but are not limited to:

- Water resources and quality assessment
- Rivers, lakes and estuary systems
- Wastewater treatment and sludge biotreatment
- Water purification and water supply
- Water source protection and sustainable use
- Modeling, measuring and prediction of water pollution
- Ground water pollution control
- Reactions and degradation of wastewater contaminants
- Other topics about water pollution

We are also interested in short papers (letters) that clearly address a specific problem, and short survey or position papers that sketch the results or problems on a specific topic. Authors of selected short papers would be invited to write a regular paper on the same topic for future issues of the *JWARP.*

Notes for Intending Authors

Submitted papers should not have been previously published nor be currently under consideration for publication elsewhere. Paper submission will be handled electronically through the website. All papers are refereed through a peer review process. For more details about the submissions, please access the website.

Website and E-Mail

http://www.scirp.org/journal/jwarp Email: jwarp@scirp.org

J. Water Resource and Protection, 2010, 2, 191-290.
Published Online March 2010 in SciRes (http://www.SciRP.org/journal/jwarp).

TABLE OF CONTENTS

Volume 2 Number 3 **March 2010**

9771945309004 09